Archiv der Pharmazie

DPhG

FULL PAPER OPEN ACCESS

Design, Synthesis, In Vitro, and In Silico Studies of 5-(Diethylamino)-2-Formylphenyl Naphthalene-2-Sulfonate Based Thiosemicarbazones as Potent Anti-Alzheimer Agents

Urva Farooq[1] | Muhammad Islam[2,3] | Zahra Batool[1] | Suraj N. Mali[4] | Rahul D. Jawarkar[5] | Shailesh S. Gurav[6] | Rima D. Alharthy[7] | Halil Şenol[8] | Nastaran Sadeghian[9] | Parham Taslimi[9] | Zahid Shafiq[1] | Silvia Schenone[10]

[1]Institute of Chemical Sciences, Bahauddin Zakariya University, Multan, Pakistan | [2]Department of Basic Sciences and Humanities (Chemistry), Muhammad Nawaz Sharif University of Engineering and Technology (MNSUET), Multan, Pakistan | [3]School of Pharmaceutical Science and Technology, Tianjin University, Tianjin, China | [4]School of Pharmacy, D.Y. Patil University (Deemed to be University), Navi Mumbai, India | [5]Department of Medicinal Chemistry, Dr. Rajendra Gode Institute of Pharmacy, University-Mardi Road, Amravati, India | [6]Department of Chemistry, VIVA College, Virar (W), Maharashtra, India | [7]Department of Chemistry, Science & Arts College, Rabigh Branch, King Abdulaziz University, Rabigh, Saudi Arabia | [8]Department of Pharmaceutical Chemistry, Faculty of Pharmacy, Bezmialem Vakif University, Fatih, Istanbul, Türkiye | [9]Department of Biotechnology, Faculty of Science, Bartin University, Bartin, Türkiye | [10]Department of Pharmacy, University of Genoa, Genoa, Italy

Correspondence: Zahid Shafiq (zahidshafiq@bzu.edu.pk) | Silvia Schenone (silvia.schenone@unige.it)

Received: 17 April 2025 | **Revised:** 17 June 2025 | **Accepted:** 24 June 2025

Funding: This Project was funded by the Deanship of Scientific Research (DSR) at King Abdulaziz University, Jeddah, under grant no. GPIP: 46-665-2024.

Keywords: anti-Alzheimer | MD simulation | molecular docking | naphthalene-2-sulfonate | thiosemicarbazones

ABSTRACT

Alzheimer's disease (AD) is known as one of the more devastating neurodegenerative diseases diagnosed in older people. Cholinesterase inhibitors (ChEI) can be used as an effective palliative treatment for AD. An extensive range of new biologically active 4-(diethylamino) salicylaldehyde-based thiosemicarbazone derivatives **5(a–u)** was synthesized and evaluated as inhibitors of cholinesterase (ChE) and monoamine oxidase (MAO) enzymes. 2,3-Dichloro-substituted compound **5u** was the most potent inhibitor of AChE and MAO-A with IC_{50} values of 12.89 and 96.25 nM, respectively. In contrast, the 2,3-dichlorophenyl-substituted compound **5a** was the most powerful inhibitor of BChE, with an IC_{50} value of 124.72 nM. Structure–activity analysis revealed that the electron-withdrawing substituents on the phenyl ring play a crucial role in the inhibition potential of synthesized compounds. Compound **5a** showed the strongest binding with 4BDS (−11.3 kcal/mol) via hydrogen bonds and π-interactions. Compound **5u** exhibited high affinity with 1B41 (−8.2 kcal/mol), 2Z5X (−8.6 kcal/mol), and 2V5Z (−7.8 kcal/mol), forming key hydrogen bonds, salt bridges, and π-interactions, highlighting its multi-target potential. In silico ADME, pharmacokinetics, and drug-likeness studies were conducted and compared with the standard drugs galantamine and clorgyline.

1 | Introduction

Alzheimer's disease (AD) is a severe neurological condition linked to behavioral, psychological, and language disorders as well as memory loss [1, 2]. Numerous research studies have demonstrated that pathological conditions involving overexpression of monoamine oxidase (MAOs) and cholinesterase (ChEs) can lead to various pathological changes, such as reduced cerebral blood flow, Aβ

Urva Farooq and Muhammad Islam contributed equally.

aggregation [3], neurofibrillary tangles (NFT) [4], neuronal death, neuro-inflammation [5], and free radical metabolic disorder [6–8]. These enzymes (ChEs and MAOs) inactivate neurotransmitters such as acetylcholine (ACh), dopamine, adrenaline, noradrenaline, and histamine in the brain [9]. The dopaminergic and cholinergic neurotransmitters in the synaptic cleft can be increased by inhibition of MAOs and ChEs [10].

ChE, specifically acetylcholinesterase (AChE, EC 3.1.1.7) and butyrylcholinesterase (BChE, EC 3.1.1.8), catalyze the hydrolysis of cholinergic neurotransmitters such as ACh and BChE. Since AChE degrades ACh more frequently than BChE, inhibiting AChE to raise ACh levels is still an effective treatment for AD [11]. This enzyme's crystal structure shows a 20 Å long gorge connecting the catalytic active site (CAS) and peripheral anionic site (PAS). Moreover, it has been noted that AChE contributes to the development of AD by inducing pro-aggregation activity in the Aβ protein, producing reactive oxygen species (ROS), dysregulating calcium, and causing neuronal dysfunction. Thus, bioactive compounds that can specifically bind with the residues of either catalytic site (PAS or CAS) may be very helpful in inhibiting AChE while removing Aβ aggregation [12]. BChE, on the other hand, hydrolyzes both choline and aliphatic esters and is known as nonspecific pseudocholinesterase, serum ChE, or BChE [13]. It is an α-glycoprotein and is present in the liver, most tissues, and the central and peripheral nervous systems [14].

The half-life of BChE is about 12 days and generally falls within the range of 5900 and 13,200 IU/L [15]. It has been documented that individuals with obesity, diabetes, uremia, hyperthyroidism, and hyperlipidemia exhibit elevated activity of this enzyme [16]. Since the liver produces BChE, hepatocellular impairment causes a drop in enzyme activity. It is a biochemical indicator of organ damage; its plasma levels decrease in cirrhosis, acute and chronic liver injury, and liver metastases. In addition, low plasma BChE levels have been linked to stress (acute and chronic), inflammation, protein-energy deficiency, and other clinical disorders [17].

Neuropsychiatric diseases such as Parkinson's disease (PD), AD, and depression, which have all become serious health problems in the world, still do not have an effective treatment, mainly due to an insufficient understanding of the multi-component pathogenesis [18, 19]. Various approaches have been used for the treatment of neurological disorders, including natural products and prodrug strategy [20, 21]. Among the well-studied etiologies, the irregular expression of mitochondrial enzyme MAO (EC 1.4.3.4) has been recognized as a main cause. The neurotransmitter-catabolizing MAOs are classified into the A and B isoforms [22]. The MAO enzyme catalyzes the oxidative deamination of both endogenous and exogenous monoamines. It has important roles in metabolizing released neurotransmitters and is mainly involved in the breakdown of norepinephrine, melatonin, serotonin, and epinephrine. MAO-A is expressed almost everywhere in the human body. MAO-B, which degrades and metabolizes dopamine and β-phenethylamine, is highly expressed in the central nervous system (CNS) [23]. The potential application of MAO-B inhibitors in the treatment of neurodegenerative diseases has drawn more attention, not just for their roles in the metabolism of monoamine neurotransmitters and in mitigating oxidative stress but also for their additional neuroprotective and neurorescue properties, which are advantageous for AD treatment. Novel MAO-B inhibitors with anti-AD activities (such as inhibiting Aβ aggregation, chelating properties, antioxidative ability, and AChE inhibition) have recently been developed by researchers as multifunctional ligands. This bodes well for the successful treatment of several neurodegenerative diseases, including AD and PD [24, 25].

Heterocyclic derivatives are valuable precursors for the development of potential enzyme inhibitors for AD [26–29]. Thiosemicarbazones are a class of chemicals with an imine moiety because of their multifunctional structure, which includes an aryl substituent that functions as a hydrophobic domain and coordination sites that contain C=S and NH groups as electron donors [30–33]. They display an extensive array of pharmacological characteristics [34], which includes antifungal [35], anticancer [36], antiviral, antimalarial [37], anti-AChE, anti-BChE, and anti-MAO [38] properties. Additionally, they are used as dyes [39], stabilizers [40], catalysts [41], and in the polymer industry [42, 43].

Due to the inability of conventional monotherapies to provide long-term relief, alternative multitargeting techniques must be investigated to address the complexity of AD. Various thiosemicarbazones have been reported to have exceptional properties, such as AChE, BChE, and MAO-A inhibitors and MAO-B inhibitors (Figure 1) [10, 44–47].

The second pharmacophore was salicylic derivatives, which show promising properties as scaffolds for anti-AD design. This moiety is known to have a wide range of beneficial bioactive properties, including the capacity to function as metal chelators, antioxidants, and β-amyloid aggregation inhibitors [48, 49]. In the past, we synthesized a novel series of 4-(diethylamino)-salicylaldehyde thiosemicarbazones and probed them as ChE inhibitors [44].

In the present work, 4-(diethylamino)-salicylaldehyde-based thiosemicarbazones **5(a–u)** are prepared and evaluated as multipotent analogs capable of concurrently inhibiting the enzymes ChE and monoamine oxidase (MAO), suggesting that they may be potentially used to treat AD.

2 | Results and Discussion

2.1 | Chemistry

A series of 21 derivatives, **5a–u,** have been synthesized to explore the biological potential of 4-(diethylamino) salicylaldehyde-based thiosemicarbazones as ChE and MAO-A and B inhibitors. The targeted thiosemicarbazones **5a–u** were synthesized in two steps (Scheme 1).

In the first step, compound **3** was synthesized by reacting 4-(diethylamino)salicylaldehyde **1** with naphthalene sulfonyl chloride **2** in the presence of triethylamine and DMF in an ice bath to obtain *O*-substituted naphthalene sulfonyl-based 4-(diethylamino)salicylaldehyde **3**, with an excellent yield of 90%.

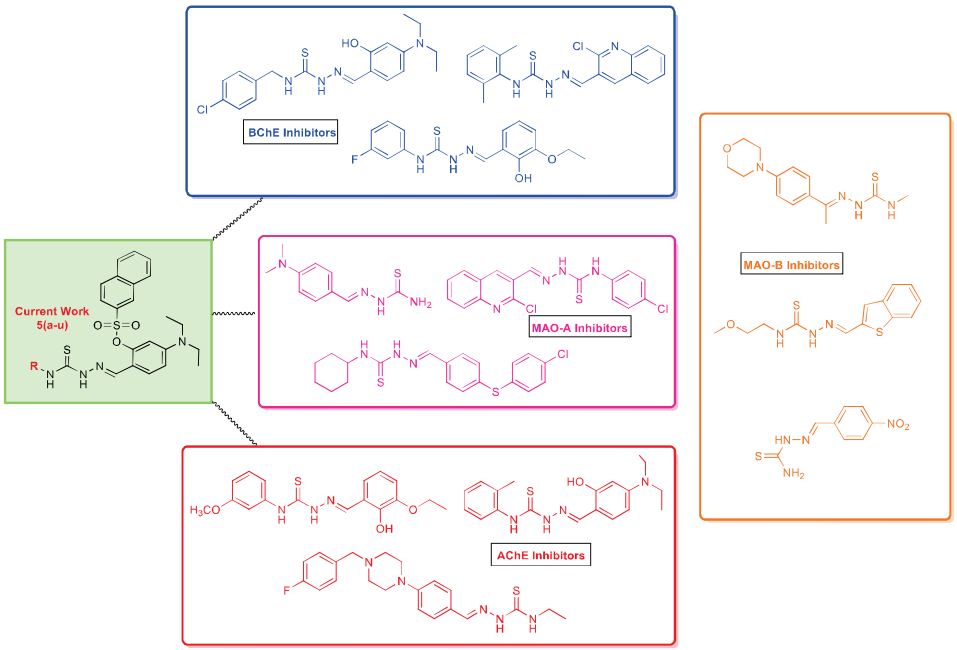

FIGURE 1 | Reported structures of thiosemicarbazone-based AChE, BChE, and MAO inhibitors.

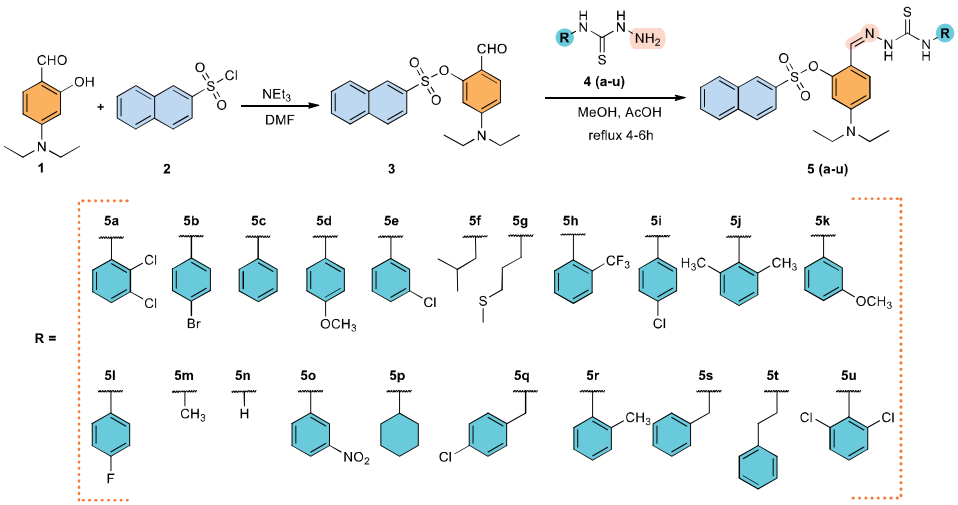

SCHEME 1 | Synthetic route for the preparation of 4-(diethylamino)salicylaldehyde-based thiosemicarbazones.

In the second step, to synthesize the 4-(diethylamino) salicylaldehyde-based thiosemicarbazones **5a–u**, the equimolar ratio of compound **3** and respective thiosemicarbazides **4a–u** was refluxed in methanol, and acetic acid was used as a catalyst. The thiosemicarbazones **5a–u** were obtained as solid residues in 85%–95% yield.

The structures of the synthesized thiosemicarbazones were confirmed using the spectral data. In ^{1}H-NMR spectra, NH–C═S protons showed a singlet between δ 9.72 and 9.93 ppm, while a broad singlet peak appeared from 11.29 to 11.97 ppm for NH–N═C protons. A singlet is observed in the 8.32–8.15 ppm range, which can be attributed to the azomethine hydrogen, finalizing the condensation with aldehydes. Furthermore, peaks that appeared in ^{13}C-NMR spectra also confirmed the formation of the thiosemicarbazones.

2.2 | Biological Activity

2.2.1 | Structure–Activity Relationship

The current work has synthesized and evaluated a series of thiosemicarbazone derivatives **5a–u** for their activity against AChE, BChE, MAO-A, and MAO-B enzymes. These activity results are reported in Table 1 as IC_{50} values in the nanomolar range. SAR was explored by varying the **R** group attached to the N^4 position of the thiosemicarbazide moiety. The results revealed that the **R** group is critical for the strong inhibitory effects. The **R** group is varied with aromatic, nonaromatic, aliphatic, and heterocyclic substituents. The synthesized compounds displayed excellent to moderate inhibition against all the isoforms of enzymes, that is, AChE, BChE, MAO-A, and MAO-B enzymes. It is a very encouraging behavior for the synthesized compounds, given the fact that these compounds can multitarget various enzymes that influence AD, such as AChE, BChE, MAO-A, and MAO-B [50]. Moreover, it is also evident from the Ki values that the compounds displayed competitive inhibition against AChE and BChE.

2.2.2 | AChE Inhibition

The synthesized compounds displayed excellent to moderate inhibition against AChE, with IC_{50} values ranging between 12.89 and 116.01 nM. Twenty compounds displayed superior inhibition potential compared with the standard galantamine, possessing an IC_{50} value of 101.24 nM.

Compounds **5c** and **5s** with phenyl and benzyl rings displayed IC_{50} values of 38.42 ($K_i = 25.43 \pm 5.32$ nM) and 71.43 nM ($K_i = 63.86 \pm 7.54$ nM), respectively. The derivatives are varied by changing the substitutions on the phenyl and benzyl rings. From the results, it can be seen that compounds with substituted phenyl and benzyl rings displayed better inhibition potential as compared with the unsubstituted rings, which revealed the importance of the substitutions.

The substitution pattern and activities of the phenyl ring can be explored as follows. The trend of IC_{50} values of the monosubstituted derivatives is given as **5o** (3-nitrophenyl, $IC_{50} = 18.93$ nM) > **5i** (4-chlorophenyl, $IC_{50} = 24.81$ nM) > **5r** (*o*-tolyl, $IC_{50} = 27.39$ nM) > **5l** (4-fluorophenyl, $IC_{50} = 29.54$ nM) > **5e** (3-chlorophenyl, $IC_{50} = 31.04$ nM) > **5b** (4-bromophenyl, $IC_{50} = 33.81$ nM) > **5d** (4-methoxyphenyl, $IC_{50} = 39.37$ nM) > **5k** (3-methoxyphenyl, $IC_{50} = 116.01$ nM). It can be seen from the trend that the inhibition potential of the compounds with electron-withdrawing substituents, such as nitro group and halogens, outshone the compounds with electron-donating groups such as methoxy and ethyl groups. Other than that, compounds with *para*-substitution displayed better inhibition potency than *meta*-substitution.

The trend of IC_{50} values of the disubstituted derivatives is given as **5u** (2,6-dichlorophenyl, $IC_{50} = 12.89$ nM) > **5a** (2,3-dichlorophenyl, $IC_{50} = 14.90$ nM) > **5h** (2-trifluoromethylphenyl, $IC_{50} = 16.76$ nM) > **5j** (2,6-dimethylphenyl, $IC_{50} = 40.62$ nM). From the IC_{50} values, it can be seen that disubstitution plays a key role in the inhibition potential of the derivatives. The three most potent members of the series are the disubstituted derivatives. Compound **5u** ($K_i = 9.82 \pm 1.76$ nM) with 2,6-dichloro substitution on the phenyl ring is the most potent member of the series.

The comparison of the strengths of aliphatic substituents as R group is as follows: **5m** (methyl, $IC_{50} = 38.49$ nM) > **5n** (H, $IC_{50} = 47.70$ nM) > **5f** (isobutyl, $IC_{50} = 49.53$ nM) > **5p** (cyclohexyl, $IC_{50} = 54.46$ nM) > **5t** (phenethyl, $IC_{50} = 56.21$ nM) > **5g** (3-methylthiopropyl, $IC_{50} = 80.43$ nM). Compound **5m** with a methyl group displayed the highest activity in this group, but with the increase in the size of the substituent, activity starts decreasing gradually.

2.2.3 | BChE Inhibition

The inhibition pattern of the synthesized compounds against BChE is almost similar to the activity on AChE, with IC_{50} values ranging from 124.72 to 308.43 nM. Sixteen of the synthesized compounds displayed higher inhibition potential than the standard galantamine (IC_{50} value = 261.62 nM).

Compound **5c** and **5s** with phenyl and benzyl rings as R group displayed IC_{50} values of 217.78 ($K_i = 182.65 \pm 15.04$ nM) and 220.34 nM ($K_i = 195.21 \pm 13.45$ nM), respectively. Unlike against AChE, **5v** and **5s** displayed almost similar potential. The trend for monosubstitution on the phenyl ring is given as **5o** (3-nitrophenyl, $IC_{50} = 192.09$ nM) > **5i** (4-chlorophenyl, $IC_{50} = 199.54$ nM) > **5l** (4-fluorophenyl, $IC_{50} = 200.34$ nM) > **5b** (4-bromophenyl, $IC_{50} = 202.05$ nM) > **5e** (3-chlorophenyl, $IC_{50} = 208.43$ nM) > **5d** (4-methoxyphenyl, $IC_{50} = 252.54$ nM) > **5k** (3-methoxyphenyl, $IC_{50} = 252.64$ nM) > **5r** (o-tolyl, $IC_{50} = 293.55$ nM). With slight variations in the IC_{50} values of the compounds, the inhibition potential is exactly similar to that observed for AChE. Compounds with electron-withdrawing groups displayed superior potency as compared with compounds with electron-donating groups.

The ranking order of disubstitution on the phenyl ring is as follows: **5a** (2,3-dichlorophenyl, $IC_{50} = 124.72$ nM) > **5h** (2-trifluoromethyl phenyl, $IC_{50} = 145.03$ nM) > **5u** (2,6-dichloro phenyl, $IC_{50} = 148.18$ nM) > **5j** (2, 6-dimethylphenyl, $IC_{50} = 265.38$ nM). Compound **5a** with the 2,3-dichloro substitution is the most potent compound of the series against BChE ($K_i = 101.32 \pm 22.43$ nM). It is the second and third most powerful

TABLE 1 | Anti-cholinesterase (AChE and BChE) and anti-MAO-A and anti-MAO-B potentials of synthesized compounds **5a–u** and their structures.

	IC_{50} (nM)								K_i (nM)	
Comp.	**AChE**	r^2	**BChE**	r^2	**MAO-A**	r^2	**MAO-B**	r^2	**AChE**	**BChE**
5a	14.90 ± 1.54	0.913	124.72 ± 9.13	0.982	104.17 ± 4.58	0.960	391.03 ± 9.04	0.989	11.37 ± 3.06	101.32 ± 22.43
5b	33.81 ± 3.41	0.906	202.05 ± 5.66	0.937	132.05 ± 7.01	0.931	409.76 ± 7.47	0.928	26.55 ± 3.34	190.57 ± 15.65
5c	38.42 ± 5.03	0.904	217.78 ± 8.41	0.929	188.54 ± 6.46	0.933	296.47 ± 6.01	0.990	25.43 ± 5.32	182.65 ± 15.04
5d	39.37 ± 2.87	0.968	252.54 ± 10.46	0.923	170.66 ± 10.42	0.935	406.18 ± 8.24	0.942	32.23 ± 5.93	234.84 ± 15.04
5e	31.04 ± 4.16	0.921	208.43 ± 7.53	0.951	117.13 ± 7.33	0.923	> 1000	0.935	25.36 ± 3.32	195.34 ± 11.53
5f	49.53 ± 5.21	0.947	253.53 ± 6.31	0.964	133.50 ± 8.04	0.901	388.10 ± 5.37	0.957	38.82 ± 6.18	239.89 ± 18.65
5g	80.43 ± 7.62	0.978	287.26 ± 8.57	0.970	187.66 ± 5.36	0.964	398.57 ± 7.93	0.902	72.43 ± 10.08	258.50 ± 16.14
5h	16.76 ± 1.35	0.949	145.03 ± 8.96	0.913	100.38 ± 4.57	0.930	249.01 ± 9.10	0.944	14.59 ± 3.36	136.01 ± 9.17
5i	24.81 ± 2.41	0.958	199.54 ± 9.41	0.902	121.24 ± 3.15	0.924	285.25 ± 4.02	0.912	21.02 ± 4.12	190.27 ± 13.60
5j	40.62 ± 2.77	0.979	265.38 ± 7.90	0.970	136.93 ± 6.21	0.981	395.37 ± 8.35	0.966	36.52 ± 5.23	228.42 ± 12.35
5k	116.01 ± 8.42	0.906	252.64 ± 9.15	0.977	144.71 ± 8.03	0.976	> 1000	0.952	95.75 ± 9.54	205.34 ± 10.16
5l	29.54 ± 2.68	0.918	200.34 ± 6.88	0.985	112.33 ± 2.78	0.907	276.97 ± 6.33	0.938	27.41 ± 3.45	182.09 ± 9.05
5m	38.49 ± 3.21	0.909	214.30 ± 7.13	0.963	132.28 ± 4.96	0.954	368.58 ± 11.25	0.926	30.22 ± 5.02	193.05 ± 11.62
5n	47.70 ± 5.67	0.970	308.43 ± 9.98	0.932	137.19 ± 6.55	0.976	395.72 ± 8.09	0.930	42.44 ± 4.10	270.16 ± 13.54
5o	18.93 ± 1.33	0.998	192.09 ± 6.36	0.981	122.65 ± 7.01	0.932	267.07 ± 6.35	0.905	14.25 ± 2.32	160.33 ± 9.01
5p	54.46 ± 4.57	0.915	254.24 ± 8.08	0.965	145.32 ± 3.57	0.985	326.68 ± 9.13	0.955	47.09 ± 6.35	226.45 ± 12.57
5q	19.34 ± 1.28	0.984	202.31 ± 14.86	0.963	119.06 ± 9.24	0.926	308.44 ± 6.07	0.927	17.63 ± 3.34	182.76 ± 11.48
5r	27.39 ± 2.42	0.912	293.55 ± 7.14	0.912	142.55 ± 6.78	0.944	495.13 ± 8.36	0.995	21.17 ± 1.05	249.09 ± 15.30
5s	71.43 ± 8.92	0.954	220.34 ± 8.53	0.954	131.09 ± 5.34	0.976	369.46 ± 12.04	0.975	63.86 ± 7.54	195.21 ± 13.45
5t	56.21 ± 4.58	0.902	271.12 ± 6.90	0.981	138.74 ± 6.02	0.932	289.02 ± 9.11	0.945	48.30 ± 7.32	226.65 ± 16.08
5u	12.89 ± 1.02	0.987	148.18 ± 7.35	0.973	96.25 ± 5.77	0.906	208.95 ± 5.84	0.978	9.82 ± 1.76	112.06 ± 7.61
*	101.24 ± 5.72	0.984	261.62 ± 9.03	0.945	—	—			84.05 ± 8.70	242.17 ± 13.88
**	—	—	—	—	150.62 ± 4.03	0.979	468.63 ± 16.05	0.987	—	—

Note: *, Galantamine; **, Clorgyline.

against the other two enzymes, AChE ($K_i = 11.37 \pm 3.06$ nM) and MAO-A, respectively.

The ranking order of the aliphatic substituents is as follows: **5m** (methyl, $IC_{50} = 214.30$ nM) > **5f** (isobutyl, $IC_{50} = 253.53$ nM) > **5p** (cyclohexyl, $IC_{50} = 254.24$ nM) > **5t** (phenethyl, $IC_{50} = 271.12$ nM) > **5g** (3-methylthiopropyl, $IC_{50} = 287.26$ nM) > **5n** (H, $IC_{50} = 308.43$ nM). The aliphatic substitution also followed the same pattern as in AChE. In fact, with the increase in size of the substituent, the activity against BChE is diminished.

2.2.4 | MAO-A Inhibition

Exploring the structure–activity relationship, the synthesized compounds displayed excellent to moderate inhibition potentials with IC_{50} values ranging between 96.25 and 188.54 nM. Eighteen compounds displayed higher inhibition potentials than the standard clorgyline, which has an IC_{50} value of 150.62 nM. It is interesting to note that the inhibition pattern of the synthesized compounds against all three enzymes, that is, AChE, BChE, and MAO-A, is almost similar with slight variations.

Compound **5c** with unsubstituted phenyl ring displayed lower inhibition potential with an IC_{50} value of 188.54 nM than the standard clorgyline and is the least potent member of the series, while the mono and disubstituted derivatives displayed much higher potency. The ranking order of monosubstitution on the phenyl ring is given as **5l** (4-fluorophenyl, $IC_{50} = 112.33$ nM) > **5i** (4-chlorophenyl, $IC_{50} = 121.24$ nM) > **5o** (3-nitrophenyl, $IC_{50} = 122.65$ nM) > **5b** (4-bromophenyl, $IC_{50} = 132.05$ nM) > **5r** (o-tolyl, $IC_{50} = 142.55$ nM) > **5k** (3-methoxyphenyl, $IC_{50} = 144.71$ nM) > **5d** (4-methoxyphenyl, $IC_{50} = 170.66$ nM). From the trend of IC_{50} values, the following observations can be made that electron-withdrawing substituents are more favorable toward the inhibition against MAO-A. With the increase in the size of the halogen substituents, the inhibition potency of the synthesized compounds starts declining (Figure 2).

The inhibition pattern for the disubstituted derivatives against MAO-A is exactly similar to that of AChE. For the aliphatic substituents, the ranking order is as follows: **5m** (methyl, $IC_{50} = 132.28$ nM) > **5f** (isobutyl, $IC_{50} = 133.50$ nM) > **5n** (H, $IC_{50} = 137.19$ nM) > **5t** (phenethyl, $IC_{50} = 138.74$ nM) > **5p** (cyclohexyl, $IC_{50} = 145.32$ nM) > **5g** (3-methylthiopropyl, $IC_{50} = 187.66$ nM). With the increase in the size of the substituent, the potency starts declining. All synthesized compounds contribute similarly toward inhibiting AChE, BChE, and MAO-A and MAO B enzymes.

2.3 | Molecular Docking Study

Molecular docking is vital for identifying potential binding sites and interactions between target molecules and proteins. This computational technique seeks an optimal conformation that minimizes the system's free energy. Predicting how a molecule interacts with a target protein aids in the design and development of new therapeutic agents by highlighting the most promising structures for further investigation [51, 52]. The docking study was accomplished using AutoDockTools 1.5.6 software [53]. Several approaches are being employed in the development of therapies for AD, with a focus on targeting key enzymes such as AChE, BChE, and MAO-A and -B. Both AChE and BChE play critical roles in the regulation of neurotransmitter levels, though they differ in their distribution across brain regions. AChE is the primary target for ChE inhibitors, which aim to slow the breakdown of ACh, a neurotransmitter involved in memory and cognition. BChE, though less abundant than AChE, is also important as it functions as a co-regulator of ACh, particularly in the later stages of AD when AChE activity decreases. Targeting both enzymes has become a promising approach in modulating cholinergic function and alleviating the cognitive decline associated with AD [10, 54, 55]. Additionally, MAO-A enzymes are being investigated due to their role in the degradation of monoamine neurotransmitters, which also influence cognitive and behavioral symptoms in AD patients. Combining these therapeutic targets offers a multifaceted approach to addressing the complex biochemical processes underlying AD [56, 57]. With this consideration, the docking study was achieved with three target proteins with PDB Id: 1B41 (*h*-AChE), 4BDS (*h*-AChE), 2V5Z (*h*-MAO-B), and 2Z5X (*h*-MAO-A) (Table 2). Target 1B41 is a crystal structure of human AChE complexed with fasciculin-II, a glycosylated protein (resolution: 2.76 Å). The receptor 4BDS is a crystal structure (resolution: 2.1 Å) of the human BChE in complex with tacrine [10, 54, 55]. The receptor 2V5Z is a crystal structure (resolution: 1.60 Å) of the human monoamine oxidase B with inhibitor safinamide [31]. And 2Z5X is a crystal structure (resolution: 2.20 Å) of human monoamine oxidase A with harmine [56–58].

The molecular docking analysis revealed that compound **5u** demonstrated the highest binding affinity (−8.2 kcal/mol) against 1B41 (Figure 3). The thione moiety established hydrogen bonding

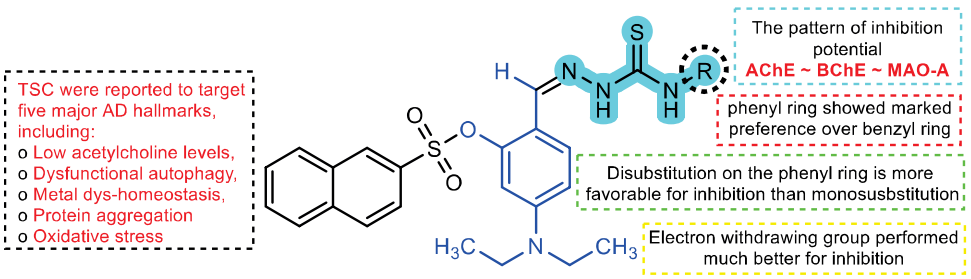

FIGURE 2 | Representation of the diversity point and effect of chemical manipulation on biological activity.

TABLE 2 | The binding residues and interactions of most and least bioactive scaffolds in comparison with the standard.

Target PDB Id	Comp. Id/Std.	Docking score (kcal/mol)	Binding residues and interactions [residue code (type of interaction)]
1B41 (*h*-AChE)	5u	−8.2	ASN A:233 (hydrogen bond); ASN A:533 (hydrogen bond); GLU A:313 (hydrogen bond, salt bridge); THR A:311 (pi-sigma); PRO A:235 (pi-sigma, carbon-hydrogen bond); PRO A:312 (carbon-hydrogen bond); THR A:238 (unfavorable acceptor-acceptor); VAL A:303 (pi-alkyl)
	5k	−7.1	ASN A:233 (hydrogen bond); GLY A:234 (hydrogen bond); HIS A:405 (pi-cation); GLU A:313 (pi-anion); PRO A:235 (pi-alkyl); VAL A:239 (alkyl)
	Galantamine	−6.9	GLU A:313 (hydrogen bond); HIS A:405 (carbon-hydrogen bond, pi-pi T-shaped); PRO A:410, CYS A:409, TRP A:532 (pi-alkyl); PRO A:235 (pi-alkyl, alkyl)
4BDS (*h*-BChE)	5a	−11.3	HIS A:438 (hydrogen bond, pi-pi stacked, unfavorable positive-positive); PHE A:329 (pi-pi T-shaped, Amide-pi stacked, pi-cation); TRP A:231 (pi-pi stacked); GLY A:116 (pi-pi stacked); TRP A:82 (pi-pi stacked); LEU A:286 (pi-alkyl); PRO A:285, TYR A:332 (alkyl)
	5n	−9.3	TYR A:332 (hydrogen bond); ASP A:70 (attractive charge); TRP A:82 (pi-pi stacked); HIS A:438, PHE A:329 (pi-alkyl)
	Galantamine	−9.3	HIS A:438 (hydrogen bond); SER A:198, (hydrogen bond, unfavorable donor-donor); GLY A:115, GLY A:117 (hydrogen bond); GLU A:197 (unfavorable acceptor-acceptor); TRP A:82, TRP A:231 (pi-alkyl)
2Z5X (*h*MAO-A)	5u	−8.6	TYR A:121 (hydrogen bond, pi-alkyl); GLU A:492 (hydrogen bond, salt bridge, pi-anion); PHE A:112 (pi-pi T-shaped); TYR A:124 (pi-sulfur); TRP A:116 (pi-sigma, pi-alkyl); PRO A:114 (pi-alkyl, alkyl)
	5c	−8.2	ARG A:109 (hydrogen bond); GLU A:492 (pi-anion); TRP A:116, TYR A:121 (pi-sigma, pi-alkyl); TRP A:128, PHE A:112 (pi-pi T-shaped); TYR A:124 (pi-pi T-shaped, pi-sulfur); TYR A:121 (pi-sulfur); ALA A:111 (pi-alkyl)
	Harmine	−8.6	GLY A:67 (carbon-hydrogen bond); TYR A:407 (pi-pi stacked); TYR A:444 (pi-pi stacked); LEU A:337 (pi-alkyl); PHE A:352 (pi-alkyl); MET A:445, TYR A:69 (alkyl); FAD A:600 (unfavorable bump)
2V5Z (*h*MAO-B)	**5u**	−7.8	GLU A:391 (2 hydrogen bonds, attractive charge); GLN A:392 (hydrogen bond); LEU A:250 (pi-sigma, pi-alkyl); TYR A:393 (pi-sulfur, unfavorable donor-donor); ARG A:36 (pi-alkyl, unfavorable donor-donor); PRO A:234 (pi-alkyl); PRO A:277 (pi-alkyl)
	5k	−6.7	GLU A:391 (hydrogen bond, attractive charge); ASP A:37 (hydrogen bond); TYR A:393 (pi-pi T-shaped); TYR A:44 (pi-pi T-shaped); ARG A:38 (carbon-hydrogen bond); ARG A:36, PRO A:277 (pi-alkyl); PRO A:234 (alkyl)
	Safinamide	−9.8	TYR A:398 (pi-pi stacked); PRO A:102 (hydrogen bond); GLN A:206 (hydrogen bond); LEU A:171 (pi-sigma); TYR A:326 (pi-pi T-shaped); CYS A:172 (pi-sulfur); LEU A:164, LEU A:167 (pi-alkyl); TRP A:119, ILE A:199 (alkyl)

(3.56 Å) with ASN A:233, while the carbothioamide NH engaged ASN A:533 (2.76 Å).

Critically, the sulfonate oxygen formed a strong hydrogen bond (2.43 Å) and a salt bridge (2.59 Å) with GLU A:313, emphasizing electrostatic stabilization. π–σ and π–alkyl interactions were observed between the naphthalene ring and THR A:311 (3.65 Å) and VAL A:303 (3.72, 5.22 Å). The diethylamino-phenyl group displayed π–σ (3.94 Å) and C–H bond (3.36 Å) contacts with PRO A:235, while an unfavorable acceptor–acceptor interaction (2.71 Å) was noted with THR A:238.

The least active analog, **5k** (−7.1 kcal/mol), formed two hydrogen bonds with ASN A:233 (2.30, 2.63 Å) and one with GLY A:234 (2.40 Å). It showed a π–cation interaction with HIS A:405 (4.86 Å), a π–anion interaction with GLU A:313 (3.25 Å), and π–alkyl contacts with PRO A:235 (4.75, 5.04 Å). Reference

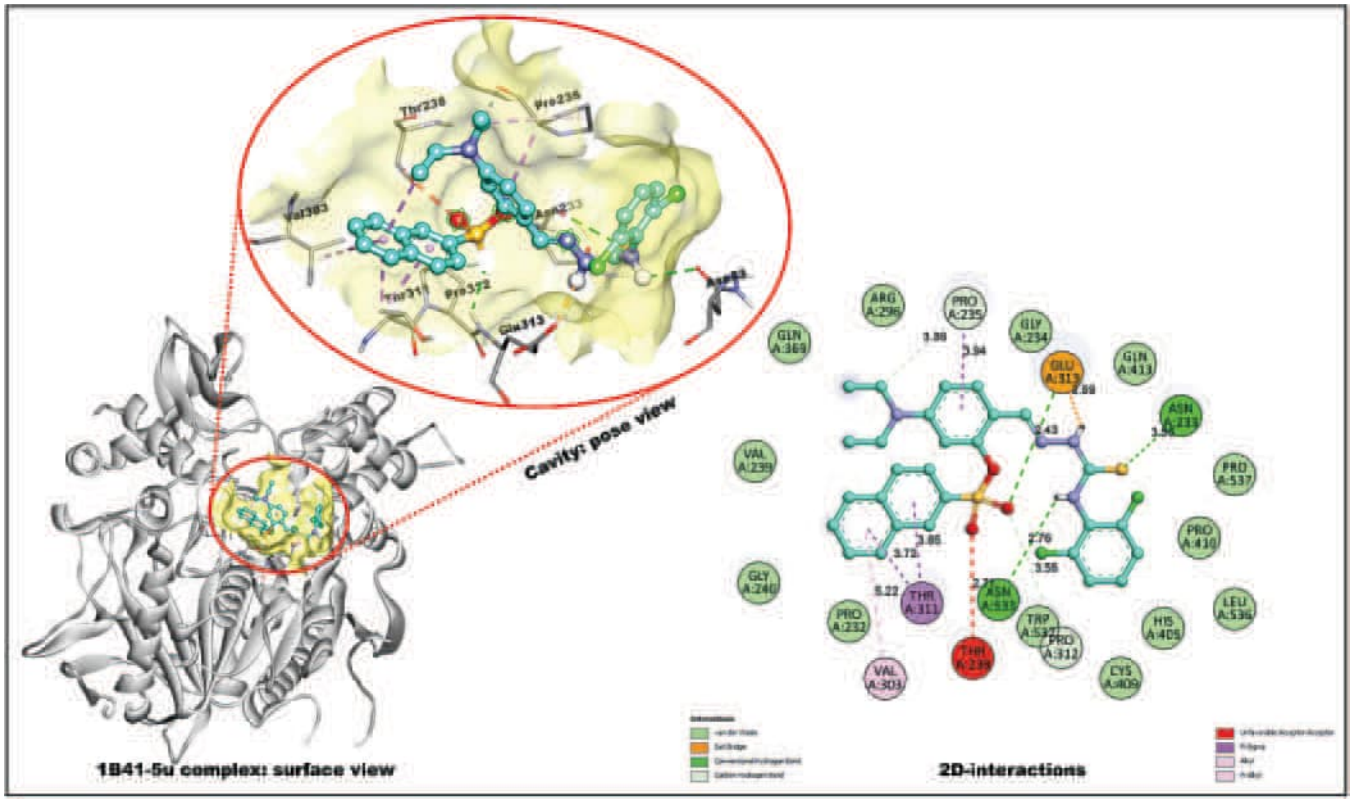

FIGURE 3 | Binding interactions of compound **5u** within the 1B41 site.

drug galantamine (−6.9 kcal/mol) interacted via H-bonding with GLU A:313, π–π T-shaped and C–H bonding with HIS A:405, and π–alkyl contacts with PRO A:410, CYS A:409, and TRP A:532.

Against 4BDS, compound **5a** showed the strongest binding (−11.3 kcal/mol). Its NH moiety engaged HIS A:438 via hydrogen bonding (2.28 Å), while the tricyclic naphthalene core established π–π stacking with PHE A:329, GLY A:116, and both TRP A:82 and TRP A:231 (4.32–6.25 Å) (Figure 4). Additionally, alkyl and π–alkyl interactions occurred with LEU A:286, PRO A:285, and TYR A:332. The least active **5n** (−9.3 kcal/mol) displayed a H-bond with TYR A:332 (2.80 Å), π–π stacking with TRP A:82 (4.28, 4.73 Å), and a π–alkyl contact with HIS A:438.

In 2Z5X, **5u** (−8.6 kcal/mol) formed hydrogen and electrostatic interactions with GLU A:492 (2.31, 2.55 Å), π–anion interaction (3.93 Å), and π–π stacking with PHE A:112. TYR A:121 participated in both H-bonding (2.25 Å) and π–alkyl bonding (4.93 Å), while TYR A:124 established a π–sulfur bond (5.24 Å). Comparatively, harmine bound less efficiently, forming π–π and π-alkyl interactions with TYR A:407 and LEU A:337. In 2V5Z, **5u** formed strong interactions with GLU A:391 (H-bonds 2.32, 3.54 Å, salt bridge 4.31 Å), GLN A:392 (H-bond 2.65 Å), and multiple π–alkyl contacts (Figure 5). The reference safinamide showed the highest binding (−9.8 kcal/mol) through extensive π–π (TYR A:398, TYR A:326), π–sulfur (CYS A:172), and hydrogen bonding (GLN A:206, PRO A:102). Detailed interactions for selected compounds have been provided in the Supporting Information.

2.4 | Docking Validation

Redocking is carried out to validate molecular docking studies, ensuring the accuracy of predicted ligand–receptor binding poses. The same protocol used in the initial docking was employed for redocking. Upon completion, the redocked complex was superimposed using Discovery Studio software. Remarkably, the redocked complex was aligned with the native complex, without any modifications (Figure 6). Some crucial amino acid residues were identified in the active pocket of each receptor, and these residues were preserved in the redocked complex of the synthesized ligand.

2.5 | Evaluation of GA-MLR QSAR Model

To ensure proper feature selection, the data set was split into training (≈80%) and prediction (≈20%) sets to avoid data losses. We used the "GA-MLR" approach using "QSARINS-2.2.4" for subjective feature selection (SFS), employing Q^2_{LOO} as a fitness parameter [7]. The final model was evaluated for internal and external validity, selecting the top QSAR model based on higher Q^2 and R^2 metrics. Thus, we developed four models for each activity, Models 1-4 as given below:

Pki = 7.897 + −0.214 * **fnotringSC7B** + −0.271 * **fsp2Ssp3C7B** + 0.249 * **notringC_Cl_8B"**-----model 1 (For AChE)

(**fnotringSC7B:** frequency of occurrence of carbon atom exactly at seven bonds from the non-ring sulfur atoms; **fsp2Ssp3C7B:** frequency of occurrence of sp3 hybridized carbon atom exactly at seven bonds from the sp2 hybridized sulfur atoms;

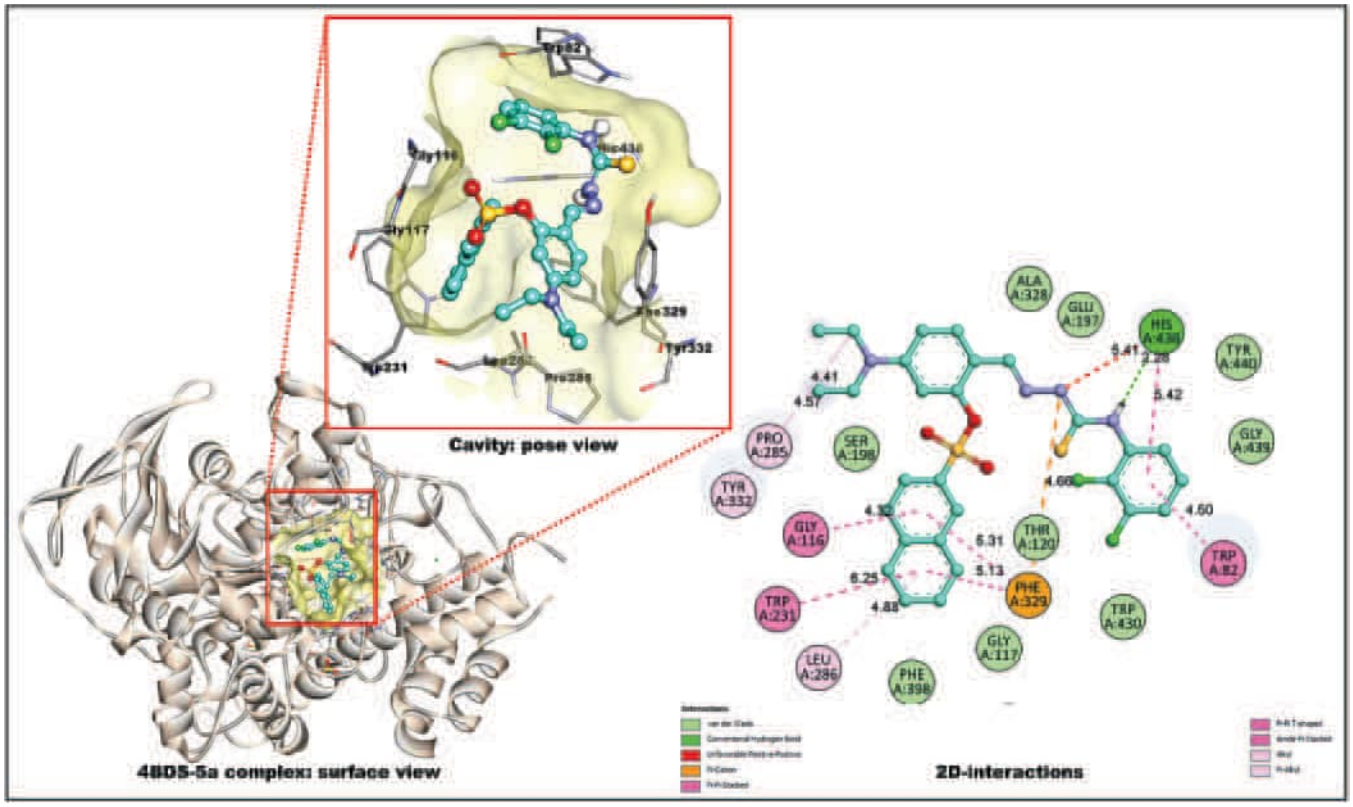

FIGURE 4 | Binding interactions of compound **5a** within the 4BDS site.

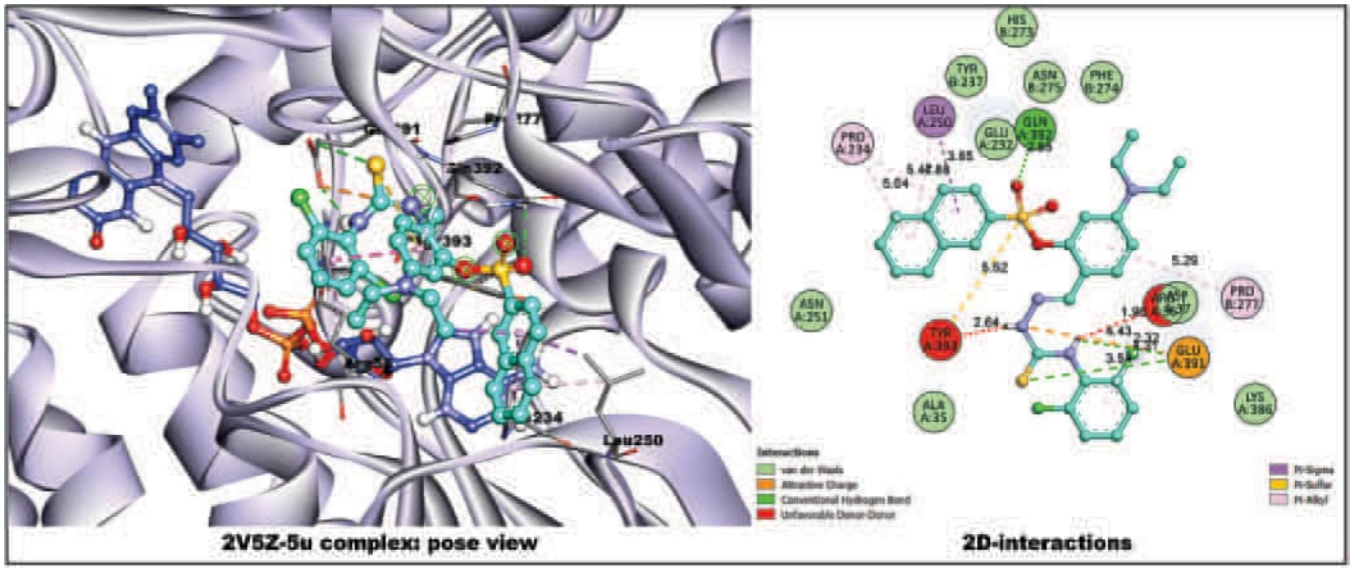

FIGURE 5 | Complex of compound **5u** and target protein 2V5Z co-crystalized with FAD molecule (blue-colored) and their 2D-binding interactions.

notringC_Cl_8B: occurrence of chlorine atom within eight bonds from the non-ring carbon atoms).

"**pKi** = 6.565 + 0.133 * **Cl_S_6B** + 0.036 * **faccaroC6B** "----------model 2 (For BChE)

(**Cl_S_6B**- occurrence of sulfur atom within six bonds from the chlorine atom; **faccaroC6B:** frequency of occurrence of aromatic carbon atom exactly at six bonds from the acceptor atoms).

"$_{p}$**IC$_{50}$** = 6.898 + −0.034 * **com_sp3C_6A** + 0.052 * **Cl_notringC_6B** + −0.148 * **fdonnotringC6B**"----model 3 (For MAO-A)

(**com_sp3C_6A**: occurrence of sp3 hybridized carbon atom within 6 angstrom units from the center of mass of molecule; **Cl_notringC_6B**: occurrence of non-ring carbon atoms within six bonds from the chlorine atom; **fdonnotringC6B**: frequency of occurrence of non-ring carbon atoms exactly at 6 bonds from the donor atoms).

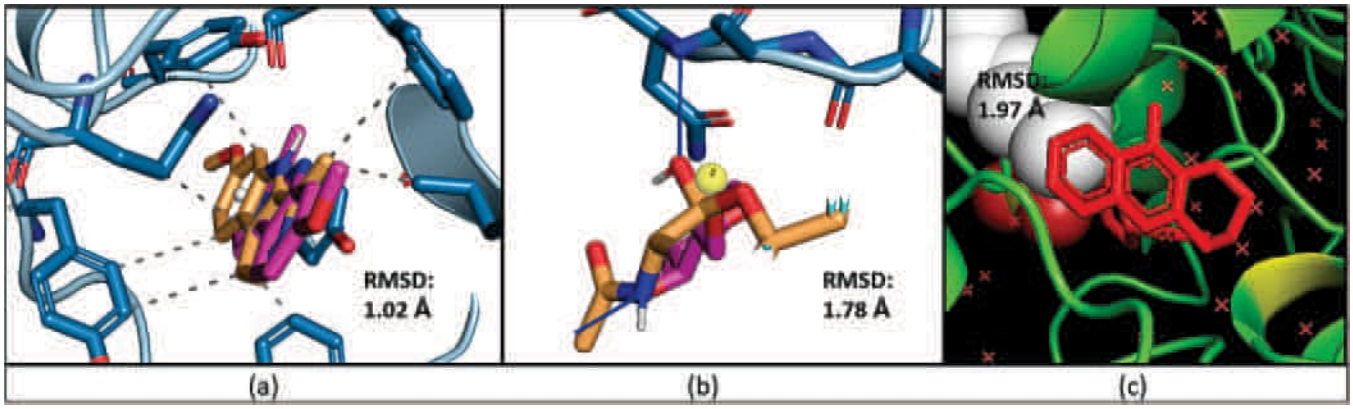

FIGURE 6 | Redocking analysis and their corresponding RMSD values for target (a) *h*MAO-A (PDB ID: 2Z5X), (b) AChE (PDB ID: 1B41), and (c) BChE (PDB ID: 4BDS).

$_{p}IC_{50} = 5.414 + 0.051 * com\_Chyd\_8A + 0.473 * fOS7B + -0.035 * C\_sp3C\_9B$-----model 3 (For MAO-B)

(**com_Chyd_8A:** occurrence of hydrophobic carbon atoms within 8 angstrom units from the center of mass of the molecule; **fOS7B:** frequency of occurrence of sulfur atom exactly at 7 bonds from the oxygen atoms; **C_sp3C_9B:** occurrence of sp3 hybridized carbon atoms within 9 bonds from the carbon atoms).

All four models are depicted in Table 3 for their respective statistics and show statistical robustness among them. The QSAR plots for the correlation between experimental and observed activities are also shown in Figure 7. Other necessary plots are provided in *the* Supporting Information.

2.6 | Interpretations of QSAR Models

2.6.1 | For Model-1

The analysis focuses on three molecular descriptors and their effects on the binding affinity (pK_i) of compounds. The descriptor **fnotringSC7B** measures the frequency of carbon atoms located exactly seven bonds away from non-ring sulfur atoms, which are not part of any cyclic structure. This descriptor has a negative coefficient (−0.214), indicating that an increase in the occurrence of these carbon atoms correlates with a decrease in pK_i, suggesting reduced binding affinity for the compound. The second descriptor, **fsp2Ssp3C7B**, tracks the occurrence of sp3 hybridized carbon atoms positioned seven bonds away from sp2 hybridized sulfur atoms, which are involved in double bonds or planar structures. This descriptor also shows a negative effect on pK_i (−0.271), meaning that more frequent configurations of sp3 carbon atoms in this arrangement lead to lower predicted pK_i values, further indicating a decrease in binding affinity. In contrast, the descriptor **notringC_Cl_8B** measures the presence of chlorine atoms within eight bonds of non-ring carbon atoms. This arrangement positively impacts pK_i, implying that the proximity of chlorine to non-ring carbon enhances binding affinity. The model's interpretation highlights these contrasting influences: the presence of chlorine near non-ring carbon atoms increases binding affinity, while specific configurations involving carbon and sulfur atoms decrease it.

2.6.2 | For Model-2

The analysis examines two molecular descriptors, **Cl_S_6B** and **faccaroC6B**, and their influence on the binding affinity (pK_i) of compounds. **Cl_S_6B** quantifies the occurrence of sulfur atoms within six bonds of chlorine atoms. This descriptor has a positive coefficient (+0.133), indicating that a greater frequency of sulfur near chlorine enhances the compound's binding affinity, thus improving its potency against its target. The presence of this molecular feature is seen as beneficial for chemical activity. **faccaroC6B** assesses the frequency of aromatic carbon atoms that are exactly six bonds away from electron-accepting atoms, such as oxygen or nitrogen. This descriptor also has a positive coefficient (+0.036), suggesting that while aromatic carbon atoms near acceptor atoms slightly contribute to increasing pKi, their effect is less pronounced than that of the Cl_S_6B descriptor. In summary, both descriptors positively influence the binding affinity of compounds: **Cl_S_6B** has a significant impact, enhancing potency, while **faccaroC6B** provides a minor boost.

2.6.3 | For Model-3

The analysis explores three molecular descriptors and their impact on the inhibitory potency (pIC_{50}) of compounds: **com_sp3C_6A**, **Cl_notringC_6B**, and **fdonnotringC6B**. Descriptor "**com_sp3C_6A**" refers to the occurrence of sp3 hybridized carbon atoms within a 6-angstrom radius of the molecule's center of mass. The negative coefficient (–0.034) indicates that an increase in these carbon atoms correlates with a slight decrease in pIC_{50}, suggesting that their presence weakens the biological activity of the compound. "**Cl_notringC_6B**" measures non-ring carbon atoms located within six bonds of chlorine atoms. This descriptor has a positive coefficient (+0.052), meaning that such proximity enhances the pIC_{50} value, thereby increasing the compound's inhibitory potency and making it more effective. "**fdonnotringC6B**" assesses the frequency of non-ring carbon atoms exactly six bonds away from electron donor atoms, like oxygen or nitrogen. This descriptor has a negative coefficient (–0.148), indicating that more non-ring carbon atoms at this distance decrease pIC_{50}, which diminishes the compound's potency.

TABLE 3 | Statistical parameters for developed QSAR models.

Statistical parameter	Model 1	Model 2	Model 3	Model 4
R^2_tr	0.94	0.86	0.78	0.80
Adj-R^2	0.92	0.84	0.73	0.76
F(3-13)	62.39	44.21	15.33	17.69
RSS_tr	0.09	0.03	0.03	0.09
MSE_tr	0.01	0.00	0.00	0.01
RMSE_tr	0.07	0.04	0.04	0.07
MAE_tr	0.06	0.03	0.03	0.06
s	0.08	0.04	0.04	0.08
AIC	−31.73	−52.77	−51.98	−30.39
BIC	−27.56	−49.43	−47.81	−26.23
CCC_tr	0.97	0.93	0.88	0.89
Q^2_cv	0.90	0.80	0.65	0.78
RMSE_cv	0.09	0.05	0.05	0.33
MSE_cv	0.01	0.00	0.00	0.11
PRESS_cv	0.13	0.04	0.04	0.53
MAE_cv	0.08	0.04	0.04	0.25
R^2_Y_{scr}	0.18	0.14	0.18	0.20
MSE_{ex}	0.11	0.02	0.00	0.11
$RMSE_{ex}$	0.33	0.13	0.05	0.33
$PRESS_{ex}$	0.53	0.08	0.01	0.53
Q^2F_1	−0.52	−0.68	0.47	0.81
Q^2F_2	−1.84	−0.71	0.09	0.84
Q^2F_3	−0.38	−0.32	0.61	0.84
$MAE_{\_ex}$	0.32	0.12	0.04	0.23
K	1.02	1.00	1.01	0.98
K_prime	0.98	1.00	0.99	1.02
R^2ext	0.17	0.02	0.53	0.36
CCC_ex	0.30	−0.12	0.47	−0.37
r^2m_ExPy	0.13	−0.01	−0.04	−0.65
r^2m_EyPx	-0.02	0.00	0.44	−0.02
R^2_o	−1.14	−0.70	0.50	−0.75
R^2_o_dash	0.11	−2.28	−0.65	−7.49
Clos_dash	0.34	141.02	2.24	21.77
Clos	7.85	44.06	0.06	3.08
$r^2_{m_}$avg	0.05	0.00	0.20	−0.33
$r^2_{m__}$delta	−0.15	0.01	0.48	0.63

2.6.4 | For Model-4

Important molecular descriptors give us important information about how structural features affect biological activity in the QSAR model for MAO-B inhibitors. We measure hydrophobic carbon atoms (com_Chyd_8A) within an 8-angstrom radius from the molecule's center of mass. Because of their hydrophobic nature, the enzyme's active region contains residues like Ile-199 and Leu-171. These atoms are necessary to stop MAO-B from working. When these residues and inhibitors interact hydrophobically, the binding affinity gofes up. Non-polar parts of the inhibitor stay in the binding pocket. A positive coefficient in the QSAR model means that the inhibitory activity (PIC_{50}) goes up when the hydrophobic carbon density at the center of the molecule goes up. This is what drugs like rasagiline and selegiline do to make their effects more selective and potent. One important indicator is sulfur-oxygen connectivity (fOS7B), which measures the number of sulfur atoms that are exactly

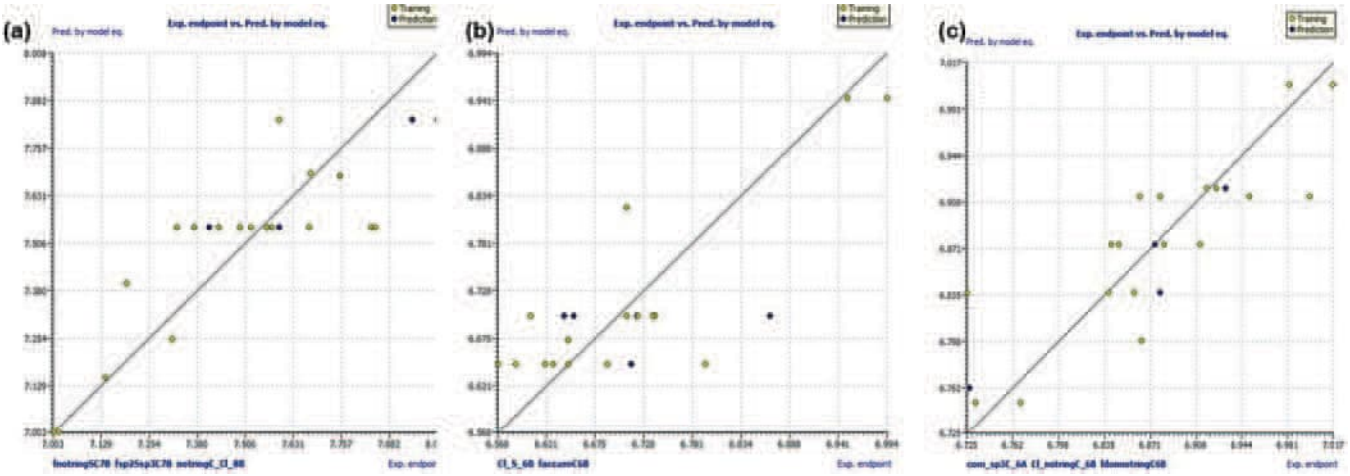

FIGURE 7 | Experimental vs. predicted activities for model-1 (a); model-2 (b) and (c) for model-3 obtained with QSAR equations.

seven bonds away from oxygen atoms. Sulfur-containing groups, like thiols and thioethers, help biological activity through electron transfer and redox interactions. Oxygen atoms, on the other hand, help hydrogen bonds form and make the substance more soluble in water. This particular connection arrangement facilitates ligand binding via both polar and non-polar interactions. A positive coefficient ($\beta > 0$) shows how important this feature is for improving MAO-B binding efficiency. For example, sulfur-containing scaffolds like thiochromones can selectively block MAO-B. Finally, the term sp3-hybridized carbon atoms (C_sp3C_9B) quantifies the number of such carbons within nine bonds of any carbon atom. Excessive carbons, prevalent in aliphatic chains and saturated hydrocarbons, often diminish molecular planarity. Lack of planarity could make it harder for molecules to π-stack, which is needed to bind to aromatic residues in MAO-B, like Tyr-398 and Tyr-435. On the other hand, molecules that are too flexible might not fit correctly into the enzyme's binding pocket. If the coefficient is less than zero, it means that reducing the number of sp3-hybridized carbons increases the inhibitory effect by making molecules flatter and more compact.

In summary, the model-3 identifies contrasting influences on inhibitory activity: non-ring carbon atoms near chlorine atoms enhance potency, while sp3 hybridized carbons near the center of mass and non-ring carbons near donor atoms reduce it. These insights emphasize how specific structural arrangements can significantly affect a compound's biological activity, guiding future design efforts to optimize potency.

2.7 | Molecular Dynamics (MD) Simulation

MD simulations provide crucial insights into the stability and dynamics of protein–ligand complexes. This study explored four distinct protein–ligand complexes to assess their stability and the molecular interactions involved. Thus, we simulated three docked complexes "1B41_**5 u**," "4BDS_**5a**," "2v5z-**5u**," and "2Z5X_**5u**" throughout 100 ns each (Figures 8 and 9). All three simulations retained a substantial stability over the period with fewer to no fluctuations among RMSD values. Compound **5u** showed promising interactions with AChE, while Compound **5a** showed strong interactions with BChE. Additionally, Compound **5u** effectively inhibited MAO-A and MAO-B. Through MD simulations, we analyzed how these molecular interactions evolved, enhancing our understanding of the dynamics within the protein–ligand complexes. These insights could pave the way for developing new drugs and therapeutics.

At the beginning of the simulation of complex "1B41_**5u**," we observed no fluctuations of amino acid residues; however, we noticed that this complex retained the root mean square deviation (RMSD) value below 2.25 Å throughout the 100 ns simulation time (Figure 8a). The overall system consists of 43,742 atoms and 11,486 water molecules. The simulation period between 20 and 100 retained the best stability of ligand–protein stability as indicated by a constant RMSD value below 1.75 Å. Ligand-fit-protein was obtained very well. To see local changes in protein chains, we usually prefer to use the "RMSF" parameter. There were minor fluctuations annotated with index residues 78, in between 300 and 400, and around 580 in both complexes, that is, "1B41_**5u**" and "4BDS_5a" (Figure 8d). By analyzing the "protein secondary structure (SSE)," it was clear that there was the involvement of 22.78% Helix, 16.35% strands, and 39.14% total SSE. For both complexes, that is, "1B41_**5u**" and "4BDS_**5a**," ligand root mean square fluctuation (L-RMSF) values indicated key changes in ligand atom positions. For complex, "1B41_**5u**," hydrophobic interactions were seen with Leu76, Tyr77, Glu358, Val365, Arg24, Pro30, Arg37, and Tyr61 (Figure 8g). Three H-bonds were seen with amino acid residues such as Gly342, Gly345, and Lys32. Water bridges were observed with Val340, Gly342, Ala343, Phe346, and Lys32. Arg24 retained 91% Pi-cationic type interaction with target 1B41.

In the case of complex, "4BDS_**5a**," we observed a stable RMSD value below 2 Å (Figure 8b). RMSF plot also depicted fewer fluctuations around residue index 100, between 200 and 300 (Figure 8e). SSE elements showed involvement of 27.25% Helix and 14.04% strand, accounting for 41.29% total SSE. The L-RMSF value was retained mostly below 2 Å. Four H-bonding interactions were seen with amino acid residues such as Gln67, Asp70, Thr82, and Thr120. We annotated mostly hydrophobic interactions with Asn68, Asp70, Phe73, Trp82, Trp231, Leu274,

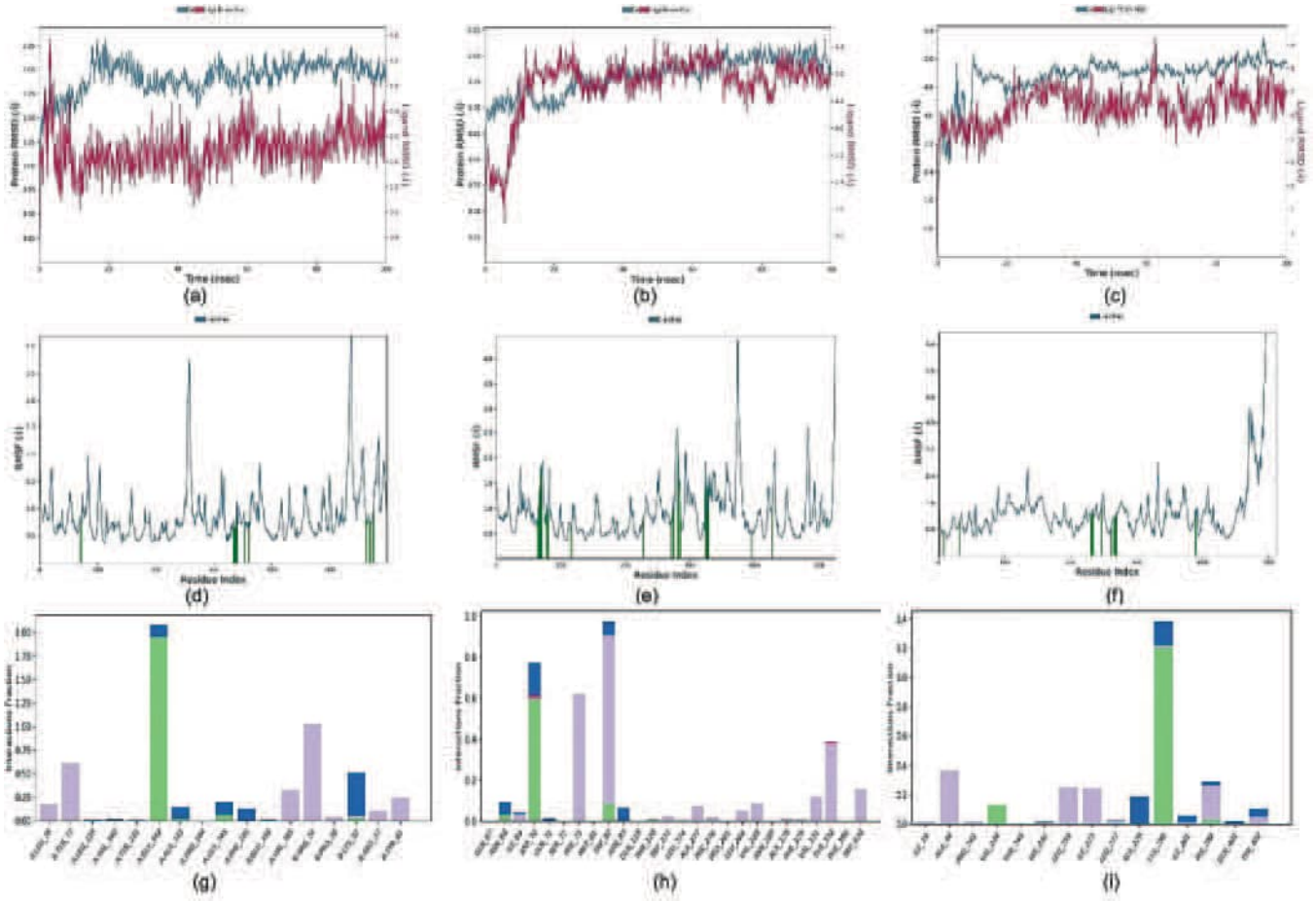

FIGURE 8 | MD simulation plots for complexes "1B41_**5u**," "4BDS_**5a**," and "2Z5X_**5u**" over the period of 100 ns, each for (a–c) RMSD analysis; (d–f) RMSF analysis; and (g–i) ligand–protein contact plots, respectively.

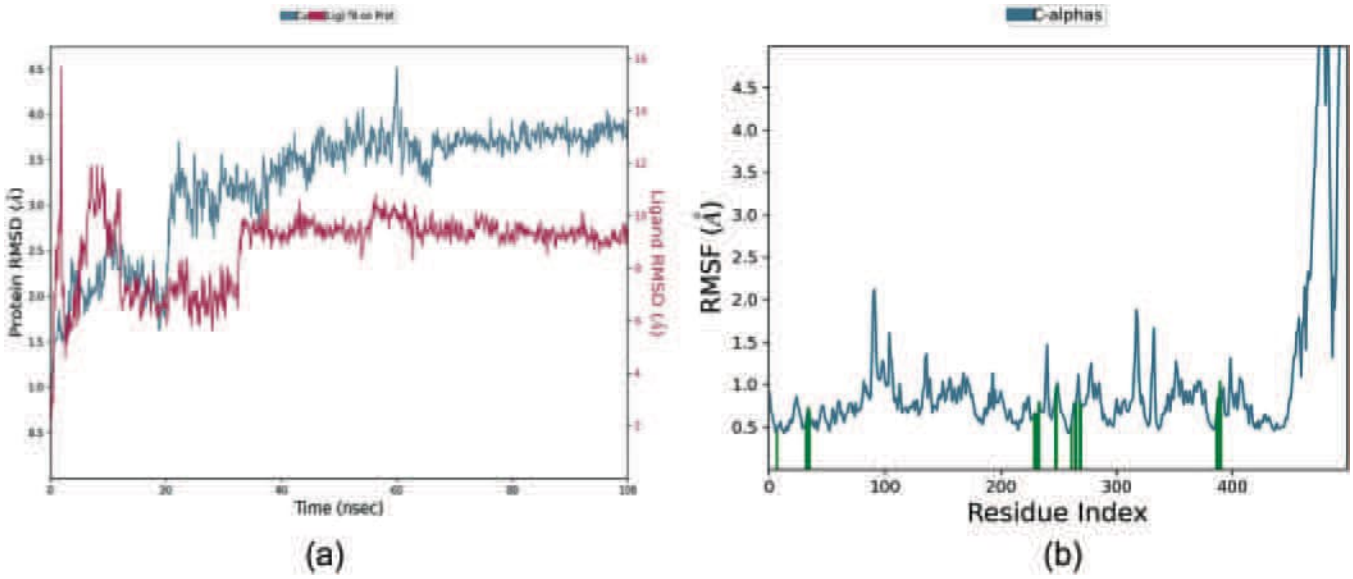

FIGURE 9 | MD simulation plots (a) RMSD and (b) RMSF for complex "2v5z-**5u**" for the period of 100 ns.

and Trp430 (Figure 8h). Ionic interactions were seen with amino acids such as Asp70, Pro285, and Tyr332. The majority of Phe73 denoted the highest π–π stacking (34% total) interaction with ligand **5a**. While Asp70 indicated a strong negative-charged interaction with the S atom (60%). From Figure 8, it was clear that compound **5u** also had good binding toward the MAO-B target. This complex had 36530 atoms in the system while it was simulated. The RMSD value was retained below

4.5 Å for most of the simulation. Only minor fluctuations can be seen from the RMSF plot (Figure 9b). Protein secondary structure analysis showed 25.13% involvement of helices and 16.30% of strands in it.

In our investigation of the protein–ligand complex "2Z5X_**5u**," we observed a stable root mean square deviation (RMSD) value consistently below 4.8 Å (Figure 8c), indicating robust stability throughout the simulation period. The RMSF analysis further illustrated minimal fluctuations, particularly around residue index 400 and within the range of 200–300, suggesting a stable structural conformation in these regions (Figure 8f). The secondary structure elements (SSE) analysis revealed a composition of 25.98% alpha helices and 15.34% beta strands, contributing to a total of 41.31% SSE, which underscores the structural integrity of the complex. The local RMSF (L-RMSF) values were predominantly maintained below 3 Å, reinforcing the notion of localized stability among the residues. Analysis of molecular interactions highlighted four hydrogen bonds involving key amino acid residues, specifically Val244, Lys280, and His282. Additionally, we annotated several hydrophobic interactions with residues including Ile19, Ala44, Pro243, His246, Leu259, Ile273, and Tyr402 (Figure 8i), which likely contribute to the overall stability of the complex. Notably, no ionic interactions were identified within the system, indicating a lack of charge-based stabilization. Furthermore, we observed water-mediated interactions, or water bridges, involving residues Ala279, Ile281, Tyr402, and Lys280, which may enhance the solvation dynamics and contribute to the overall stability of the protein–ligand interaction. These findings provide valuable insights into the molecular interactions and stability characteristics of the "2Z5X_**5u**" complex, contributing to a deeper understanding of its functional dynamics.

3 | Conclusion

A series of thiosemicarbazone derivatives (**5a–u**) were successfully synthesized and characterized through ^{1}HNMR and ^{13}CNMR. All the derivatives were evaluated against AChE, BChE, and MAO-A enzymes in search of lead candidates. All compounds showed varied degrees of inhibition, ranging between 12.89 and 116.01 nM (AChE) and between 124.72 and 308.43 nM (BChE) as compared with the standard drug galantamine (IC_{50} values of 101.24 and 261.62 nM, respectively). Compound **5u** ($IC_{50} = 12.89$ nM) has a 2,6-diCl substitution on the phenyl ring, and compound **5a** ($IC_{50} = 124.72$ nM) has a 2,3-diCl substitution on the phenyl ring, showing strong binding interaction with the active site of enzyme, reducing the catalytic activity, and was identified to be the most active inhibitor of AChE and BChE enzymes. Compound **5u** ($IC_{50} = 96.25$ nM) showed the most active inhibitor of monoamine oxidase (MAO-A) enzyme. Among all compounds, **5a** exhibited the strongest binding affinity with 4BDS (−11.3 kcal/mol), forming multiple stabilizing interactions with HIS A:438, PHE A:329, and TRP A:82. For 1B41, compound **5u** showed the best binding (−8.2 kcal/mol), engaging residues GLU A:313 and ASN A:233 through hydrogen bonding and salt bridges. Against 2Z5X, **5u** again demonstrated potent affinity (−8.6 kcal/mol), interacting via hydrogen bonds and π–anion interactions with GLU A:492 and TYR A:124. Finally, **5u** also bound strongly to 2V5Z (−7.8 kcal/mol), forming hydrogen bonds and charge interactions with GLU A:391 and GLN A:392, confirming its multi-target potential. The promising inhibitory activities of compounds **5a** and **5u** against key enzymes related to neurological disorders, along with supportive ADME and QSAR analyses, suggest their potential as lead candidates for further drug development targeting CNS diseases. These findings encourage continued exploration and optimization of this compound series to enhance efficacy and pharmacokinetic profiles.

Our results suggested that **5a** and **5u** can be considered potential candidates for the treatment of neurological disorders such as AD.

4 | Experimental

4.1 | Chemistry

4.1.1 | General

For the synthesis of indole-based thiosemicarbazones, all the starting materials, such as 4-(diethylamino)salicylaldehyde, were bought from Sigma Aldrich. Chemicals and solvents, including triethylamine, methanol, DMF, glacial acetic acid, petroleum ether, and ethyl acetate, were bought from Merck and used as original. Silica gel plates with aluminum back were utilized to check the reaction progress and completion. A Bruker Ascend 400 MHz NMR spectrometer was utilized to get ^{1}H and ^{13}C-NMR spectra in deuterated solvent DMSO-d_6 at 25°C (400 MHz for ^{1}H and 101 MHz for ^{13}C). NMR spectra were presented as chemical shifts (ppm), and coupling constants (*J*) were demonstrated in Hertz (Hz) to detail signal multiplicity.

The InChI codes of the investigated compounds, together with some biological activity data, are provided as Supporting Information.

4.1.2 | General Procedure for the Synthesis of 5-(Diethylamino)-2-Formylphenyl Naphthalene-2-Sulfonate (3)

In a round-bottom flask, 0.5 g (2.5 mmol) of 4-(diethylamino) salicylaldehyde **1** and 0.348 mL (2.5 mmol) of triethylamine were added. DMF (3 mL) was added while stirring in an ice bath. After that, 0.56 g (2.5 mmol) of naphthalene sulfonyl chloride **2** was added with continued stirring. TLC was used to track the progress of the reaction. The reaction was terminated after an hour upon completion. The reaction mixture was poured into 20 mL of ice-cold water. The precipitated solid was filtered and dried to obtain the product **3** in 95% yield.

4.1.3 | General Procedure for the Synthesis of Thiosemicarbazones 5a–u

The targeted thiosemicarbazones were synthesized in a single-step condensation reaction. In an oven-dried one-neck round-bottom flask, equimolar quantities of 4-(diethylamino)salicylaldehyde

(0.1 g, 0.01 mmol) and respective thiosemicarbazides (**4a–u**) were added in methanol (10 mL). Three to four drops of glacial acetic acid were used as a catalyst in the reaction mixture. The reaction mixture was refluxed for 5–6 h, and then TLC was used to determine the progress of the reaction using a mixture of 1:2 petroleum ether and ethyl acetate as the eluent. After completion of the reaction, the solid product so formed was filtered, washed, and dried. The residue was crystallized with ethanol.

(E)-2-({2-[(2,3-Dichlorophenyl)carbamothioyl]hydrazono}methyl)-5-(diethylamino)phenyl naphthalene-2-sulfonate (**5a**): Yield: 92%; M.P: 202°C–204°C; Color: yellow; ^{1}H-NMR: δ (400 MHz, DMSO-d_6) 11.96 (1 H, s, NH-N=C), 9.93 (1 H, s, S=C–NH–R), 8.66 (1 H, d, J = 2.0, Ar), 8.30 (1 H, s, HC=N), 8.24 (2 H, t, J = 8.5 Hz, Ar), 8.11 (1 H, d, J = 8.2 Hz, Ar), 8.04=7.91 (2 H, m, Ar), 7.75 (3 H, dqd, J = 16.3, 7.8, 3.7 Hz, Ar), 7.55 (1 H, dd, J = 8.1, 1.5 Hz, Ar), 7.40 (1 H, t, J = 8.1 Hz, Ar), 6.61 (1 H, dd, J = 9.1, 2.5 Hz, Ar), 5.94 (1 H, d, J = 2.5 Hz, Ar), 3.11 (4 H, q, J = 7.0 Hz, CH_2), 0.81 (6 H, t, J = 6.9 Hz, CH_3); ^{13}C-NMR (100 MHz, DMSO-d_6) δ 176.04 (C=S), 150.07 (C=N), 149.97 (Ar), 139.09 (Ar), 138.96 (Ar), 135.69 (Ar), 132.02 (Ar), 131.97 (Ar), 131.83 (Ar), 131.06 (Ar), 130.55 (Ar), 130.52 (Ar), 130.09 (Ar), 129.42 (Ar), 128.67 (Ar), 128.58 (Ar), 128.51 (Ar), 128.42 (Ar), 128.32 (Ar), 127.98 (Ar), 123.14 (Ar), 113.61 (Ar), 111.19 (Ar), 104.09 (Ar), 44.26 (CH_2), 12.42 (CH_3); FT-IR Vmax (cm^{-1}): 3261 (*N–H stretch*), 3136 (*Ar–H or N–H stretch*), 2970 (*C–H stretch, N-ethyl*), 1611 (*C=N or Ar–C=C*), 1589 (*C=N or N–C=S,*), 1574 (*Ar–C=C stretch*), 1524 (*N–H bend or Ar–C=C*), 1498 (*Ar–C–C stretch*), 1451 (*CH_2 bend, N-ethyl*), 1345 (*S=O sym. stretch, sulfonate*), 1264 (*S=O asym. stretch, sulfonate*), 1167 (*C–N or S–O stretch*), 1016 (*C–N stretch or Ar–C–H bend*), 956 (*N–H wag or C=S,*), 798 (*Ar–C–H out-of-plane*); HPLC: CH_3CN:H_2O = 80:20; R_t: 7.620 min, purity: 98.7%; Elemental Analysis: CHN, Calcd: C, 55.90; H, 4.36; N, 9.31; found: C, 55.95; H, 4.39; N, 9.34; ESI-HRMS (m/z): chemical formula: $C_{28}H_{26}{}^{35}Cl_2N_4O_3S_2$, calcd [M-H]$^+$: 599.07451, found [M + H]$^+$: 599.07455 *(0.04 ppm deviation)*, chemical formula: $C_{28}H_{26}{}^{37}Cl_2N_4O_3S_2$, calcd [M-H]$^+$: 601.06860, found [M + H]$^+$: 601.07213 *(3.53 ppm deviation)*.

(*E*)-2-({2-[(4-Bromophenyl)carbamothioyl]hydrazono}methyl)-5-(diethylamino)phenyl naphthalene-2-sulfonate (**5b**): Yield: 90%; M.P: 198°C–200°C; Color: yellow; ^{1}H-NMR: δ (400 MHz, DMSO-d_6) 11.78 (1 H, s, NH–N=C), 9.85 (1 H, s, S=C–NH–R), 8.65 (1 H, d, J = 2.0 Hz, Ar), 8.24 (3 H, dd, J = 15.7, 7.0 Hz, Ar, HC=N), 8.11 (1 H, d, J = 8.1 Hz, Ar), 8.04–7.94 (2 H, m, Ar), 7.75 (2 H, dddd, J = 26.4, 8.0, 6.9, 1.3 Hz, Ar), 7.63–7.47 (4 H, m, Ar), 6.59 (1 H, dd, J = 9.1, 2.5 Hz, Ar), 5.95 (1 H, d, J = 2.5 Hz, Ar), 3.11 (4 H, q, J = 7.0 Hz, CH_2), 0.81 (6 H, t, J = 7.0 Hz, CH_3); ^{13}C-NMR (100 MHz, DMSO-d_6) δ 175.34 (C=S), 149.97 (C=N), 149.91 (Ar), 139.02 (Ar), 135.67 (Ar), 131.95 (Ar), 131.88 (Ar), 131.27 (Ar), 131.02 (Ar), 130.53 (Ar), 130.09 (Ar), 129.21 (Ar), 128.57 (Ar), 128.42 (Ar), 127.75 (Ar), 123.14 (Ar), 117.64 (Ar), 113.63 (Ar), 110.99 (Ar), 104.10 (Ar), 44.27 (CH_2), 12.43 (CH_3); FT-IR Vmax (cm^{-1}): 3318 (*N–H stretch*), 3129 (*Ar–H or N–H stretch*), 2968 (*C–H stretch, N-ethyl*), 1613 (*C=N or Ar–C=C*), 1583 (*C=N or N–C=S,*), 1551 (*N–H bend or Ar–C=C*), 1483 (*Ar–C–C stretch*), 1367 (*S=O sym. stretch, sulfonate*), 1266 (*S=O asym. stretch, sulfonate*), 1180 (*C–N or S–O stretch*), 1058 (*C–N stretch or Ar–C–H bend*), 907 (*N–H wag or C=S,*), 876 (*C–H out-of-plane, aromatic*), 756 (*Ar–C–H out-of-plane bend*); HPLC: CH_3CN:H_2O = 80: 20; R_t: 5.766 min, purity: 98.01%; Elemental Analysis: CHN Calcd: C, 54.99; H, 4.45; N, 9.16; found: C, 55.23; H, 4.49; N, 9.19; ESI-HRMS (*m/z*): chemical formula: $C_{28}H_{27}{}^{79}BrN_4O_3S_2$, calcd [M + H]$^+$: 611.07862, found [M + H]$^+$: 611.07625 *(4.12 ppm deviation)*, chemical formula: $C_{28}H_{27}{}^{81}BrN_4O_3S_2$, calcd [M + H]$^+$: 613.07270, found [M + H]$^+$: 613.07456 *(1.86 ppm deviation)*, $C_{28}H_{27}{}^{79}BrN_4O_3S_2$, calcd [M +Na]$^+$: 633.06056, found [M+Na]$^+$: 633.05825 *(2.31 ppm deviation)*, chemical formula: $C_{28}H_{27}{}^{81}BrN_4O_3S_2$, calcd [M+Na]$^+$: 635.05460, found [M + H]$^+$: 635.05629 *(1.69 ppm deviation)*.

(*E*)-5-(Diethylamino)-2-{[2-(phenylcarbamothioyl)hydrazono]methyl}phenyl naphthalene-2-sulfonate (**5c**): Yield: 90%; M.P: 204°C–206°C; Color: yellow; ^{1}H-NMR: δ (400 MHz, DMSO-d_6) 11.71 (1 H, s, NH–N=C), 9.82 (1 H, s, S=C–NH–R), 8.66 (1 H, d, J = 1.9 Hz, Ar), 8.28 (1 H, s, HC=N), 8.24 (2 H, t, J = 8.5 Hz, Ar), 8.12 (1 H, d, J = 8.1 Hz, Ar), 8.05–7.95 (2 H, m, Ar), 7.78 (1 H, ddd, J = 8.2, 6.9, 1.3 Hz, Ar), 7.72 (1 H, ddd, J = 8.1, 6.9, 1.3 Hz, Ar), 7.62–7.53 (2 H, m, Ar), 7.36 (2 H, t, J = 7.9 Hz, Ar), 7.23–7.13 (1 H, m, Ar), 6.59 (1 H, dd, J = 9.1, 2.5 Hz, Ar), 5.94 (1 H, d, J = 2.5 Hz, Ar), 3.11 (4 H, q, J = 7.0 Hz, CH_2), 0.81 (6 H, t, J = 7.0 Hz, CH_3); ^{13}C-NMR (100 MHz, DMSO-d_6) δ 175.48 (C=S), 149.91, 149.83 (C=N), 139.57 (Ar), 138.72 (Ar), 135.67 (Ar), 131.96 (Ar), 131.93 (Ar), 131.02 (Ar), 130.54 (Ar), 130.51 (Ar), 130.09 (Ar), 129.24 (Ar), 128.57 (Ar), 128.47 (Ar), 128.42 (Ar), 125.84 (Ar), 125.49 (Ar), 123.15 (Ar), 113.75 (Ar), 111.00 (Ar), 104.09 (Ar), 44.26 (CH_2), 12.43 (CH_3); FT-IR Vmax (cm^{-1}): 3310 (*N–H stretch*), 3133 (*Ar–H or N–H stretch*), 2969 (*C–H stretch, N-ethyl*), 1610 (*C=N or Ar–C=C*), 1590 (*C=N or N–C=S,*), 1548 (*N–H bend or Ar–C=C*), 1502 (*Ar–C–C stretch*), 1443 (*CH_2 bend, N-ethyl*), 1360 (*S=O sym. stretch, sulfonate*), 1314 (*S=O asym. stretch, sulfonate*), 1264 (*C–N or S–O stretch*), 1180 (*C–N or S–O stretch*), 1079 (*C–N stretch or Ar–C–H bend*), 1013 (*C–N stretch or Ar–C–H bend*), 952 (*N–H wag or C=S,*), 840 (*C–H out-of-plane, aromatic*), 757 (*Ar–C–H out-of-plane bend*), 688 (*aromatic ring deformation*); HPLC: CH_3CN:H_2O = 80:20; Rt: 3.790 min, purity: 99.4805%; Elemental Analysis: CHN Calcd: C, 63.13; H, 5.30; N, 10.52; found: C, 63.17; H, 5.34; N, 10.67; ESI-HRMS (*m/z*): chemical formula: $C_{28}H_{28}N_4O_3S_2$, calcd [M + H]$^+$: 533.16811, found [M + H]$^+$: 533.16634 *(1.77 ppm deviation)*, calcd [M+Na]$^+$: 555.15005, found [M+Na]$^+$: 555.14798 *(2.07 ppm deviation)*.

(*E*)-5-(Diethylamino)-2-({2-[(4-methoxyphenyl)carbamothioyl]hydrazono}methyl)phenyl naphthalene-2-sulfonate (**5d**): Yield: 89%; M.P: 206°C–208°C; Color: off-white; ^{1}H-NMR: δ (400 MHz, DMSO-d_6) 11.62 (1 H, s, NH–N=C), 9.72 (1 H, s, S=C–NH–R), 8.65 (1 H, d, J = 2.0 Hz, Ar), 8.30–8.17 (3 H, m, Ar, HC=N), 8.16–8.08 (1 H, m, Ar), 8.04–7.95 (2 H, m, Ar), 7.79 (1 H, ddd, J = 8.2, 6.9, 1.3 Hz, Ar), 7.72 (1 H, ddd, J = 8.1, 6.9, 1.3 Hz, Ar), 7.43–7.34 (2 H, m, Ar), 6.96–6.88 (2 H, m, Ar), 6.58 (1 H, dd, J = 9.1, 2.5 Hz, Ar), 5.94 (1 H, d, J = 2.5 Hz, Ar), 3.76 (3 H, s, O–CH_3), 3.11 (4 H, q, J = 7.0 Hz, CH_2), 0.81 (6 H, t, J = 7.0 Hz, CH_3); ^{13}C-NMR (100 MHz, DMSO-d_6) δ 175.92 (C=S), 157.25 (C=N), 149.85 (Ar), 149.76 (Ar), 138.41 (Ar), 135.67 (Ar), 132.49 (Ar), 131.96 (Ar), 131.01 (Ar), 130.52 (Ar), 130.09 (Ar), 129.19 (Ar), 128.57 (Ar), 128.43 (Ar), 127.66 (Ar), 123.16 (Ar), 113.85 (Ar), 113.69 (Ar), 110.99 (Ar), 104.07 (Ar), 55.71 (O–CH_3), 44.25 (CH_2), 12.43 (CH_3); FT-IR Vmax (cm^{-1}): 3278 (N–H stretch), 3104 (Ar–H or N–H stretch), 2964 (C–H stretch, N-ethyl), 1611 (C=N or Ar–C=C), 1590 (C=N or N–C=S,), 1539 (N–H bend or Ar–C=C), 1509 (Ar–C–C stretch), 1435 (CH_2 bend, N-ethyl),

1399 (S=O sym. stretch, sulfonate), 1289 (S=O asym. stretch, sulfonate), 1235 (C–N or S–O stretch), 1184 (C–N or S–O stretch), 1099 (C–N stretch or Ar–C–H bend), 1069 (C–N stretch or Ar–C–H bend), 961 (N–H wag or C=S), 840 (C–H out-of-plane, aromatic), 769 (Ar–C–H out-of-plane bend); HPLC: $CH_3CN:H_2O = 80:20$; R_t: 3.314 min, purity: 99.27%. Elemental Analysis: CHN Calcd: C, 61.90; H, 5.37; N, 9.96; found: C, 62.30; H, 5.557; N, 10.12; ESI-HRMS (*m/z*): chemical formula: $C_{29}H_{30}N_4O_4S_2$, calcd $[M + H]^+$: 563.17867, found $[M + H]^+$: 563,17662 *(2.05 ppm deviation)*, calcd $[M+Na]^+$: 585.16062, found $[M + Na]^+$: 585,15840 *(2.22 ppm deviation)*.

(*E*)-2-({2-[(3-chlorophenyl)carbamothioyl]hydrazono}methyl)-5-(diethylamino)phenyl naphthalene-2-sulfonate (**5e**): Yield: 90%; M.P: 195°C–197°C; Color: yellow; ^{1}H-NMR: δ (400 MHz, DMSO-d_6) 11.83 (1 H, s, NH–N=C), 9.90 (1 H, s, S=C–NH–R), 8.66 (1 H, d, $J = 2.0$ Hz, Ar), 8.29 (1 H, s, HC=N), 8.24 (2 H, t, $J = 8.3$ Hz, Ar), 8.15–8.09 (1 H, m, Ar), 8.06–7.96 (2 H, m, Ar), 7.81–7.75 (2 H, m, Ar), 7.72 (1 H, ddd, $J = 8.1$, 6.9, 1.3 Hz, Ar), 7.60 (1 H, ddd, $J = 8.2$, 2.1, 1.0 Hz, Ar), 7.38 (1 H, t, $J = 8.1$ Hz, Ar), 7.23 (1 H, ddd, $J = 8.1$, 2.2, 1.0 Hz, Ar), 6.60 (1 H, dd, $J = 9.1$, 2.5 Hz, Ar), 5.95 (1 H, d, $J = 2.5$ Hz, Ar), 3.12 (4 H, q, $J = 7.0$ Hz, CH_2), 0.81 (6 H, t, $J = 7.0$ Hz, CH_3); ^{13}C-NMR (100 MHz, DMSO-d_6) δ 175.22 (C=S), 150.01 (C=N), 149.94 (Ar), 141.08 (Ar), 139.15 (Ar), 135.68 (Ar), 132.57 (Ar), 131.96 (Ar), 131.88 (Ar), 131.02 (Ar), 130.54 (Ar), 130.50 (Ar), 130.09 (Ar), 130.00 (Ar), 129.20 (Ar), 128.56 (Ar), 128.42 (Ar), 125.08 (Ar), 124.08 (Ar), 123.15 (Ar), 113.59 (Ar), 110.99 (Ar), 104.09 (Ar), 44.28 (CH_2), 12.42 (CH_3); FT-IR Vmax (cm^{-1}): 3308 (*N–H stretch*), 3130 (*Ar–H or N–H stretch*), 3080 (*Ar–H stretch*), 2967 (*C–H stretch, N-ethyl*), 2923 (*C–H stretch, aliphatic*), 1611 (*C=N or Ar–C=C*), 1584 (*C=N or N–C=S*), 1546 (*N–H bend or Ar–C=C*), 1503 (*Ar–C–C stretch*), 1472 (*CH_2 bend, N-ethyl*), 1356 (*S=O sym. stretch, sulfonate*), 1302 (*S=O asym. stretch, sulfonate*), 1262 (*C–N or S–O stretch*), 1181 (*C–N or S–O stretch*), 1128 (*C–N stretch or Ar–C–H bend*), 1056 (*C–N stretch or Ar–C–H bend*), 952 (*N–H wag or C=S*), 851 (*C–H out-of-plane, aromatic*), 794 (*Ar–C–H out-of-plane bend*); HPLC: $CH_3CN:H_2O = 80:20$; Rt: 5.299 min, purity: 98.44%; Elemental Analysis: CHN Calcd: C, 59.30; H, 4.80; N, 9.88; found: C, 59.50; H, 4.98; N, 10.20; ESI-HRMS (*m/z*): chemical formula: $C_{28}H_{27}{}^{35}ClN_4O_3S_2$, calcd $[M + H]^+$: 567.12914, found $[M + H]^+$: 567.12726 *(1.88 ppm deviation)*, chemical formula: $C_{28}H_{27}{}^{35}ClN_4O_3S_2$, calcd $[M+Na]^+$: 589.11108, found $[M+Na]^+$: 589.10885 *(2.23 ppm deviation)*, chemical formula: $C_{28}H_{27}{}^{37}ClN_4O_3S_2$, calcd $[M + H]^+$: 569,12320, found $[M + H]^+$: 569,12462 *(1.42 ppm deviation)*, chemical formula: $C_{28}H_{27}{}^{37}ClN_4O_3S_2$, calcd $[M + Na]^+$: 591.10510, found $[M + Na]^+$: 591.10634 *(1.24 ppm deviation)*.

(*E*)-5-(Diethylamino)-2-{[2-(isobutylcarbamothioyl)hydrazono] methyl}phenyl naphthalene-2-sulfonate (**5f**): Yield: 86%; M.P: 164°C–166°C; Color: yellow; ^{1}H-NMR: δ (400 MHz, DMSO-d_6) 11.33 (1 H, s, NH–N=C), 8.65 (1 H, d, $J = 2.0$ Hz, S=C–NH–R), 8.27–8.15 (4 H, m, Ar, HC=N), 8.11 (1 H, dd, $J = 8.2$, 1.2 Hz, Ar), 7.98 (1 H, dd, $J = 8.7$, 2.0 Hz, Ar), 7.84 (1 H, d, $J = 9.0$ Hz, Ar), 7.78 (1 H, ddd, $J = 8.2$, 6.9, 1.3 Hz, Ar), 7.71 (1 H, ddd, $J = 8.1$, 6.9, 1.3 Hz, Ar), 6.59 (1 H, dd, $J = 9.0$, 2.5 Hz, Ar), 5.92 (1 H, d, $J = 2.5$ Hz, Ar), 3.40–3.34 (2 H, m, isopr. CH_2), 3.10 (4 H, q, $J = 7.0$ Hz, CH_2), 1.98 (1 H, dt, $J = 13.6$, 6.8 Hz isopr. CH), 0.87 (6 H, d, $J = 6.7$ Hz, isopr. CH_3), 0.80 (6 H, t, $J = 7.0$ Hz, CH_3); ^{13}C-NMR (100 MHz, DMSO-d_6) δ 177.13 (C=S), 149.66 (C=N), 149.58 (Ar), 137.72 (Ar), 135.65 (Ar), 132.00 (Ar), 131.95 (Ar), 130.98 (Ar), 130.49 (Ar), 130.05 (Ar), 128.75 (Ar), 128.55 (Ar), 128.40 (Ar), 123.13 (Ar), 114.03 (Ar), 111.08 (Ar), 104.12 (Ar), 51.16 (*N*-CH_2), 44.24 (CH_2), 28.30 (isopr. CH_2), 20.56 (isopr. CH_3), 12.42 (CH_3); FT-IR Vmax (cm^{-1}): 3350 (*N–H stretch*,), 3250 (*N–H stretch*), 3089 (*Ar–H stretch*), 2950 (*C–H stretch, N-ethyl/aliphatic*), 1615 (*C=N or Ar–C=C*), 1598 (*C=N or N–C=S*,), 1475 (*CH_2 bend, N-ethyl*), 1385 (*S=O sym. stretch, sulfonate*), 1250 (*S=O asym. stretch, sulfonate*), 1145 (*C–N or S–O stretch*), 1039 (*C–N stretch or Ar–C–H bend*), 978 (*N–H wag or C=S*,), 854 (*C–H out-of-plane, aromatic*), 765 (*Ar–C–H out-of-plane bend*); HPLC: $CH_3CN:H_2O = 80:20$; R_t: 4.213 min, purity: 98.15%; Elemental Analysis: CHN Calcd: C, 60.91; H, 6.29; N, 10.93; found: C, 61.41; H, 6.49; N, 10.98; ESI-HRMS (*m/z*): chemical formula: $C_{26}H_{32}N_4O_3S_2$, calcd $[M + H]^+$: 513.19941, found $[M + H]^+$: 513.19768 *(1.73 ppm deviation)*, chemical formula: $C_{26}H_{32}N_4O_3S_2$, calcd $[M + Na]^+$: 535.18135, found $[M + Na]^+$: 535.17948 *(1.87 ppm deviation)*.

(*E*)-5-(Diethylamino)-2-{[2-(isobutylcarbamothioyl)hydrazono] methyl}phenyl naphthalene-2-sulfonate (**5g**): Yield: 87%; M.P: 133°C–135°C; Color: yellow; ^{1}H-NMR: δ (400 MHz, DMSO-d_6) 11.34 (1 H, s, NH–N=C), 8.64 (1 H, d, $J = 1.9$ Hz, S = C–NH–R), 8.29 (1 H, t, $J = 5.9$ Hz, Ar), 8.23 (2 H, dd, $J = 8.6$, 6.4 Hz, Ar), 8.17 (1 H, s, HC=N), 8.13–8.08 (1 H, m, Ar), 7.98 (1 H, dd, $J = 8.8$, 2.0 Hz, Ar), 7.86 (1 H, d, $J = 9.0$ Hz, Ar), 7.79 (1 H, ddd, $J = 8.2$, 6.9, 1.3 Hz, Ar), 7.71 (1 H, ddd, $J = 8.1$, 6.8, 1.3 Hz, Ar), 6.58 (1 H, dd, $J = 9.1$, 2.5 Hz, Ar), 5.93 (1 H, d, $J = 2.5$ Hz, Ar), 3.60 (2 H, q, $J = 6.7$ Hz, CH_2), 3.10 (4 H, q, $J = 7.0$ Hz, CH_2), 2.53–2.45 (4 H, m, CH_2), 2.06 (3 H, s, S-CH_3), 1.84 (2 H, p, $J = 7.2$ Hz, CH_2), 0.81 (6 H, t, $J = 7.0$ Hz, CH_3); ^{13}C-NMR (100 MHz, DMSO-d_6) δ 176.93 (C=S), 149.70 (C=N), 149.61 (Ar), 137.70 (Ar), 135.65 (Ar), 131.95 (Ar), 130.98 (Ar), 130.49 (Ar), 130.06 (Ar), 128.66 (Ar), 128.55 (Ar), 128.40 (Ar), 123.14 (Ar), 114.02 (Ar), 111.03 (Ar), 104.09 (Ar), 44.24 (CH_2), 43.05 (S-CH_3), 31.22 (CH_2), 28.85 (CH_2), 15.11 (CH_2), 12.42 (CH_3); FT-IR Vmax (cm^{-1}): 3361 (*N–H stretch*), 3148 (*Ar–H or N–H stretch*), 2969 (*C–H stretch, N-ethyl*), 2914 (*C–H stretch, aliphatic*), 1613 (*C=N or Ar–C=C*), 1509 (*Ar–C–C stretch*), 1450 (*CH_2 bend, N-ethyl*), 1358 (*S=O sym. stretch, sulfonate*), 1310 (*S=O asym. stretch, sulfonate*), 1262 (*C–N or S–O stretch*), 1160 (*C–N or S–O stretch*), 1065 (*C–N stretch or Ar–C–H bend*), 1014 (*C–N stretch or Ar–C–H bend*), 952 (*N–H wag or C=S*,), 885 (*C–H out-of-plane, aromatic*), 795 (*Ar–C–H out-of-plane bend*), 755 (*Ar–C–H out-of-plane bend*); HPLC: $CH_3CN:H_2O = 80:20$; R_t: 3.451 min, purity: 98.32%; Elemental Analysis: CHN Calcd: C, 57.32; H, 5.92; N, 10.28; found: C, 57.84; H, 6.40; N, 10.68; ESI-HRMS (*m/z*): chemical formula: $C_{26}H_{32}N_4O_3S_3$, calcd $[M + H]^+$: 545.17148, found $[M + H]^+$: 545.16982 *(1.66 ppm deviation)*, calcd $[M + Na]^+$: 567.15342, found $[M + Na]^+$: 567.15149 *(1.93 ppm deviation)*.

(*E*)-5-(Diethylamino)-2-[(2-{[2-(trifluoromethyl)phenyl] carbamothioyl}hydrazineylidene) methyl]phenyl naphthalene-2-sulfonate (**5h**): Yield: 90%; M.P: 185°C–187°C; Color: yellow; ^{1}H-NMR: δ (400 MHz, DMSO-d_6) 11.94 (1 H, s, NH–N=C), 9.74 (1 H, s, S=C-NH-R), 8.67 (1 H, d, $J = 2.0$ Hz, Ar), 8.31 (1 H, s, HC = N), 8.25 (2 H, t, $J = 9.1$ Hz, Ar), 8.12 (1 H, d, $J = 8.2$ Hz, Ar), 7.99 (1 H, dd, $J = 8.7$, 2.0 Hz, Ar), 7.89 (1 H, d, $J = 9.0$ Hz, Ar), 7.83–7.67 (5 H, m, Ar), 7.48 (1 H, t, $J = 7.6$ Hz, Ar), 6.62 (1 H, dd, $J = 9.1$, 2.5 Hz, Ar), 5.91 (1 H, d, $J = 2.5$ Hz, Ar), 3.10 (4 H, q, $J = 7.0$ Hz, CH_2), 0.79 (6 H, t, $J = 7.0$ Hz, CH_3); ^{13}C-NMR (100 MHz, DMSO-d_6) δ 176.68 (C=S), 150.05 (C=N), 149.96 (Ar),

138.90 (Ar), 135.70 (Ar), 132.88 (Ar), 131.98 (Ar), 131.89 (Ar), 131.59 (Ar), 131.05 (Ar), 130.56 (Ar), 130.53 (Ar), 130.08 (Ar), 128.58 (Ar), 128.42 (Ar), 127.23 (Ar), 126.50 (Ar), 125.41 (Ar), 123.12 (Ar), 113.63 (Ar), 111.25 (Ar), 104.07 (Ar), 44.23 (CH_2), 12.40 (CH_3); FT-IR Vmax (cm^{-1}): 3305 (*N–H stretch*), 2798 (*C–H stretch, aliphatic*), 1610 (*C═N or Ar–C═C*), 1588 (*C═N or N–C═S,*), 1554 (*N–H bend or Ar–C═C*), 1511 (*Ar–C–C stretch*), 1457 (*CH_2 bend, N-ethyl*), 1371 (*S═O sym. stretch, sulfonate*), 1314 (*S═O asym. stretch, sulfonate*), 1271 (*C–N or S–O stretch; possible C–F stretch contribution*), 1186 (*C–N or S–O stretch*), 1096 (*C–N stretch or Ar–C–H bend*), 1063 (*C–N stretch or Ar–C–H bend*), 956 (*N–H wag or C═S*), 755 (*Ar–C–H out-of-plane bend*), 545 (*S–O bending or sulfonate fingerprint*); HPLC: $CH_3CN:H_2O = 80:20$; R_t: 5.205 min, purity: 96.52%; Elemental Analysis: CHN Calcd: C, 57.99; H, 4.53; N, 9.33; found: C, 58.40; H, 4.87; N, 9.45; ESI-HRMS (*m/z*): chemical formula: $C_{29}H_{27}F_3N_4O_3S_2$, calcd $[M + H]^+$: 601.15549, found $[M + H]^+$: 601.15356 *(1.93 ppm deviation)*, calcd $[M + Na]^+$: 623.13744, found $[M + Na]^+$: 623.13537 *(2.07 ppm deviation)*.

(*E*)-2-({2-[(4-Chlorophenyl)carbamothioyl]hydrazono}methyl)-5-(diethylamino)phenyl naphthalene-2-sulfonate (**5i**): Yield: 92%; M.P: 199°C–201°C; Color: pale yellow; ^{1}H-NMR: δ (400 MHz, DMSO-d_6) 11.78 (1 H, s, NH–N═C), 9.86 (1 H, s, S═C–NH–R), 8.65 (1 H, d, $J = 2.0$ Hz, Ar), 8.27 (1 H, s, HC═N), 8.24 (2 H, t, $J = 8.3$ Hz, Ar), 8.11 (1 H, d, $J = 8.1$ Hz, Ar), 8.05–7.94 (2 H, m, Ar), 7.78 (1 H, ddd, $J = 8.1$, 6.9, 1.3 Hz, Ar), 7.76–7.68 (1 H, m, Ar), 7.67–7.58 (2 H, m, Ar), 7.47–7.34 (2 H, m, Ar), 6.59 (1 H, dd, $J = 9.1$, 2.5 Hz, Ar), 5.95 (1 H, d, $J = 2.5$ Hz, Ar), 3.11 (4 H, q, $J = 7.0$ Hz, CH_2), 0.81 (6 H, t, $J = 7.0$ Hz, CH_3); ^{13}C-NMR (100 MHz, DMSO-d_6) δ 175.43 (C═S), 149.97 (C═N), 149.90 (Ar), 139.00 (Ar), 138.57 (Ar), 135.68 (Ar), 131.96 (Ar), 131.89 (Ar), 131.02 (Ar), 130.53 (Ar), 130.09 (Ar), 129.43 (Ar), 129.20 (Ar), 128.57 (Ar), 128.42 (Ar), 128.34 (Ar), 127.44 (Ar), 123.15 (Ar), 113.65 (Ar), 110.99 (Ar), 104.09 (Ar), 44.26 (CH_2), 12.43 (CH_3). FT-IR Vmax (cm^{-1}): 3314 (*N–H stretch*), 3132 (*Ar–H or N–H stretch*), 2970 (*C–H stretch, N-ethyl*), 1613 (*C═N or Ar–C═C*), 1587 (*C═N or N–C═S,*), 1550 (*N–H bend or Ar–C═C*), 1509 (*Ar–C–C stretch*), 1406 (*CH_2 bend, N-ethyl*), 1367 (*S═O sym. stretch, sulfonate*), 1314 (*S═O asym. stretch, sulfonate*), 1180 (*C–N or S–O stretch*), 1132 (*C–N or S–O stretch*), 1080 (*C–N stretch or Ar–C–H bend*), 1012 (*C–N stretch or Ar–C–H bend*), 952 (*N–H wag or C═S*), 907 (*C–H out-of-plane, aromatic*), 757 (*Ar–C–H out-of-plane bend*), 690 (*aromatic ring deformation*); HPLC: $CH_3CN:H_2O = 80:20$; Rt: 5.440 min, purity: 98.10%; Elemental Analysis: CHN Calcd: C, 59.30; H, 4.80; N, 9.88; found: C, 59.54; H, 4.94; N, 9.97; ESI-HRMS (m/z): chemical formula: $C_{28}H_{27}{}^{35}ClN_4O_3S_2$, calcd $[M + H]^+$: 567.12914, found $[M + H]^+$: 567.12717 *(1.97 ppm deviation)*, calcd $[M+Na]^+$: 589.11108, found $[M+Na]^+$: 589.10886 *(2.22 ppm deviation)*, chemical formula: $C_{28}H_{27}{}^{37}ClN_4O_3S_2$, calcd $[M + H]^+$: 569.12320, found $[M + H]^+$: 569.12464 *(1.44 ppm deviation)*, calcd $[M + Na]^+$: 591.10510, found $[M + Na]^+$: 591.10654 *(1.44 ppm deviation)*.

(*E*)-5-(Diethylamino)-2-({2-[(2,6-dimethylphenyl)carbamothioyl] hydrazono}methyl)phenyl naphthalene-2-sulfonate (**5j**): Yield: 86%; M.P: 219°C–221°C; Color: off-white; ^{1}H-NMR: δ (400 MHz, DMSO-d_6) 11.62 (1 H, s, NH-N═C), 9.60 (1 H, s, S═C-NH-R), 8.68 (1 H, d, $J = 2.0$ Hz, Ar), 8.25 (3 H, dd, $J = 16.0$, 7.7 Hz, Ar), 8.09 (2 H, dd, $J = 20.5$, 8.6 Hz, Ar), 8.00 (1 H, dd, $J = 8.7$, 2.0 Hz, Ar), 7.80 (1 H, t, $J = 7.5$ Hz, Ar), 7.72 (1 H, t, $J = 7.5$ Hz, Ar), 7.20–7.02 (3 H, m, Ar), 6.55 (1 H, dd, $J = 9.0$, 2.5 Hz, Ar), 5.90 (1 H, d, $J = 2.5$ Hz, Ar), 3.09 (4 H, q, $J = 7.0$ Hz, CH_2), 2.16 (6 H, s, CH_3), 0.79 (6 H, t, $J = 6.9$ Hz, CH_3); ^{13}C-NMR (100 MHz, DMSO-d_6) δ 176.59 (C═S), 149.78 (C═N), 149.64 (Ar), 137.87 (Ar), 137.72 (Ar), 136.95 (Ar), 135.68 (Ar), 131.98 (Ar), 131.05 (Ar), 130.52 (Ar), 130.07 (Ar), 129.09 (Ar), 128.58 (Ar), 128.42 (Ar), 127.97 (Ar), 127.22 (Ar), 123.19 (Ar), 114.13 (Ar), 111.05 (Ar), 104.00 (Ar), 44.22 (CH_2), 18.56 (CH_3), 12.42 (CH_3); FT-IR Vmax (cm^{-1}): 3295 (*N–H stretch*), 3094 (*Ar–H or N–H stretch*), 2966 (*C–H stretch, N-ethyl*), 1612 (*C═N or Ar–C═C*), 1590 (*C═N or N–C═S*), 1509 (*Ar–C–C stretch*), 1435 (*CH_2 bend, N-ethyl*), 1395 (*S═O sym. stretch, sulfonate*), 1284 (*S═O asym. stretch, sulfonate*), 1262 (*C–N or S–O stretch*), 1187 (*C–N or S–O stretch*), 1068 (*C–N stretch or Ar–C–H bend*), 1017 (*C–N stretch or Ar–C–H bend*), 965 (*N–H wag or C═S*), 855 (*C–H out-of-plane, aromatic*), 759 (*Ar–C–H out-of-plane bend*), 548 (*S–O bending or sulfonate fingerprint*); HPLC: $CH_3CN:H_2O = 80:20$; R_t: 4.186 min, purity: 99.77%; Elemental Analysis: CHN Calcd: C, 64.26; H, 5.75; N, 9.99; found: C, 64.45; H, 5.93; N, 10.46; ESI-HRMS (*m/z*): chemical formula: $C_{30}H_{32}N_4O_3S_2$, calcd $[M + H]^+$: 561.19941, found $[M + H]^+$: 561.19732 *(2.09 ppm deviation)*, calcd $[M + Na]^+$: 583.18135, found $[M + Na]^+$: 583.17899 *(2.36 ppm deviation)*.

(*E*)-5-(Diethylamino)-2-({2-[(3-methoxyphenyl)carbamothioyl] hydrazono}methyl)phenyl naphthalene-2-sulfonate (**5k**): Yield: 90%; M.P: 185°C–187°C; Color: pale yellow; ^{1}H-NMR: δ (400 MHz, DMSO-d_6) 11.72 (1 H, s, NH–N═C), 9.77 (1 H, s, S═C–NH–R), 8.66 (1 H, d, $J = 2.0$ Hz, Ar), 8.25 (3 H, dd, $J = 15.9$, 7.0 Hz, Ar), 8.11 (1 H, d, $J = 8.1$ Hz, Ar), 8.05–7.94 (2 H, m, Ar), 7.83–7.67 (2 H, m, Ar), 7.31 (1 H, t, $J = 2.2$ Hz, Ar), 7.28–7.17 (2 H, m, Ar), 6.76 (1 H, dd, $J = 8.2$, 2.5 Hz, Ar), 6.59 (1 H, dd, $J = 9.1$, 2.5 Hz, Ar), 5.94 (1 H, d, $J = 2.5$, Ar), 3.76 (3 H, s, O-CH_3, 3.11 (4 H, q, $J = 7.0$ Hz, CH_2), 0.81 (6 H, t, $J = 7.0$ Hz, CH_3). ^{13}C-NMR (100 MHz, DMSO-d_6) δ 175.16 (C═S), 159.45 (C═N), 149.92 (Ar), 149.85 (Ar), 140.67 (Ar), 138.81 (Ar), 135.67 (Ar), 131.96 (Ar), 131.93 (Ar), 131.02 (Ar), 130.53 (Ar), 130.51 (Ar), 130.08 (Ar), 129.28 (Ar), 129.16 (Ar), 128.57, 128.42 (Ar), 123.15 (Ar), 117.67 (Ar), 113.68 (Ar), 111.17 (Ar), 111.01 (Ar), 110.93 (Ar), 104.10 (Ar), 55.60 (O-CH_3), 44.27 (CH_2), 12.42 (CH_3); FT-IR Vmax (cm^{-1}): 3309 (*N–H stretch*), 3126 (*Ar–H or N–H stretch*), 2965 (*C–H stretch, N-ethyl*), 2833 (*C–H stretch, aliphatic*), 1610 (*C═N or Ar–C═C*), 1592 (*C═N or N–C═S*), 1547 (*N–H bend or Ar–C═C*), 1511 (*Ar–C–C stretch*), 1453 (*CH_2 bend, N-ethyl*), 1407 (*CH_2 or S═O sym. stretch*), 1365 (*S═O sym. stretch, sulfonate*), 1265 (*S═O asym. stretch, sulfonate*), 1181 (*C–N or S–O stretch*), 1080 (*C–N stretch or Ar–C–H bend*), 1042 (*C–N stretch or Ar–C–H bend*), 952 (*N–H wag or C═S,*), 859 (*C–H out-of-plane, aromatic*), 759 (*Ar–C–H out-of-plane bend*), 649 (*aromatic ring deformation or S–O bend*); HPLC: CH3CN: H2O = 80: 20; tR: 3.928 min, purity: 99.42%; Elemental Analysis: CHN Calcd: C, 61.90; H, 5.37; N, 9.96; found: C, 62.45; H, 5.67; N, 10.14; ESI-HRMS (*m/z*): chemical formula: $C_{29}H_{30}N_4O_4S_2$, calcd $[M + H]^+$: 563.17867, found $[M + H]^+$: 563.17684 *(1.83 ppm deviation)*, calcd $[M + Na]^+$: 585.16062, found $[M + Na]^+$: 585.15858 *(2.04 ppm deviation)*.

(*E*)-5-(Diethylamino)-2-({2-[(4-fluorophenyl)carbamothioyl] hydrazono}methyl)phenyl naphthalene-2-sulfonate (**5l**): Yield: 95%; M.P: 183°C–185°C; Color: yellow; ^{1}H-NMR: δ (400 MHz, DMSO-d_6) 11.72 (1 H, s, NH–N═C), 9.83 (1 H, s, S═C–NH–R),

8.66 (1 H, d, $J = 1.9$ Hz, Ar), 8.31–8.20 (3 H, m, Ar), 8.15–8.07 (1 H, m, Ar), 8.05–7.95 (2 H, m, Ar), 7.79 (1 H, ddd, $J = 8.2$, 6.9, 1.3 Hz, Ar), 7.72 (1 H, ddd, $J = 8.1$, 6.8, 1.3 Hz, Ar), 7.59–7.48 (2 H, m, Ar), 7.25–7.14 (2 H, m, Ar), 6.58 (1 H, dd, $J = 9.1$, 2.5 Hz, Ar), 5.94 (1 H, d, $J = 2.5$ Hz, Ar), 3.11 (4 H, q, $J = 7.0$ Hz, CH_2), 0.81 (6 H, t, $J = 7.0$ Hz, CH_3); ^{13}C-NMR (100 MHz, DMSO-d_6) δ 175.86 (C═S), 161.16 (C═N), 158.76 (Ar), 149.93 (Ar), 149.85 (Ar), 138.77 (Ar), 135.95 (Ar), 135.92 (Ar), 135.68 (Ar), 131.96 (Ar), 131.92 (Ar), 131.02 (Ar), 130.53 (Ar), 130.09 (Ar), 129.17 (Ar), 128.57 (Ar), 128.43 (Ar), 128.20 (Ar), 128.12 (Ar), 123.15 (Ar), 115.20 (Ar), 114.98 (Ar), 113.74 (Ar), 110.98 (Ar), 104.08 (Ar), 44.26 (CH_2), 12.43 (CH_3); FT-IR Vmax (cm^{-1}): 3314 (*N–H stretch*), 3133 (*Ar–H or N–H stretch*), 2967 (*C–H stretch, N-ethyl*), 2920 (*C–H stretch, aliphatic*), 1610 (*C═N or Ar–C═C*), 1551 (*N–H bend or Ar–C═C*), 1504 (*Ar–C–C stretch*), 1404 (*CH_2 bend, N-ethyl*), 1363 (*S═O sym. stretch, sulfonate*), 1301 (*S═O asym. stretch, sulfonate*), 1266 (*C–N or S–O stretch*), 1180 (*C–N or S–O stretch*), 1057 (*C–N stretch or Ar–C–H bend*), 950 (*N–H wag or C═S*), 906 (*C–H out-of-plane, aromatic*), 860 (*C–H out-of-plane, aromatic*), 758 (*Ar–C–H out-of-plane bend*), 650 (*aromatic ring deformation or S–O bend*); HPLC: $CH_3CN:H_2O = 80:20$; R_t: 3.838 min, purity: 99.61%; Elemental Analysis: CHN Calcd: C, 61.07; H, 4.94; N, 10.17; found: C, 61.45; H, 5.43; N, 10.67; ESI-HRMS (*m/z*): chemical formula: $C_{28}H_{27}FN_4O_3S_2$, calcd $[M + H]^+$: 551.15869, found $[M + H]^+$: 551.15653 *(2.16 ppm deviation)*, calcd $[M + Na]^+$: 573.14063, found $[M + Na]^+$: 573.13842 *(2.21 ppm deviation)*.

(*E*)-5-(Diethylamino)-2-{[2-(methylcarbamothioyl)hydrazono]methyl}phenyl naphthalene-2-sulfonate (**5m**): Yield: 93%; M.P: 205°C–207°C; Color: off-white; ^{1}H-NMR: δ (400 MHz, DMSO-d_6) 11.35 (1 H, s, NH–N═C), 8.64 (1 H, d, $J = 1.9$ Hz, S═C–NH–R), 8.30–8.14 (4 H, m, Ar), 8.11 (1 H, d, $J = 8.2$ Hz, Ar), 7.98 (1 H, dd, $J = 8.8$, 2.0 Hz, Ar), 7.87 (1 H, d, $J = 9.0$ Hz, Ar), 7.75 (2 H, dt, $J = 29.8$, 7.3 Hz, Ar), 6.58 (1 H, dd, $J = 9.1$, 2.6 Hz, Ar), 5.93 (1 H, d, $J = 2.6$ Hz, Ar), 3.10 (4 H, q, $J = 7.0$ Hz, CH_2), 2.97 (3 H, d, $J = 4.5$ Hz, *N*-CH_3), 0.81 (6 H, t, $J = 6.9$ Hz, CH_3); ^{13}C-NMR (100 MHz, DMSO-d_6) δ 177.63 (C═S), 149.70 (C═N), 149.59 (Ar), 137.42 (Ar), 135.65 (Ar), 131.94 (Ar), 130.98 (Ar), 130.49 (Ar), 130.07 (Ar), 128.56 (Ar), 128.48 (Ar), 128.41 (Ar), 123.13 (Ar), 114.09 (Ar), 111.05 (Ar), 104.05 (Ar), 44.22 (CH_2), 31.14 (*N*-CH_3), 12.43 (CH_3); FT-IR Vmax (cm^{-1}): 3343 (*N–H stretch*), 3134 (*Ar–H or N–H stretch*), 2964 (*C–H stretch, N-ethyl*), 1615 (*C═N or Ar–C═C*), 1548 (*N–H bend or Ar–C═C*), 1515 (*Ar–C–C stretch*), 1470 (*CH_2 bend, N-ethyl*), 1443 (*CH_2 or C–N bend*), 1350 (*S═O sym. stretch, sulfonate*), 1260 (*S═O asym. stretch, sulfonate*), 1187 (*C–N or S–O stretch*), 1130 (*C–N or S–O stretch*), 1016 (*C–N stretch or Ar–C–H bend*), 955 (*N–H wag or C═S*), 885 (*C–H out-of-plane, aromatic*), 815 (*C–H out-of-plane, aromatic*), 758 (*Ar–C–H out-of-plane bend*); HPLC: $CH_3CN:H_2O = 80:20$; R_t: 2.489 min, purity: 96.03%; Elemental Analysis: CHN Calcd: C, 58.70; H, 5.57; N, 11.91; found: C, 58.94; H, 5.77; N, 12.30; ESI-HRMS (*m/z*): chemical formula: $C_{23}H_{26}N_4O_3S_2$, calcd $[M + H]^+$: 471.15246, found $[M + H]^+$: 471.15087 *(1.59 ppm deviation)*, calcd $[M + Na]^+$: 493.13440, found $[M + Na]^+$: 493.13249 *(0.91 ppm deviation)*.

(*E*)-2-[(2-Carbamothioylhydrazono)methyl]-5-(diethylamino) phenyl naphthalene-2-sulfonate (**5n**): Yield: 91%; M.P: 245°C–247°C; Color: off-white; ^{1}H-NMR: δ (400 MHz, DMSO-d_6) 11.33 (1 H, s, NH–N═C), 8.65 (1 H, d, $J = 1.9$ Hz, S = C-NH-R), 8.27– 8.21 (2 H, m, Ar), 8.19 (1 H, s, HC═N), 8.12 (1 H, dd, $J = 8.1$, 1.2 Hz, Ar), 8.04–7.96 (2 H, m, Ar), 7.88 (1 H, d, $J = 9.0$ Hz, Ar), 7.79 (1 H, ddd, $J = 8.2$, 6.8, 1.3 Hz, Ar), 7.72 (2 H, ddd, $J = 8.1$, 5.8, 1.3 Hz, Ar), 6.57 (1 H, dd, $J = 9.1$, 2.6 Hz, Ar), 5.90 (1 H, d, $J = 2.5$ Hz, Ar), 3.09 (4 H, q, $J = 7.0$ Hz, CH_2), 0.79 (6 H, t, $J = 7.0$ Hz, CH_3); ^{13}C-NMR (101 MHz, DMSO-d_6) δ 177.70 (C═S), 149.75 (C═N), 149.64 (Ar), 138.05 (Ar), 135.66 (Ar), 131.99 (Ar), 131.95 (Ar), 131.00 (Ar), 130.51 (Ar), 130.06 (Ar), 128.67 (Ar), 128.57 (Ar), 128.42 (Ar), 123.14 (Ar), 113.99 (Ar), 111.09 (Ar), 103.99 (Ar), 44.21 (CH_2), 12.42 (CH_3); FT-IR Vmax (cm^{-1}): 3299 (*N–H stretch*), 3131 (*N–H stretch, NH or Ar–H*), 3088 (*Ar–H stretch*), 2964 (*C–H stretch, N-ethyl*), 2922 (*C–H stretch, aliphatic*), 2853 (*C–H stretch, aliphatic*), 1612 (*C═N or Ar–C═C stretch*), 1588 (*N–C═S or C═N,*), 1507 (*Ar–C–C stretch*), 1407 (*CH_2 bend, N-ethyl*), 1375 (*S═O sym. stretch, sulfonate*), 1338 (*C–N or S═O bend*), 1306 (*S═O asym. stretch, sulfonate*), 1201 (*C–N or S–O stretch*), 1127 (*C–N or S–O stretch*), 1079 (*C–N stretch or Ar–C–H bend*), 953 (*N–H wag or C═S*), 888 (*C–H out-of-plane, aromatic*), 757 (*Ar–C–H out-of-plane bend*); HPLC: $CH_3CN:H_2O = 80:20$; R_t: 1.948 min, purity: 99.38%; Elemental Analysis: CHN Calcd: C, 57.87; H, 5.30; N, 12.27; found: C, 57.93; H, 5.46; N, 12.48; ESI-HRMS (*m/z*): chemical formula: $C_{22}H_{24}N_4O_3S_2$, calcd $[M + H]^+$: 457.13681, found $[M + H]^+$: 457.13494 *(1.87 ppm deviation)*, calcd $[M + Na]^+$: 479.11875, found $[M + Na]^+$: 479.11701 *(1.74 ppm deviation)*.

(*E*)-5-(Diethylamino)-2-({2-[(3-nitrophenyl)carbamothioyl]hydrazono}methyl)phenyl naphthalene-2-sulfonate (**5o**): Yield: 94%; M.P: 176°C–178°C; Color: yellow; ^{1}H-NMR: δ (400 MHz, DMSO-d_6) 11.97 (1 H, s, NH-N═C), 10.13 (1 H, s, S═C-NH-R), 8.66 (2 H, d, $J = 2.0$ Hz, Ar), 8.32 (1 H, s, HC = N), 8.24 (2 H, t, $J = 8.2$ Hz, Ar), 8.11 (2 H, d, $J = 8.1$ Hz, Ar), 8.08–7.95 (3 H, m, Ar), 7.83–7.69 (2 H, m, Ar), 7.64 (1 H, t, $J = 8.2$ Hz, Ar), 6.62 (1 H, dd, $J = 9.1$, 2.6 Hz, Ar), 5.99 (1 H, d, $J = 2.6$ Hz, Ar), 3.13 (4 H, q, $J = 7.1$ Hz, CH_2), 0.83 (6 H, t, $J = 6.9$ Hz, CH_3); ^{13}C-NMR (100 MHz, DMSO-d_6) δ 175.26 (C═S), 150.10 (C═N), 150.04 (Ar), 147.72 (Ar), 140.84 (Ar), 139.56 (Ar), 135.68 (Ar), 131.96 (Ar), 131.83 (Ar), 131.73 (Ar), 131.03 (Ar), 130.53 (Ar), 130.49 (Ar), 130.09 (Ar), 129.60 (Ar), 129.16 (Ar), 128.55 (Ar), 128.42 (Ar), 123.14 (Ar), 119.78 (Ar), 119.69 (Ar), 113.49 (Ar), 111.01 (Ar), 104.14 (Ar), 44.29 (CH_2), 12.42 (CH_3); FT-IR Vmax (cm^{-1}): 3298 (*N–H stretch*), 3131 (*N–H stretch, NH or Ar–H*), 2964 (*C–H stretch, N-ethyl*), 2921 (*C–H stretch, aliphatic*), 2854 (*C–H stretch, aliphatic*), 1612 (*C═N or Ar–C═C stretch*), 1589 (*N–C═S or NO_2 asym. stretch*), 1508 (*Ar–C–C stretch or NO_2 asym. stretch*), 1406 (*CH_2 bend, N-ethyl*), 1374 (*NO_2 sym. stretch*), 1307 (*S═O asym. stretch, sulfonate*), 1264 (*C–N or S–O stretch*), 1061 (*C–N stretch or Ar–C–H bend*), 1009 (*C–N stretch or Ar–C–H bend*), 953 (*N–H wag or C═S*), 862 (*C–H out-of-plane, aromatic*), 757 (*Ar–C–H out-of-plane bend*); HPLC: $CH_3CN:H_2O = 80:20$; R_t: 3.987 min, purity: 98.53%; Elemental Analysis: CHN Calcd: C, 58.22; H, 4.71; N, 12.12; found: C, 58.46; H, 4.93; N, 12.43; ESI-HRMS (*m/z*): chemical formula: $C_{28}H_{27}N_5O_5S_2$, calcd $[M + H]^+$: 578.15319, found $[M + H]^+$: 578.15113 *(2.06 ppm deviation)*, calcd $[M + Na]^+$: 600.13513, found $[M + Na]^+$: 600.1299 *(2.14 ppm deviation)*.

(*E*)-2-{[2-(Cyclohexylcarbamothioyl)hydrazono]methyl}-5-(diethylamino)phenyl naphthalene-2-sulfonate (**5p**): Yield: 90%; M.P: 194°C–196°C; Color: pale yellow; ^{1}H-NMR: δ (400 MHz, DMSO-d_6) 11.29 (1 H, s, NH-N═C), 8.64 (1 H, d,

$J = 2.0$ Hz, S=C–NH–R), 8.22 (2 H, t, $J = 8.8$ Hz, Ar), 8.15 (1 H, s, HC=N), 8.11 (1 H, d, $J = 8.2$ Hz, Ar), 7.97 (1 H, dd, $J = 8.7$, 2.0 Hz, Ar), 7.83–7.68 (4 H, m, Ar), 6.58 (1 H, dd, $J = 9.1$, 2.5 Hz, Ar), 5.90 (1 H, d, $J = 2.5$ Hz, Ar), 4.16 (1 H, dp, $J = 15.6$, 5.7, 4.5 Hz, Cy. Hex), 3.08 (4 H, q, $J = 7.0$ Hz, CH_2), 1.93–1.79 (2 H, m, Cy. Hex), 1.71 (2 H, dt, $J = 12.7$, 3.3 Hz, Cy. Hex), 1.60 (1 H, d, $J = 12.7$ Hz, Cy. Hex), 1.46–1.20 (4 H, m, Cy. Hex), 1.20–1.04 (1 H, m, Cy. Hex), 0.79 (6 H, t, $J = 7.0$ Hz, CH_3); ^{13}C-NMR (100 MHz, DMSO-d_6) δ 175.59 (C=S), 149.58 (C=N), 138.17 (Ar), 135.64 (Ar), 132.06 (Ar), 131.94 (Ar), 130.95 (Ar), 130.51 (Ar), 130.49 (Ar), 130.05 (Ar), 129.21 (Ar), 128.56 (Ar), 128.40 (Ar), 123.12 (Ar), 113.87 (Ar), 111.01 (Ar), 104.18(Ar), 52.82 (*N*-Cy. Hex), 44.25 (CH_2), 32.42 (Cy. Hex), 25.63 (Cy. Hex), 25.35 (Cy. Hex), 12.39 (CH_3); FT-IR Vmax (cm^{-1}): 3338 (*N–H stretch*), 3125 (*Ar–H or N–H stretch*), 2973 (*C–H stretch, N-ethyl*), 2927 (*C–H stretch, aliphatic*), 1616 (*C=N or Ar–C=C stretch*), 1541 (*N–H bend or Ar–C=C*), 1508 (*Ar–C–C stretch*), 1448 (*CH_2 bend, N-ethyl*), 1407 (*CH_2 or S=O sym. stretch, sulfonate*), 1373 (*S=O sym. stretch, sulfonate*), 1294 (*S=O asym. stretch, sulfonate*), 1214 (*C–N or S–O stretch*), 1183 (*C–N or S–O stretch*), 1089 (*C–N stretch or Ar–C–H bend*), 986 (*C–H out-of-plane, aromatic*), 953 (*N–H wag or C=S*), 861 (*C–H out-of-plane, aromatic*), 753 (*Ar–C–H out-of-plane bend*); HPLC: $CH_3CN:H_2O = 80:20$; R_t: 6.061 min, purity: 99.24%; Elemental Analysis: CHN Calcd: C, 62.43; H, 6.36; N, 10.40; found: C, 62.64; H, 6.57; N, 10.66. ESI-HRMS (*m/z*): chemical formula: $C_{28}H_{34}N_4O_3S_2$, calcd $[M + H]^+$: 539.21506, found $[M + H]^+$: 539.21319 *(1.87 ppm deviation)*, calcd $[M + Na]^+$: 561.19700, found $[M + Na]^+$: 561.19477 *(2.23 ppm deviation)*.

(*E*)-2-({2-[(4-Chlorobenzyl)carbamothioyl]hydrazono}methyl)-5-(diethylamino)phenyl naphthalene-2-sulfonate (**5q**): Yield: 90%; M.P: 198°C–200°C; Color: pale yellow; ^{1}H-NMR: δ (400 MHz, DMSO-d_6) 11.51 (1 H, s, NH-N°C=C), 8.83 (1 H, t, $J = 6.3$ Hz, S=C–NH–R), 8.65 (1 H, d, $J = 2.0$ Hz, Ar), 8.23 (3 H, q, $J = 5.1$ Hz, Ar, HC = N), 8.11 (1 H, d, $J = 8.1$ Hz, Ar), 7.97 (1 H, dd, $J = 8.8$, 2.0 Hz, Ar), 7.90 (1 H, d, $J = 9.0$ Hz, Ar), 7.79 (1 H, ddd, $J = 8.2$, 6.9, 1.3 Hz, Ar), 7.72 (1 H, ddd, $J = 8.2$, 6.9, 1.3 Hz, Ar), 7.44–7.30 (4 H, m, Ar), 6.56 (1 H, dd, $J = 9.0$, 2.5 Hz, Ar), 5.94 (1 H, d, $J = 2.5$ Hz, Ar), 4.78 (2 H, d, $J = 6.2$ Hz, *N*-CH_2), 3.10 (4 H, q, $J = 7.0$ Hz, CH_2), 0.80 (6 H, t, $J = 7.0$ Hz, CH_3); ^{13}C-NMR (101 MHz, DMSO-d_6) δ 177.44 (C=S), 149.80 (C=N), 149.68 (Ar), 139.12 (Ar), 138.01 (Ar), 135.66 (Ar), 131.95 (Ar), 131.89 (Ar), 131.67 (Ar), 131.02 (Ar), 130.49 (Ar), 130.07 (Ar), 129.58 (Ar), 128.54 (Ar), 128.41 (Ar), 123.16 (Ar), 113.94 (Ar), 111.02 (Ar), 104.06 (Ar), 46.28 (*N*-CH_2), 44.24 (CH_2), 12.42 (CH_3); FT-IR Vmax (cm^{-1}): 3357 (*N–H stretch*), 3146 (*N–H or Ar–H stretch*), 2370 (*possible overtone or combination band*), 2908 (*C–H stretch, aliphatic*), 1615 (*C=N or Ar–C=C stretch*), 1516 (*N–H bend or Ar–C=C*), 1487 (*Ar–C–C stretch*), 1409 (*CH_2 bend, N-ethyl*), 1301 (*S=O asym. stretch, sulfonate*), 1216 (*C–N or S–O stretch*), 1085 (*C–N stretch or Ar–C–H bend*), 1013 (*C–N stretch or Ar–C–H bend*), 958 (*N–H wag or C=S*), 856 (*C–H out-of-plane, aromatic*), 759 (*Ar–C–H out-of-plane bend*), 545 (*possibly S–S or other bending mode*); HPLC: $CH_3CN:H_2O = 80:20$, R_t: 5.011 min, purity: 96.94%; Elemental Analysis: CHN Calcd: C, 59.93; H, 5.03; N, 9.64; found: C, 60.23; H, 5.67; N, 9.87; ESI-HRMS (*m/z*): chemical formula: $C_{29}H_{29}{}^{35}ClN_4O_3S_2$, calcd $[M + H]^+$: 581.14479, found $[M + H]^+$: 581.14272 *(2.07 ppm deviation)*, calcd $[M+Na]^+$: 603.12673, found $[M + Na]^+$: 603.12440 *(2.33 ppm deviation)*, chemical formula: $C_{29}H_{29}{}^{37}ClN_4O_3S_2$, calcd $[M + H]^+$: 583.13890, found $[M + H]^+$: 583.14021 *(1.31 ppm deviation)*, calcd $[M + Na]^+$: 605.12080, found $[M + Na]^+$: 603.12220 *(1.40 ppm deviation)*.

(*E*)-5-(Diethylamino)-2-{[2-(o-tolylcarbamothioyl)hydrazono]methyl}phenyl naphthalene-2-sulfonate (**5r**): Yield: 93%; M.P: 189°C–191°C; Color: off-white. ^{1}H-NMR: δ (400 MHz, DMSO-d_6) 11.68 (1 H, s, NH–N=C), 9.69 (1 H, s, S=C–NH–R), 8.67 (1 H, d, $J = 2.0$ Hz, Ar), 8.25 (3 H, dd, $J = 17.0$, 8.5 Hz, Ar, HC=N), 8.12 (1 H, d, $J = 8.2$ Hz, Ar), 8.08–7.94 (2 H, m, Ar), 7.79 (1 H, ddd, $J = 8.2$, 6.9, 1.3 Hz, Ar), 7.72 (1 H, ddd, $J = 8.2$, 6.9, 1.3 Hz, Ar), 7.32 (1 H, dd, $J = 7.3$, 1.9 Hz, Ar), 7.22 (3 H, dtt, $J = 19.0$, 7.3, 3.9 Hz, Ar), 6.57 (1 H, dd, $J = 9.1$, 2.5 Hz, Ar), 5.93 (1 H, d, $J = 2.5$ Hz, Ar), 3.34 (3 H, s, CH_3), 3.10 (4 H, q, $J = 7.0$ Hz, CH_2), 0.80 (6 H, t, $J = 6.9$ Hz, CH_3); ^{13}C-NMR (100 MHz, DMSO-d_6) δ 176.46 (C=S), 149.86 (C=N), 149.73 (Ar), 138.55 (Ar), 138.17 (Ar), 135.68 (Ar), 135.59 (Ar), 131.97 (Ar), 131.94 (Ar), 131.03 (Ar), 130.52 (Ar), 130.45 (Ar), 130.08 (Ar), 128.98 (Ar), 128.94 (Ar), 128.57 (Ar), 128.42 (Ar), 126.90 (Ar), 126.26 (Ar), 123.17 (Ar), 113.96 (Ar), 111.06 (Ar), 104.05 (Ar), 44.24 (CH_2), 18.27 (CH_3), 12.42 (CH_3); FT-IR Vmax (cm^{-1}): 317 (*N–H stretch,*), 3122 (*N–H or Ar–H stretch*), 2967 (*C–H stretch, N-ethyl*), 1618 (*C=N or Ar–C=C stretch*), 1591 (*N–C=S or C=N,*), 1540 (*N–H bend or Ar–C=C*), 1482 (*Ar–C–C stretch*), 1410 (*CH_2 bend, N-ethyl*), 1356 (*S=O sym. stretch, sulfonate*), 1265 (*S=O asym. stretch, sulfonate*), 1185 (*C–N or S–O stretch*), 1063 (*C–N stretch or Ar–C–H bend*), 956 (*N–H wag or C=S*), 852 (*C–H out-of-plane, aromatic*), 754 (*Ar–C–H out-of-plane bend*); HPLC: $CH_3CN:H_2O = 80:20$; R_t: 3.903 min, purity: 98.26%; Elemental Analysis: CHN Calcd: C, 63.71; H, 5.53; N, 10.25; found: C, 63.92; H, 5.68; N, 10.44; ESI-HRMS (*m/z*): chemical formula: $C_{29}H_{30}N_4O_3S_2$, calcd $[M + H]^+$: 547.18376, found $[M + H]^+$: 547.18202 *(1.74 ppm deviation)*, calcd $[M + Na]^+$: 569.16570, found $[M + Na]^+$: 569.16380 *(1.90 ppm deviation)*.

(*E*)-2-{[2-(Benzylcarbamothioyl)hydrazono]methyl}-5-(diethylamino)phenyl naphthalene-2-sulfonate (**5s**): Yield: 93%; M.P: 186°C–188°C, Color: yellow; ^{1}H-NMR: δ (400 MHz, DMSO-d_6) 11.46 (1 H, s, NH–N=C), 8.78 (1 H, t, $J = 6.3$ Hz, S=C–NH–R), 8.65 (1 H, d, $J = 1.9$ Hz, Ar), 8.27–8.17 (3 H, m, Ar, HC=N), 8.11 (1 H, d, $J = 8.2$ Hz, Ar), 7.97 (1 H, dd, $J = 8.7$, 2.0 Hz, Ar), 7.89 (1 H, d, $J = 9.0$ Hz, Ar), 7.84–7.75 (1 H, m, Ar), 7.75–7.64 (1 H, m, Ar), 7.32 (4 H, d, $J = 5.6$ Hz, Ar), 7.24 (1 H, td, $J = 5.8$, 2.5 Hz, Ar), 6.56 (1 H, dd, $J = 9.1$, 2.5 Hz, Ar), 5.94 (1 H, d, $J = 2.5$ Hz, Ar), 4.80 (2 H, d, $J = 6.2$ Hz, *N*-CH_2), 3.10 (4 H, q, $J = 7.0$ Hz, CH_2), 0.80 (6 H, t, $J = 7.0$ Hz, CH_3); ^{13}C-NMR (101 MHz, DMSO-d_6) δ 177.41 (C=S), 149.77 (C=N), 149.66 (Ar), 140.02 (Ar), 137.87 (Ar), 131.95 (Ar), 131.88 (Ar), 131.02 (Ar), 130.49 (Ar), 130.07 (Ar), 128.60 (Ar), 128.56 (Ar), 128.41 (Ar), 127.67 (Ar), 127.15 (Ar), 123.16 (Ar), 113.96 (Ar), 104.06 (Ar), 46.93 (*N*-CH_2), 44.24 (CH_2), 12.42 (CH_3); FT-IR Vmax (cm^{-1}): 3359 (*N–H stretch*), 3154 (*N–H or Ar–H stretch*), 2970 (*C–H stretch, N-ethyl*), 1613 (*C=N or Ar–C=C stretch*), 1518 (*N–H bend or Ar–C=C*), 1451 (*CH_2 bend, N-ethyl*), 1409 (*CH_2 bend or Ar–C–C stretch*), 1267 (*S=O asym. stretch, sulfonate*), 1217 (*C–N or S–O stretch*), 1084 (*C–N stretch or Ar–C–H bend*), 1067 (*C–N stretch or Ar–C–H bend*), 1019 (*C–N stretch or Ar–C–H bend*), 960 (*N–H wag or C=S*), 761 (*Ar–C–H out-of-plane bend*); HPLC: $CH_3CN:H_2O = 80:20$; t_R: 3.819 min, purity: 98.14%; Elemental Analysis: CHN

Calcd: C, 63.71; H, 5.53; N, 10.25; found: C, 63.791; H, 5.64; N, 10.34; ESI-HRMS (*m/z*): chemical formula: $C_{29}H_{30}N_4O_3S_2$, calcd $[M+H]^+$: 547.18376, found $[M+H]^+$: 547.18182 *(1.94 ppm deviation)*, calcd $[M+Na]^+$: 569.16570, found $[M+Na]^+$: 569.16373 *(1.97 ppm deviation)*.

(*E*)-5-(Diethylamino)-2-{[2-(phenethylcarbamothioyl)hydrazono] methyl}phenyl naphthalene-2-sulfonate (**5t**): Yield: 95%; M.P: 195°C–197°C; Color: pale yellow; ^{1}H-NMR: δ (400 MHz, DMSO-d_6) 11.40 (1 H, s, NH-N=C), 8.65 (1 H, d, $J = 2.0$ Hz, S=C–NH–R), 8.31–8.16 (4 H, m, Ar, HC=N), 8.11 (1 H, d, $J = 8.2$ Hz, Ar), 7.98 (1 H, dd, $J = 8.8$, 2.0 Hz, Ar), 7.84–7.75 (2 H, m, Ar), 7.72 (1 H, ddd, $J = 8.2$, 6.8, 1.3 Hz, Ar), 7.37–7.17 (5 H, m, Ar), 6.60 (1 H, dd, $J = 9.1$, 2.5 Hz, Ar), 5.94 (1 H, d, $J = 2.5$ Hz, Ar), 3.73 (2 H, ddd, $J = 9.4$, 7.6, 5.8 Hz, *N*-CH_2), 3.11 (4 H, q, $J = 7.0$ Hz, CH_2), 2.89 (2 H, dd, $J = 9.1$, 6.4 Hz, CH_2), 0.81 (6 H, t, $J = 7.0$ Hz, CH_3); ^{13}C-NMR (100 MHz, DMSO-d_6) δ 176.83 (C=S), 149.75 (C=N), 149.66 (Ar), 139.75 (Ar), 137.68 (Ar), 135.66 (Ar), 131.95 (Ar), 131.93 (Ar), 131.00 (Ar), 130.50 (Ar), 130.06 (Ar), 129.06 (Ar), 128.93 (Ar), 128.56 (Ar), 128.42 (Ar), 126.65 (Ar), 123.14 (Ar), 113.99 (Ar), 111.05 (Ar), 104.10 (Ar), 45.37 (*N*-CH_2), 44.24 (CH_2), 35.42 (CH_3), 12.43 (CH_3); FT-IR Vmax (cm^{-1}): 3351 (*N–H stretch*,), 3124 (*N–H or Ar–H stretch*), 3055 (*Ar–H stretch*), 2964 (*C–H stretch, N-ethyl*), 2925 (*C–H stretch, aliphatic*), 1612 (*C=N or Ar–C=C stretch*), 1542 (*N–H bend or Ar–C=C*), 1513 (*Ar–C–C stretch*), 1451 (*CH_2 bend, N-ethyl*), 1401 (*CH_2 bend or Ar–C–C stretch*), 1378 (*S=O sym. stretch, sulfonate*), 1266 (*S=O asym. stretch, sulfonate*), 1123 (*C–N or S–O stretch*), 949 (*N–H wag or C=S*), 857 (*C–H out-of-plane, aromatic*), 754 (*Ar–C–H out-of-plane bend*); HPLC: $CH_3CN:H_2O = 80:20$; R_t: 4.649 min, purity: 99.32%; Elemental Analysis: CHN Calcd: C, 64.26; H, 5.75; N, 9.99; found: C, 64.48; H, 5.93; N, 10.19; ESI-HRMS (*m/z*): chemical formula: $C_{30}H_{32}N_4O_3S_2$, calcd $[M+H]^+$: 561.19941, found $[M+H]^+$: 561.19773 *(1.68 ppm deviation)*, calcd $[M+Na]^+$: 583.18135, found $[M+Na]^+$: 583.17930 *(2.05 ppm deviation)*.

(*E*)-2-({2-[(2,6-Dichlorophenyl)carbamothioyl]hydrazono} methyl)-5-(diethylamino)phenyl naphthalene-2-sulfonate (**5u**): Yield: 94%; M.P: 226°C–228°C; Color: pale yellow; ^{1}H-NMR: δ (400 MHz, DMSO-d_6) 11.89 (1 H, s, NH–N=C), 9.86 (1 H, s, S=C–NH–R), 8.68 (1 H, d, $J = 1.9$ Hz, Ar), 8.32 (1 H, s, HC=N), 8.25 (2 H, t, $J = 8.4$ Hz, Ar), 8.17–8.04 (2 H, m, Ar), 8.01 (1 H, dd, $J = 8.7$, 2.0 Hz, Ar), 7.80 (1 H, ddd, $J = 8.2$, 6.9, 1.3 Hz, Ar), 7.72 (1 H, ddd, $J = 8.1$, 6.9, 1.3 Hz, Ar), 7.54 (2 H, d, $J = 8.1$ Hz, Ar), 7.36 (1 H, dd, $J = 8.6$, 7.6 Hz, Ar), 6.58 (1 H, dd, $J = 9.2$, 2.5 Hz, Ar), 5.92 (1 H, d, $J = 2.5$ Hz, Ar), 3.10 (4 H, q, $J = 7.0$ Hz, CH_2), 0.79 (6 H, t, $J = 7.0$ Hz, CH_3); ^{13}C-NMR (100 MHz, DMSO-d_6) δ 176.95 (C=S), 149.97 (C=N), 149.83 (Ar), 138.55 (Ar), 135.74 (Ar), 135.72 (Ar), 135.69 (Ar), 131.98 (Ar), 131.91 (Ar), 131.07 (Ar), 130.53 (Ar), 130.08 (Ar), 129.68 (Ar), 128.91 (Ar), 128.71 (Ar), 128.61 (Ar), 128.44 (Ar), 123.18 (Ar), 113.86 (Ar), 111.03 (Ar), 103.98 (Ar), 44.24 (CH_2), 12.41 (CH_3); FT-IR Vmax (cm^{-1}): 3318 (*N–H stretch*), 3130 (*N–H or Ar–H stretch*), 2970 (*C–H stretch, N-ethyl*), 1612 (*C=N or Ar–C=C stretch*), 1588 (*N–C=S or C=N*), 1543 (*N–H bend or Ar–C=C*), 1521 (*N–H bend or Ar–C=C*), 1435 (*CH_2 bend, N-ethyl*), 1373 (*S=O sym. stretch, sulfonate*), 1350 (*S=O sym. stretch, sulfonate*), 1222 (*S=O asym. stretch, sulfonate*), 1166 (*C–N or S–O stretch*), 1068 (*C–N stretch or Ar–C–H bend*), 956 (*N–H wag or C=S*), 842 (*C–H out-of-plane, aromatic*), 777 (*C–Cl stretch, dichlorobenzene*), 757 (*C–Cl stretch, dichlorobenzene*), 546 (*C–Cl bending or skeletal vibration*); HPLC: $CH_3CN:H_2O = 80:20$; R_t: 3.388 min, purity: 98.81%; Elemental Analysis: CHN anal. Calcd: C, 55.90; H, 4.36; N, 9.31; found: C, 56.34; H, 4.47; N, 9.52; ESI-HRMS (*m/z*): chemical formula: $C_{28}H_{26}{}^{35}Cl_2N_4O_3S_2$, calcd $[M+H]^+$: 601.09016, found $[M+H]^+$: 601.08809 *(2.07 ppm deviation)*, calcd $[M+Na]^+$: 623.07211, found $[M+Na]^+$: 623.06722 *(4.89 ppm deviation)*, chemical formula: $C_{28}H_{26}{}^{37}Cl_2N_4O_3S_2$, calcd $[M+H]^+$: 603.08420, found $[M+H]^+$: 603.08546 *(1.26 ppm deviation)*, calcd $[M+Na]^+$: 625.06620, found $[M+Na]^+$: 625.06722 *(1.02 ppm deviation)*.

4.2 | Inhibition Assays

4.2.1 | Activity and Inhibition Test for AChE and BChE

Both acetylcholine iodide (AChI) and butyrylcholine iodide (BChI) were used as substrates for the enzymatic hydrolysis reactions, with 5,5′-dithiobis(2-nitrobenzoic acid) (DTNB) serving as a common reagent for detecting the activities of AChE and BChE. The assay was conducted: 1 mL of 1.0 M Tris/HCl buffer (pH 8.0) was mixed with 10 µL of the sample solution in deionized water. To this mixture, 50 µL of AChE or BChE enzyme solution was added, and the reaction was incubated at room temperature for 10 min. After incubation, 50 µL of DTNB (0.5 mM) was introduced, followed by the addition of 50 µL of either AChI or BChI (10 mM), initiating the enzymatic reaction. The hydrolysis of the substrates was monitored spectrophotometrically by measuring the absorbance at 412 nm, corresponding to the formation of the yellow-colored 5-thio-2-nitrobenzoate anion. This color change is due to the reaction of DTNB with thiocholine released during the hydrolysis of AChI or BChI. For every inhibitor that was utilized, IC_{50} and K_i values were determined. In this study, C7512- BChE from equine serum and C3389- AChE from *Electrophorus electricus* (electric eel) were purchased from Sigma Aldrich. For inhibitors exhibiting an inhibitory effect, an activity (%)-[I] graph was created, and from this graph, inhibitor doses (IC_{50} values) resulting in 50% inhibition were computed [59–62].

4.2.2 | Study of MAO-A inhibition

The in vitro fluorometric technique was used to assess each newly generated substance's inhibitory activity against hMAO-A and hMAO-B. In a horseradish peroxidase coupling reaction, the oxired reagent (10-acetyl-3,7-dihydroxyphenoxazine) detects H_2O_2, a result of the oxidative deamination of tyramine, which is utilized as an MAO substrate. The test was carried out in two steps. First, each compound's concentrations of 10^{-3} and 10^{-4} M were investigated. In the second step, substances that demonstrated inhibitory activity at a concentration of 10^{-5}–10^{-9} M more than 50% were subjected to additional analysis. Table 1 displays the IC50 values for the recently produced compounds against the hMAO-A and hMAO-B isoforms. These parameters of this study were made as in previous studies [63]. We purchased these two enzymes from Sigma Aldrich (M7316-Monoamine Oxidase A human and M7441- Monoamine Oxidase A human) [64].

4.3 | Computational Methods

4.3.1 | Molecular Docking Studies

Protein and ligand preparation, grid generation, and docking were performed using AutoDockTools 1.5.6 [51–53]. Ligand stability was achieved by minimizing energy at the MM2 level with Chem3D Pro [51–53]. The protein structures were obtained from the Protein Data Bank (https://www.rcsb.org/), specifically *h*MAO-A (PDB ID: 2Z5X), MAO-B (PDB ID: 2V5Z), AChE (PDB-ID: 1B41), and BChE (PDB ID: 4BDS), based on previous studies [31, 55, 56, 62]. Interactions between ligands and receptors were analyzed in both 2D and 3D using BIOVIA Discovery Studio Visualizer software [53]. Detailed docking methodology is provided in the supplementary information (SI) file.

4.3.2 | 2D-MLR-Based QSAR Study

In our analysis, we utilized "QSARINS-2.2.4" for QSAR analysis based on GA-MLR (Genetic Algorithm-Multiple Linear Regression). The chemical structures in "SMILES" format were converted to 3D using "Openbabel 3.1," and descriptors were computed with "PyDescriptor." The process eliminated highly intercorrelated descriptors, resulting in over 1600+ for subsequent QSAR modeling. The methodology employed for the QSAR analysis was based on our previous publication [65].

4.3.3 | Molecular Dynamics studies

For MDS analysis, we simulated complexes "1B41_**5 u**," "4BDS_**5a**," "2v5z-5u," and "2Z5X_**5u**" using the "Desmond" module. An explicit solvent model with TIP3P water and the OPLS-2005 force field was used in a 10 Å × 10 Å × 10 Å periodic box. Na^+ ions and NaCl were added for charge balance and physiological conditions. The system was simulated for 100 ns. The details for setting up the complex were followed from earlier literature [66].

Acknowledgments

This Project was funded by the Deanship of Scientific Research (DSR) at King Abdulaziz University, Jeddah, under grant no. GPIP: 46-665-2024. The authors, therefore, acknowledge with thanks DSR for technical and financial support. Z.S. is thankful to the Alexander von Humboldt Foundation for the award of Return Fellowship. Open access publishing facilitated by Universita degli Studi di Genova, as part of the Wiley - CRUI-CARE agreement.

Conflicts of Interest

The authors declare no conflicts of interest.

Data Availability Statement

The data that support the findings of this study are available in the supporting material of this article.

References

1. R. M. Anderson, C. Hadjichrysanthou, S. Evans, and M. M. Wong, "Why Do so Many Clinical Trials of Therapies for Alzheimer's Disease Fail?," *Lancet* 390, no. 10110 (2017): 2327–2329.

2. J. Zhang, Y. Zhang, J. Wang, et al. "Recent Advances in Alzheimer's Disease: Mechanisms, Clinical Trials and New Drug Development Strategies," *Signal Transduction and Targeted Therapy* 9, no. 211 (2024), https://doi.org/10.1038/s41392-024-01911-3.

3. S. Manzoor and N. Hoda, "A Comprehensive Review of Monoamine Oxidase Inhibitors as Anti-Alzheimer's Disease Agents: A Review," *European Journal of Medicinal Chemistry* 206 (2020): 112787.

4. B. S. Thawkar and G. Kaur, "Zebrafish as a Promising Tool for Modeling Neurotoxin-Induced Alzheimer's Disease," *Neurotoxicity Research* 39 (2021): 949–965.

5. Ł. J. Walczak-Nowicka and M. Herbet, "Acetylcholinesterase Inhibitors in the Treatment of Neurodegenerative Diseases and the Role of Acetylcholinesterase in Their Pathogenesis," *International Journal of Molecular Sciences* 22, no. 17 (2021): 9290.

6. N. I. Bohnen, M. J. Grothe, N. J. Ray, M. L. T. M. Müller, and S. J. Teipel, "Recent Advances in Cholinergic Imaging and Cognitive Decline—Revisiting the Cholinergic Hypothesis of Dementia," *Current Geriatrics Reports* 7 (2018): 1–11.

7. T. Iizuka and M. Kameyama, "Cholinergic Enhancement Increases Regional Cerebral Blood Flow to the Posterior Cingulate Cortex in Mild Alzheimer's Disease," *Geriatrics & Gerontology International* 17, no. 6 (2017): 951–958.

8. K. Abd El-Moneim Ibrahim, S. Mohamed Abdelrahman, H. KA Elhakim, and E. Ali Ragab, "Single or Combined Exposure to Chlorpyrifos and Cypermethrin Provoke Oxidative Stress and Downregulation in Monoamine Oxidase and Acetylcholinesterase Gene Expression of the Rat's Brain," *Environmental Science and Pollution Research* 27 (2020): 12692–12703.

9. J. P. S. Ferreira, H. M. T. Albuquerque, S. M. Cardoso, A. M. S. Silva, and V. L. M. Silva, "Dual-Target Compounds for Alzheimer's Disease: Natural and Synthetic AChE and BACE-1 Dual-Inhibitors and Their Structure-Activity Relationship (SAR)," *European Journal of Medicinal Chemistry* 221 (2021): 113492.

10. S. Jalil, R. Basri, M. Aziz, et al., "Pristine 2-Chloroquinoline-Based-Thiosemicarbazones as Multitarget Agents Against Alzheimer's Disease: In Vitro and In Silico Studies of Monoamine Oxidase (MAO) and Cholinesterase (ChE) Inhibitors," *Journal of Molecular Structure* 1306 (2024): 137841.

11. M. Bortolami, F. Pandolfi, D. De Vita, et al., "New Deferiprone Derivatives as Multi-Functional Cholinesterase Inhibitors: Design, Synthesis and In Vitro Evaluation," *European Journal of Medicinal Chemistry* 198 (2020): 112350.

12. S. Zaib, R. Munir, M. T. Younas, et al., "Hybrid Quinoline-Thiosemicarbazone Therapeutics as a New Treatment Opportunity for Alzheimer's Disease–Synthesis, In Vitro Cholinesterase Inhibitory Potential and Computational Modeling Analysis," *Molecules* 26, no. 21 (2021): 6573.

13. L. Santarpia, I. Grandone, F. Contaldo, and F. Pasanisi, "Butyrylcholinesterase as a Prognostic Marker: A Review of the Literature," *Journal of Cachexia, Sarcopenia and Muscle* 4 (2013): 31–39.

14. L. Davis, J. J. Britten, and M. Morgan, "Cholinesterase Its Significance in Anaesthetic Practice," *Anaesthesia* 52, no. 3 (1997): 244–260.

15. Y. Pan, J. L. Muzyka, and C.-G. Zhan, "Model of Human Butyrylcholinesterase Tetramer by Homology Modeling and Dynamics Simulation," *Journal of Physical Chemistry B* 113, no. 18 (2009): 6543–6552.

16. M. Cucuianu, T. Nistor, N. Hâncu, P. Orbai, C. Muscurel, and I. Stoian, "Serum Cholinesterase Activity Correlates With Serum Insulin, C-Peptide and Free Fatty Acids Levels in Patients With Type 2 Diabetes," *Romanian Journal of Internal Medicine* 40, no. 1/4 (2002): 43–51.

17. N. Lampón, E. F. Hermida-Cadahia, A. Riveiro, and J. C. Tutor, "Association Between Butyrylcholinesterase Activity and Low-Grade Systemic Inflammation," *Annals of Hepatology* 11, no. 3 (2012): 356–363.

18. P. Narayan, S. Ehsani, and S. Lindquist, "Erratum: Corrigendum: Combating Neurodegenerative Disease With Chemical Probes and Model Systems," *Nature Chemical Biology* 11, no. 2 (2015): 172.

19. P. C. Trippier, K. Jansen Labby, D. D. Hawker, J. J. Mataka, and R. B. Silverman, "Target-And Mechanism-Based Therapeutics for Neurodegenerative Diseases: Strength in Numbers," *Journal of Medicinal Chemistry* 56, no. 8 (2013): 3121–3147.

20. Z. Hui, W. Lai-Fa, W. Xue-Qin, D. Ling, H. Bin-Sheng, and J.-M. Li, "Mechanisms and Therapeutic Potential of Chinonin in Nervous System Diseases," *Journal of Asian Natural Products Research* 26, no. 12 (2024): 1405–1420.

21. A. Nayak, R. Raju, P. Das, et al., "Ibuprofen With Amino Acid Dipeptide Conjugation: A Novel Prodrug for the Management of Alzheimer's Disease Complications," *International Journal of Pharmacology* 20, no. 1 (2024): 62–71.

22. R. Hong and X. Li, "Discovery of Monoamine Oxidase Inhibitors by Medicinal Chemistry Approaches," *MedChemComm* 10, no. 1 (2019): 10–25.

23. D. Osmaniye, B. Kurban, B. N. Sağlık, S. Levent, Y. Özkay, and Z. A. Kaplancıklı, "Novel Thiosemicarbazone Derivatives: In Vitro and In Silico Evaluation as Potential inhibitors," *Molecules* 26, no. 21 (2021): 6640.

24. J. Hroudová, N. Singh, Z. Fišar, and K. K. Ghosh, "Progress in Drug Development for Alzheimer's Disease: An Overview in Relation to Mitochondrial Energy Metabolism," *European Journal of Medicinal Chemistry* 121 (2016): 774–784.

25. J. Xie, R. Liang, Y. Wang, J. Huang, X. Cao, and B. Niu, "Progress n Target Drug Molecules for Alzheimer's Disease," *Current Topics in Medicinal Chemistry* 20, no. 1 (2020): 4–36.

26. X. H. Gao, J. J. Tang, H. R. Liu, L. B. Liu, and Y. Z. Liu, "Structure–Activity Study of Fluorine or Chlorine-Substituted Cinnamic Acid Derivatives With Tertiary Amine Side Chain in Acetylcholinesterase and Butyrylcholinesterase Inhibition," *Drug Development Research* 80, no. 4 (2019): 438–445.

27. Q. Q. Lu, Y. M. Chen, H. R. Liu, et al., "Nitrogen-Containing Flavonoid and Their Analogs With Diverse B-Ring in Acetylcholinesterase and Butyrylcholinesterase Inhibition," *Drug Development Research* 81, no. 8 (2020): 1037–1047.

28. L. Kang, X.-H. Gao, H.-R. Liu, et al., "Structure–Activity Relationship Investigation of Coumarin–Chalcone Hybrids With Diverse Side-Chains as Acetylcholinesterase and Butyrylcholinesterase Inhibitors," *Molecular Diversity* 22 (2018): 893–906.

29. A. R. Pasha, S. Ullah, A. Khan, et al., "Synthesis, In Vitro α-glucosidase Inhibitory Potential and In Silico Study of 2-Chloro Pyridine Incorporated Thiosemicarbazones," *Journal of Molecular Structure* 1317 (2024): 139089.

30. Z. Batool, S. Ullah, A. Khan, et al., "Design, Synthesis, and In Vitro and In Silico Study of 1-Benzyl-Indole Hybrid Thiosemicarbazones as Competitive Tyrosinase Inhibitors," *RSC Advances* 14, no. 39 (2024): 28524–28542.

31. Z. Batool, S. Ullah, A. Khan, et al., "Design, Synthesis, QSAR Modelling and Molecular Dynamic Simulations of N-Tosyl-Indole Hybrid Thiosemicarbazones as Competitive Tyrosinase Inhibitors," *Scientific Reports* 14, no. 1 (2024): 25754.

32. A. Rasool, Z. Batool, M. Khan, et al., "Bis-Pharmacophore of Cinnamaldehyde-Clubbed Thiosemicarbazones as Potent Carbonic Anhydrase-Ii Inhibitors," *Scientific Reports* 12, no. 1 (2022): 16095.

33. M. Islam, S. Ullah, A. Khan, et al., "Design, Synthesis, In Vitro, and In Silico Studies of 4-Fluorocinnamaldehyde Based Thiosemicarbazones as Urease Inhibitors," *Scientific Reports* 15, no. 1 (2025): 609.

34. M. Tasleem, J. Pelletier, J. Sévigny, et al., "Synthesis, In Vitro, and In Silico Studies of Morpholine-Based Thiosemicarbazones as Ectonucleotide Pyrophosphatase/Phosphodiesterase-1 and-3 Inhibitors," *International Journal of Biological Macromolecules* 266 (2024): 131068.

35. H. P. Ebrahimi, J. S. Hadi, T. A. Alsalim, T. S. Ghali, and Z. Bolandnazar, "A Novel Series of Thiosemicarbazone Drugs: From Synthesis to Structure," *Spectrochimica Acta, Part A: Molecular and Biomolecular Spectroscopy* 137 (2015): 1067–1077.

36. P. Kinthada and R. Gust, "Synthesis and Characterization, Nuclease Activity Studies and Anti-Cancer Studies of Au (Iii)-Isatinthiosemicarbazone Complexes as Potential Anticancer Drugs," *Journal of Drug Development and Delivery* 1 (2018): 01–06.

37. R. Matsa, P. Makam, M. Kaushik, S. L. Hoti, and T. Kannan, "Thiosemicarbazone Derivatives: Design, Synthesis and In Vitro Antimalarial Activity Studies," *European Journal of Pharmaceutical Sciences* 137 (2019): 104986.

38. S. U. Qazi, A. Naz, A. Hameed, et al., "Semicarbazones, Thiosemicarbazone, Thiazole and Oxazole Analogues as Monoamine Oxidase Inhibitors: Synthesis, Characterization, Biological Evaluation, Molecular Docking, and Kinetic Studies," *Bioorganic Chemistry* 115 (2021): 105209.

39. K. M. Abuamer, A. A. Maihub, M. M. El-Ajaily, A. M. Etorki, M. M. Abou-Krisha, and M. A. Almagani, "The Role of Aromatic Schiff Bases in the Dyes Techniques," *International Journal of Organic Chemistry* 04 (2014): 7–15.

40. J. Y. W. Mak, W. Xu, R. C. Reid, et al., "Stabilizing Short-Lived Schiff Base Derivatives of 5-Aminouracils That Activate Mucosal-Associated Invariant T Cells," *Nature Communications* 8, no. 1 (2017): 14599.

41. K. C. Gupta and A. K. Sutar, "Catalytic Activities of Schiff Base Transition Metal Complexes," *Coordination Chemistry Reviews* 252, no. 12–14 (2008): 1420–1450.

42. R. Rasool, S. Hasnain, and N. Nishat, "Metal-Based Schiff Base Polymers: Preparation, Spectral, Thermal and Their In Vitro Biological Investigation," *Designed Monomers and Polymers* 17, no. 3 (2014): 217–226.

43. S. B. Zahra, A. Khan, N. Ahmed, et al., "Versatile Biological Activities of Thiosemicarbazones and Their Metal Complexes," *Journal of Molecular Structure* 1322 (2025): 140511, https://doi.org/10.1016/j.molstruc.2024.140511.

44. S. Hashmi, S. Khan, Z. Shafiq, et al., "Probing 4-(Diethylamino)-Salicylaldehyde-Based Thiosemicarbazones as Multi-Target Directed Ligands Against Cholinesterases, Carbonic Anhydrases and α-Glycosidase Enzymes," *Bioorganic Chemistry* 107 (2021): 104554.

45. M. Ishaq, P. Taslimi, Z. Shafiq, et al., "Synthesis, Bioactivity and Binding Energy Calculations of Novel 3-ethoxysalicylaldehyde Based Thiosemicarbazone Derivatives," *Bioorganic Chemistry* 100 (2020): 103924.

46. M. Erdoğan, M. Serdar Çavuş, H. Muğlu, et al., "Synthesis, Theoretical, In Silico and In Vitro Biological Evaluation Studies of New Thiosemicarbazones as Enzyme Inhibitors," *Chemistry & Biodiversity* 20, no. 11 (2023): 202301063.

47. G. E. Mathew, J. M. Oh, K. Mohan, A. Tengli, B. Mathew, and H. Kim, "Development of Methylthiosemicarbazones as New Reversible Monoamine Oxidase-B Inhibitors for the Treatment of Parkinson's Disease," *Journal of Biomolecular Structure and Dynamics* 39, no. 13 (2021): 4786–4794.

48. G. F. Makhaeva, N. V. Kovaleva, N. P. Boltneva, et al., "Bis-Amiridines as Acetylcholinesterase and Butyrylcholinesterase Inhibitors: N-Functionalization Determines the Multitarget Anti-Alzheimer's Activity Profile," *Molecules* 27, no. 3 (2022): 1060.

49. Q. Song, Y. Li, Z. Cao, X. Qiang, Z. Tan, and Y. Deng, "Novel Salicylamide Derivatives as Potent Multifunctional Agents for the Treatment of Alzheimer's Disease: Design, Synthesis and Biological Evaluation," *Bioorganic Chemistry* 84 (2019): 137–149.

50. C. Yamali, F. S. Engin, S. Bilginer, et al., "Phenothiazine-Based Chalcones as Potential Dual-Target Inhibitors Toward Cholinesterases (AChE, BuChE) and Monoamine Oxidases (Mao-A, Mao-B)," *Journal of Heterocyclic Chemistry* 58, no. 1 (2021): 161–171.

51. S. S. Gurav, K. T. Waghmode, S. N. Dandekar, et al., "New 2-Chloroimidazo [1, 2-a] Pyridine Induced Schiff Bases: Synthesis, Characterization, Antimicrobial and A-498 and A-549 Anticancer Activity, Molecular Modeling, In-Silico Pharmacokinetics, and DFT Studies," *Chemical Physics Impact* 8 (2024): 100494.

52. M. Kurbanova, S. N. Mali, F. Gurbanova, H. Yasin, S. S. Gurav, and C.-H. Lai, "Synthesis, Structure, DFT Study and Molecular Docking Inspection of Spirobi [Hexahydropyrimidine]-Diones Derivative," *Chemical Physics Impact* 9 (2024): 100716.

53. O. Trott and A. J. Olson, "Autodock Vina: Improving the Speed and Accuracy of Docking With a New Scoring Function, Efficient Optimization, and Multithreading," *Journal of Computational Chemistry* 31, no. 2 (2010): 455–461.

54. C. Lemke, J. Christmann, J. Yin, et al., "Chromenones as Multineurotargeting Inhibitors of Human Enzymes," *ACS Omega* 4, no. 26 (2019): 22161–22168.

55. K. Teralı, "An Evaluation of Neonicotinoids′ Potential to Inhibit Human Cholinesterases: Protein–Ligand Docking and Interaction Profiling Studies," *Journal of Molecular Graphics and Modelling* 84 (2018): 54–63.

56. B. N. Sağlık, B. Kaya Çavuşoğlu, D. Osmaniye, et al., "In Vitro and In Silico Evaluation of New Thiazole Compounds as Monoamine Oxidase Inhibitors," *Bioorganic Chemistry* 85 (2019): 97–108.

57. B. Evranos-Aksöz, S. Yabanoğlu-Çiftçi, G. Uçar, K. Yelekçi, and R. Ertan, "Synthesis of Some Novel Hydrazone and 2-Pyrazoline Derivatives: Monoamine Oxidase Inhibitory Activities and Docking Studies," *Bioorganic & Medicinal Chemistry Letters* 24, no. 15 (2014): 3278–3284.

58. N. Gökhan-Kelekçi, O. O. Simşek, A. Ercan, et al., "Synthesis and Molecular Modeling of Some Novel Hexahydroindazole Derivatives as Potent Monoamine Oxidase Inhibitors," *Bioorganic & Medicinal Chemistry* 17, no. 18 (2009): 6761–6772.

59. M. Ali, S. Shamim, U. Salar, et al., "2-Amino-6-Ethoxy-4-Arylpyridine-3, 5-Dicarbonitrile Scaffolds as Potential Acetylcholinesterase and Butyrylcholinesterase Inhibitors," *Journal of Molecular Structure* 1321 (2025): 139863.

60. S. Zareei, M. Mohammadi-Khanaposhtani, M. Shahali, et al., "Phenyldiazenyl-Phenoxy-1,2,3-Triazol-Acetamide Derivatives as New Dual Cholinesterase Inhibitors: Design, Synthesis, In Vitro, and In Silico Enzymatic Inhibition Evaluations," *Journal of Molecular Structure* 1321 (2025): 139686.

61. V. P. Ol'ga, D. N. Tomilin, H. Şenol, et al., "Synthesis of Pyrrole-Heterocyclic Derivatives as Anti-Alzheimer and Antidiabetic Candidates: An In Vitro-In Silico Study," *Journal of Molecular Structure* 1315 (2024): 138998.

62. D. G. Solğun, N. Sadeghian, P. Taslimi, T. Taskin-Tok, and M. S. Ağırtaş, "Synthesis of Zinc Phthalocyanine Containing 1,2-Phenylene Bis (3-Chloropropanoate) Substituted Groups and Investigation of Their Metabolic Enzyme Inhibitory Effects," *Polyhedron* 264 (2024): 117251.

63. P. Bissel, M. C. Bigley, K. Castagnoli, and N. Castagnoli Jr., "Synthesis and Biological Evaluation of MAO-A Selective 1,4-Disubstituted-1,2,3,6-Tetrahydropyridinyl Substrates," *Bioorganic & Medicinal Chemistry* 10, no. 9 (2002): 3031–3041.

64. L. O. El-Halaby, W. M. El-Husseiny, S. M. El-Messery, and F. E. Goda, "Synthesis, In Vitro, and In Silico Studies of New Derivatives of Diphenylpiperazine Scaffold: A Key Substructure for MAO Inhibition," *Bioorganic Chemistry* 143 (2024): 107011.

65. S. N. Mali, A. Pandey, B. R. Thorat, and C.-H. Lai, "Multiple 3D-and 2D-quantitative Structure–Activity Relationship Models (QSAR), Theoretical Study and Molecular Modeling to Identify Structural Requirements of Imidazopyridine Analogues as Anti-Infective Agents Against Tuberculosis," *Structural Chemistry* 33, no. 3 (2022): 679–694.

66. A. Alghamdi, A. S. Abouzied, A. Alamri, et al., "Synthesis, Molecular Docking, and Dynamic Simulation Targeting Main Protease (Mpro) of New, Thiazole Clubbed Pyridine Scaffolds as Potential COVID-19 Inhibitors," *Current Issues in Molecular Biology* 45, no. 2 (2023): 1422–1442.

Supporting Information

Additional supporting information can be found online in the Supporting Information section.

		IC_{50} (nM)								Ki (nM)	
Comp.	**InChI**	**AChE**	**r^2**	**BChE**	**r^2**	**MAO-A**	**r^2**	**MAO-B**	**r^2**	**AChE**	**BChE**
5a	**1S/C28H26Cl2N4O3S2/c1-3-34(4-2)22-14-12-21(18-31-33-28(38)32-25-11-7-10-24(29)27(25)30)26(17-22)37-39(35,36)23-15-13-19-8-5-6-9-20(19)16-23/h5-18H,3-4H2,1-2H3,(H2,32,33,38)/b31-18+**	14.90±1.54	0.913	124.72±9.13	0.982	104.17±4.58	0.960	391.03±9.04	0.989	11.37±3.06	101.32±22.43
5b	**1S/C28H27BrN4O3S2/c1-3-33(4-2)25-15-9-22(19-30-32-28(37)31-24-13-11-23(29)12-14-24)27(18-25)36-38(34,35)26-16-10-20-7-5-6-8-21(20)17-26/h5-19H,3-4H2,1-2H3,(H2,31,32,37)/b30-19+**	33.81±3.41	0.906	202.05±5.66	0.937	132.05±7.01	0.931	409.76±7.47	0.928	26.55±3.34	190.57±15.65
5c	**1S/C28H28N4O3S2/c1-3-32(4-2)25-16-14-23(20-29-31-28(36)30-24-12-6-5-7-13-24)27(19-25)35-37(33,34)26-17-15-21-10-8-9-11-22(21)18-26/h5-20H,3-4H2,1-2H3,(H2,30,31,36)/b29-20+**	38.42±5.03	0.904	217.78±8.41	0.929	188.54±6.46	0.933	296.47±6.01	0.990	25.43±5.32	182.65±15.04
5d	**1S/C29H30N4O4S2/c1-4-33(5-2)25-14-10-23(20-30-32-29(38)31-24-12-15-26(36-3)16-**	39.37±2.87	0.968	252.54±10.46	0.923	170.66±10.42	0.935	406.18±8.24	0.942	32.23±5.93	234.84±15.04

	13-24)28(19-25)37-39(34,35)27-17-11-21-8-6-7-9-22(21)18-27/h6-20H,4-5H2,1-3H3,(H2,31,32,38)/b30-20+										
5e	**1S/C28H27ClN4O3S2/c1-3-33(4-2)25-14-12-22(19-30-32-28(37)31-24-11-7-10-23(29)17-24)27(18-25)36-38(34,35)26-15-13-20-8-5-6-9-21(20)16-26/h5-19H,3-4H2,1-2H3,(H2,31,32,37)/b30-19+**	31.04±4.16	0.921	208.43±7.53	0.951	117.13±7.33	0.923	>1000	0.935	25.36±3.32	195.34±11.53
5f	**1S/C26H32N4O3S2/c1-5-30(6-2)23-13-11-22(18-28-29-26(34)27-17-19(3)4)25(16-23)33-35(31,32)24-14-12-20-9-7-8-10-21(20)15-24/h7-16,18-19H,5-6,17H2,1-4H3,(H2,27,29,34)/b28-18+**	49.53±5.21	0.947	253.53±6.31	0.964	133.50±8.04	0.901	388.10±5.37	0.957	38.82±6.18	239.89±18.65
5g	**1S/C26H32N4O3S3/c1-4-30(5-2)23-13-11-22(19-28-29-26(34)27-15-8-16-35-3)25(18-23)33-36(31,32)24-14-12-20-9-6-7-10-21(20)17-24/h6-7,9-14,17-19H,4-5,8,15-16H2,1-3H3,(H2,27,29,34)/b28-19+**	80.43±7.62	0.978	287.26±8.57	0.970	187.66±5.36	0.964	398.57±7.93	0.902	72.43±10.08	258.50±16.14
5h	**1S/C29H27F3N4O3S2/c1-3-36(4-2)23-15-13-22(19-33-35-**	16.76±1.35	0.949	145.03±8.96	0.913	100.38±4.57	0.930	249.01±9.10	0.944	14.59±3.36	136.01±9.17

	28(40)34-26-12-8-7-11-25(26)29(30,31)32)27(18-23)39-41(37,38)24-16-14-20-9-5-6-10-21(20)17-24/h5-19H,3-4H2,1-2H3,(H2,34,35,40)/b33-19+										
5i	**1S/C28H27ClN4O3S2/c1-3-33(4-2)25-15-9-22(19-30-32-28(37)31-24-13-11-23(29)12-14-24)27(18-25)36-38(34,35)26-16-10-20-7-5-6-8-21(20)17-26/h5-19H,3-4H2,1-2H3,(H2,31,32,37)/b30-19+**	24.81±2.41	0.958	199.54±9.41	0.902	121.24±3.15	0.924	285.25±4.02	0.912	21.02±4.12	190.27±13.60
5j	**1S/C30H32N4O3S2/c1-5-34(6-2)26-16-14-25(20-31-33-30(38)32-29-21(3)10-9-11-22(29)4)28(19-26)37-39(35,36)27-17-15-23-12-7-8-13-24(23)18-27/h7-20H,5-6H2,1-4H3,(H2,32,33,38)/b31-20+**	40.62±2.77	0.979	265.38±7.90	0.970	136.93±6.21	0.981	395.37±8.35	0.966	36.52±5.23	228.42±12.35
5k	**1S/C29H30N4O4S2/c1-4-33(5-2)25-15-13-23(20-30-32-29(38)31-24-11-8-12-26(18-24)36-3)28(19-25)37-39(34,35)27-16-14-21-9-6-7-10-22(21)17-27/h6-20H,4-5H2,1-3H3,(H2,31,32,38)/b30-**	116.01±8.42	0.906	252.64±9.15	0.977	144.71±8.03	0.976	>1000	0.952	95.75±9.54	205.34±10.16

	20+										
5l	**1S/C28H27FN4O3S2/c1-3-33(4-2)25-15-9-22(19-30-32-28(37)31-24-13-11-23(29)12-14-24)27(18-25)36-38(34,35)26-16-10-20-7-5-6-8-21(20)17-26/h5-19H,3-4H2,1-2H3,(H2,31,32,37)/b30-19+**	29.54±2.68	0.918	200.34±6.88	0.985	112.33±2.78	0.907	276.97±6.33	0.938	27.41±3.45	182.09±9.05
5m	**1S/C23H26N4O3S2/c1-4-27(5-2)20-12-10-19(16-25-26-23(31)24-3)22(15-20)30-32(28,29)21-13-11-17-8-6-7-9-18(17)14-21/h6-16H,4-5H2,1-3H3,(H2,24,26,31)/b25-16+**	38.49±3.21	0.909	214.30±7.13	0.963	132.28±4.96	0.954	368.58±11.25	0.926	30.22±5.02	193.05±11.62
5n	**1S/C22H24N4O3S2/c1-3-26(4-2)19-11-9-18(15-24-25-22(23)30)21(14-19)29-31(27,28)20-12-10-16-7-5-6-8-17(16)13-20/h5-15H,3-4H2,1-2H3,(H3,23,25,30)/b24-15+**	47.70±5.67	0.970	308.43±9.98	0.932	137.19±6.55	0.976	395.72±8.09	0.930	42.44±4.10	270.16±13.54
5o	**1S/C28H27N5O5S2/c1-3-32(4-2)24-14-12-22(19-29-31-28(39)30-23-10-7-11-25(17-23)33(34)35)27(18-24)38-40(36,37)26-15-13-20-8-5-6-9-21(20)16-26/h5-19H,3-4H2,1-**	18.93±1.33	0.998	192.09±6.36	0.981	122.65±7.01	0.932	267.07±6.35	0.905	14.25±2.32	160.33±9.01

	2H3,(H2,30,31,39)/b29-19+										
5p	**1S/C28H34N4O3S2/c1-3-32(4-2)25-16-14-23(20-29-31-28(36)30-24-12-6-5-7-13-24)27(19-25)35-37(33,34)26-17-15-21-10-8-9-11-22(21)18-26/h8-11,14-20,24H,3-7,12-13H2,1-2H3,(H2,30,31,36)/b29-20+**	54.46±4.57	0.915	254.24±8.08	0.965	145.32±3.57	0.985	326.68±9.13	0.955	47.09±6.35	226.45±12.57
5q	**1S/C29H29ClN4O3S2/c1-3-34(4-2)26-15-11-24(20-32-33-29(38)31-19-21-9-13-25(30)14-10-21)28(18-26)37-39(35,36)27-16-12-22-7-5-6-8-23(22)17-27/h5-18,20H,3-4,19H2,1-2H3,(H2,31,33,38)/b32-20+**	19.34±1.28	0.984	202.31±14.86	0.963	119.06±9.24	0.926	308.44±6.07	0.927	17.63±3.34	182.76±11.48
5r	**1S/C29H30N4O3S2/c1-4-33(5-2)25-16-14-24(20-30-32-29(37)31-27-13-9-6-10-21(27)3)28(19-25)36-38(34,35)26-17-15-22-11-7-8-12-23(22)18-26/h6-20H,4-5H2,1-3H3,(H2,31,32,37)/b30-20+**	27.39±2.42	0.912	293.55±7.14	0.912	142.55±6.78	0.944	495.13±8.36	0.995	21.17±1.05	249.09±15.30
5s	**1S/C29H30N4O3S2/c1-3-33(4-2)26-16-14-25(21-31-32-**	71.43±8.92	0.954	220.34±8.53	0.954	131.09±5.34	0.976	369.46±12.04	0.975	63.86±7.54	195.21±13.45

	29(37)30-20-22-10-6-5-7-11-22)28(19-26)36-38(34,35)27-17-15-23-12-8-9-13-24(23)18-27/h5-19,21H,3-4,20H2,1-2H3,(H2,30,32,37)/b31-21+										
5t	**1S/C30H32N4O3S2/c1-3-34(4-2)27-16-14-26(22-32-33-30(38)31-19-18-23-10-6-5-7-11-23)29(21-27)37-39(35,36)28-17-15-24-12-8-9-13-25(24)20-28/h5-17,20-22H,3-4,18-19H2,1-2H3,(H2,31,33,38)/b32-22+**	56.21±4.58	0.902	271.12±6.90	0.981	138.74±6.02	0.932	289.02±9.11	0.945	48.30±7.32	226.65±16.08
5u	**1S/C28H26Cl2N4O3S2/c1-3-34(4-2)22-14-12-21(18-31-33-28(38)32-27-24(29)10-7-11-25(27)30)26(17-22)37-39(35,36)23-15-13-19-8-5-6-9-20(19)16-23/h5-18H,3-4H2,1-2H3,(H2,32,33,38)/b31-18+**	12.89±1.02	0.987	148.18±7.35	0.973	96.25±5.77	0.906	208.95±5.84	0.978	9.82±1.76	112.06±7.61
*		101.24±5.72	0.984	261.62±9.03	0.945	-	-			84.05±8.70	242.17±13.88
**		-	-	-	-	150.62±4.03	0.979	468.63±16.05	0.987	-	-

Design, synthesis, in vitro and in silico studies of 5-(diethylamino)-2-formylphenyl naphthalene-2-sulfonate based thiosemicarbazones as potent anti-Alzheimer agents

Urva Farooq[a, ≠], Muhammad Islam[b,c, ≠], Zahra Batool[a], Suraj N. Mali[d], Rahul D. Jawarkar[e], Shailesh S. Gurav[f], Rima D. Alharthy[g], Halil Şenol[h], Nastaran Sadeghian[i], Parham Taslimi[i], Zahid Shafiq[a]* and Silvia Schenone[j]*

[a]*Institute of Chemical Sciences, Bahauddin Zakariya University, 60800, Multan, Pakistan.*

[b]*Department of Chemistry, Muhammad Nawaz Sharif University of Engineering and Technology (MNSUET), 60000, Multan, Pakistan*

[c]*School of Pharmaceutical Science and Technology, Tianjin University, 92 Weijin Road, Tianjin 300072, China.*

[d]*School of Pharmacy, D.Y. Patil University (Deemed to be University), Sector 7, Nerul, Navi Mumbai 400706, India*

[e]*Department of Medicinal Chemistry, Dr. Rajendra Gode Institute of Pharmacy, University-Mardi Road, Amravati, India*

[f]*Department of Chemistry, VIVA College, Virar (W), Maharashtra-401303, India.*

[g]*Department of Chemistry, Science & Arts College, Rabigh Branch, King Abdulaziz University, Rabigh 21911, Saudi Arabia*

[h]*Bezmialem Vakif University, Faculty of Pharmacy, Department of Pharmaceutical Chemistry, 34093 Fatih, Istanbul, Türkiye*

[i]*Department of Biotechnology, Faculty of Science, Bartin University, 74110 Bartin, Türkiye*

[j]*Department of Pharmacy, University of Genoa, Viale Benedetto XV, 3, Genoa 16132, Italy*

***Corresponding Authors*:**

Prof. Dr. Zahid Shafiq: zahidshafiq@bzu.edu.pk

Prof. Dr. Silvia Schenone: silvia.schenone@unige.it

≠ = Contributed equally

TABLE OF CONTENTS

Molecular Docking Studies Further Analysis

Materials and methods

The structure of compounds 5a-5v was built using ChemDraw Ultra 12.0 software package. The stable configuration of ligands was obtained by minimizing energy via the MM2 level, utilizing the Chem3D Pro 12.0. A known protein database bank (https://www.rcsb.org/) was used to retrieve 3D-crystal structures of proteins with PDB IDs: 1B41, 4BDS, 2V5Z and 2Z5X. Three-dimensional coordinates of the enzymes were retrieved in the PDB format. The protein and ligand preparation, grid generation, and docking were executed using a molecular modelling tool, AutoDockTools 1.5.6 software. Target proteins were pre-processed to remove all water molecules, ions, and co-crystallized ligands as they may interfere with docking. Further optimization was achieved by adding all hydrogen atoms, and assigning partial charges- Kollman charges and saved the prepared protein structure in PDBQT format.

The ligand preparation was achieved by adding the Gasteiger charges followed by merging all non-polar hydrogen atoms and then saving the ligand in PDBQT format, which is required by AutoDock Vina. The ligand was set up for docking with the help of AutoDockTools (ADT; Version 1.5.6) to define the torsional degrees of freedom to be considered during the docking process and all acyclic dihedral angles in the ligand were allowed to rotate freely. Using AutoDockTools, the grid box was defined that specifies the docking parameters was defined. The center and dimensions of the grid box were set to cover the binding site properly. The grid box parameters, including center coordinates and box size, were saved in the AutoDock Vina configuration file. Exhaustiveness (a parameter controlling the thoroughness of the search) was 8 as default.

The docking was executed by means of the AutoDock Vina program using a configuration file. After docking, the pose with the least binding energy was selected as the best-docked ligand with the corresponding receptor using the PyMOL software and; the ligand-protein complex was saved in PDB format. Further, 2D and 3D ligand-receptor interactions were analyzed using Discovery Studio visualizer software.

The protein structure 4BDS is human butyrylcholinesterase in complex with tacrine. Thus, for the docking against 4BDS, the grid center (x, y, z) coordinates of co-crystalized ligand-Tacrine were used. For 4BDS, the grid box was built with size (x,y,z) of 60 × 60 × 60 points and it was positioned with co-crystalized ligand coordinates (x,y,z): 132.994, 116.013, and 41.214. Correspondingly, For protein 2Z5X, a grid box of size (x,y,z) 40 × 40 × 40 was set along with coordinates (x,y,z): 37.986, 29.585, and -17.813 of co-crystalized ligand. For receptor 2V5Z the grid center (x, y, z) coordinates of co-crystalized inhibitor safinamide were

used, center (x, y, z) = 51.886, 156.452, 28.559 and size (x,y,z) 40 × 40 × 40.For protein 1B41 (PDB ID), the grid box was positioned in the middle of the protein having coordinates (x,y,z) 116.546, 110.33, and -134.181. The grid box constituted a large region to include the entire protein target, following the blind docking method in the absence of co-crystalized ligand [2-4].

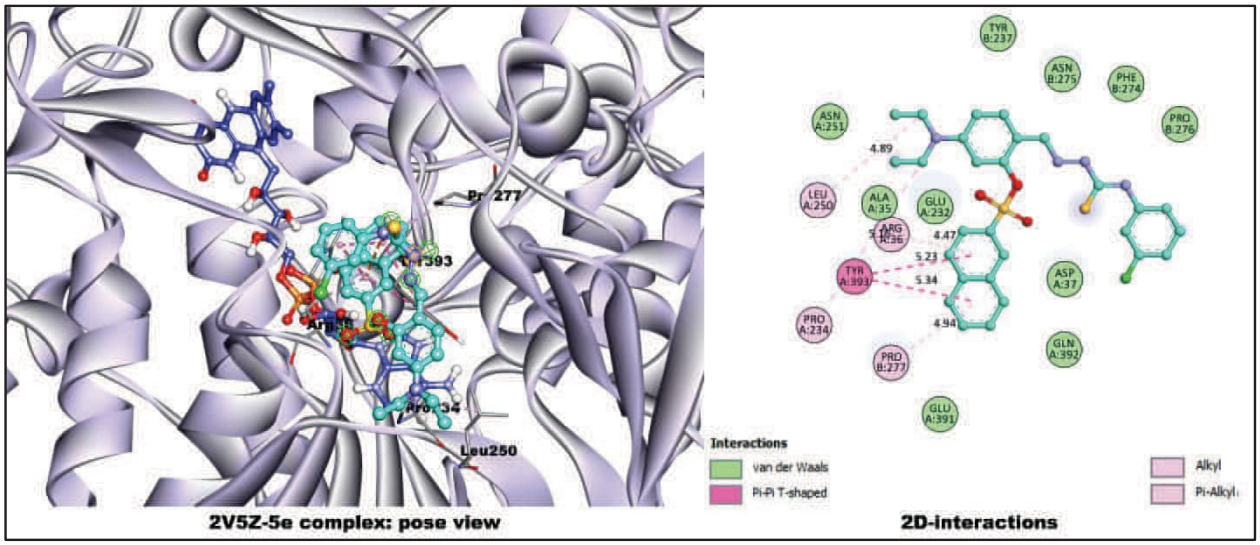

Figure S 1. Complex of **5e**-2V5Z co-crystalized with FAD molecule (blue-colored) and their 2D-binding interactions.

References

[1]. O. Trott A. J. Olson, Software News and update autodock vina: improving the speed and accuracy of docking with a new scoring function, efficient optimization, and multithreading, J Comput Chem. 31 (2009) 455–461. https://doi.org/10.1002/jcc.21334.

[2]. Lemke, C., et al., Chromenones as multineurotargeting inhibitors of human enzymes. ACS Omega 2019, 4, 22161−22168. DOI: 10.1021/acsomega.9b03409

[3]. Saquib Jalil, Rabia Basri, Mubashir Aziz, Zahid Shafiq, Syeda Abida Ejaz, Abdul Hameed, Jamshed Iqbal,Pristine 2-chloroquinoline-based-thiosemicarbazones as multitarget agents against alzheimer's disease: In vitro and in silico studies of monoamine oxidase (MAO) and cholinesterase (ChE) inhibitors, Journal of Molecular Structure, 1306, 2024, 137841,https://doi.org/10.1016/j.molstruc.2024.137841.

[4]. Qazi, S. U.; Naz, A.; Hameed, A.; Osra, F. A.; Jalil, S.; Iqbal, J.; Shah, S. A. A.; Mirza, A. Z. Semicarbazones, thiosemicarbazone, thiazole and oxazole analogues as

monoamine oxidase inhibitors: Synthesis, characterization, biological evaluation, molecular docking, and kinetic studies. Bioorganic chemistry 2021, 115, 105209.

QSAR Model

$_{P}IC_{50}$=5.414 + 0.051 * com_Chyd_8A + 0.473 * fOS7B + -0.035 * C_sp3C_9B

com_Chyd_8A: occurrence of hydrophobic carbon atoms within 8 angstrom unit from the center of mass of the molecule.

fOS7B: frequency of occurrence of sulphur atom exactly at 7 bonds from the oxygen atoms.

C_sp3C_9B: occurrence of sp3 hybridized carbon atoms within 9 bonds from the carbon atoms.

Qsar parameters

R2_tr	0.8032	RMSE_ex	0.3257
Adj-R2	0.7578	PRESS_ex	0.5304
F(3-13)	17.6891	Q2F1	0.8131
RSS_tr	0.0925	Q2F2	0.8415
MSE_tr	0.0054	Q2F3	0.8364
RMSE_tr	0.0738	MAE_ex	0.2318
MAE_tr	0.058	K	0.9812
s	0.0843	K_prime	1.0169
AIC	-30.3916	R2ext	0.3604
BIC	-26.2255	CCC_ex	-0.3737
CCC_tr	0.8909	r2m_ExPy	-0.6492
Q2_cv	0.78	r2m_EyPx	-0.0196
RMSE_cv	0.3257	R2o	-0.7511
MSE_cv	0.1061	R2o_dash	-7.4853
PRESS_cv	0.5304	Clos_dash	21.7668
MAE_cv	0.2453	Clos	3.0837
R2_Yscr	0.1978	r2m_avg	-0.3344
		r2m_delta	0.6296
MSE_ex	0.1061		

Important molecular descriptors give us important information about how structural features affect biological activity in the QSAR model for MAO-B inhibitors. We measure hydrophobic carbon atoms (com_Chyd_8A) within an 8-angstrom radius from the molecule's center of mass. Because of their hydrophobic nature, the enzyme's active region contains residues like Ile-199 and Leu-171. These atoms are necessary to stop MAO-B from working. When these residues and inhibitors interact hydrophobically, the binding affinity goes up. Non-polar parts of the inhibitor stay in the binding pocket. A positive coefficient in the QSAR model means that the inhibitory activity (PIC50) goes up when the hydrophobic carbon density at the center of the molecule goes up. This is what drugs like rasagiline and selegiline do to make their effects more selective and potent.

One important indicator is sulfur-oxygen connectivity (fOS7B), which measures the number of sulfur atoms that are exactly seven bonds away from oxygen atoms. Sulfur-containing groups, like thiols and thioethers, help biological activity through electron transfer and redox interactions. Oxygen atoms, on the other hand, help hydrogen bonds form and make the substance more soluble in water. This particular connection arrangement facilitates ligand binding via both polar and nonpolar interactions. A positive coefficient ($\beta > 0$) shows how important this feature is for improving MAO-B binding efficiency. For example, sulfur-containing scaffolds like thiochromones can selectively block MAO-B.

Finally, the term sp3-hybridized carbon atoms (C_sp3C_9B) quantify the number of such carbons within nine bonds of any carbon atom. Excessive carbons, prevalent in aliphatic chains and saturated hydrocarbons, often diminish molecular planarity. Lack of planarity could make it harder for molecules to π-stack, which is needed to bind to aromatic residues in MAO-B like Tyr-398 and Tyr-435. On the other hand, molecules that are too flexible might not fit correctly into the enzyme's binding pocket. If the coefficient is less than zero, it means that reducing the number of sp3-hybridized carbons increases the inhibitory effect by making molecules flatter and more compact. Safinamide exemplifies a balance between stiff aromatic groups and little aliphatic branching; hence, it optimizes its effectiveness as a selective MAO-B inhibitor. All of these traits make the complicated connection between molecular structure and inhibitory function stand out. This makes it easier to come up with effective MAO-B inhibitors.

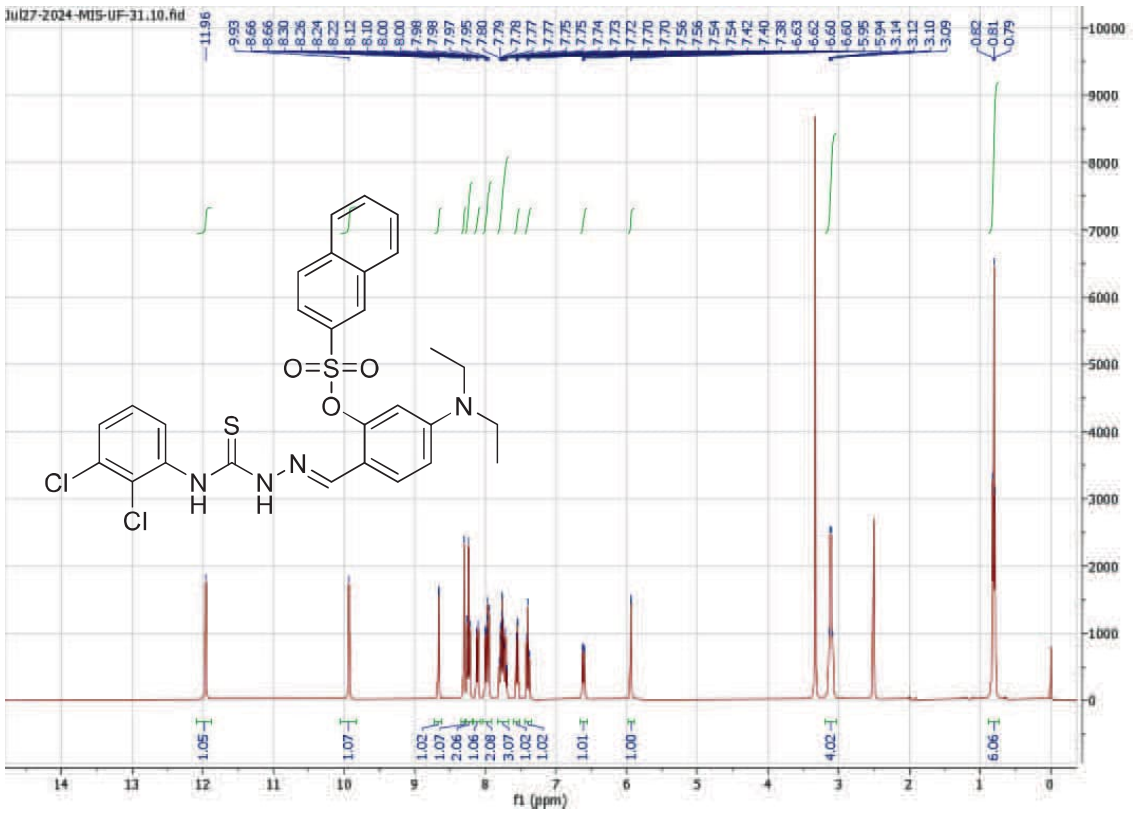

Figure S 2. ^{1}H-NMR Spectrum of Compound **5a** (DMSO-*d6*, 400 MHz

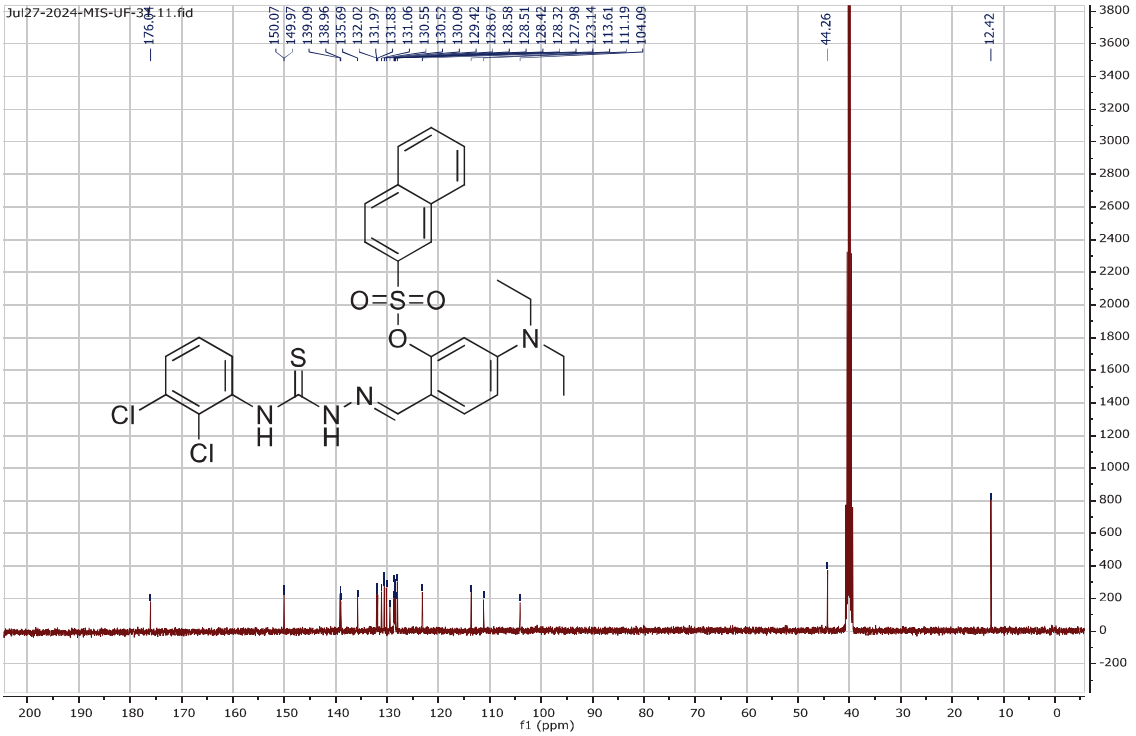

Figure S 3. ^{13}C-NMR Spectrum of Compound **5a** (DMSO-*d6*, 100 MHz)

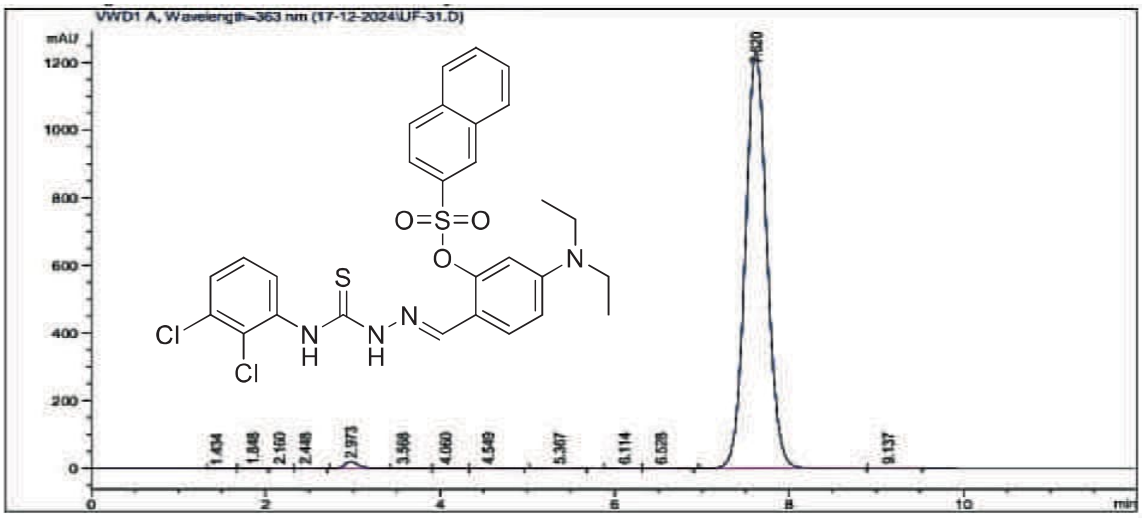

Area Percent Report

Sorted By : Signal
Multiplier : 1.0000
Dilution : 1.0000
Use Multiplier & Dilution Factor with ISTDs

Signal 1: VWD1 A, Wavelength=363 nm

Peak #	RetTime [min]	Type	Width [min]	Area [mAU*s]	Height [mAU]	Area %
1	1.434	BB	0.1358	1.45805	1.47357e-1	6.813e-3
2	1.848	BV E	0.1532	1.65824	1.40984e-1	7.749e-3
3	2.160	VV R	0.1810	8.27829	7.26445e-1	0.0387
4	2.448	VB	0.1445	9.07875	9.54357e-1	0.0424
5	2.973	BV R	0.1582	203.99185	19.53420	0.9532
6	3.568	VV E	0.1886	5.28300	3.90007e-1	0.0247
7	4.060	VB E	0.1771	3.61506	3.06103e-1	0.0169
8	4.549	BB	0.1848	4.71880	3.63877e-1	0.0221
9	5.367	BB	0.2111	13.58404	9.63324e-1	0.0635
10	6.114	BV	0.1945	6.49481	4.79369e-1	0.0304

Data File D:\HPLC-DATA\Data\17-12-2024\UF-31.D
Sample Name: UF-31

Peak #	RetTime [min]	Type	Width [min]	Area [mAU*s]	Height [mAU]	Area %
11	6.528	VB	0.2337	14.22781	9.38505e-1	0.0665
12	7.620	BB	0.2658	2.11223e4	1230.59741	98.7042
13	9.137	BB	0.2338	4.91372	2.68647e-1	0.0230
Totals :				2.13997e4	1255.81059	

Figure S 4. HPLC Purity Analysis of Compound **5a**

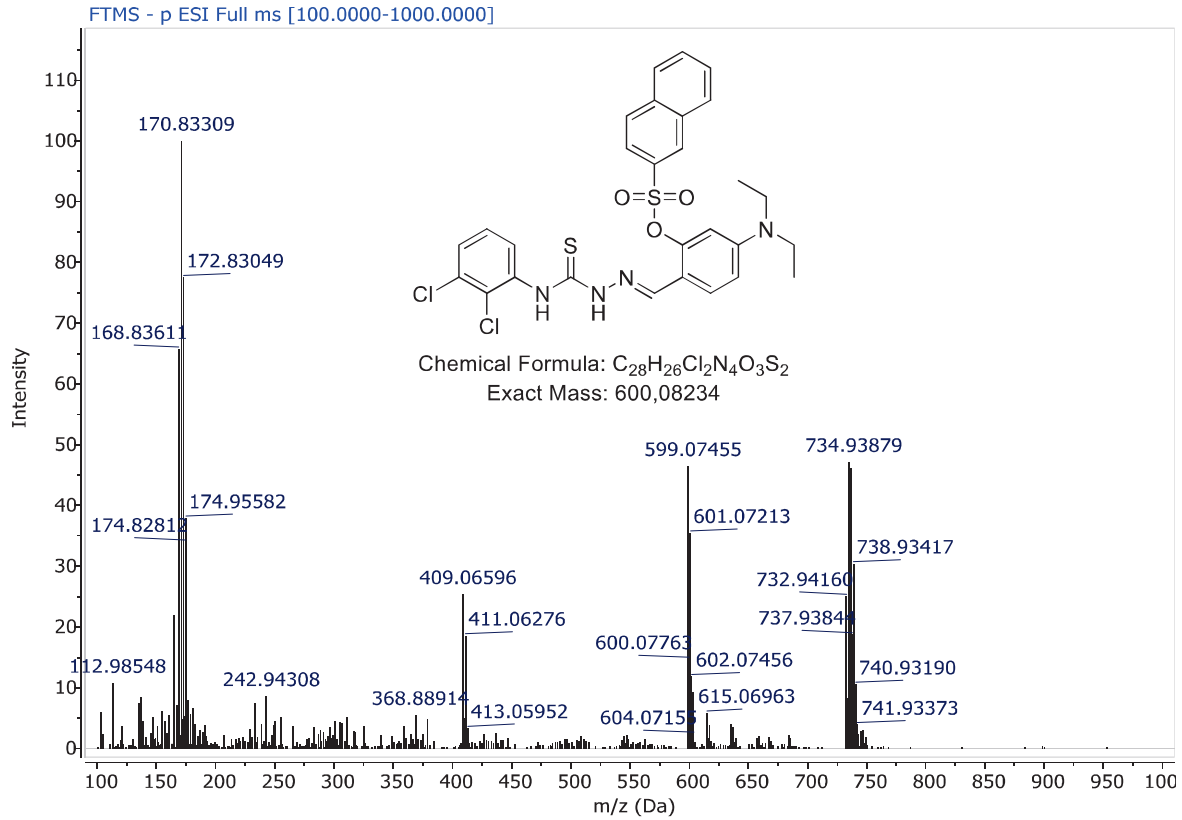

Figure S 5. ESI-HRMS Spectrum of Compound **5a**

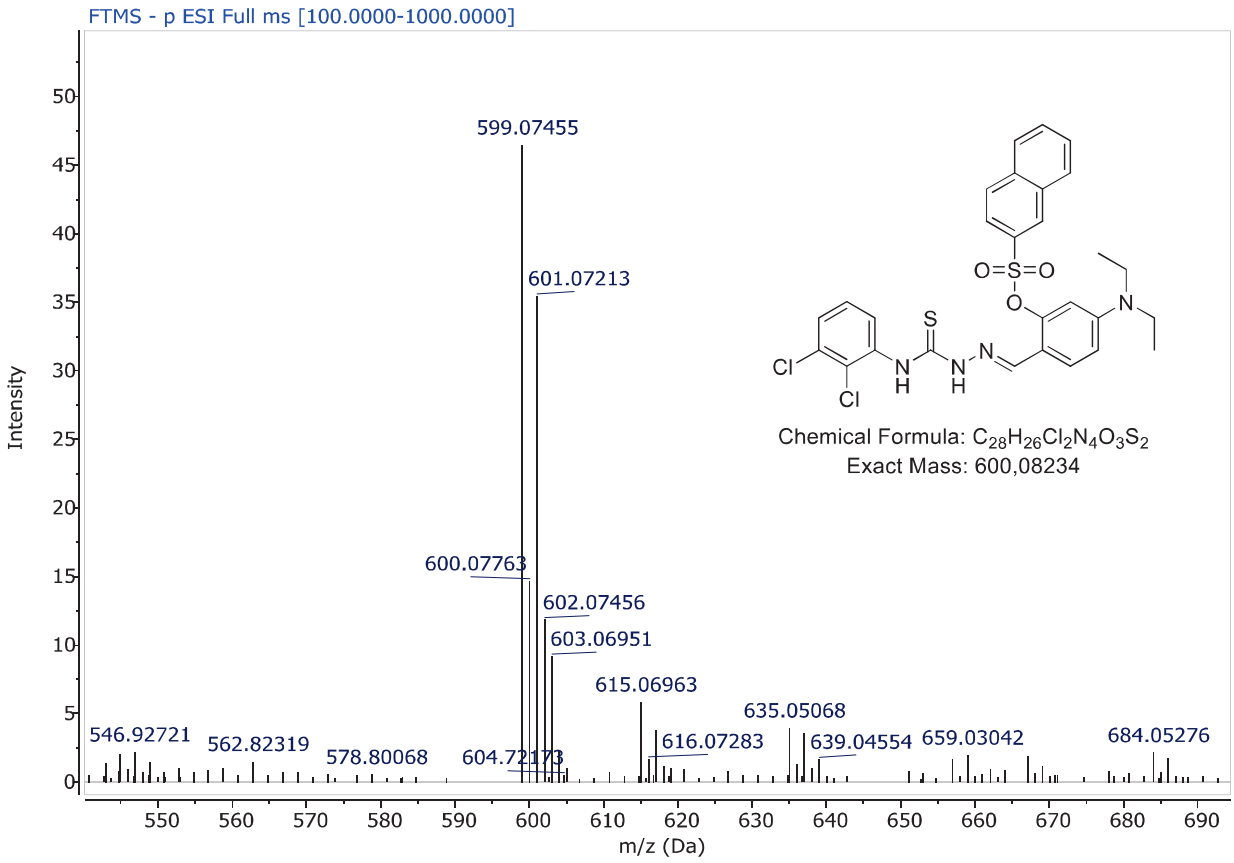

Figure S 6. ESI-HRMS Spectrum of Compound **5a** (extended)

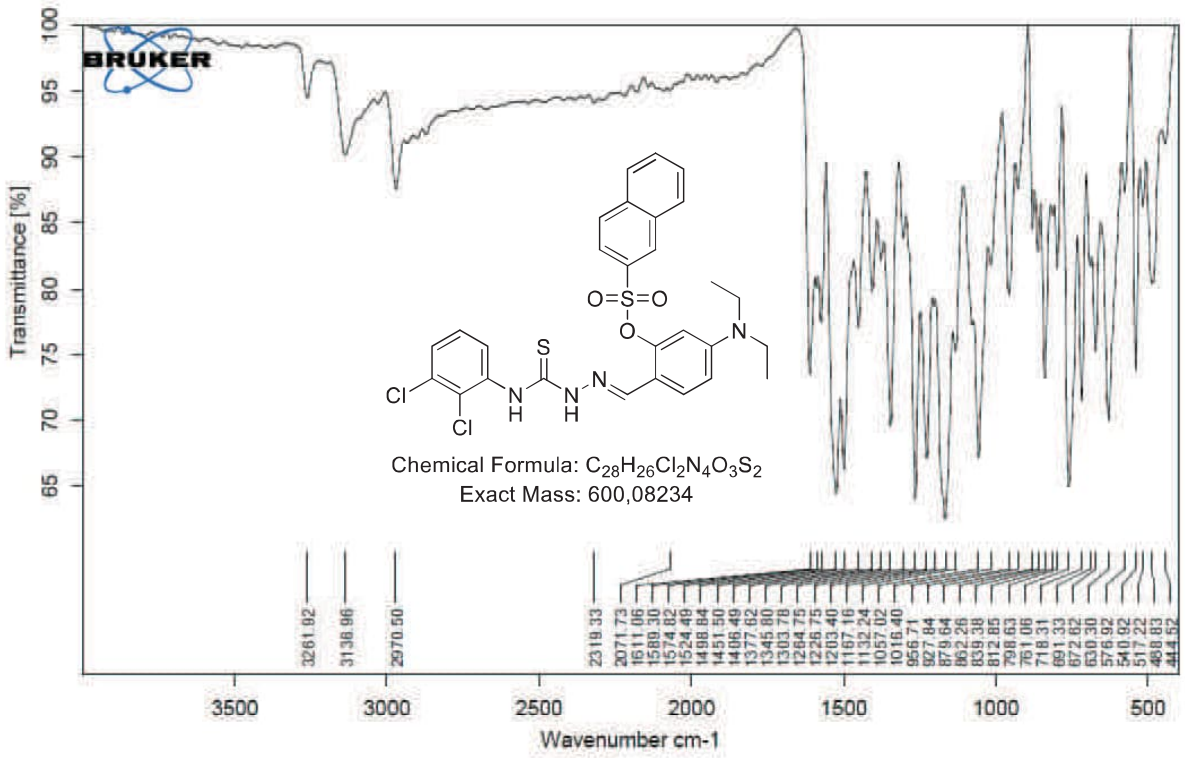

Figure S 7. FT-IR Spectrum of Compound **5a**

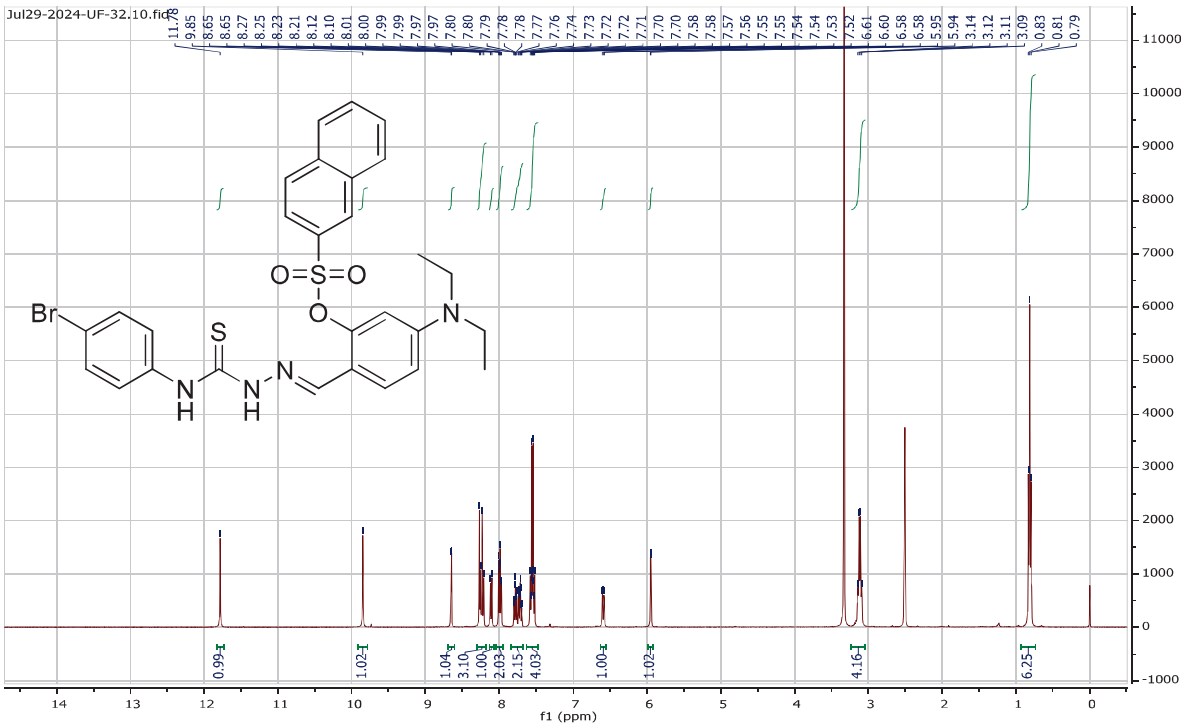

Figure S 8. ^{1}H-NMR Spectrum of Compound **5b** (DMSO-*d6*, 400 MHz)

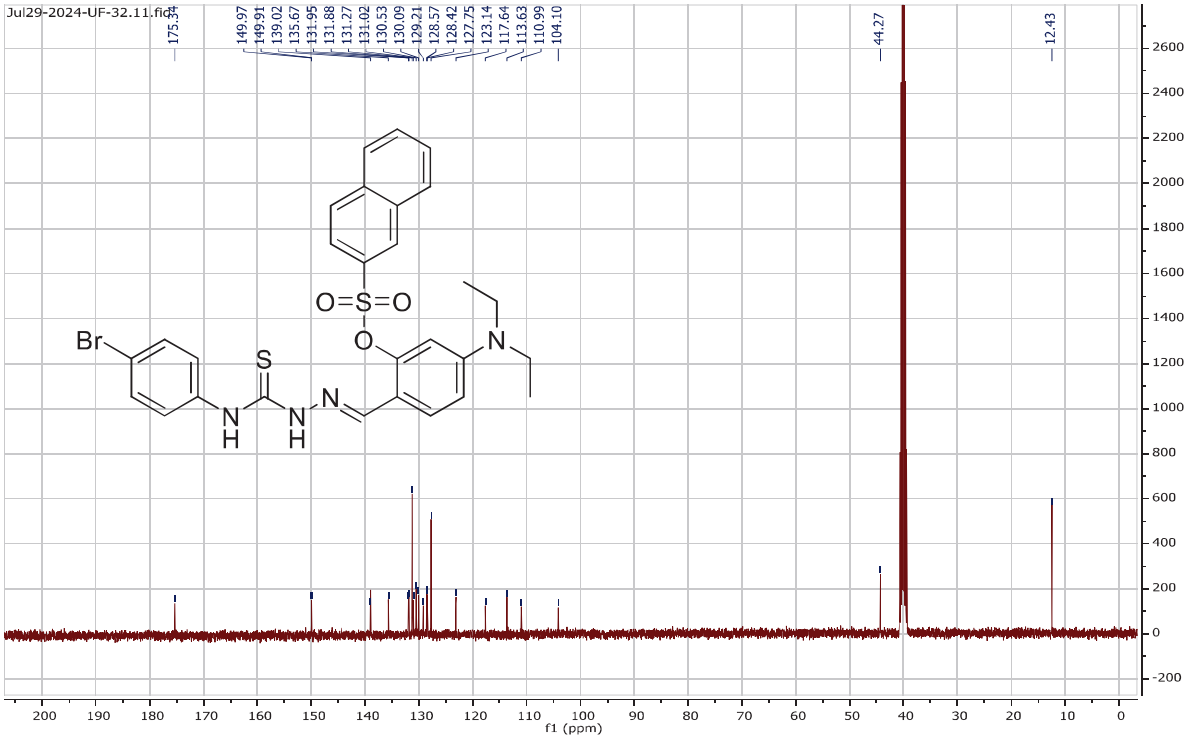

Figure S 9. ^{13}C-NMR Spectrum of Compound **5b** (DMSO-*d6*, 100 MHz)

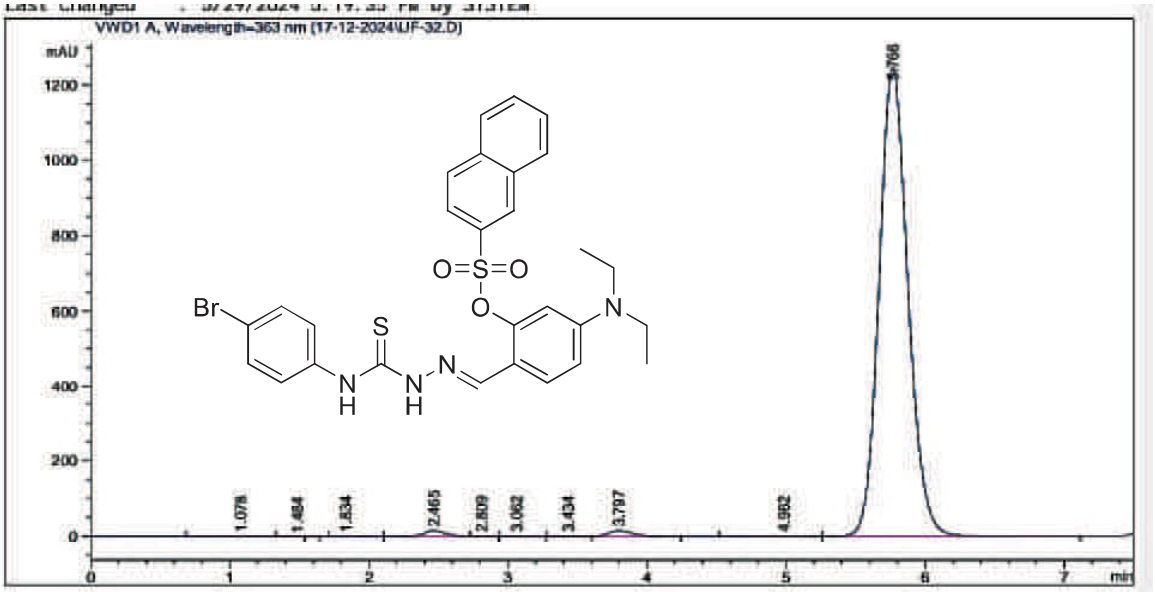

Area Percent Report

Sorted By : Signal
Multiplier : 1.0000
Dilution : 1.0000
Use Multiplier & Dilution Factor with ISTDs

Signal 1: VWD1 A, Wavelength=363 nm

Peak #	RetTime [min]	Type	Width [min]	Area [mAU*s]	Height [mAU]	Area %
1	1.078	BV R	0.2455	3.79857	1.89532e-1	0.0207
2	1.484	VV E	0.0956	2.34355e-1	3.31408e-2	1.278e-3
3	1.834	BB	0.1496	1.69731	1.54952e-1	9.257e-3
4	2.465	BV R	0.1537	157.82867	15.31502	0.8608
5	2.809	VB E	0.0877	8.23985e-1	1.28906e-1	4.494e-3
6	3.062	BB	0.1281	1.70550	1.98157e-1	9.301e-3
7	3.434	BV E	0.1497	2.13836	2.17367e-1	0.0117
8	3.797	VB R	0.1784	171.73717	14.87329	0.9366
9	4.982	BV	0.2662	23.40304	1.28592	0.1276
10	5.766	VB	0.2220	1.79727e4	1247.16541	98.0183

Data File D:\HPLC-DATA\Data\17-12-2024\UF-32.D
Sample Name: UF-32

Peak #	RetTime [min]	Type	Width [min]	Area [mAU*s]	Height [mAU]	Area %
Totals :				1.83361e4	1279.56169	

Figure S 10. HPLC Purity Analysis of Compound **5b**

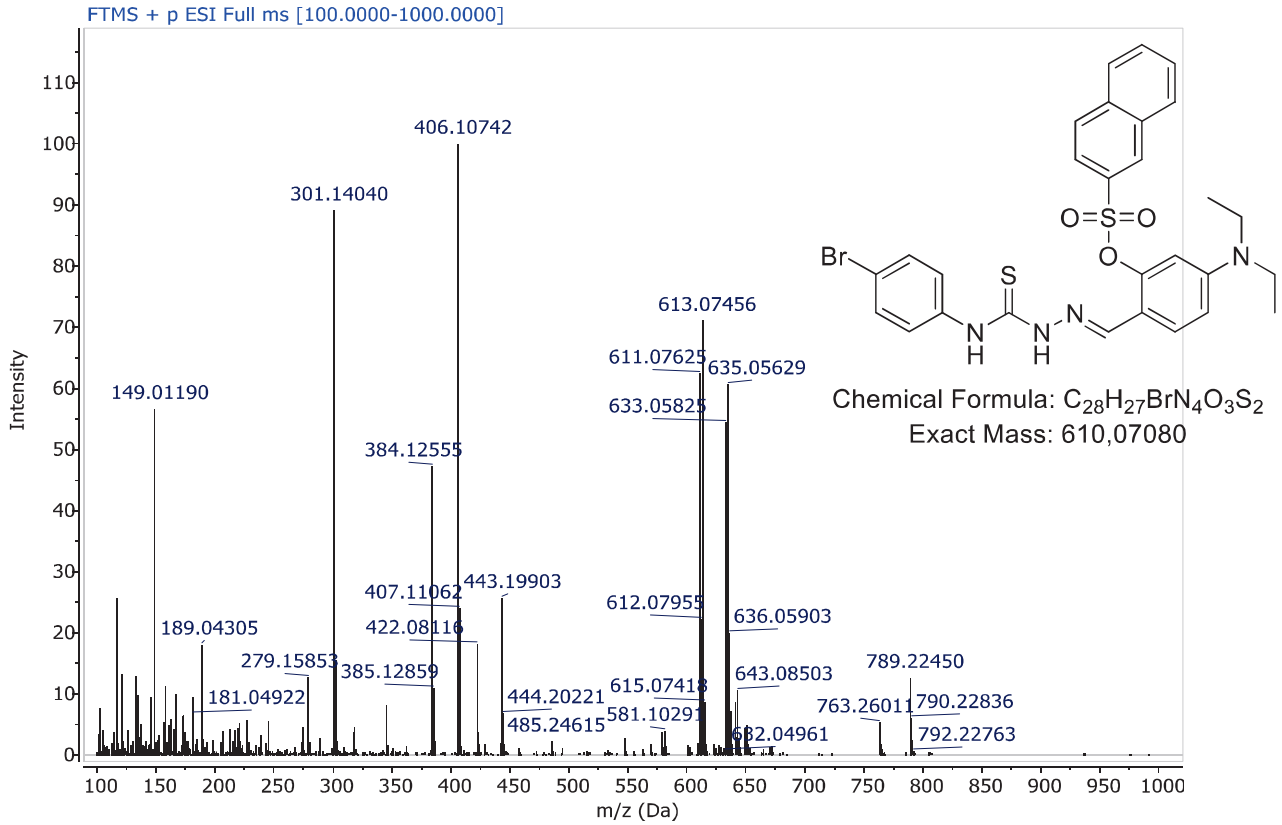

Figure S 11. ESI-HRMS Spectrum of Compound **5b**

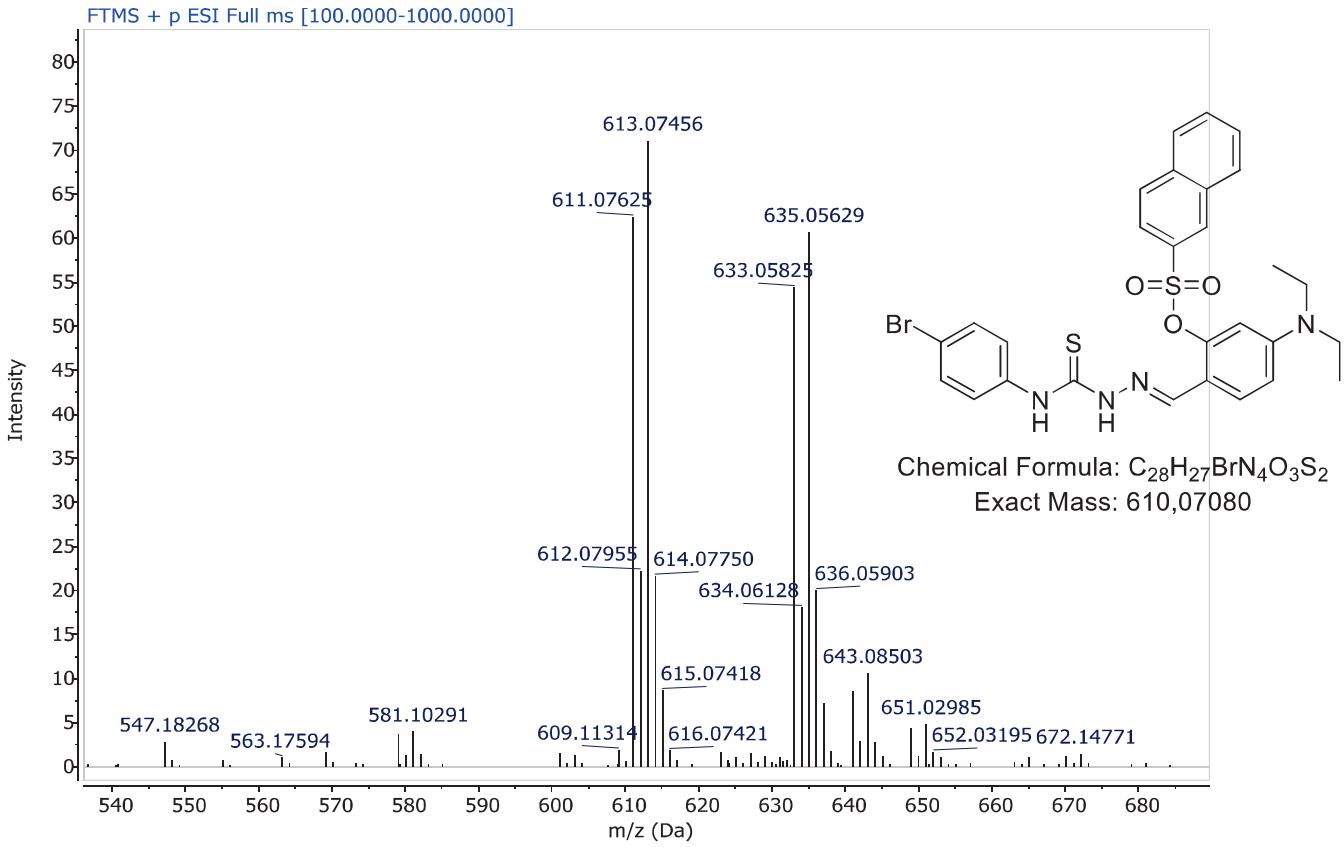

Figure S 12. ESI-HRMS Spectrum of Compound **5b** (extended)

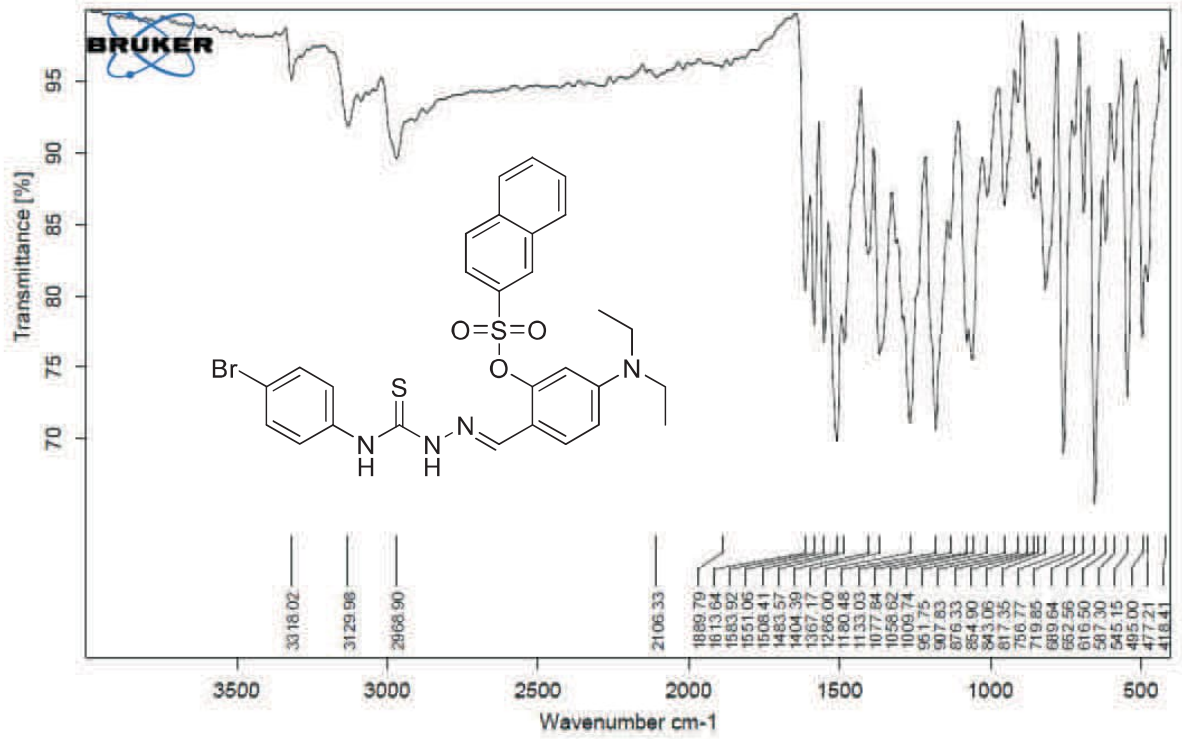

Figure S 13. FT-IR Spectrum of Compound **5b**

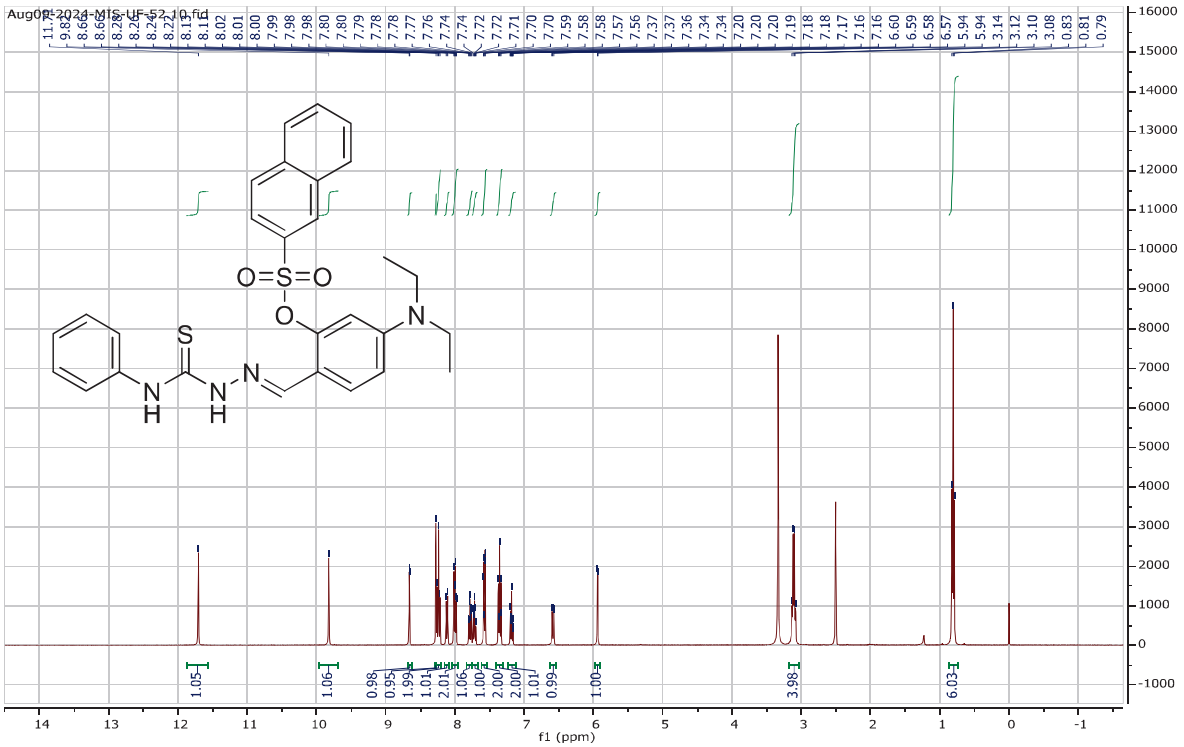

Figure S 14. [1]H-NMR Spectrum of Compound **5c** (DMSO-*d6*, 400 MHz)

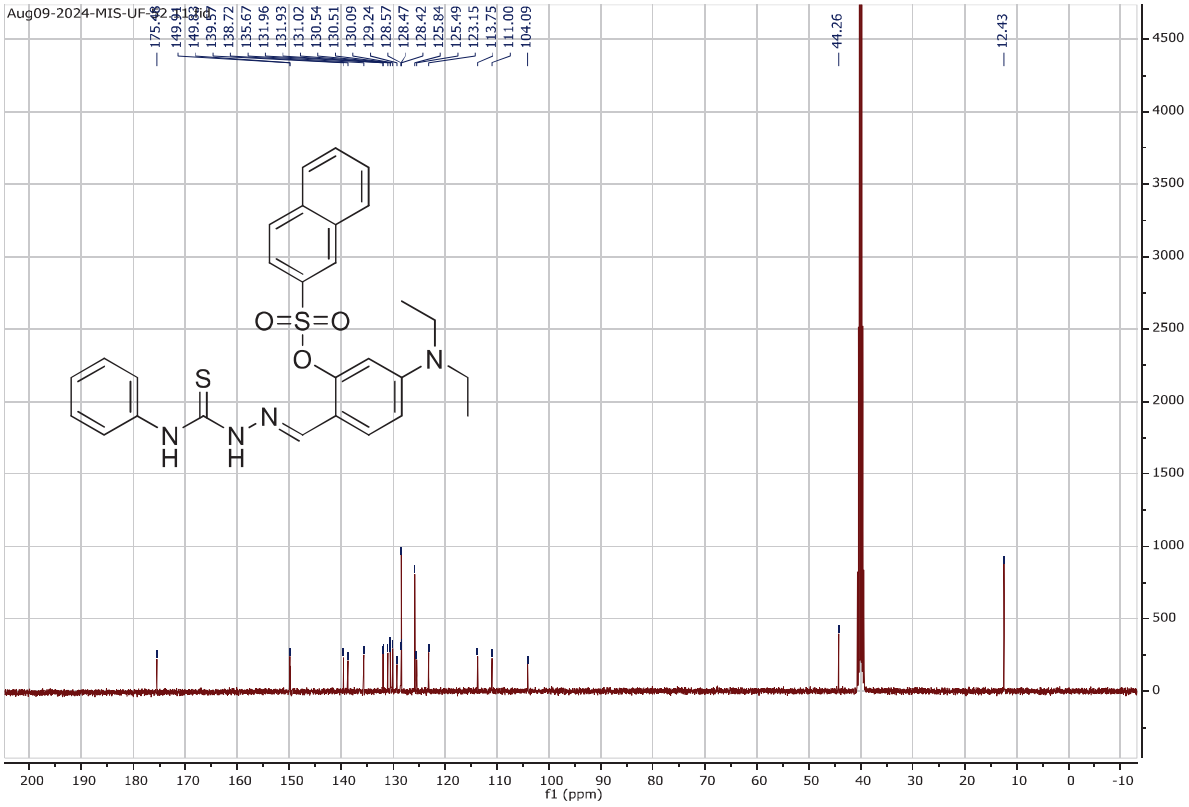

Figure S 15. [13]C-NMR Spectrum of Compound **5c** (DMSO-*d6*, 100 MHz)

Acq. Operator : SYSTEM
Sample Operator : SYSTEM
Acq. Instrument : HPLC Location : -
Injection Date : 12/21/2024 1:55:33 PM Inj : 1
Inj Volume : No Inj

Method : D:\HPLC-DATA\Method\BZ-11.M
Last changed : 5/29/2024 5:19:35 PM by SYSTEM

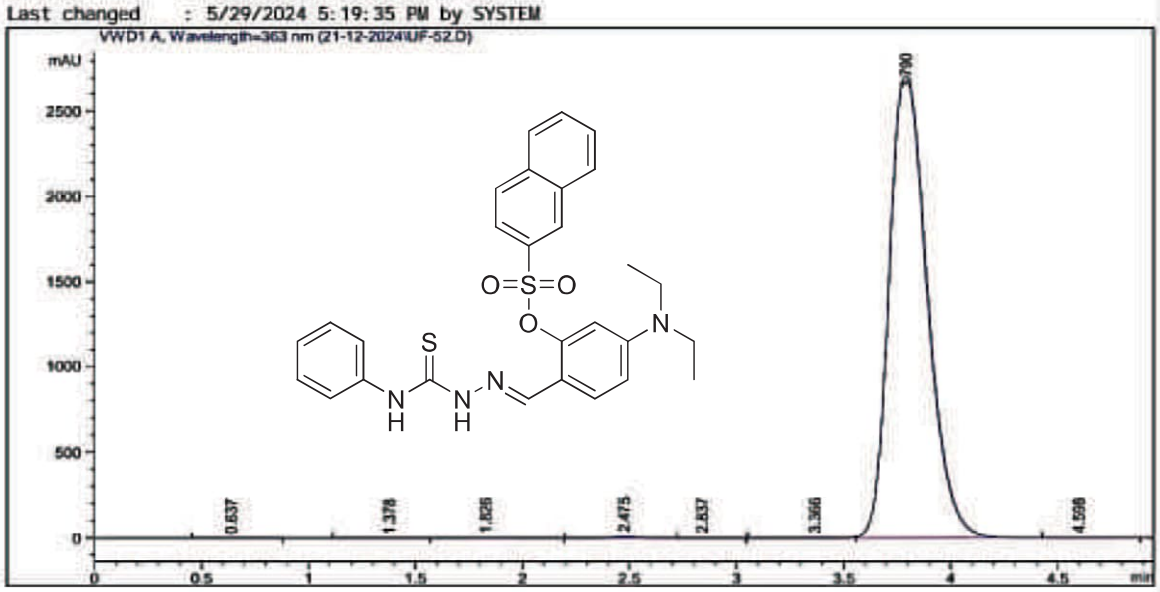

Area Percent Report

Sorted By : Signal
Multiplier : 1.0000
Dilution : 1.0000
Use Multiplier & Dilution Factor with ISTDs

Signal 1: VWD1 A, Wavelength=363 nm

Peak #	RetTime [min]	Type	Width [min]	Area [mAU*s]	Height [mAU]	Area %
1	0.637	BB	0.1682	2.47061	1.93153e-1	7.324e-3
2	1.378	BV E	0.2017	2.84027	1.74399e-1	8.420e-3
3	1.826	VB R	0.1618	28.39550	2.67245	0.0842
4	2.475	BV R	0.1613	76.41418	6.97383	0.2265
5	2.837	VB E	0.1402	3.08681	3.19680e-1	9.151e-3
6	3.366	BV E	0.1763	55.11078	4.64399	0.1634
7	3.790	VV R	0.1909	3.35574e4	2713.43994	99.4805
8	4.598	VBAE	0.1987	6.91442	5.01389e-1	0.0205
Totals :				3.37326e4	2728.91904	

Figure S 16. HPLC Purity Analysis of Compound **5c**

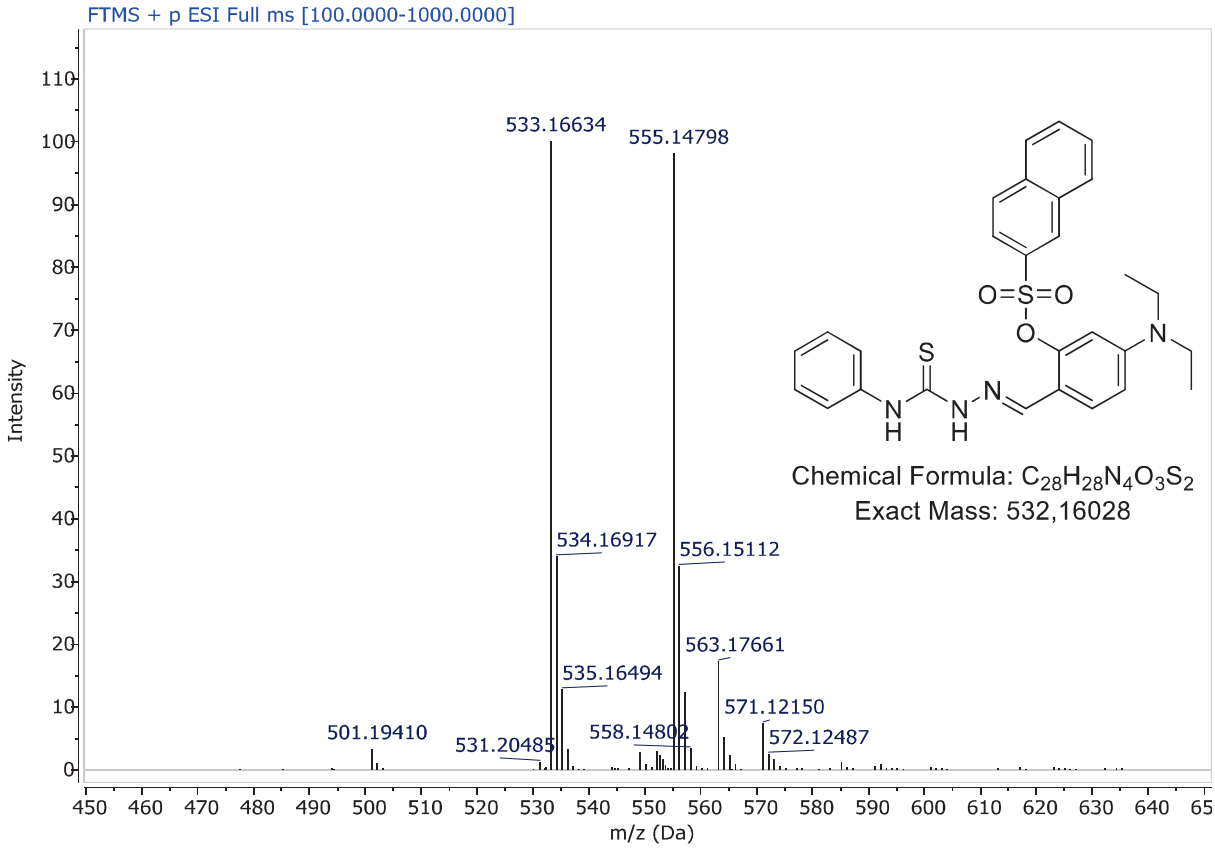

Figure S 17. ESI-HRMS Spectrum of Compound **5c**

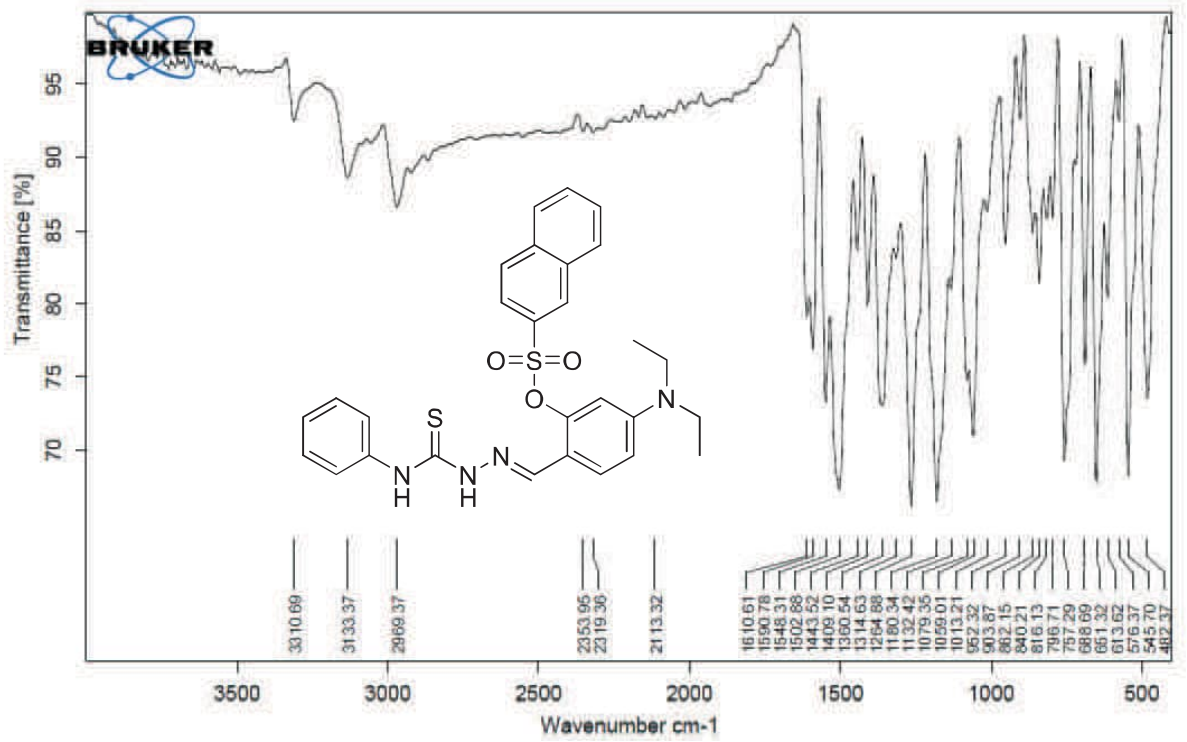

Figure S 18. FT-IR Spectrum of Compound **5c**

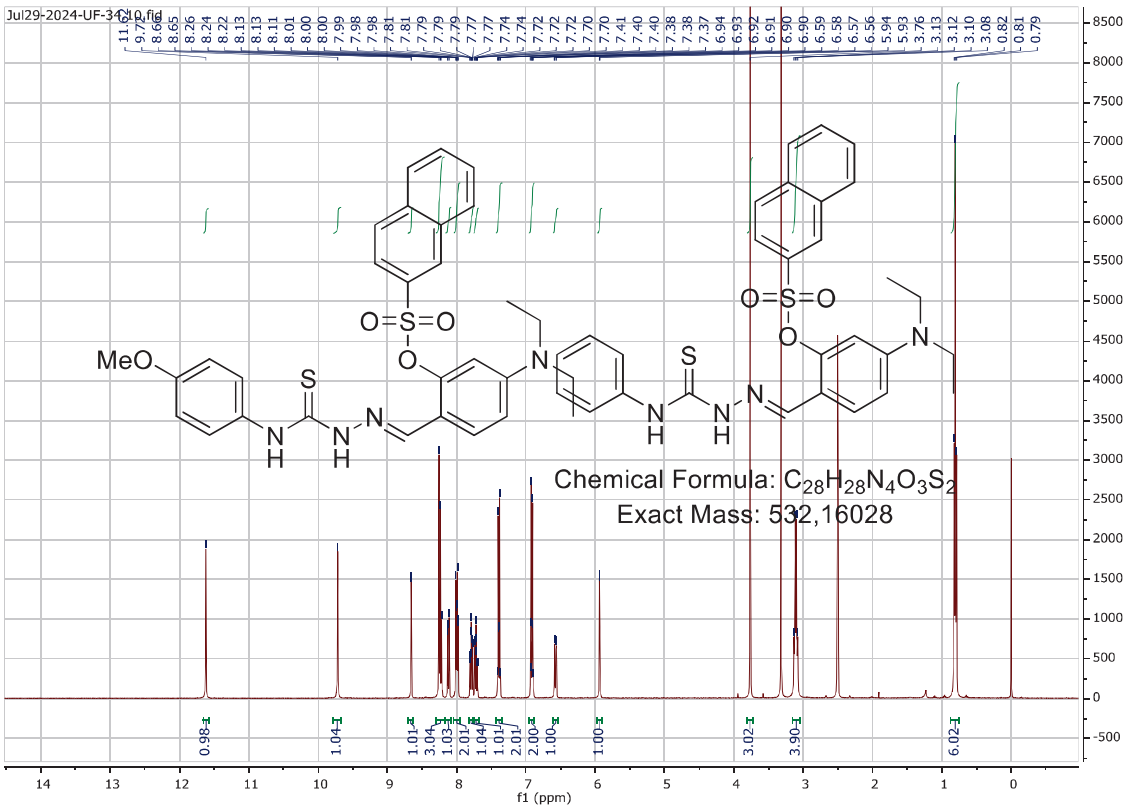

Figure S 19. [1]H-NMR Spectrum of Compound **5d** (DMSO-*d6*, 400 MHz)

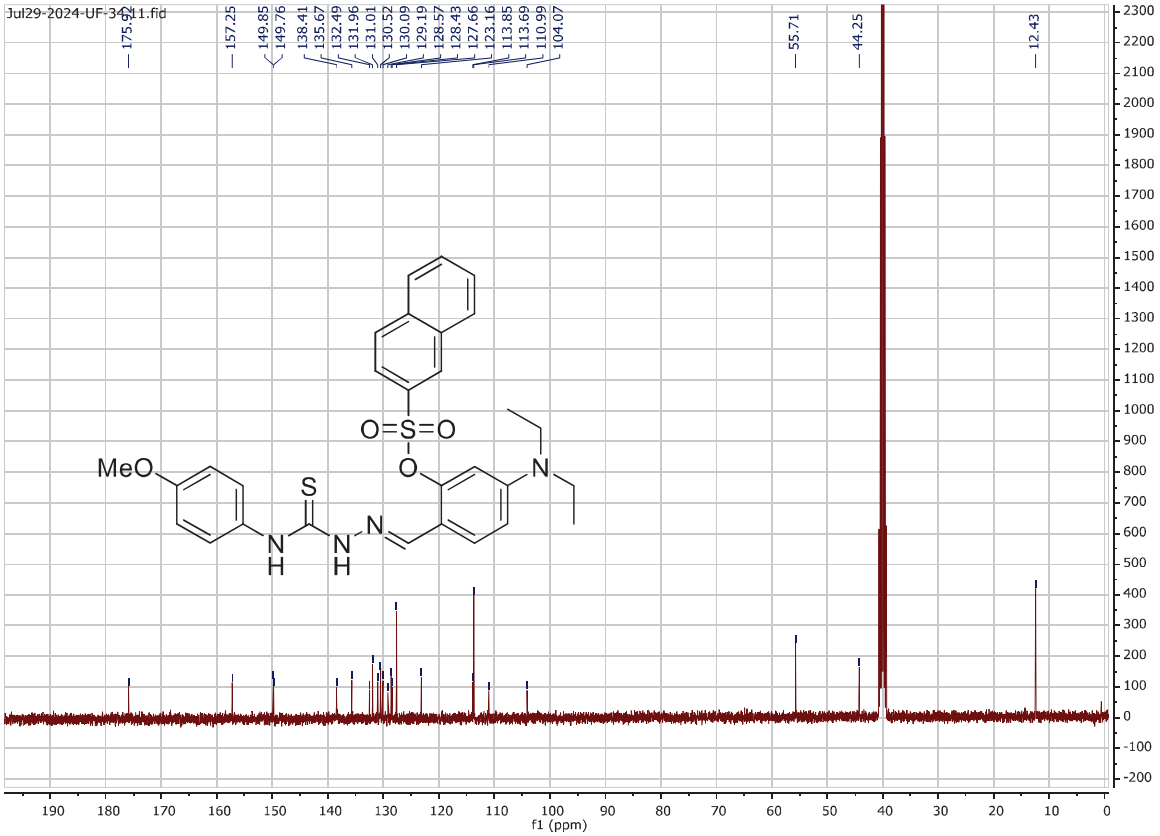

Figure S 20. [13]C-NMR Spectrum of Compound **5d** (DMSO-*d6*, 100 MHz)

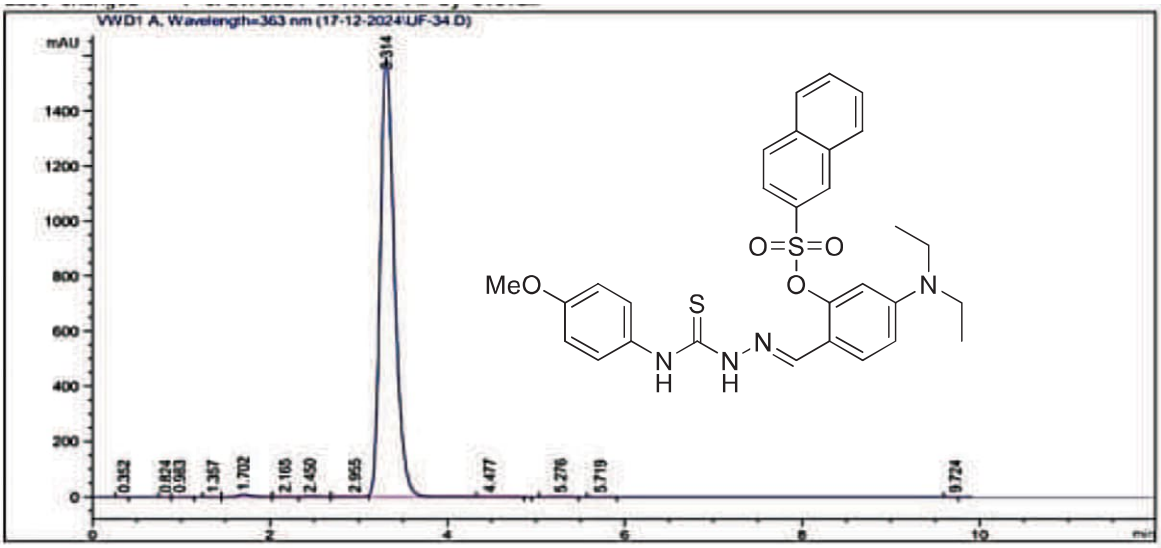

Area Percent Report

Sorted By : Signal
Multiplier : 1.0000
Dilution : 1.0000
Use Multiplier & Dilution Factor with ISTDs

Signal 1: VWD1 A, Wavelength=363 nm

Peak #	RetTime [min]	Type	Width [min]	Area [mAU*s]	Height [mAU]	Area %
1	0.352	BV	0.0679	1.31698e-1	2.87833e-2	7.366e-4
2	0.824	BB	0.0807	2.75594e-1	5.33244e-2	1.541e-3
3	0.983	BB	0.0818	3.70976e-1	6.29909e-2	2.075e-3
4	1.357	BV	0.0874	5.63858e-1	8.68938e-2	3.154e-3
5	1.702	VB	0.1424	75.30840	8.07019	0.4212
6	2.165	BV E	0.1123	2.72918	3.57561e-1	0.0153
7	2.450	VB R	0.1388	27.12757	3.00500	0.1517
8	2.955	BV E	0.1654	16.13267	1.44229	0.0902
9	3.314	VV R	0.1693	1.77502e4	1592.52966	99.2750
10	4.477	VB E	0.1926	3.63274	2.39997e-1	0.0203

Data File D:\HPLC-DATA\Data\17-12-2024\UF-34.D
Sample Name: UF-34

Peak #	RetTime [min]	Type	Width [min]	Area [mAU*s]	Height [mAU]	Area %
11	5.276	BB	0.1685	2.09760	1.75560e-1	0.0117
12	5.719	BB	0.1400	1.06263	9.54864e-2	5.943e-3
13	9.724	BB	0.0895	1.92650e-1	2.78348e-2	1.077e-3
Totals :				1.78798e4	1606.17557	

Figure S 21. HPLC Purity Analysis of Compound **5d**

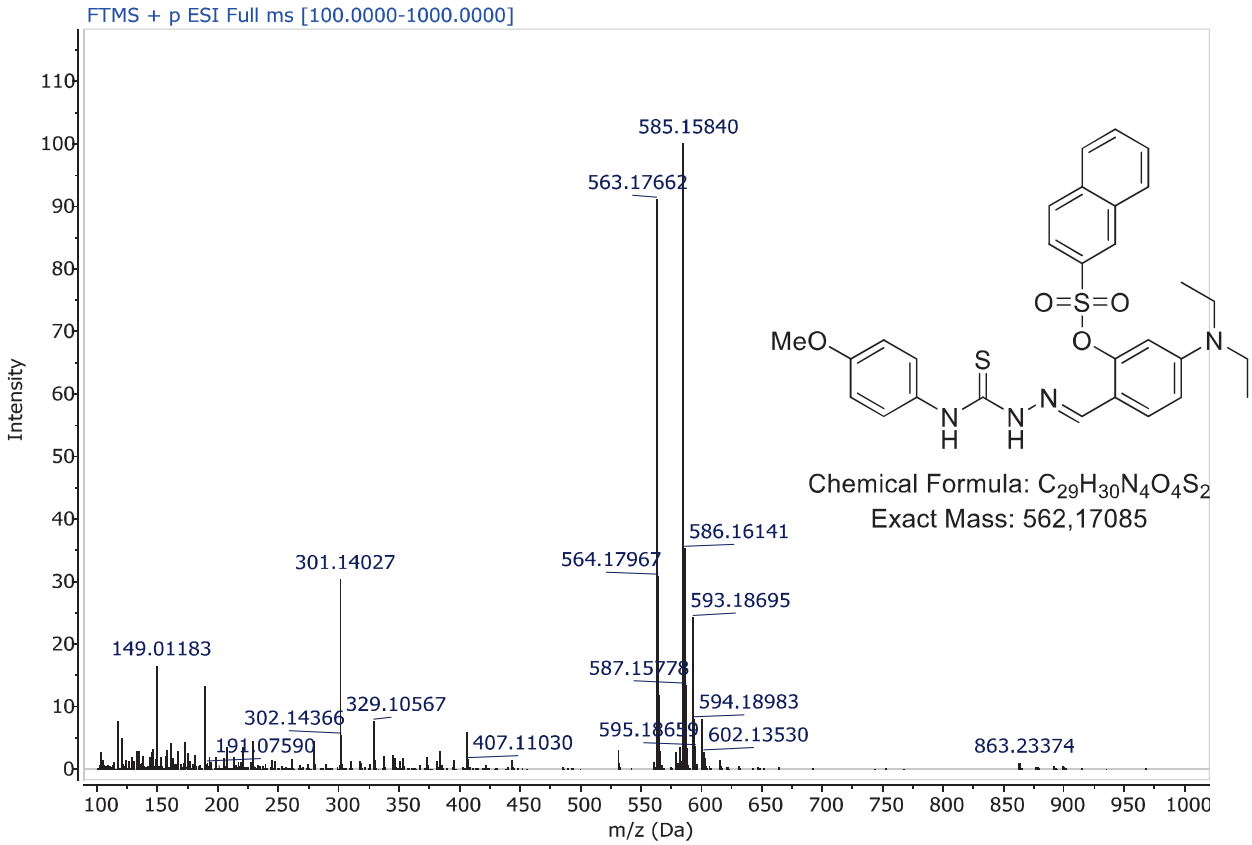

Figure S 22. ESI-HRMS Spectrum of Compound **5d**

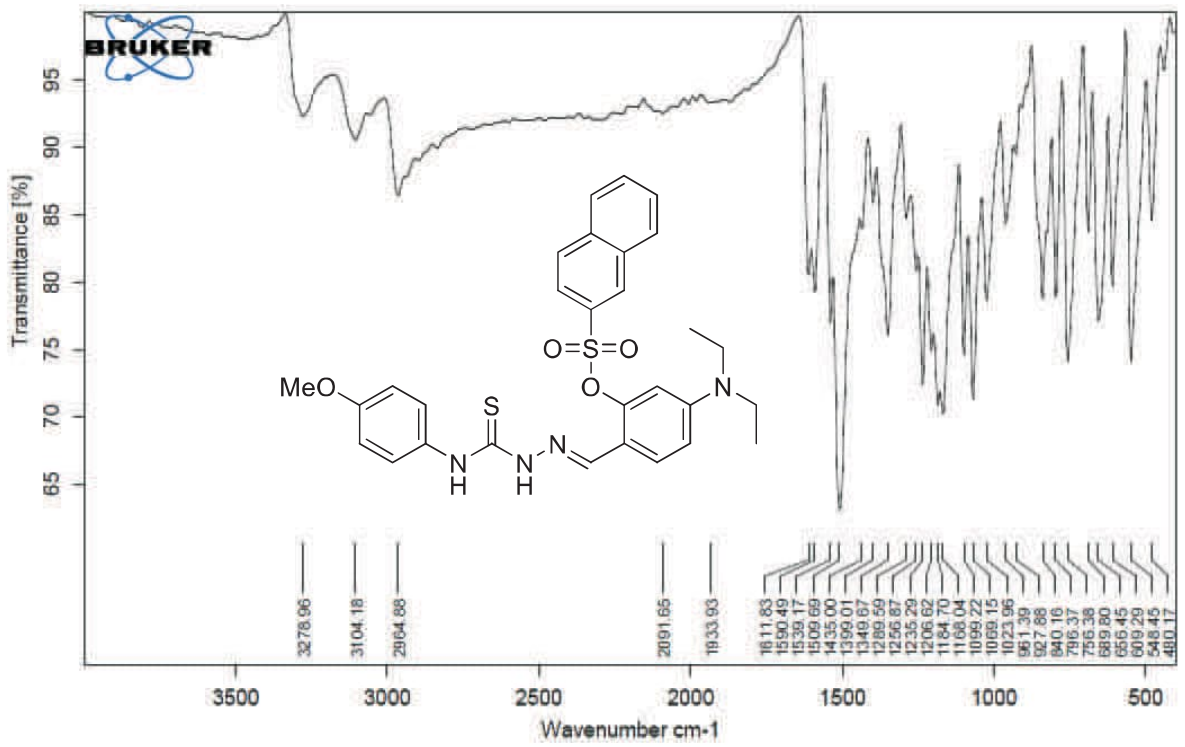

Figure S 23. FT-IR Spectrum of Compound **5d**

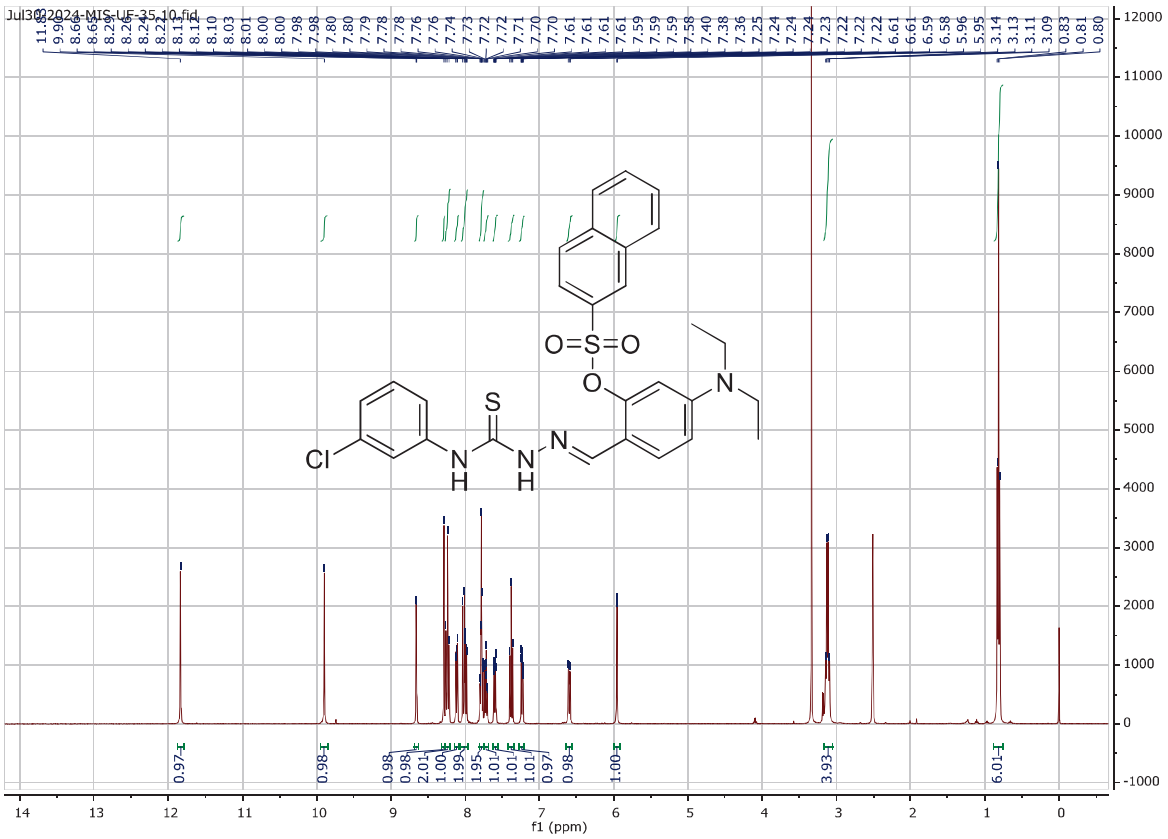

Figure S 24. ^{1}H-NMR Spectrum of Compound **5e** (DMSO-*d6*, 400 MHz)

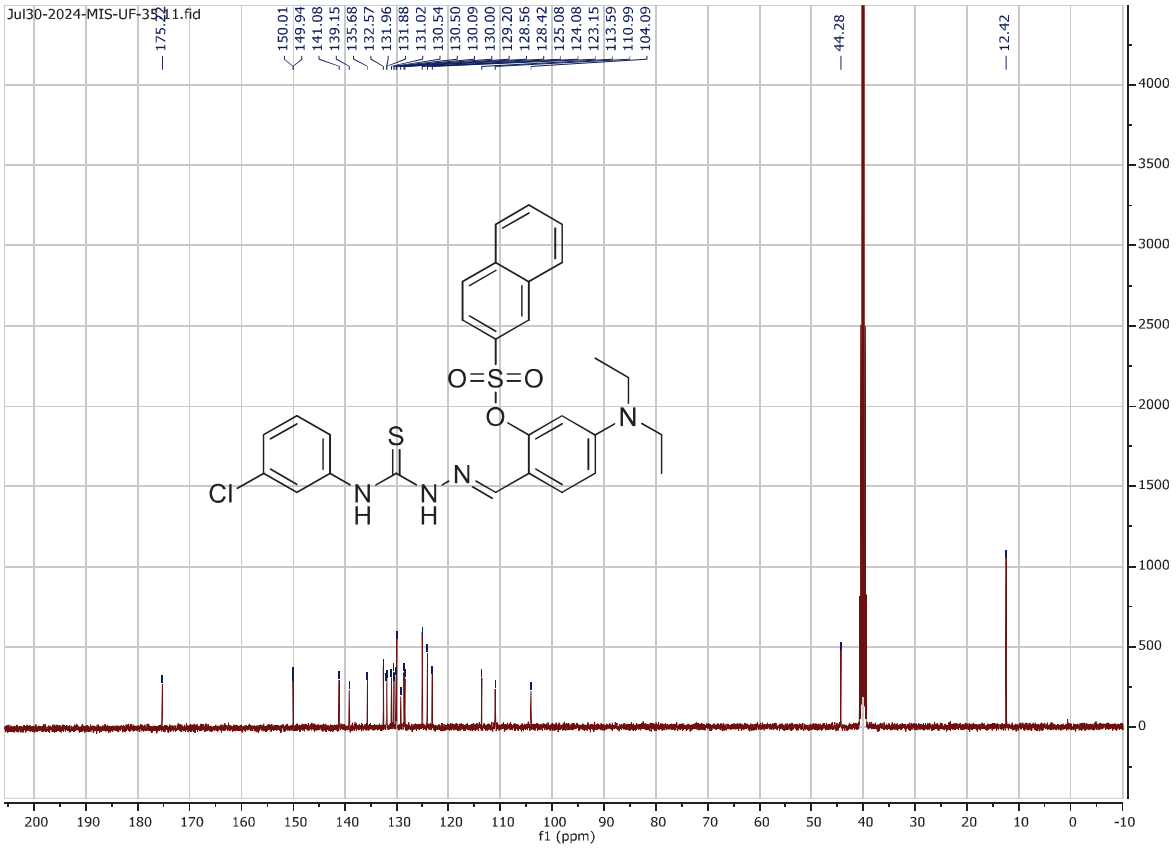

Figure S 25. ^{13}C-NMR Spectrum of Compound **5e** (DMSO-*d6*, 100 MHz)

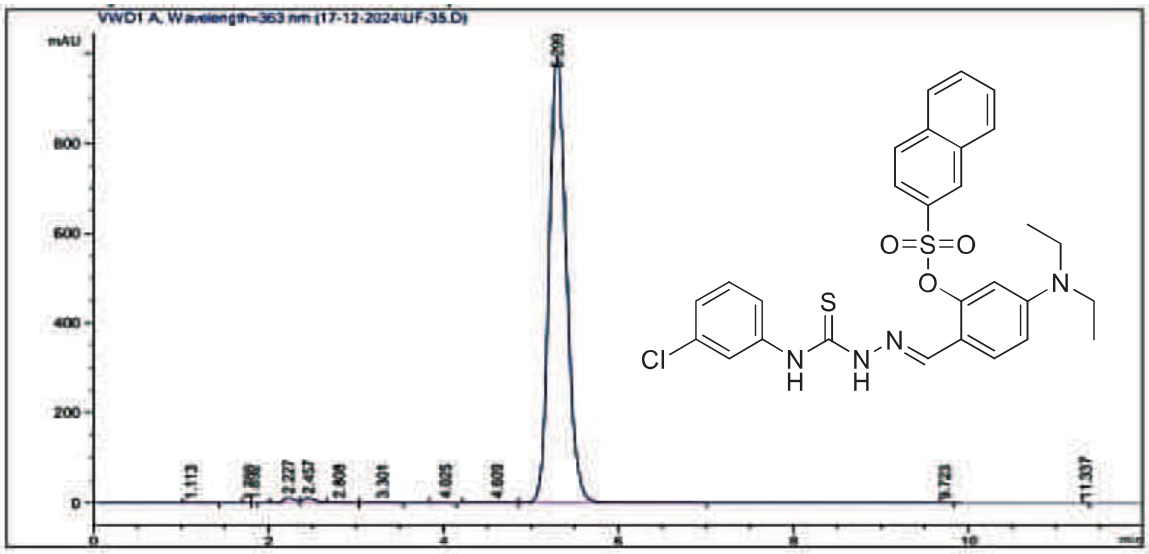

Area Percent Report

Sorted By : Signal
Multiplier : 1.0000
Dilution : 1.0000
Use Multiplier & Dilution Factor with ISTDs

Signal 1: VWD1 A, Wavelength=363 nm

Peak #	RetTime [min]	Type	Width [min]	Area [mAU*s]	Height [mAU]	Area %
1	1.113	BB	0.1303	6.28713e-1	6.10870e-2	4.541e-3
2	1.780	BV	0.0584	1.66930e-1	4.04186e-2	1.206e-3
3	1.832	VB	0.0393	7.27133e-2	2.91477e-2	5.252e-4
4	2.227	BV	0.1350	92.44135	10.62140	0.6676
5	2.457	VV R	0.1488	101.43955	10.26612	0.7326
6	2.808	VB E	0.1397	3.73237	3.93933e-1	0.0270
7	3.301	BB	0.1992	4.46080	3.16840e-1	0.0322
8	4.025	BB	0.1268	1.09115	1.16476e-1	7.881e-3
9	4.609	BV	0.2217	11.70080	8.06461e-1	0.0845
10	5.299	VB	0.2108	1.36300e4	995.16412	98.4406

Data File D:\HPLC-DATA\Data\17-12-2024\UF-35.D
Sample Name: UF-35

Peak #	RetTime [min]	Type	Width [min]	Area [mAU*s]	Height [mAU]	Area %
11	9.723	BB	0.0587	1.11746e-1	2.95632e-2	8.071e-4
12	11.337	VB	0.0434	7.36662e-2	2.83354e-2	5.320e-4
Totals :				1.38460e4	1017.87391	

Figure S 26. HPLC Purity Analysis of Compound **5e**

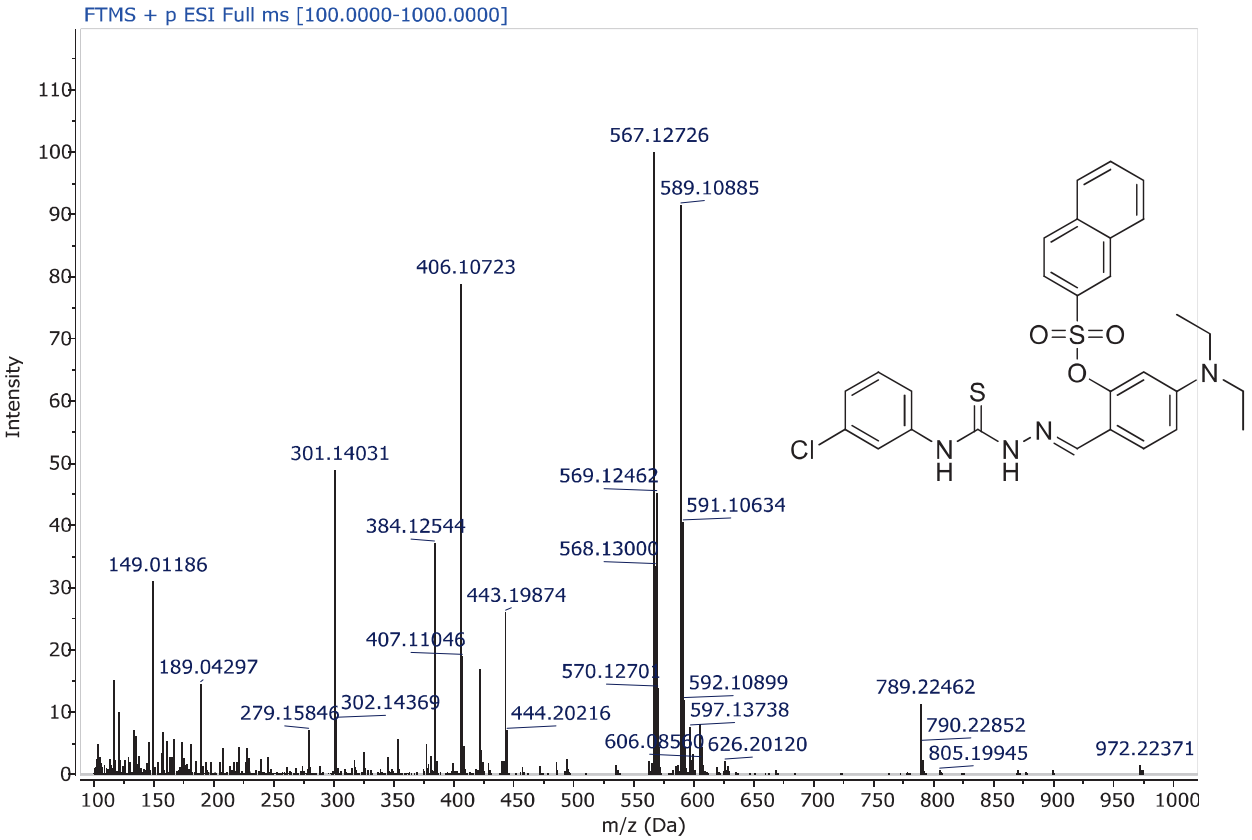

Figure S 27. ESI-HRMS Spectrum of Compound **5e**

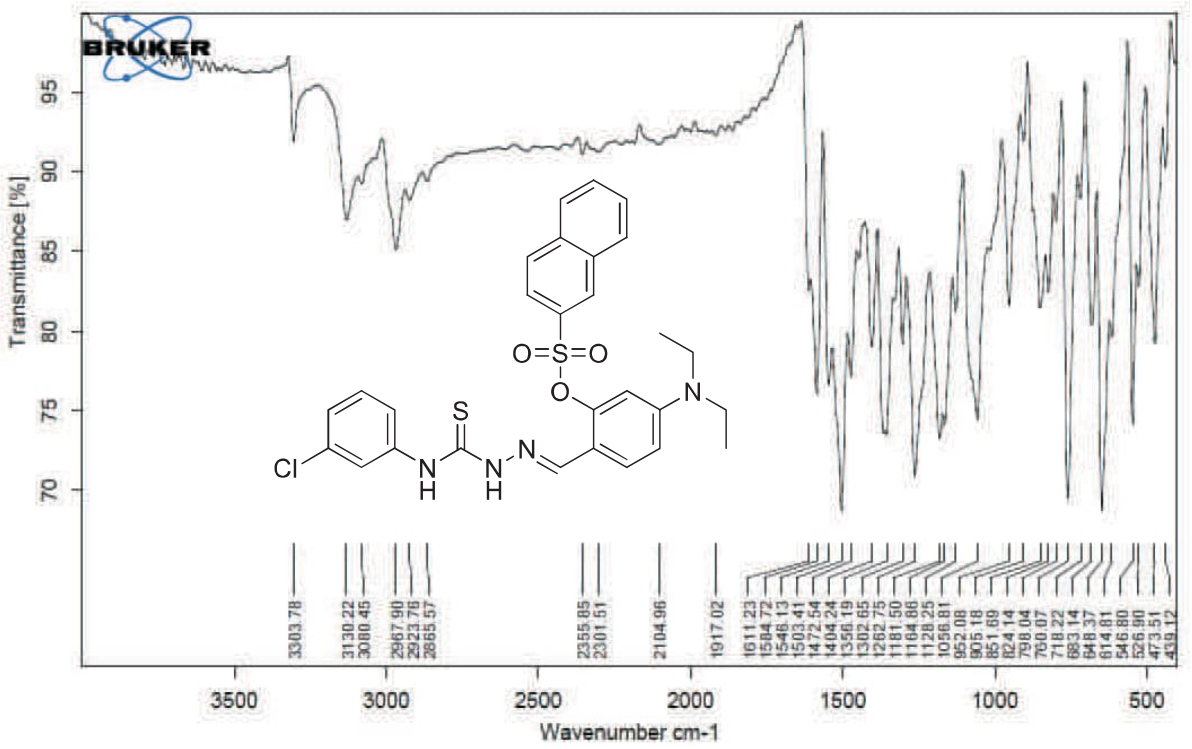

Figure S 28. FT-IR Spectrum of Compound **5e**

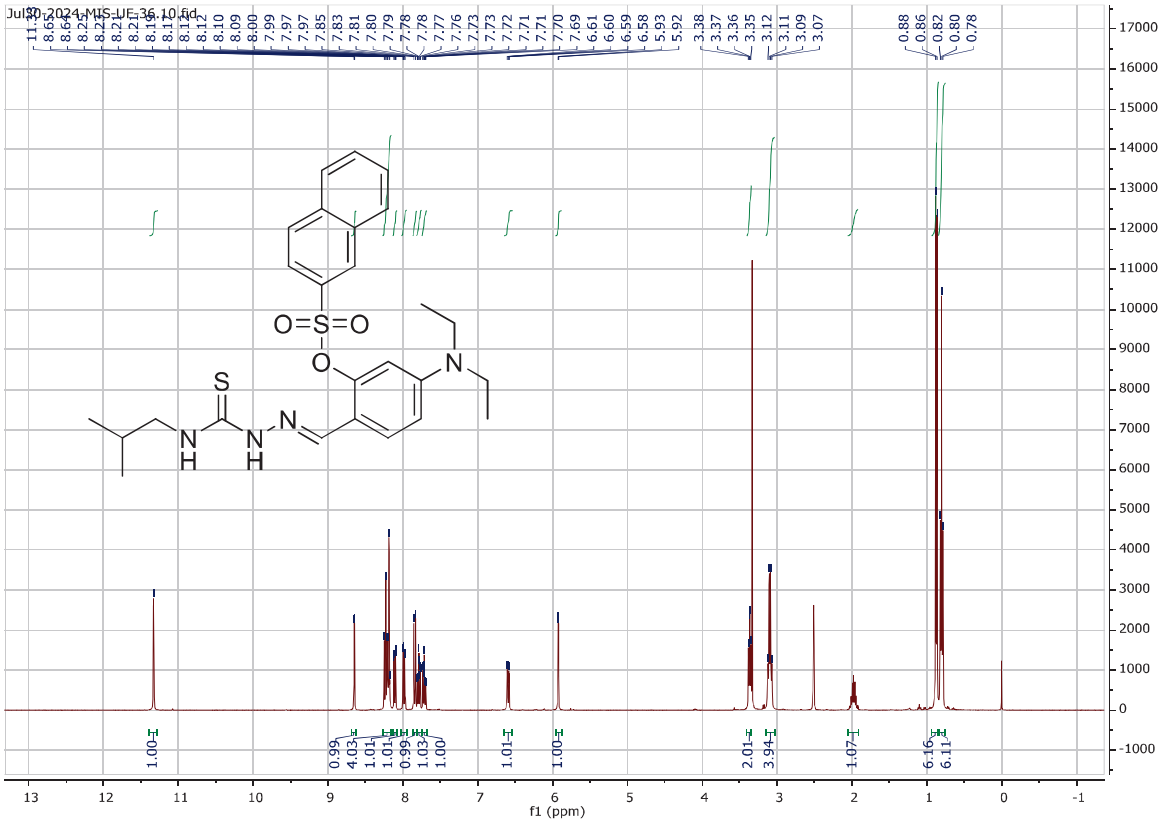

Figure S 29. ^{1}H-NMR Spectrum of Compound **5f** (DMSO-*d6*, 400 MHz)

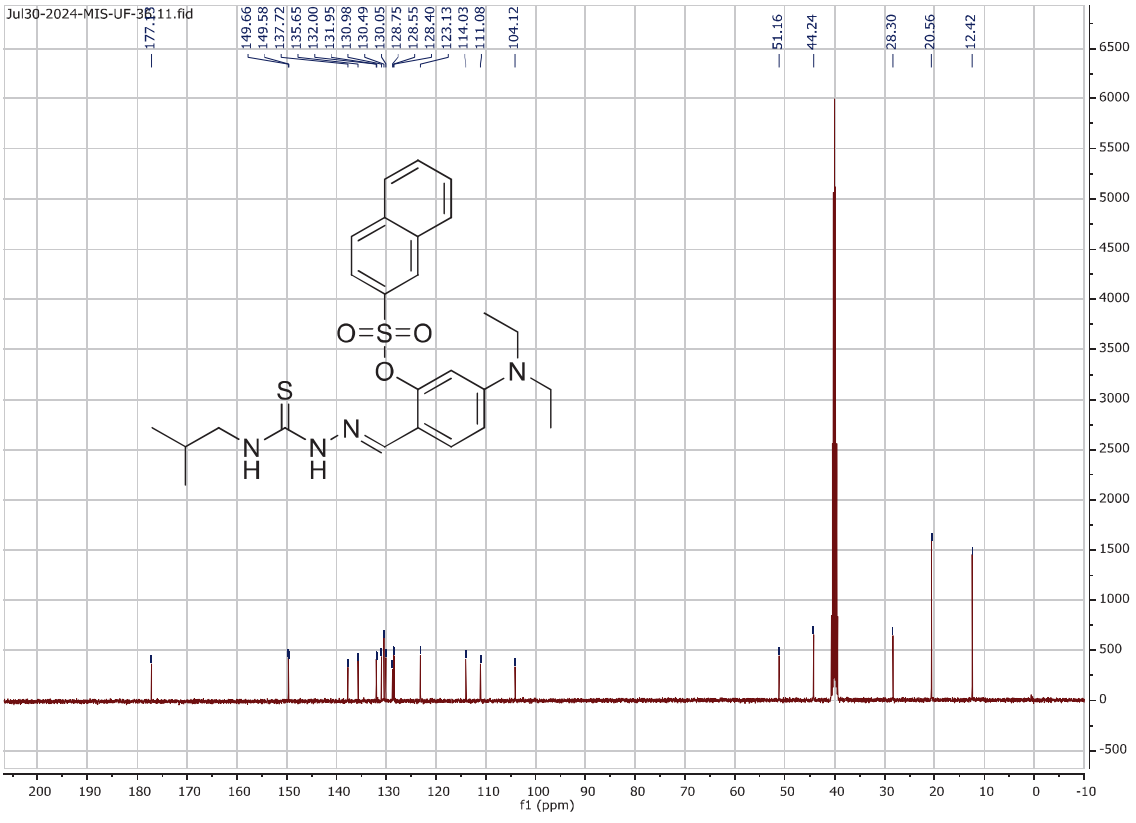

Figure S 30. ^{13}C-NMR Spectrum of Compound **5f** (DMSO-*d6*, 100 MHz)

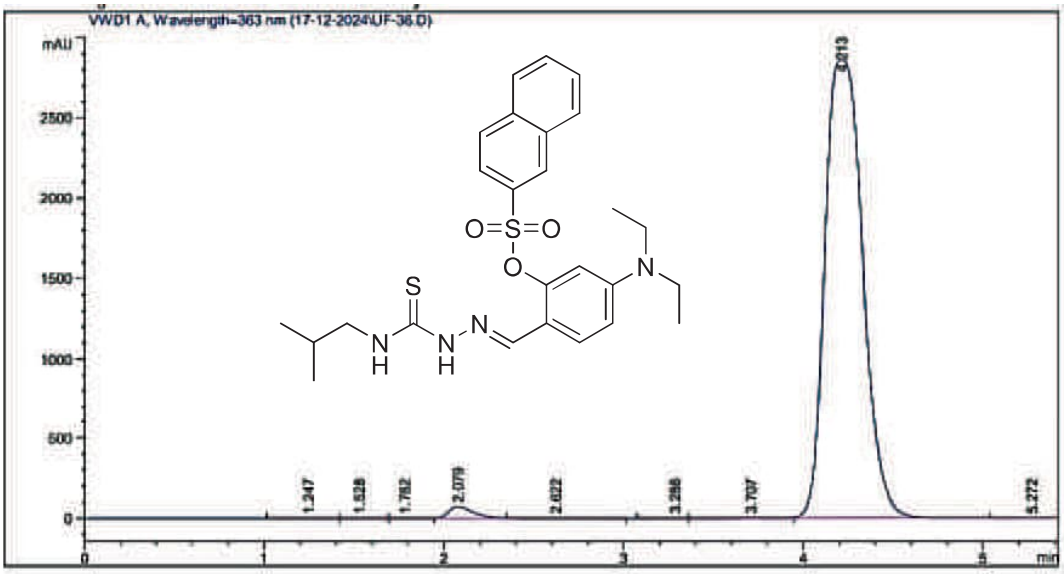

Area Percent Report

Sorted By : Signal
Multiplier : 1.0000
Dilution : 1.0000
Use Multiplier & Dilution Factor with ISTDs

Signal 1: VWD1 A, Wavelength=363 nm

Peak #	RetTime [min]	Type	Width [min]	Area [mAU*s]	Height [mAU]	Area %
1	1.247	BV E	0.1562	5.16884	4.58803e-1	0.0122
2	1.528	VV E	0.1397	11.45072	1.22425	0.0270
3	1.782	VV E	0.1429	7.14915	6.89059e-1	0.0168
4	2.079	VV R	0.1422	672.89374	72.23827	1.5857
5	2.622	VB E	0.2274	14.01569	8.24827e-1	0.0330
6	3.286	BV E	0.1593	8.30166	8.17429e-1	0.0196
7	3.707	VV E	0.2189	57.19376	3.77738	0.1348
8	4.213	VV R	0.2295	4.16524e4	2862.61401	98.1530
9	5.272	VBAE	0.2046	7.64036	5.74665e-1	0.0180

HPLC 12/17/2024 4:27:20 PM SYSTEM Page 1 of 2

Data File D:\HPLC-DATA\Data\17-12-2024\UF-36.D
Sample Name: UF-36

Totals : 4.24362e4 2943.21869

*** End of Report ***

Figure S 31. HPLC Purity Analysis of Compound **5f**

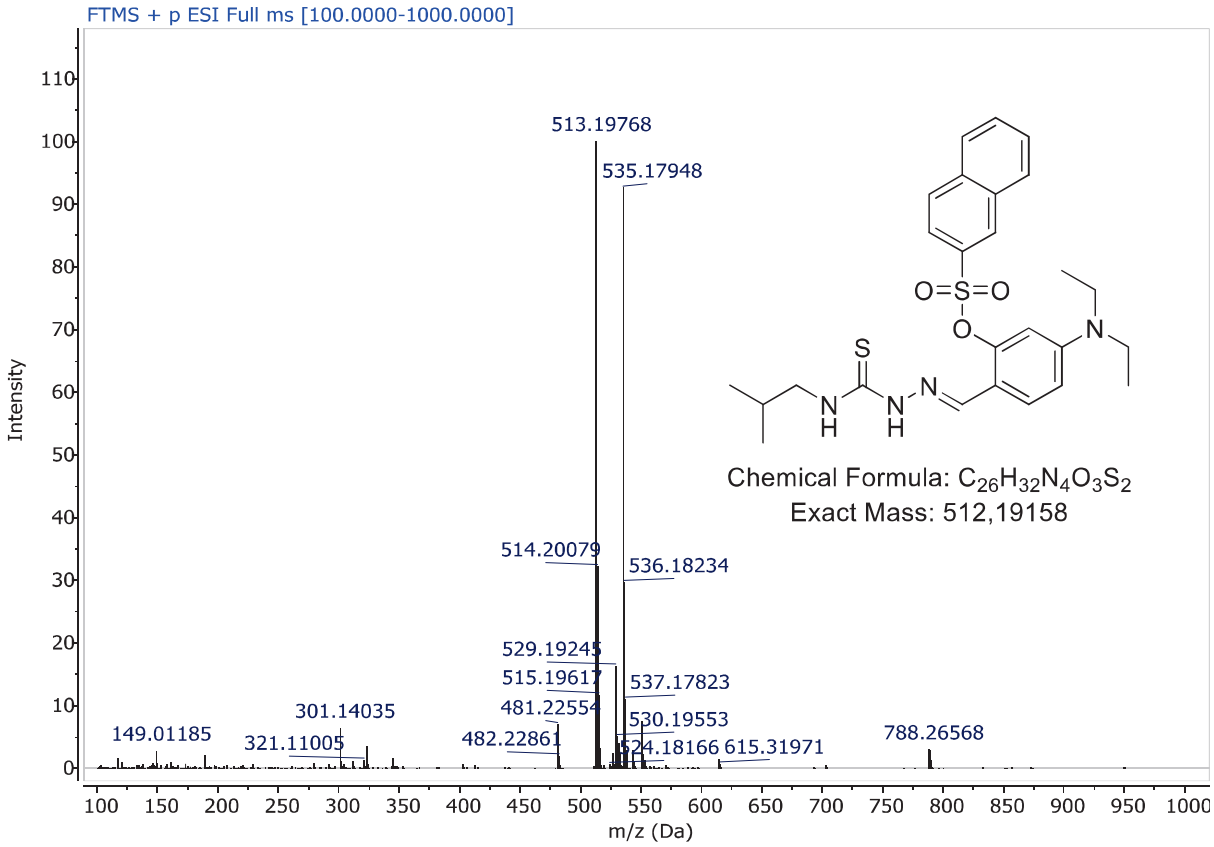

Figure S 32. ESI-HRMS Spectrum of Compound **5f**

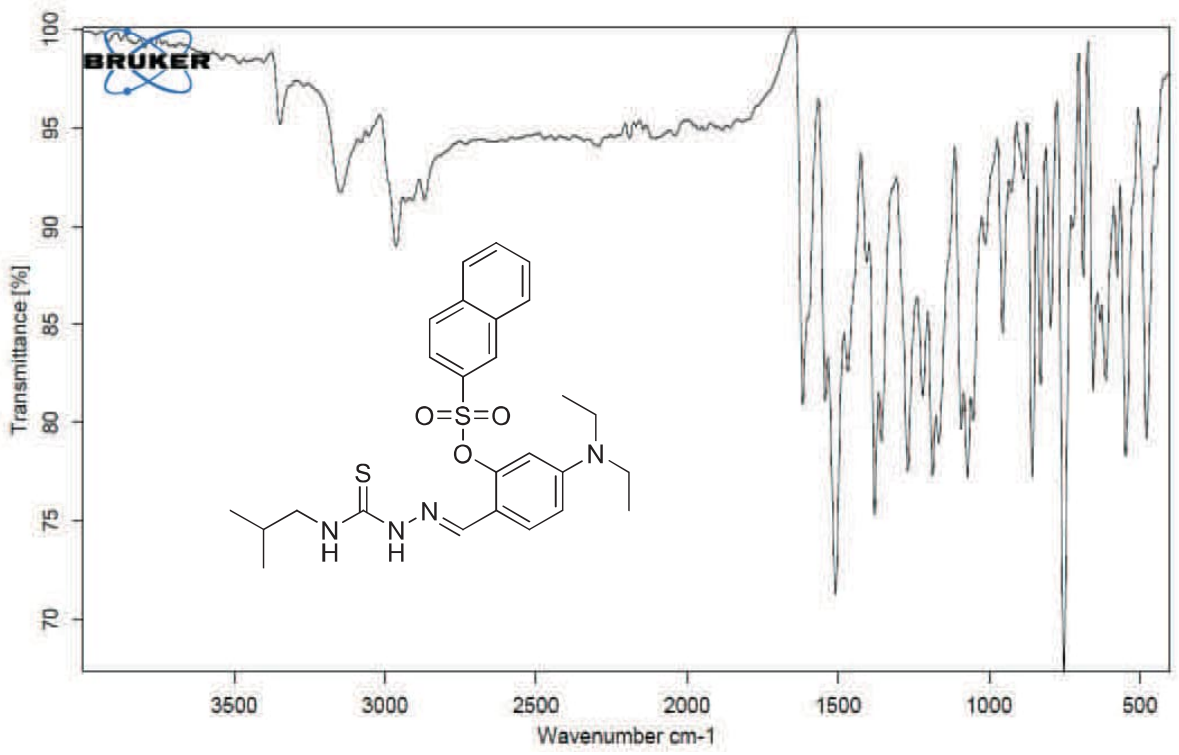

Figure S 33. FT-IR Spectrum of Compound **5f**

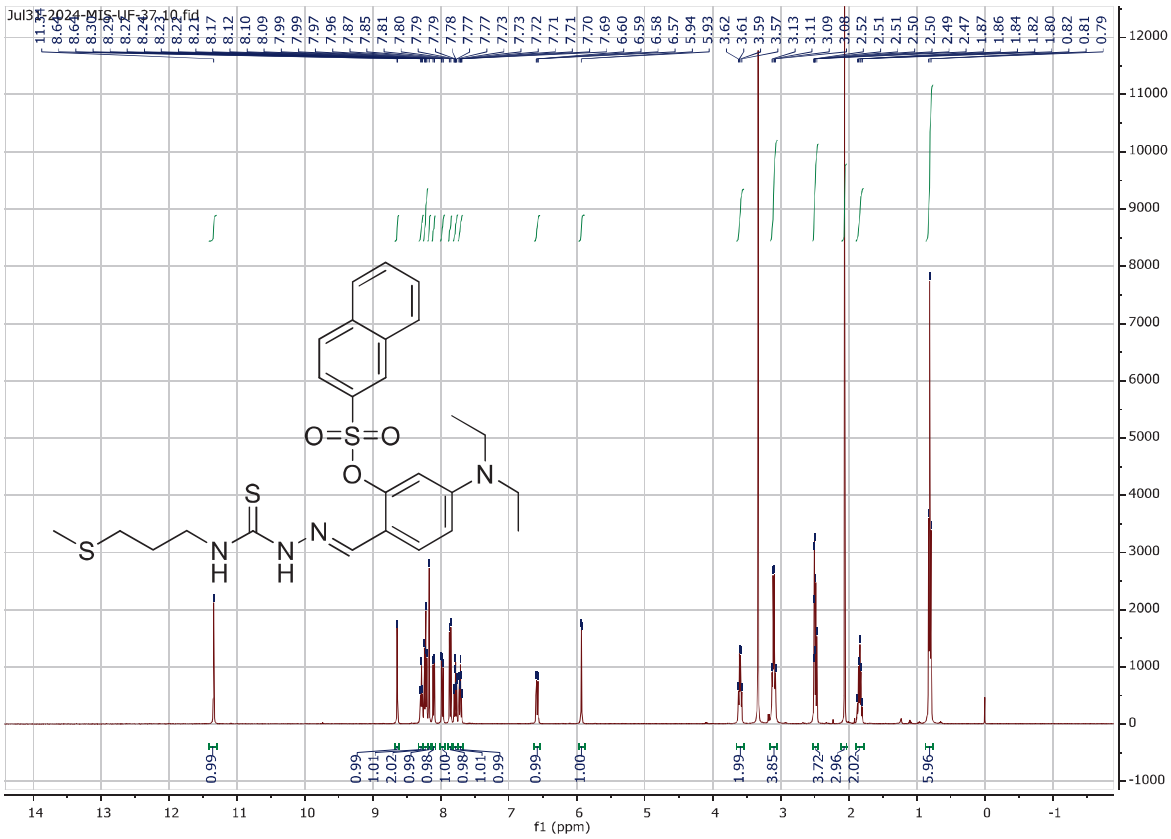

Figure S 34. ^{1}H-NMR Spectrum of Compound **5g** (DMSO-*d6*, 400 MHz)

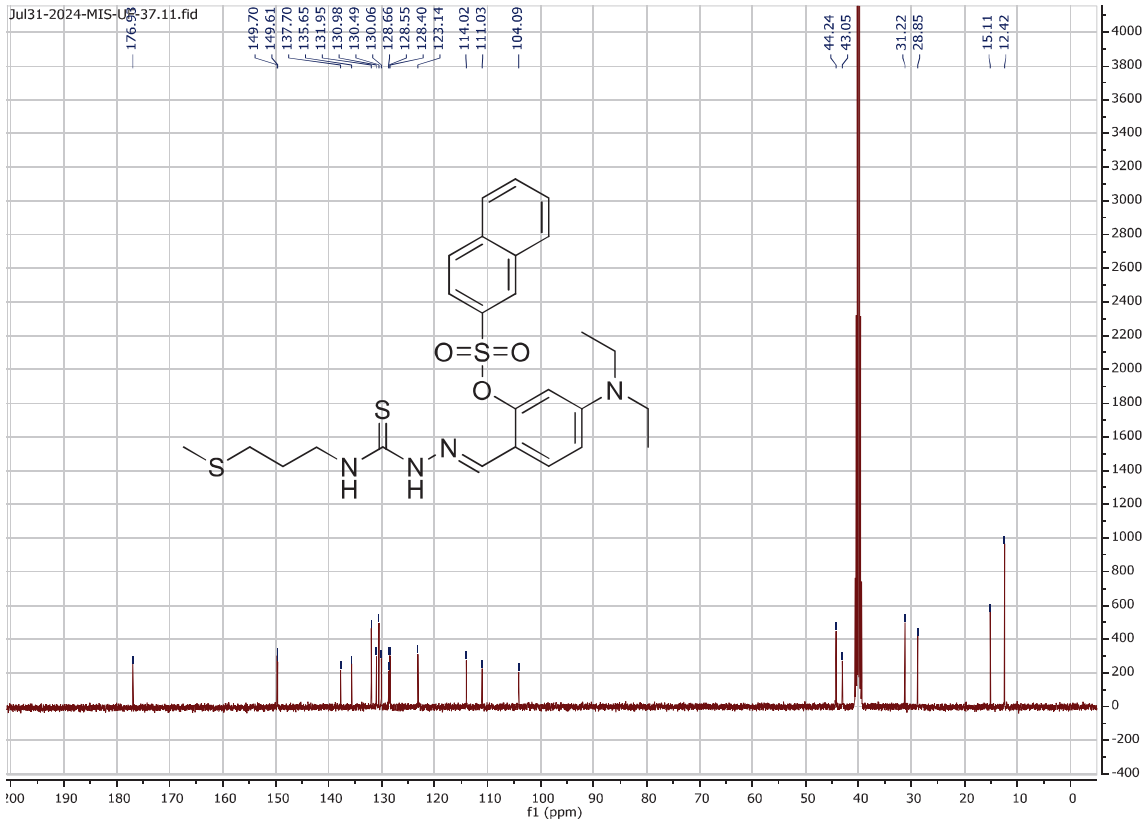

Figure S 35. ^{13}C-NMR Spectrum of Compound **5g** (DMSO-*d6*, 100 MHz)

Acq. Operator : SYSTEM
Sample Operator : SYSTEM
Acq. Instrument : HPLC Location : -
Injection Date : 12/17/2024 4:27:45 PM Inj : 1
Inj Volume : No Inj

Method : D:\HPLC-DATA\Method\BZ-11.M
Last changed : 5/29/2024 5:19:35 PM by SYSTEM

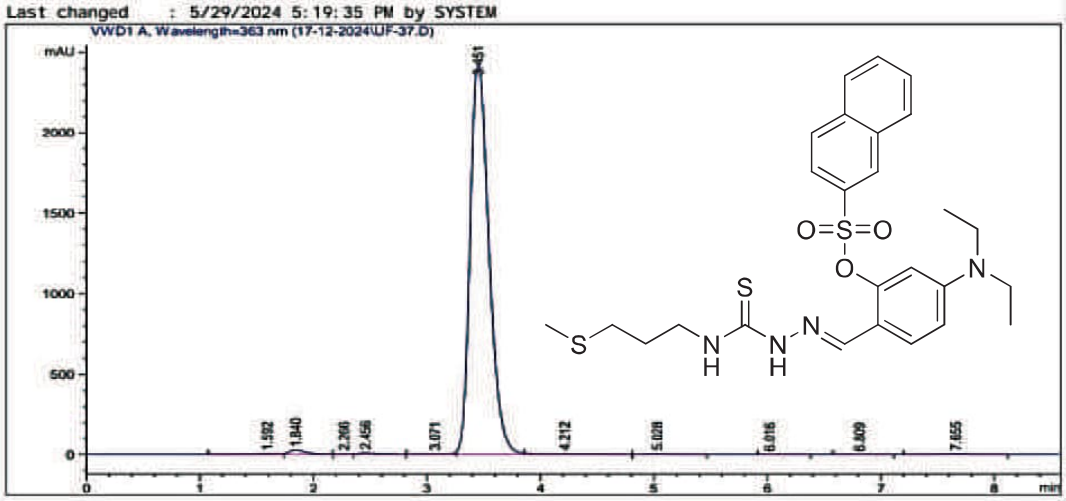

Area Percent Report

Sorted By : Signal
Multiplier : 1.0000
Dilution : 1.0000
Use Multiplier & Dilution Factor with ISTDs

Signal 1: VWD1 A, Wavelength=363 nm

Peak #	RetTime [min]	Type	Width [min]	Area [mAU*s]	Height [mAU]	Area %
1	1.592	BV E	0.1908	50.48253	4.12608	0.1767
2	1.840	VB R	0.1417	256.18890	27.26139	0.8967
3	2.266	BV E	0.0862	9.94358e-1	1.76273e-1	3.481e-3
4	2.456	VB R	0.1455	71.83395	7.58185	0.2514
5	3.071	BV E	0.1690	27.75907	2.44159	0.0972
6	3.451	VV R	0.1789	2.80901e4	2423.61255	98.3231
7	4.212	VB E	0.2604	46.22150	2.50480	0.1618
8	5.028	BB	0.2165	5.53470	3.13004e-1	0.0194
9	6.016	BB	0.2022	8.98860e-1	5.54677e-2	3.146e-3
10	6.809	BB	0.1949	2.47214	1.57429e-1	8.653e-3

Data File D:\HPLC-DATA\Data\17-12-2024\UF-37.D
Sample Name: UF-37

Peak #	RetTime [min]	Type	Width [min]	Area [mAU*s]	Height [mAU]	Area %
11	7.655	BV	0.2645	16.70424	9.25067e-1	0.0585

Totals : 2.85692e4 2469.15550

Figure S 36. HPLC Purity Analysis of Compound **5g**

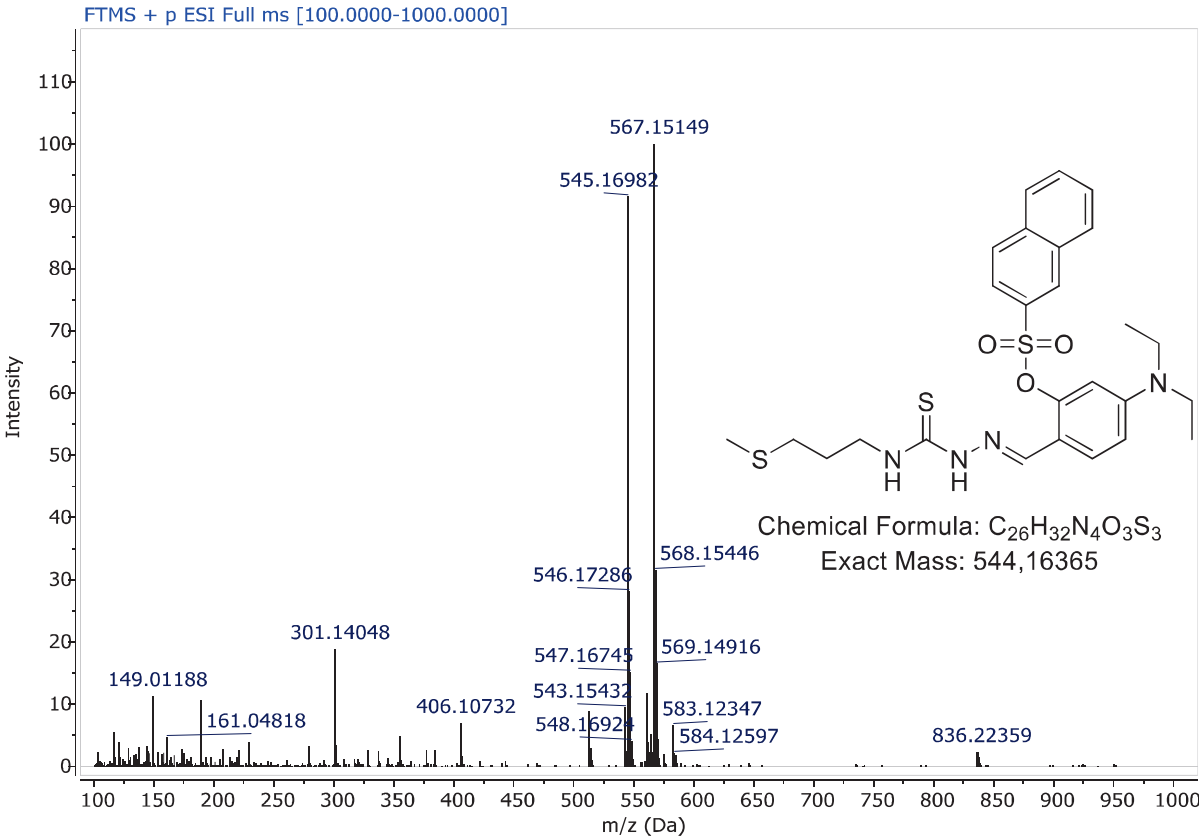

Figure S 37. ESI-HRMS Spectrum of Compound **5g**

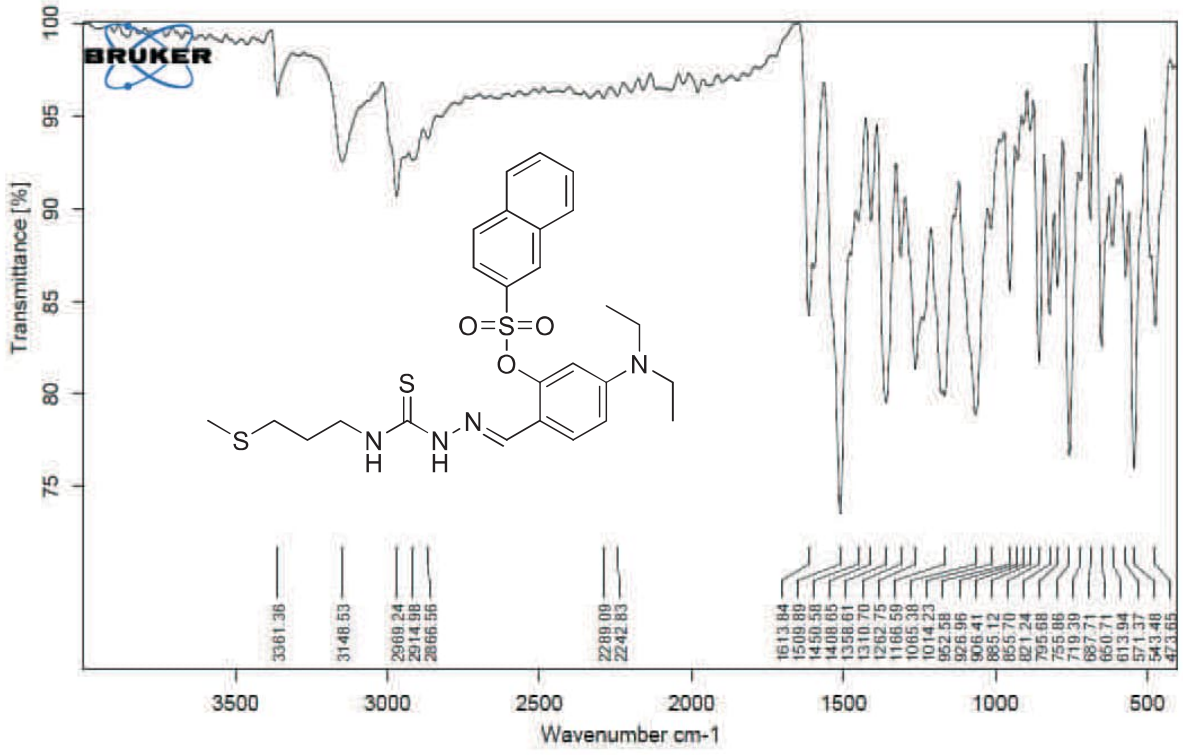

Figure S 38. FT-IR Spectrum of Compound **5g**

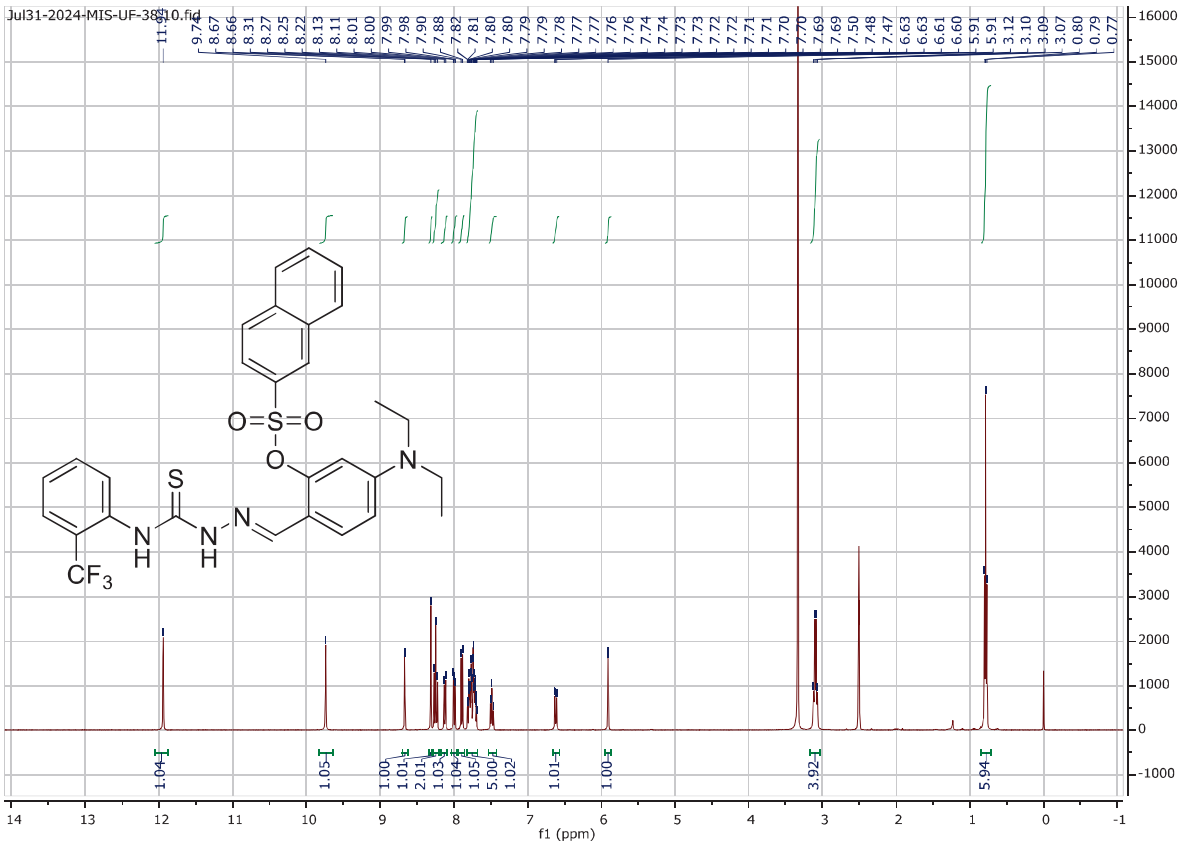

Figure S 39. ^{1}H-NMR Spectrum of Compound **5h** (DMSO-*d6*, 400 MHz)

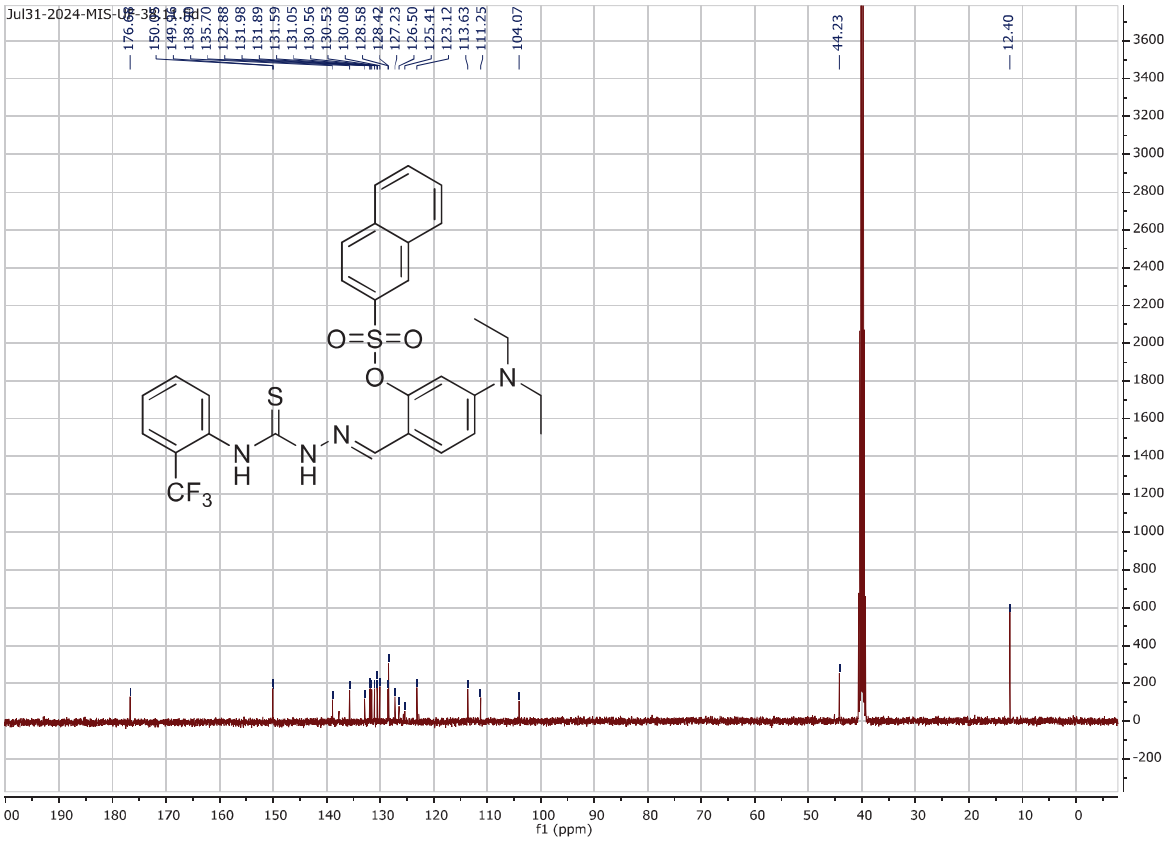

Figure S 40. ^{13}C-NMR Spectrum of Compound **5h** (DMSO-*d6*, 100 MHz)

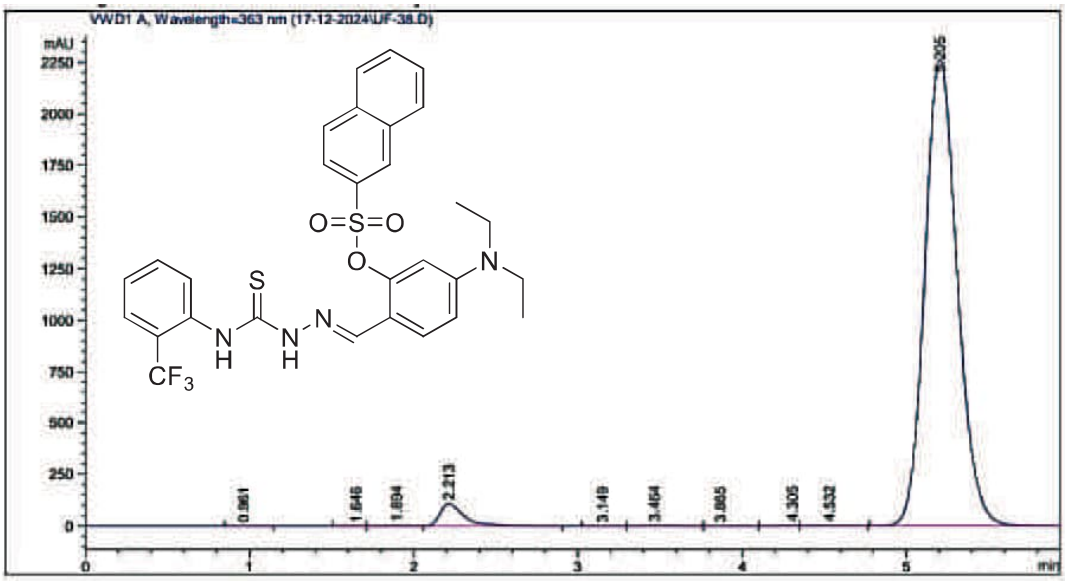

****

Area Percent Report

****

Sorted By : Signal
Multiplier : 1.0000
Dilution : 1.0000
Use Multiplier & Dilution Factor with ISTDs

Signal 1: VWD1 A, Wavelength=363 nm

Peak #	RetTime [min]	Type	Width [min]	Area [mAU*s]	Height [mAU]	Area %
1	0.961	BB	0.1183	4.54997e-1	5.42401e-2	1.408e-3
2	1.646	BV E	0.1223	1.45942	1.88630e-1	4.516e-3
3	1.894	VV E	0.1749	4.18585	3.52639e-1	0.0130
4	2.213	VB R	0.1509	1074.85986	106.79336	3.3262
5	3.149	BV	0.1512	2.09048	2.15234e-1	6.469e-3
6	3.464	VV	0.1984	8.78822	6.21574e-1	0.0272
7	3.865	VB	0.1464	2.59139	2.24413e-1	8.019e-3
8	4.305	BV	0.1177	4.29800	5.39300e-1	0.0133
9	4.532	VB	0.1889	23.69898	1.88520	0.0733
10	5.205	BBA	0.2131	3.11924e4	2264.61475	96.5266

HPLC 12/17/2024 4:43:29 PM SYSTEM Page 1 of 2

Data File D:\HPLC-DATA\Data\17-12-2024\UF-38.D
Sample Name: UF-38

Peak #	RetTime [min]	Type	Width [min]	Area [mAU*s]	Height [mAU]	Area %
Totals :				3.23148e4	2375.48934	

Figure S 41. HPLC Purity Analysis of Compound **5h**

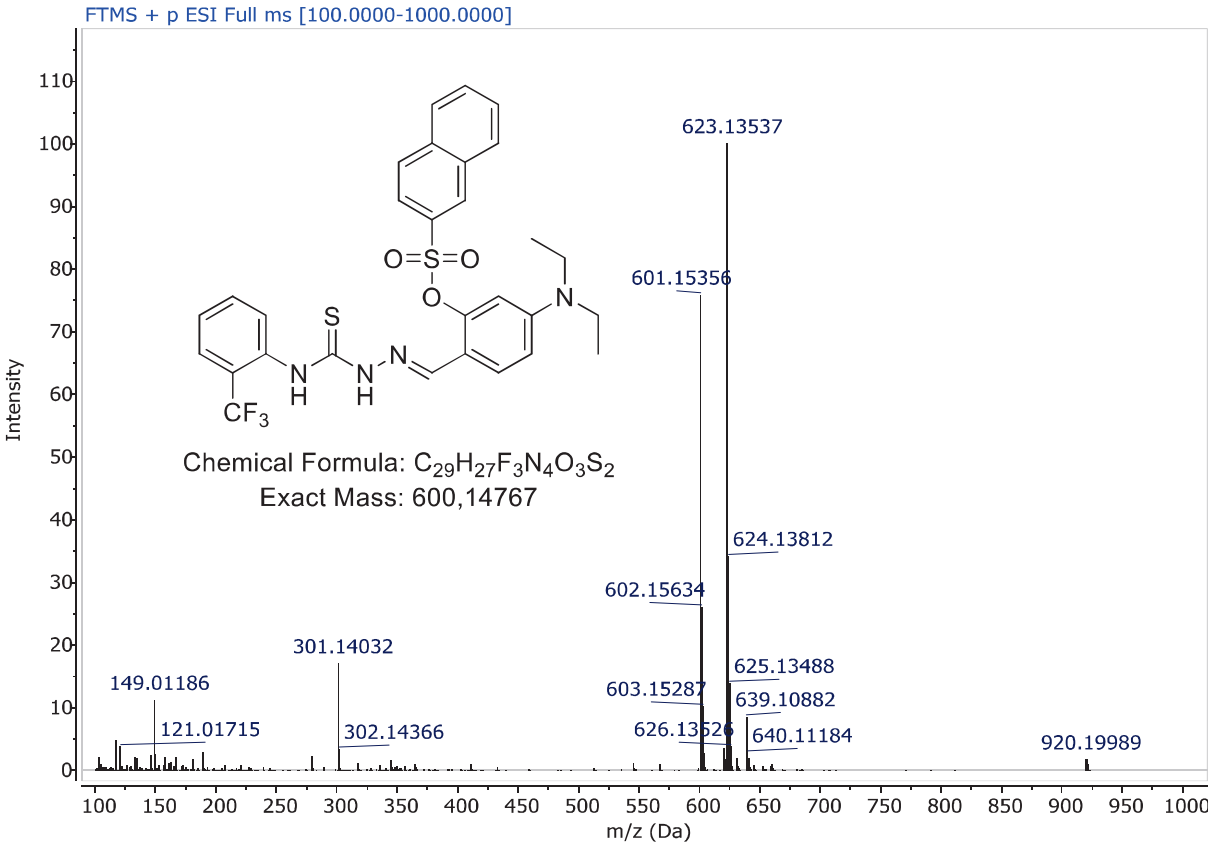

Figure S 42. ESI-HRMS Spectrum of Compound **5h**

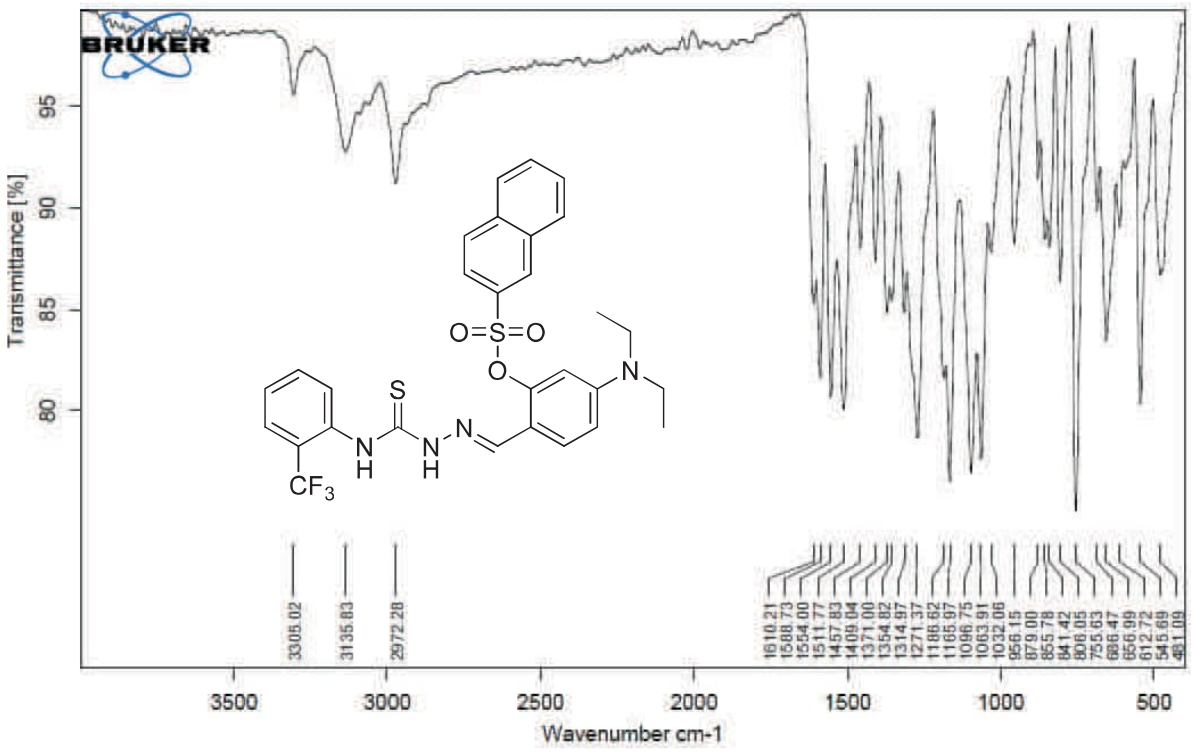

Figure S 43. FT-IR Spectrum of Compound **5h**

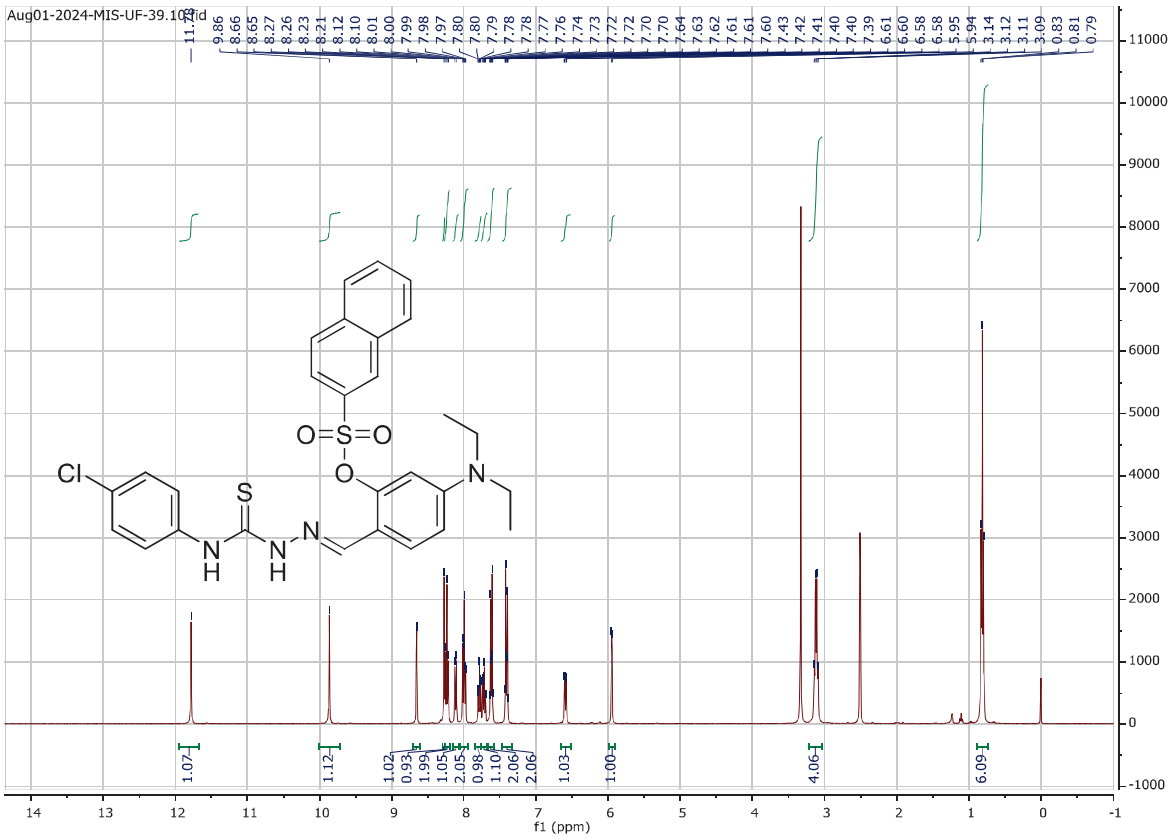

Figure S 44. ^{1}H-NMR Spectrum of Compound **5i** (DMSO-*d6*, 400 MHz)

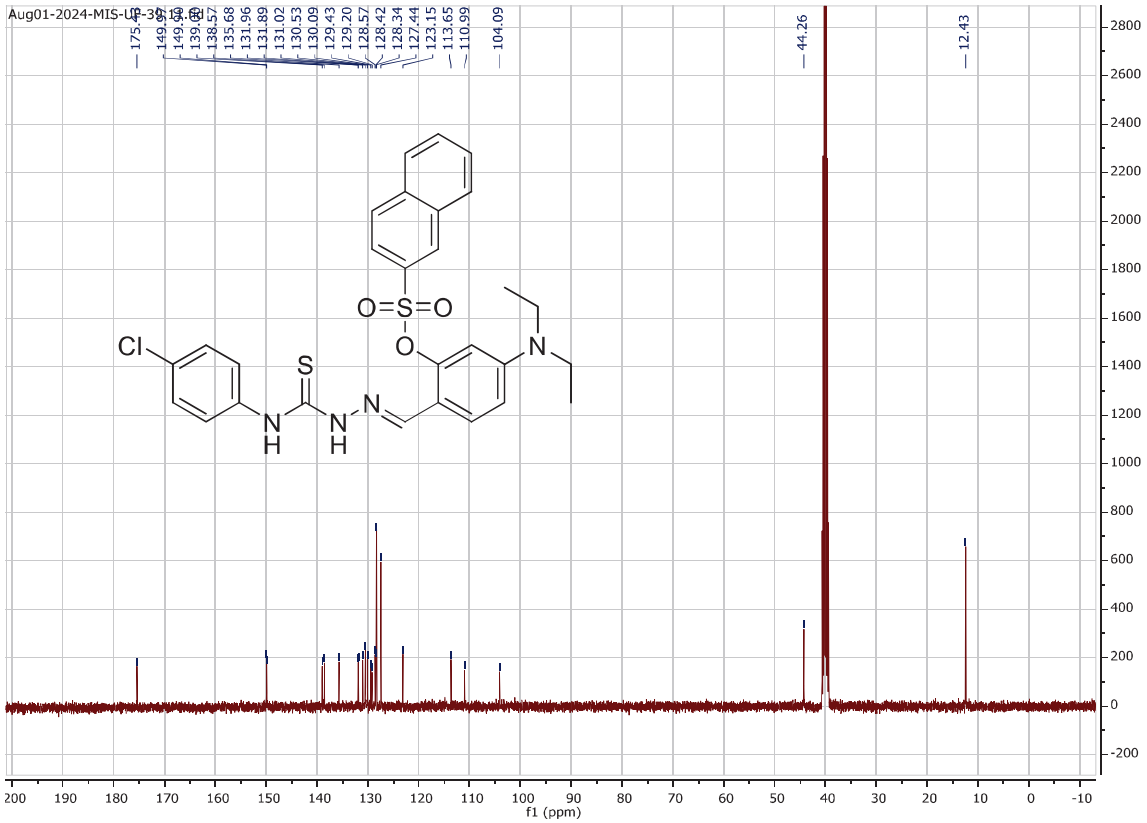

Figure S 45. ^{13}C-NMR Spectrum of Compound **5i** (DMSO-*d6*, 100 MHz)

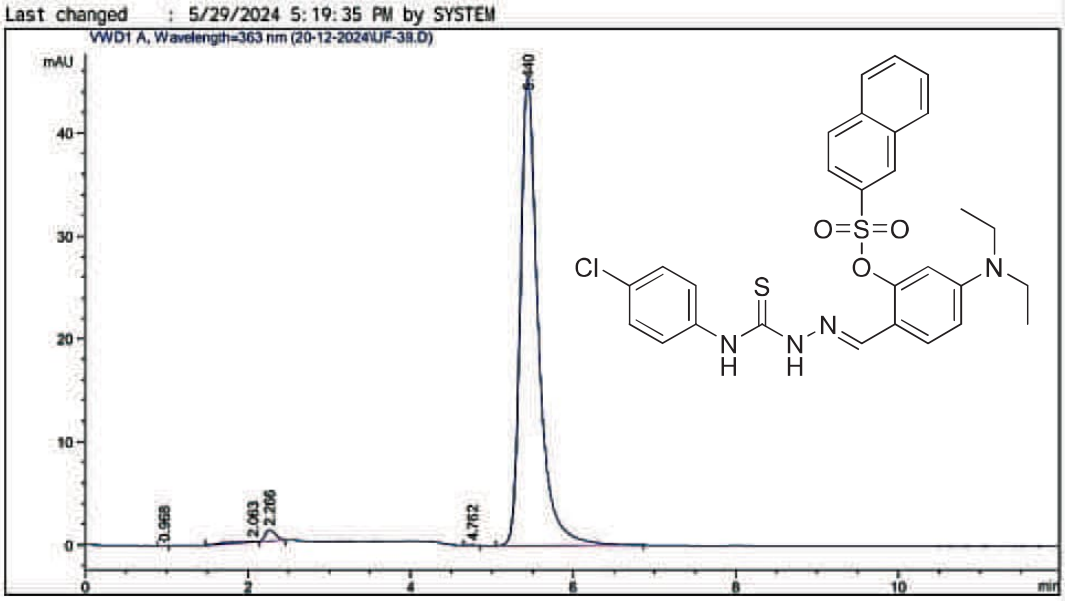

Method : D:\HPLC-DATA\Method\BZ-11.M
Last changed : 5/29/2024 5:19:35 PM by SYSTEM

Area Percent Report

Sorted By : Signal
Multiplier : 1.0000
Dilution : 1.0000
Use Multiplier & Dilution Factor with ISTDs

Signal 1: VWD1 A, Wavelength=363 nm

Peak #	RetTime [min]	Type	Width [min]	Area [mAU*s]	Height [mAU]	Area %
1	0.968	BB	0.0680	1.71663e-1	3.22127e-2	0.0242
2	2.063	BV E	0.6392	3.38553	6.26534e-2	0.4767
3	2.266	VB R	0.1423	9.68887	1.08226	1.3641
4	4.762	BB	0.0850	1.96241e-1	3.18474e-2	0.0276
5	5.440	BB	0.2269	696.80988	45.46298	98.1074
Totals :				710.25217	46.67195	

Figure S 46. HPLC Purity Analysis of Compound **5i**

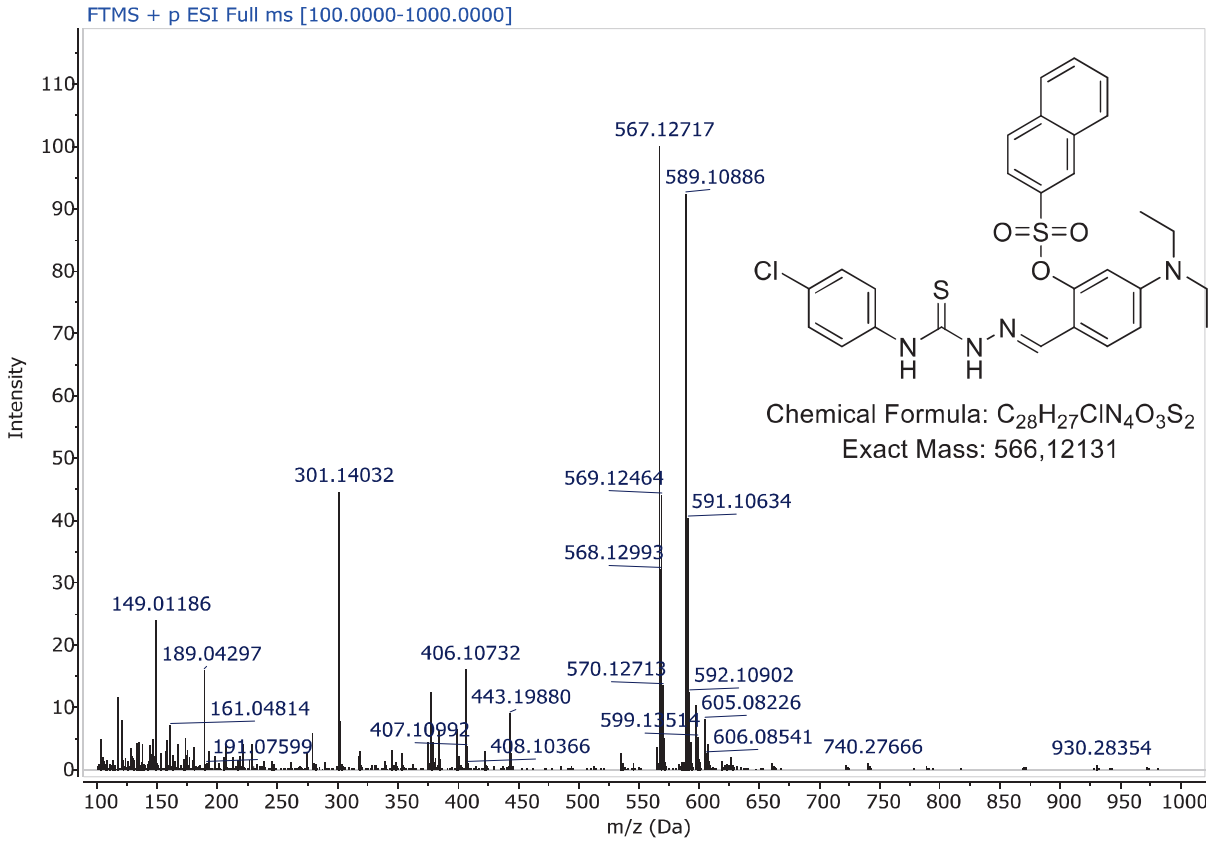

Figure S 47. ESI-HRMS Spectrum of Compound **5i**

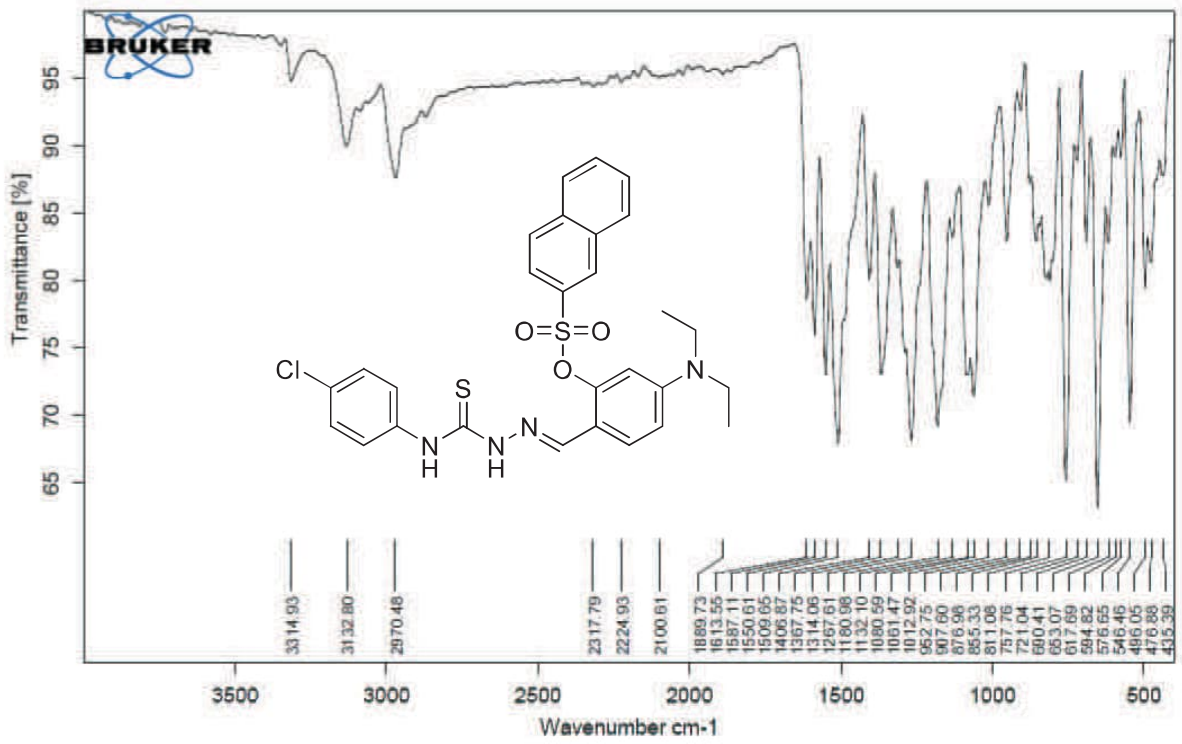

Figure S 48. FT-IR Spectrum of Compound **5i**

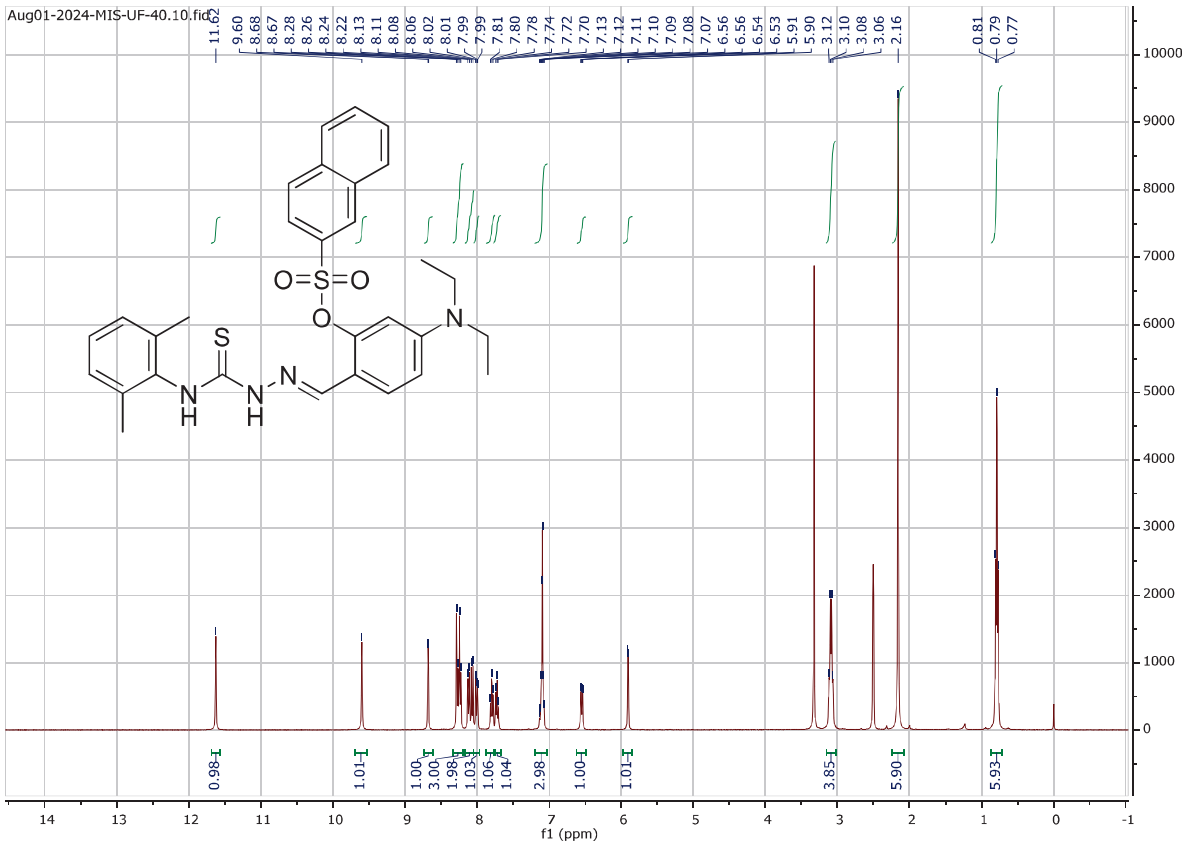

Figure S 49. ^{1}H-NMR Spectrum of Compound **5j** (DMSO-*d6*, 400 MHz)

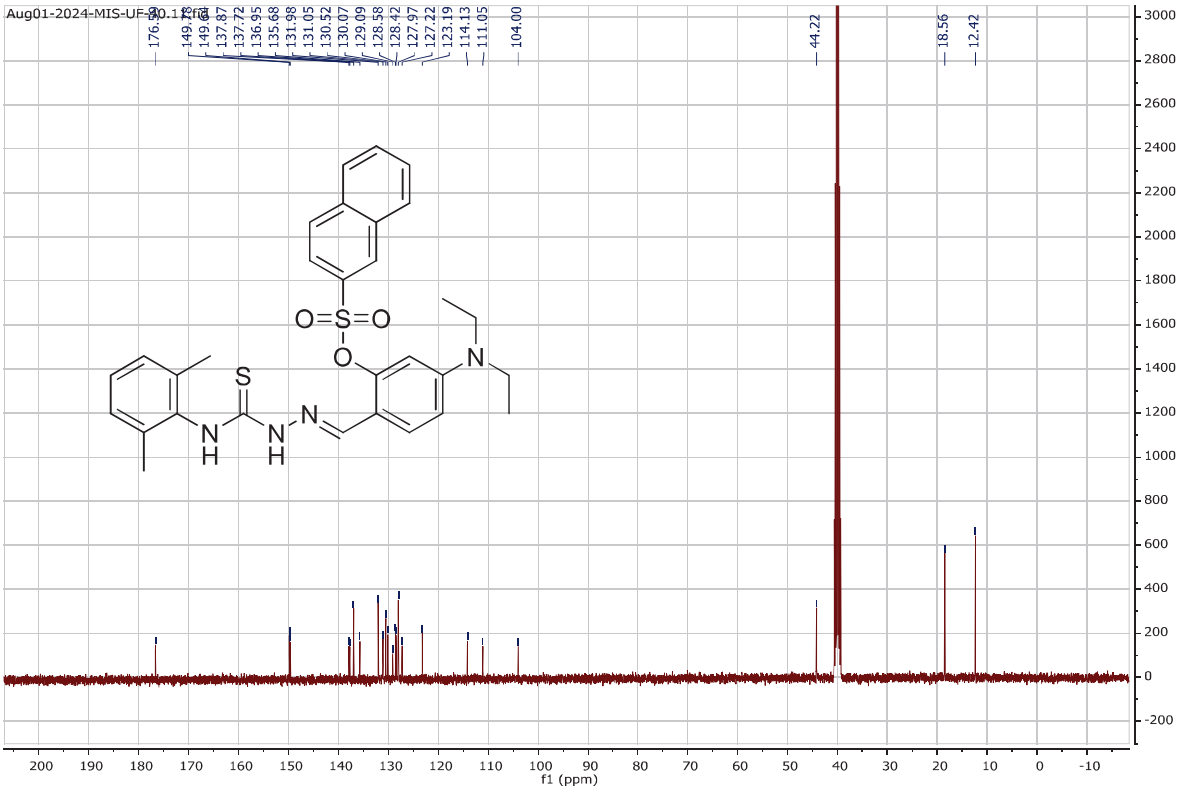

Figure S 50. ^{13}C-NMR Spectrum of Compound **5j** (DMSO-*d6*, 100 MHz)

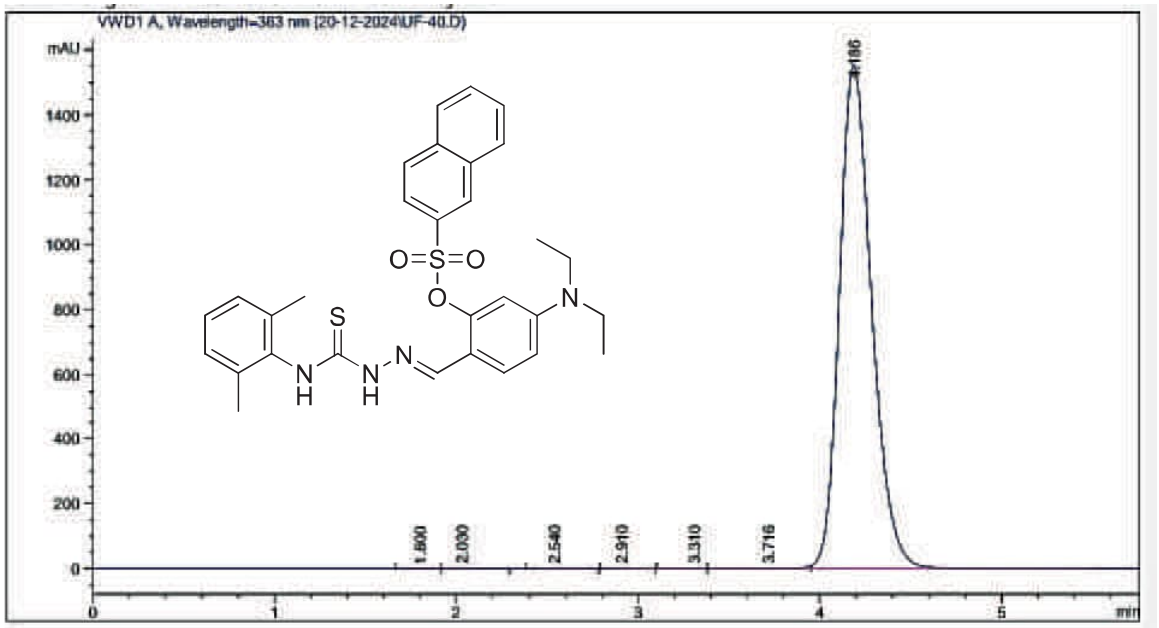

Area Percent Report

Sorted By : Signal
Multiplier : 1.0000
Dilution : 1.0000
Use Multiplier & Dilution Factor with ISTDs

Signal 1: VWD1 A, Wavelength=363 nm

Peak #	RetTime [min]	Type	Width [min]	Area [mAU*s]	Height [mAU]	Area %
1	1.800	BV	0.1125	1.16770	1.39129e-1	6.068e-3
2	2.030	VB	0.1410	4.38038	4.62744e-1	0.0228
3	2.540	BB	0.1591	16.60466	1.59797	0.0863
4	2.910	BB	0.1277	3.19885	3.84148e-1	0.0166
5	3.310	BV E	0.1210	1.09275	1.15031e-1	5.678e-3
6	3.716	VV E	0.1997	17.21306	1.23011	0.0894
7	4.186	VBAR	0.1893	1.92015e4	1554.07251	99.7732
Totals :				1.92451e4	1558.00163	

Figure S 51. HPLC Purity Analysis of Compound **5j**

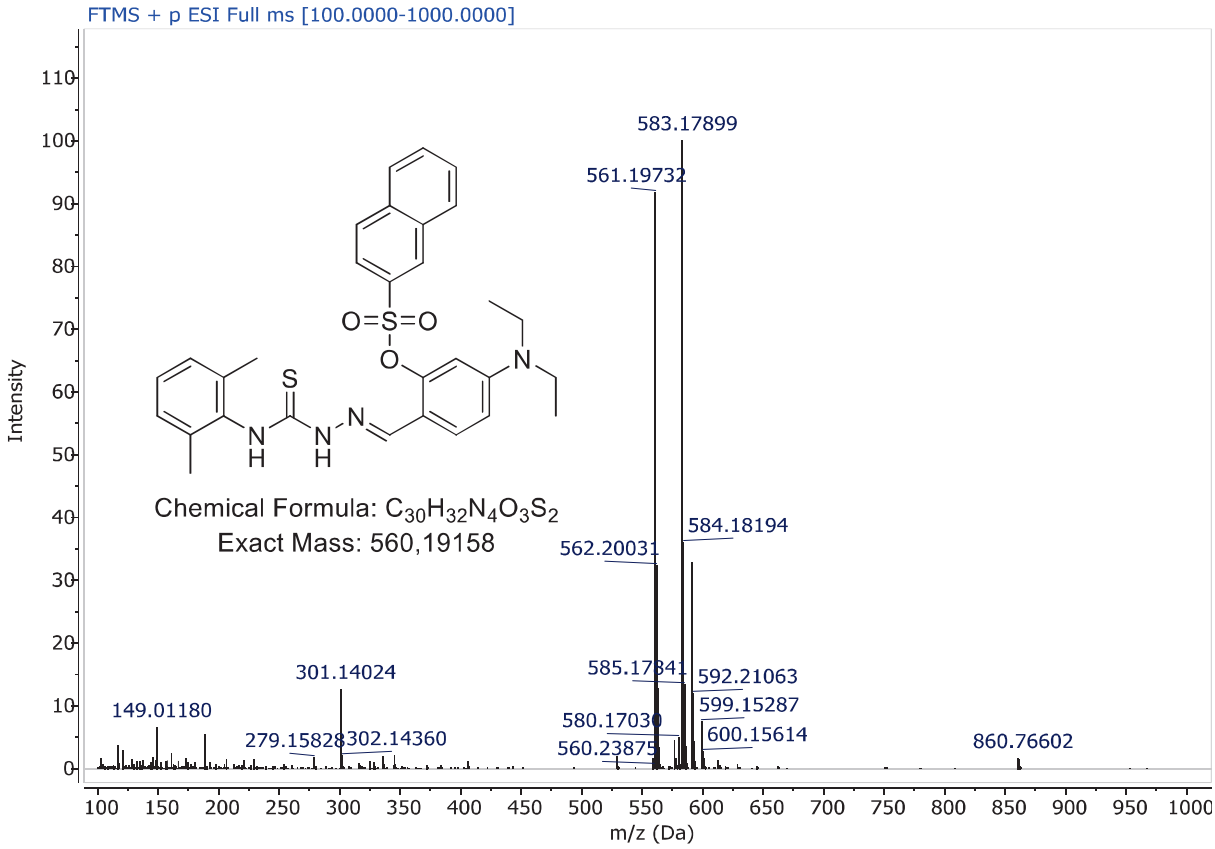

Figure S 52. ESI-HRMS Spectrum of Compound **5j**

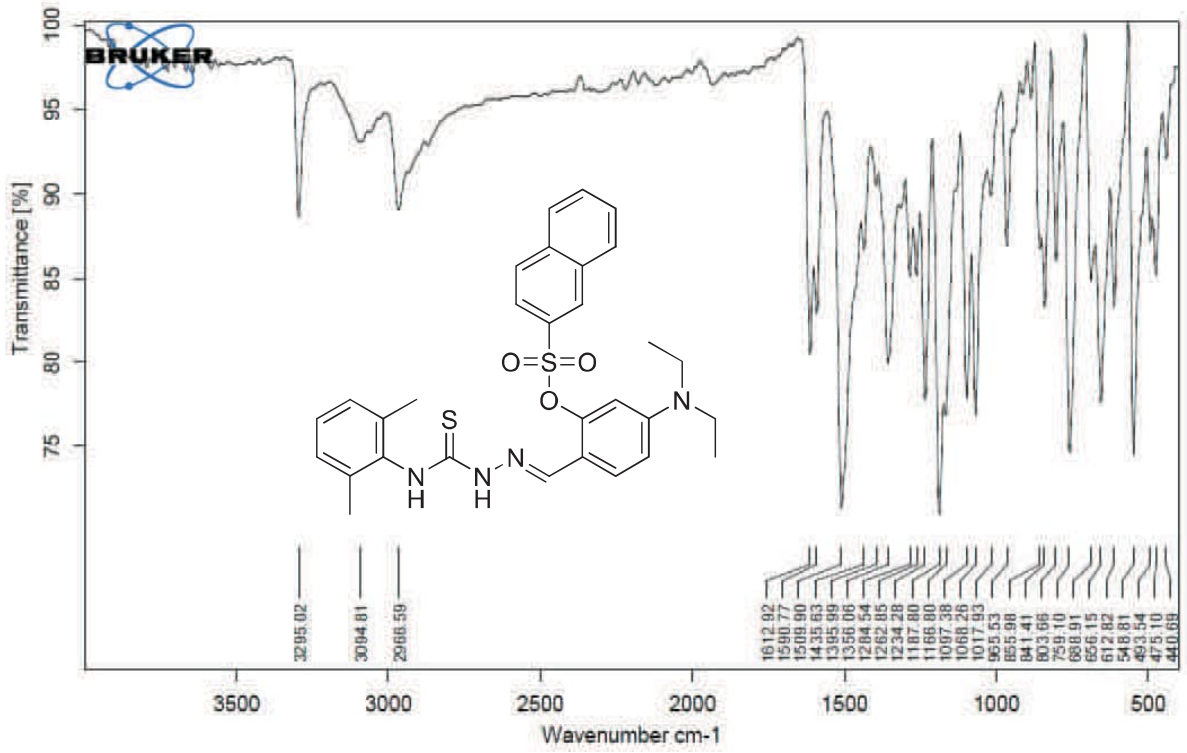

Figure S 53. FT-IR Spectrum of Compound **5j**

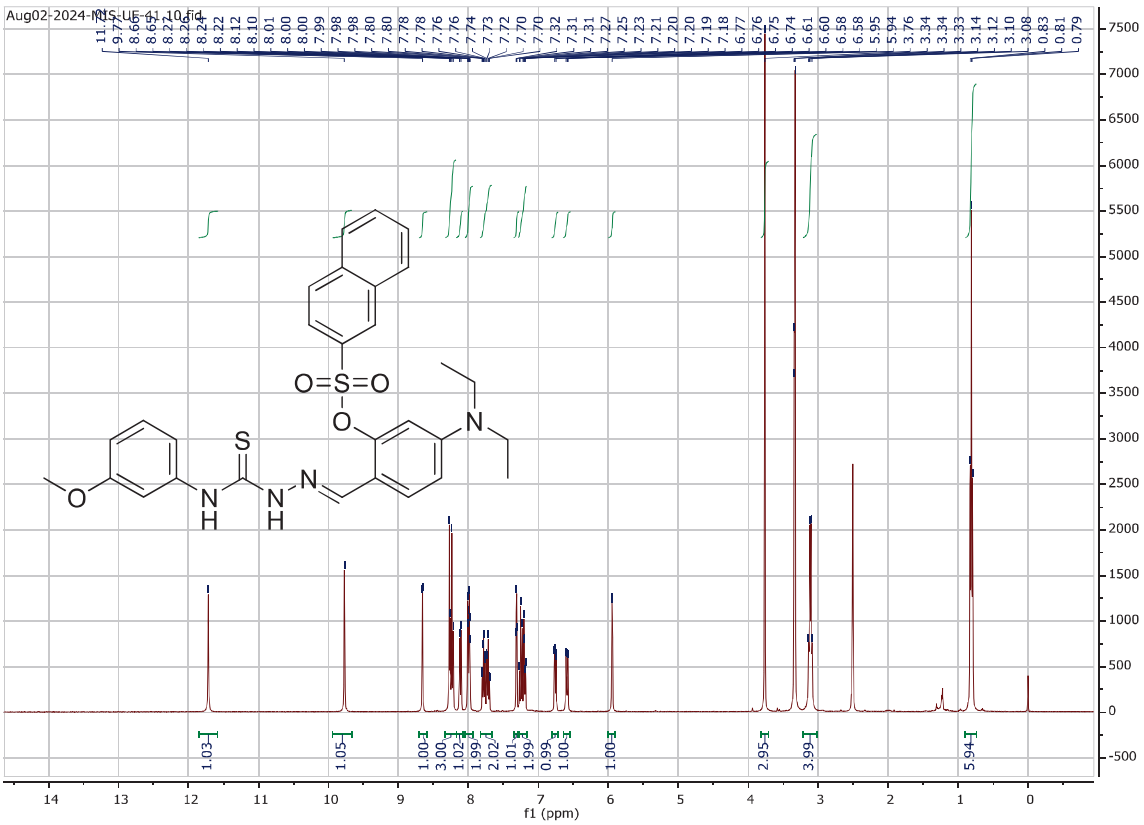

Figure S 54. ^{1}H-NMR Spectrum of Compound **5k** (DMSO-*d6*, 400 MHz)

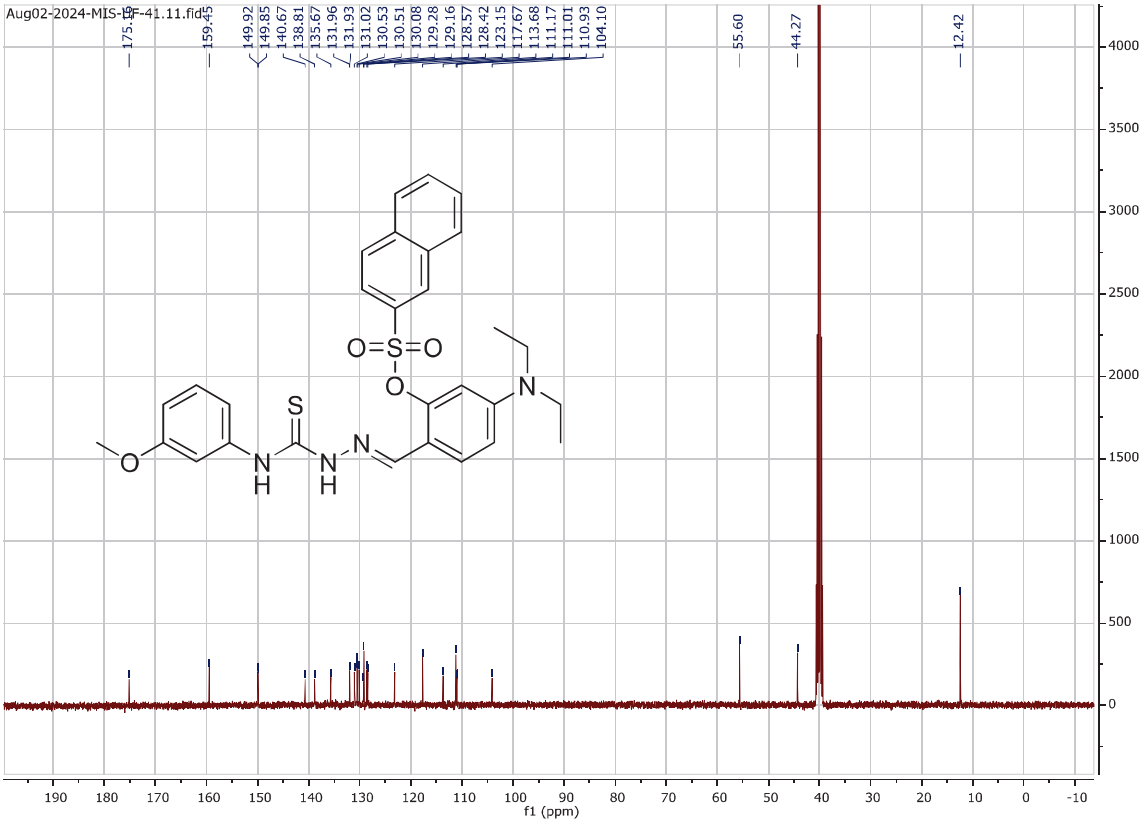

Figure S 55. ^{13}C-NMR Spectrum of Compound **5k** (DMSO-*d6*, 100 MHz)

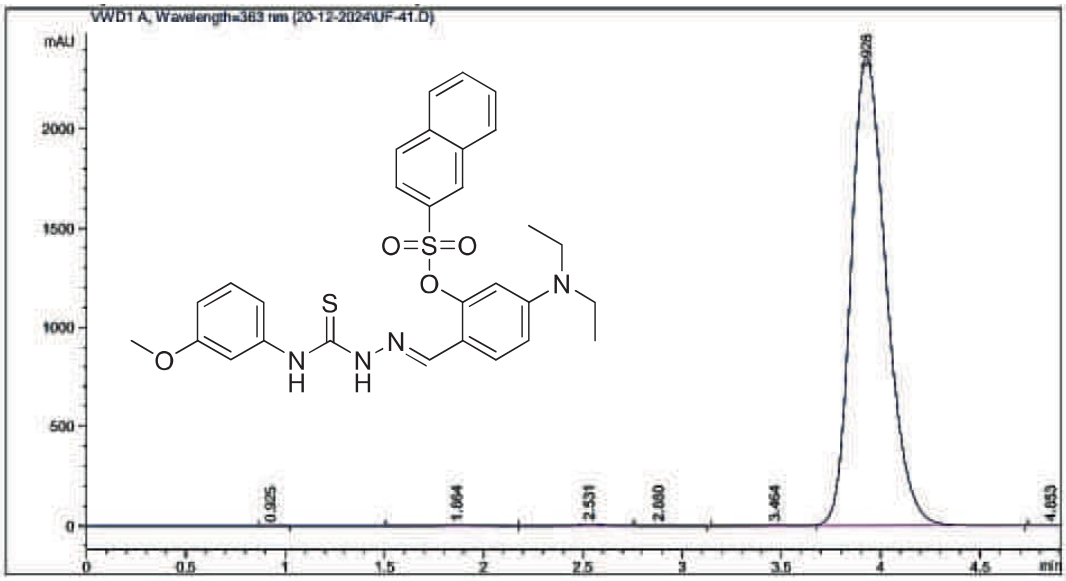

Area Percent Report

Sorted By : Signal
Multiplier : 1.0000
Dilution : 1.0000
Use Multiplier & Dilution Factor with ISTDs

Signal 1: VWD1 A, Wavelength=363 nm

Peak #	RetTime [min]	Type	Width [min]	Area [mAU*s]	Height [mAU]	Area %
1	0.925	BB	0.0761	2.00753e-1	3.55127e-2	6.891e-4
2	1.864	BV	0.1475	39.15018	4.00708	0.1344
3	2.531	VV R	0.1530	85.74770	8.37039	0.2943
4	2.880	VB E	0.1482	3.79124	3.42094e-1	0.0130
5	3.464	BV E	0.1861	36.94952	2.90814	0.1268
6	3.928	VB R	0.1897	2.89643e4	2361.51831	99.4268
7	4.853	BBA	0.0988	1.14209	1.92683e-1	3.920e-3
Totals :				2.91313e4	2377.37420	

Figure S 56. HPLC Purity Analysis of Compound **5k**

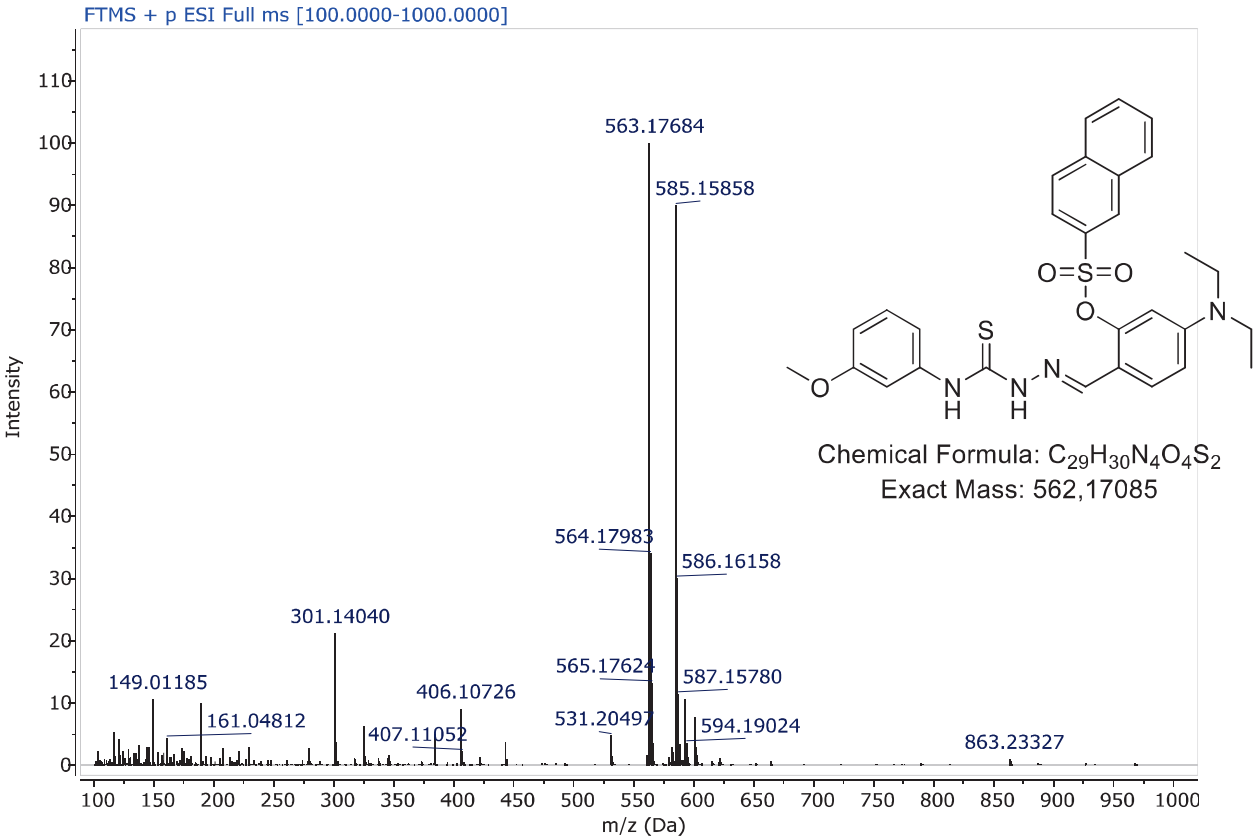

Figure S 57. ESI-HRMS Spectrum of Compound **5k**

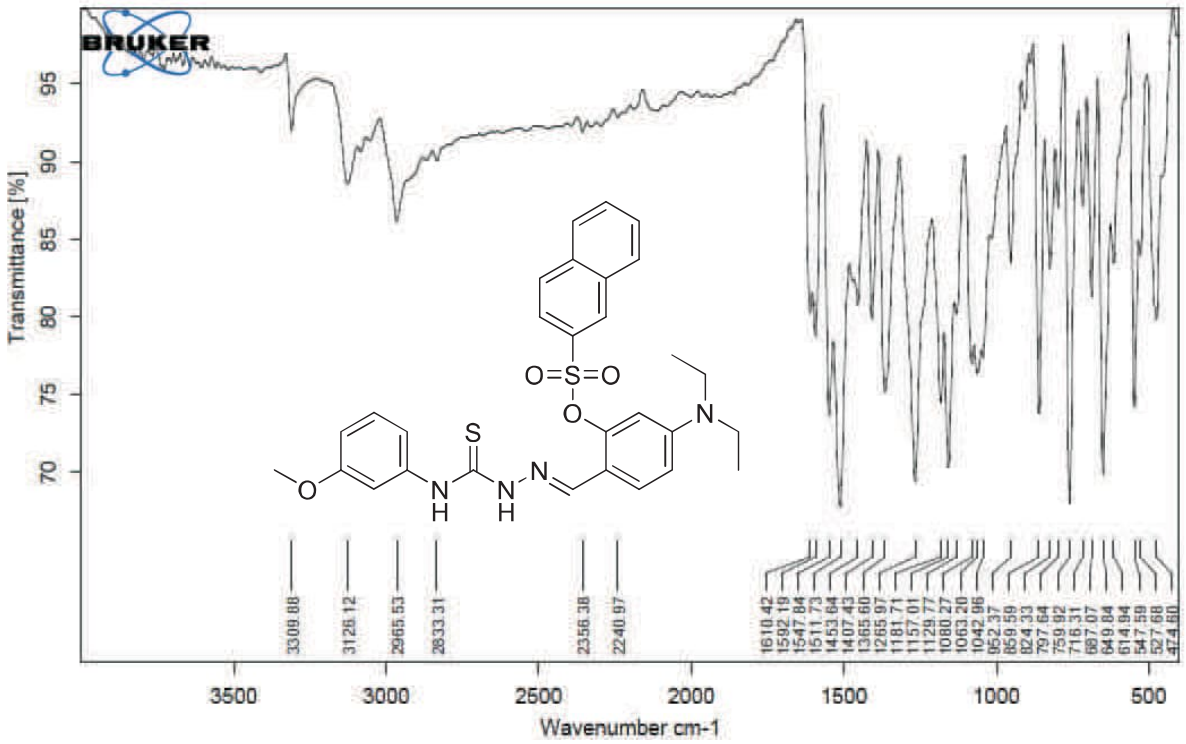

Figure S 58. FT-IR Spectrum of Compound **5k**

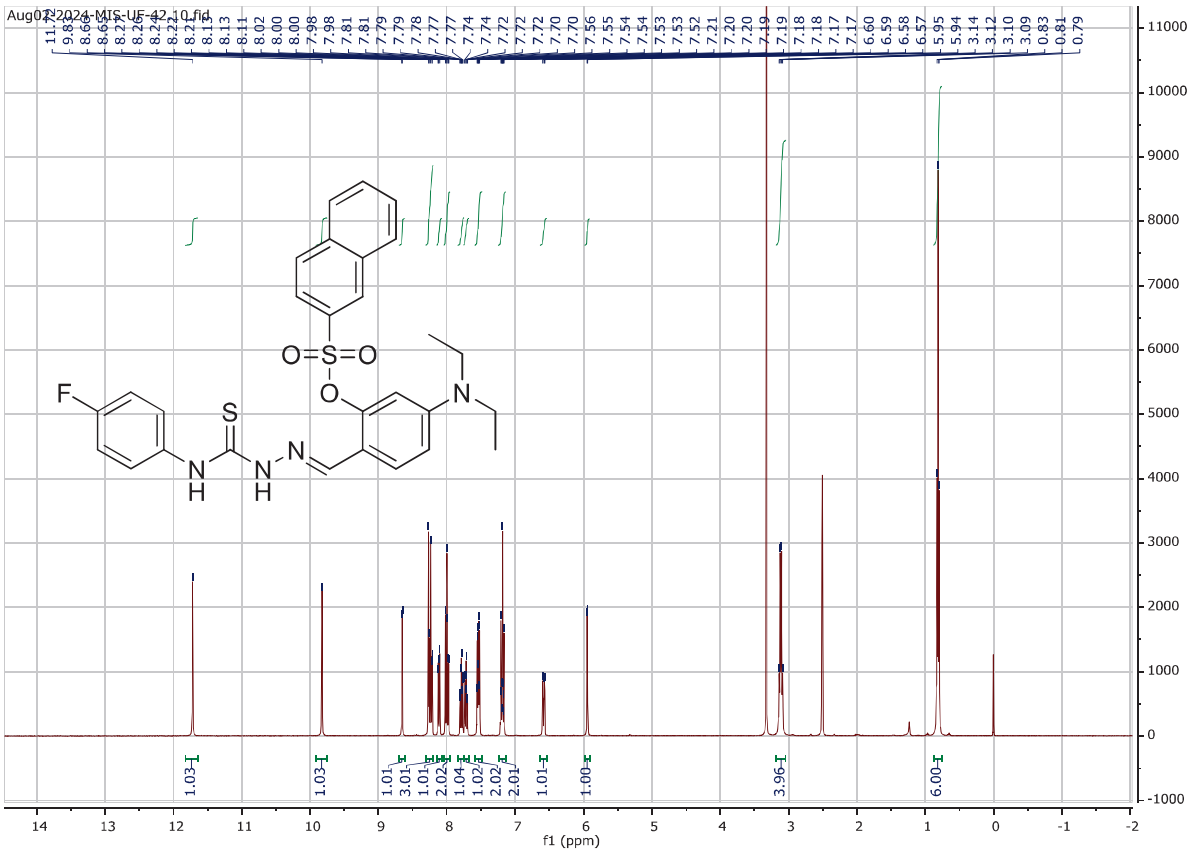

Figure S 59. ^{1}H-NMR Spectrum of Compound **5l** (DMSO-*d6*, 400 MHz)

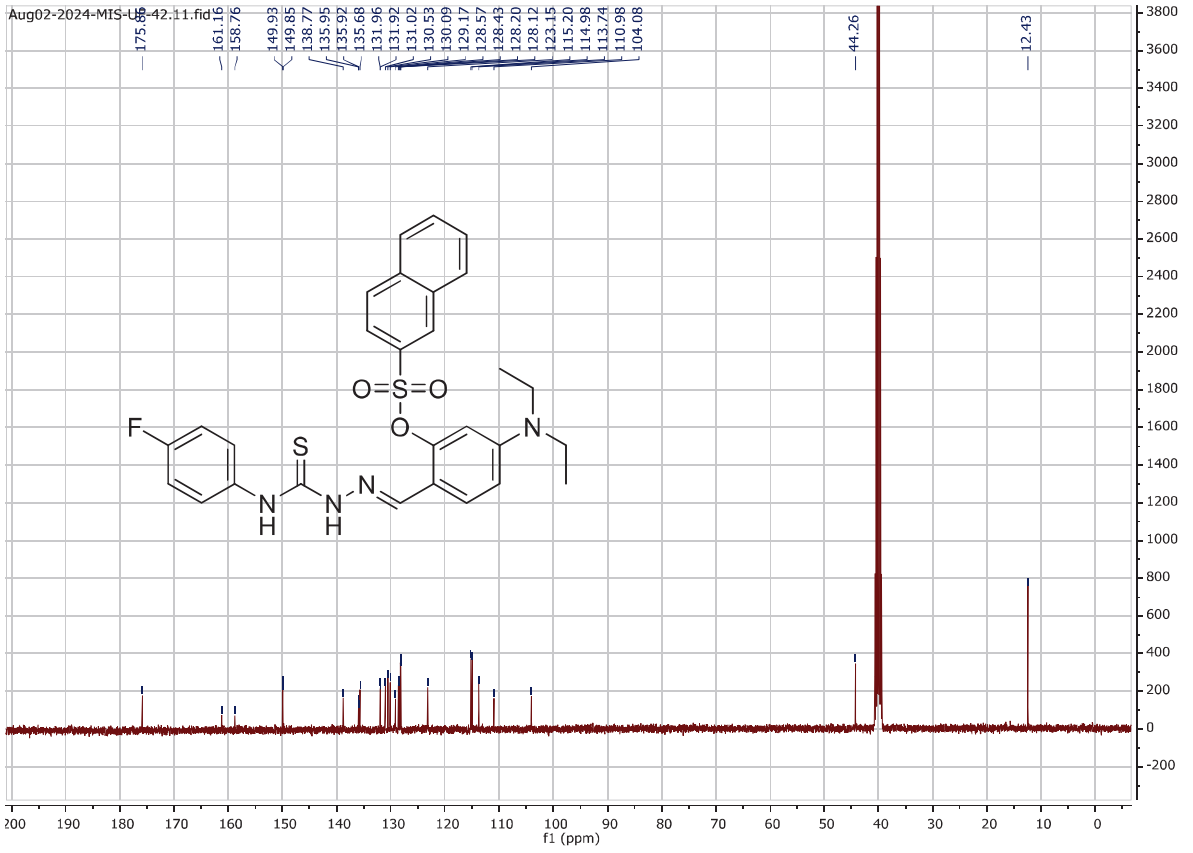

Figure S 60. ^{13}C-NMR Spectrum of Compound **5l** (DMSO-*d6*, 100 MHz)

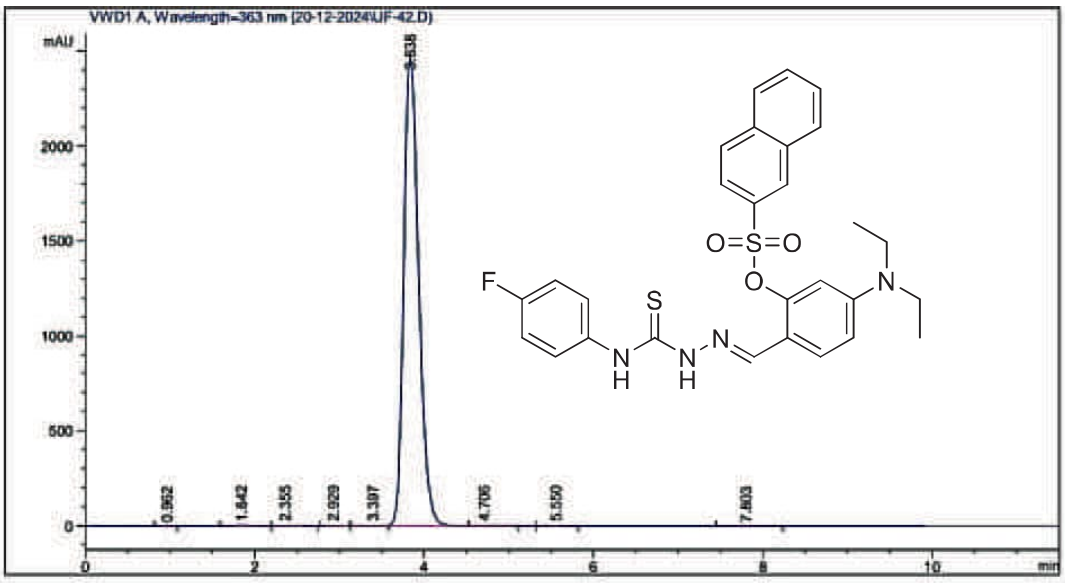

Area Percent Report

Sorted By : Signal
Multiplier : 1.0000
Dilution : 1.0000
Use Multiplier & Dilution Factor with ISTDs

Signal 1: VWD1 A, Wavelength=363 nm

Peak #	RetTime [min]	Type	Width [min]	Area [mAU*s]	Height [mAU]	Area %
1	0.962	BB	0.1055	4.28311e-1	5.86818e-2	1.412e-3
2	1.842	BV	0.1495	38.42909	3.81664	0.1267
3	2.355	VB	0.2099	16.58397	1.08800	0.0547
4	2.929	BB	0.1492	18.63580	1.97934	0.0614
5	3.397	BV E	0.1740	26.35806	2.30864	0.0869
6	3.838	VV R	0.1894	3.02208e4	2468.54541	99.6192
7	4.706	VB E	0.2160	8.20460	5.20430e-1	0.0270
8	5.550	BB	0.1800	3.07651	2.33347e-1	0.0101
9	7.803	BB	0.2318	3.79024	1.99545e-1	0.0125

Data File D:\HPLC-DATA\Data\20-12-2024\UF-42.D
Sample Name: UF-42

Totals : 3.03363e4 2478.75004

Figure S 61. HPLC Purity Analysis of Compound **5l**

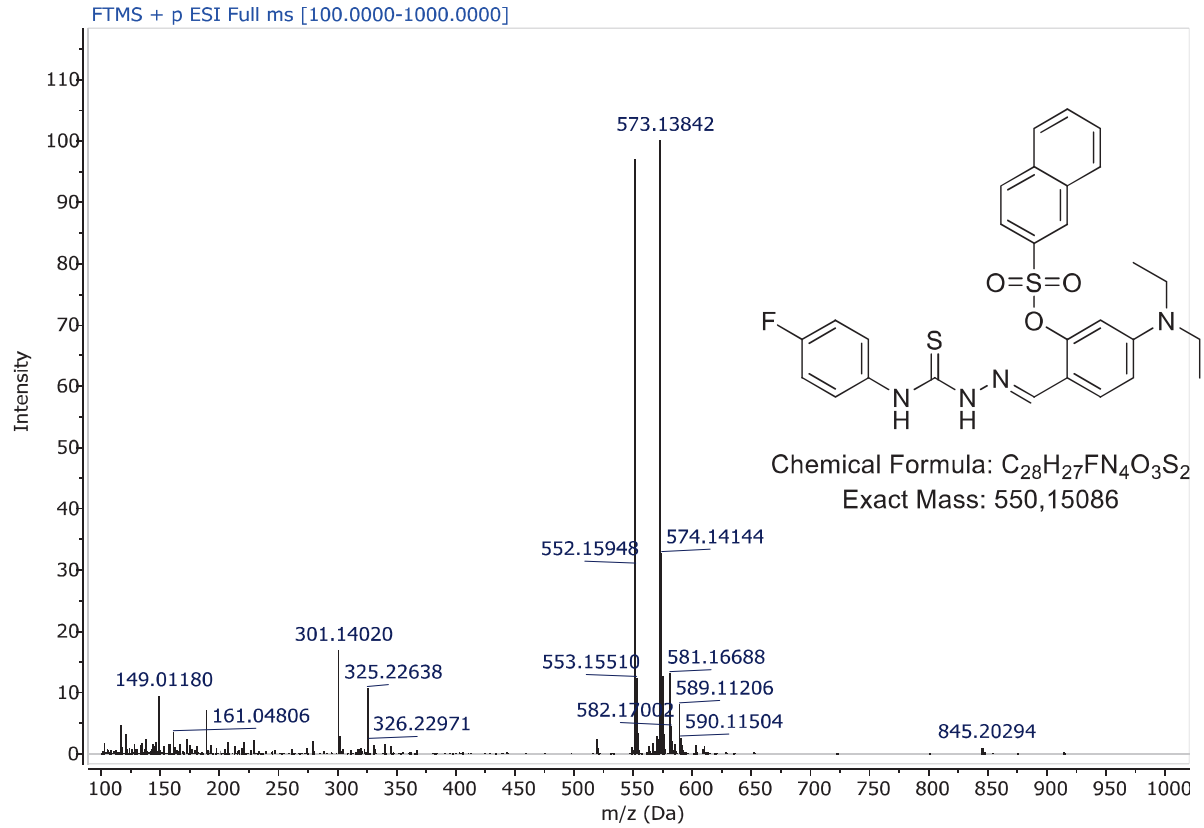

Figure S 62. ESI-HRMS Spectrum of Compound **5l**

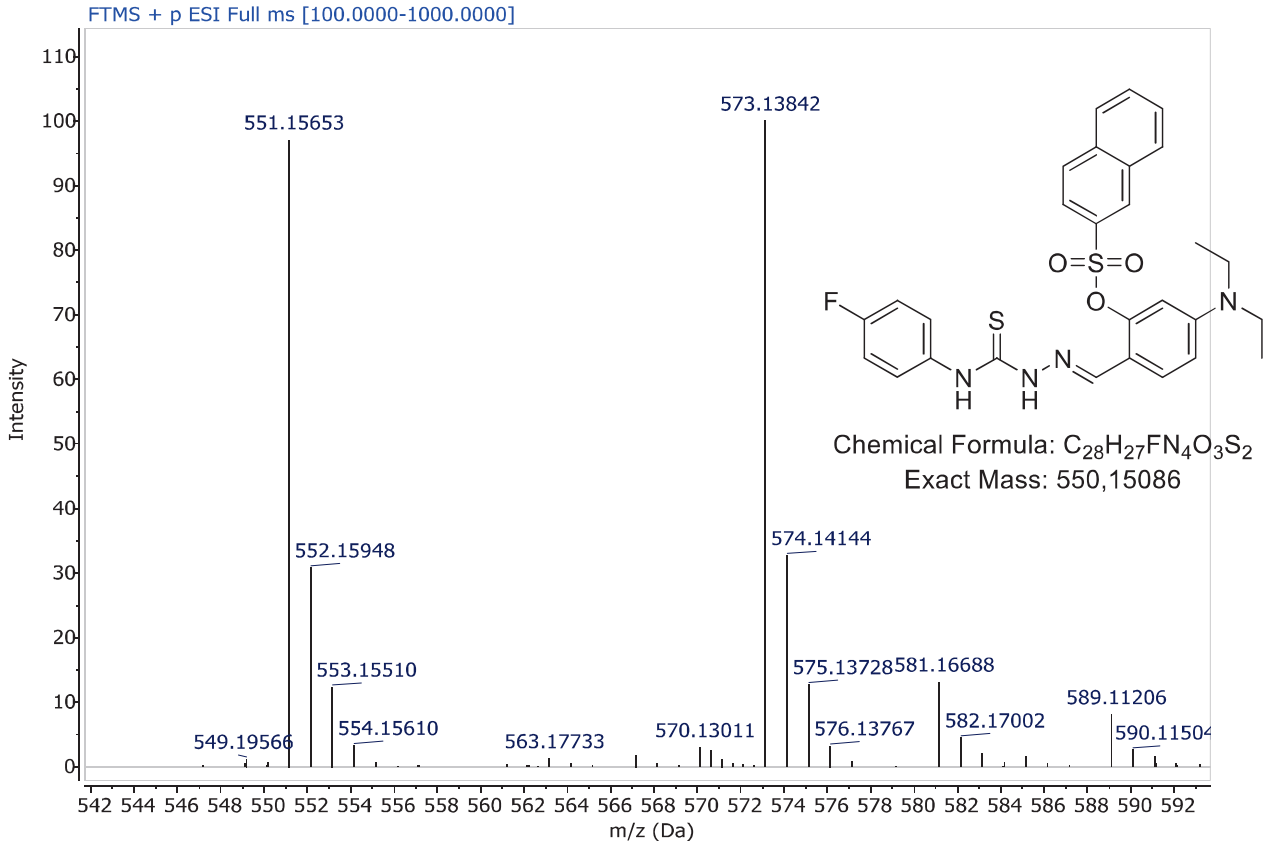

Figure S 63. ESI-HRMS Spectrum of Compound **5l** (extended)

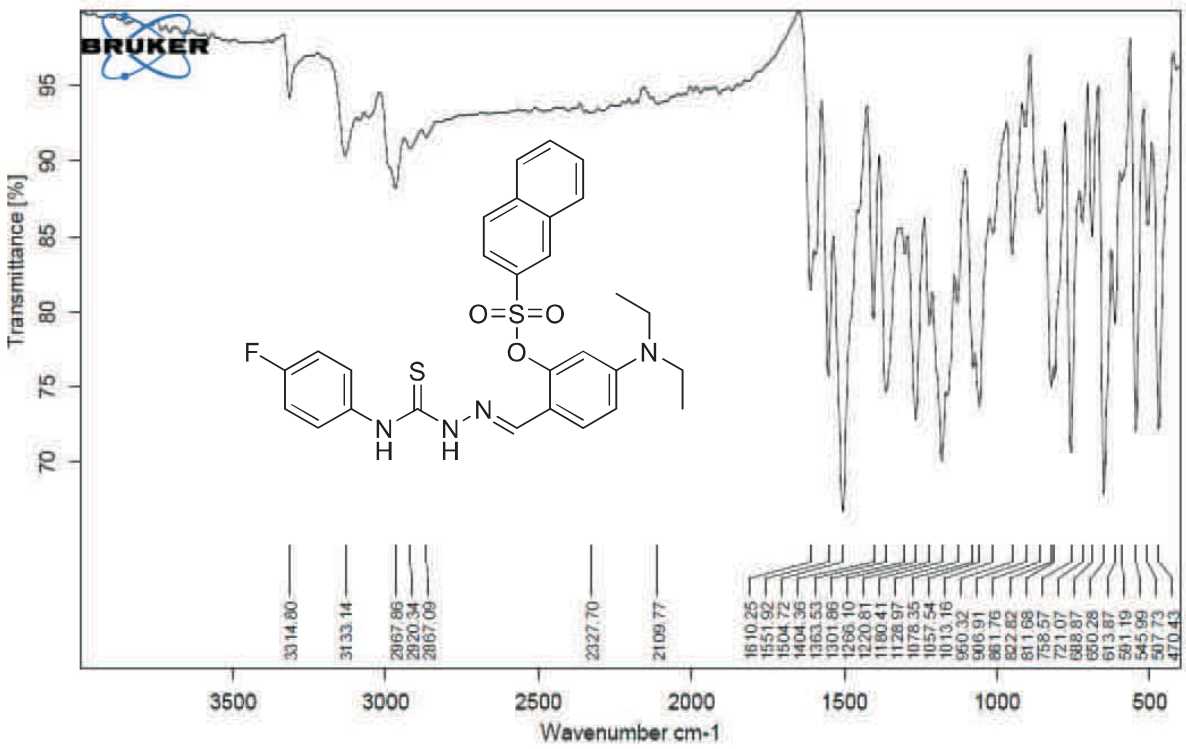

Figure S 64. FT-IR Spectrum of Compound **5l**

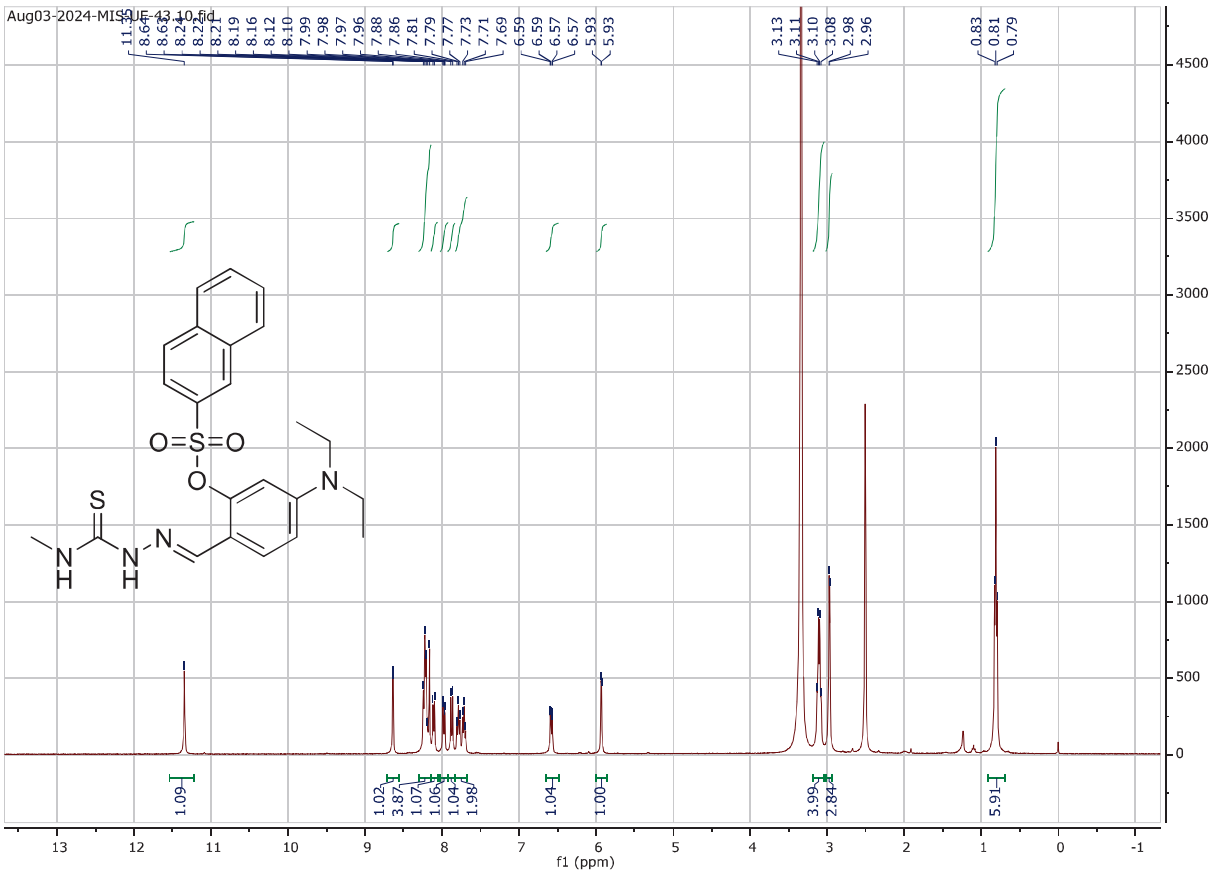

Figure S 65. [1]H-NMR Spectrum of Compound **5m** (DMSO-*d6*, 400 MHz)

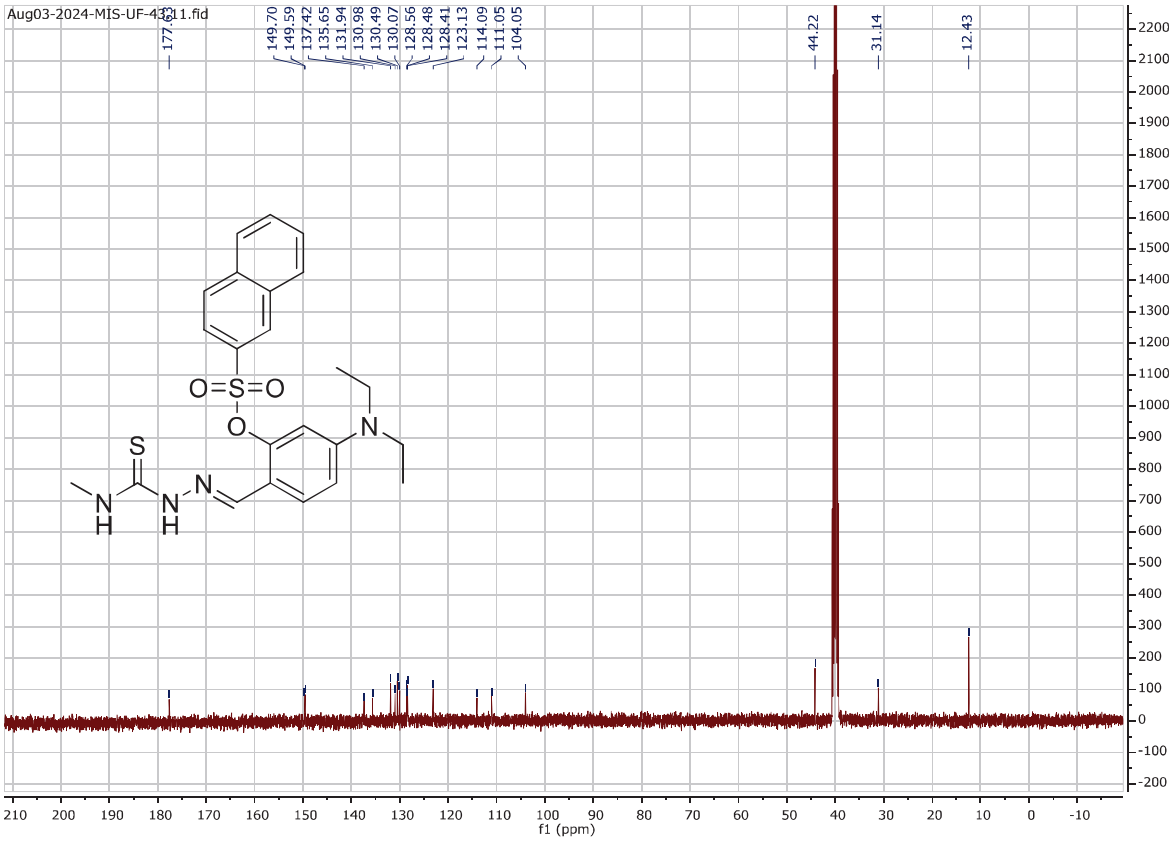

Figure S 66. ^{13}C-NMR Spectrum of Compound **5m** (DMSO-*d6*, 100 MHz)

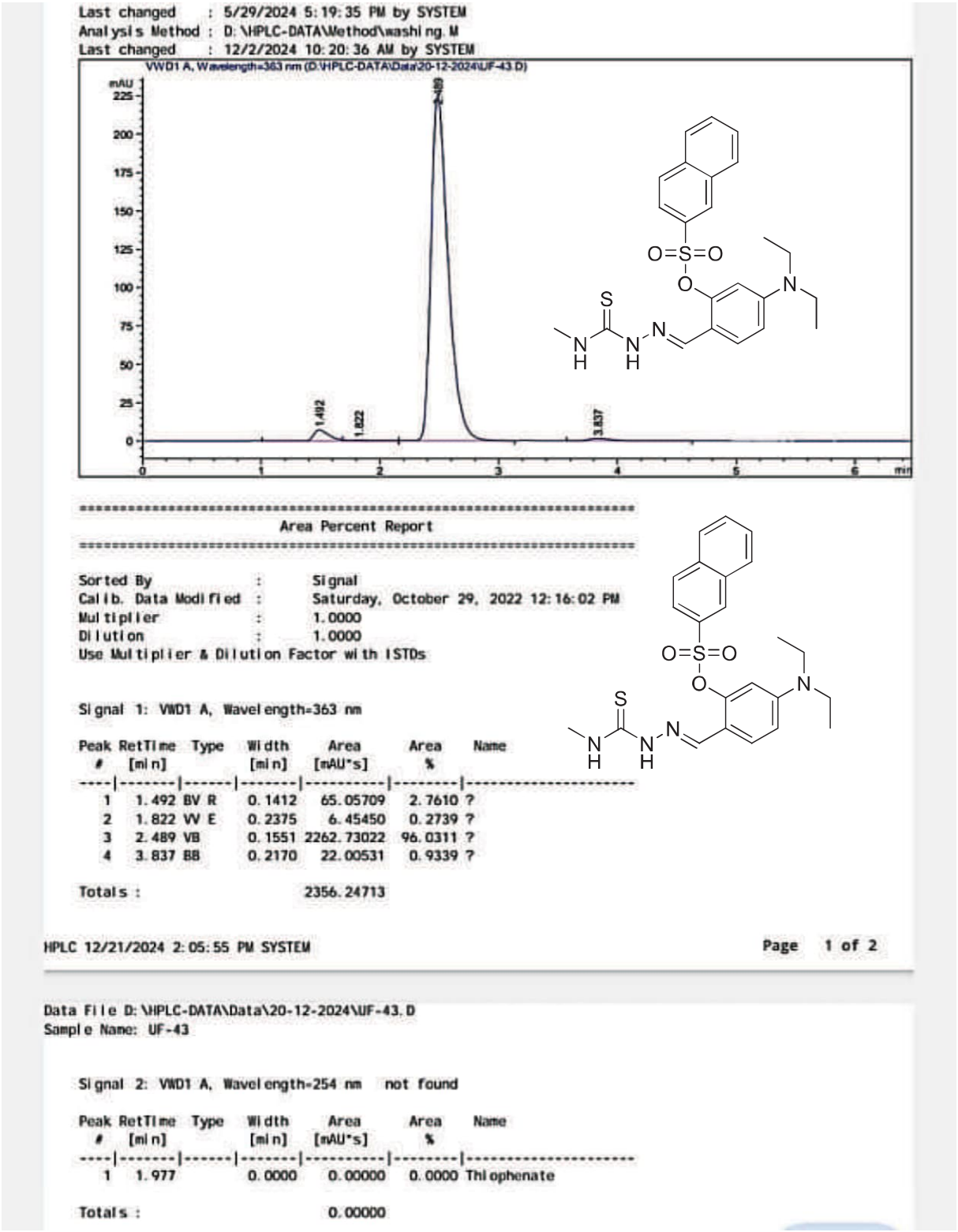

Figure S 67. HPLC Purity Analysis of Compound **5m**

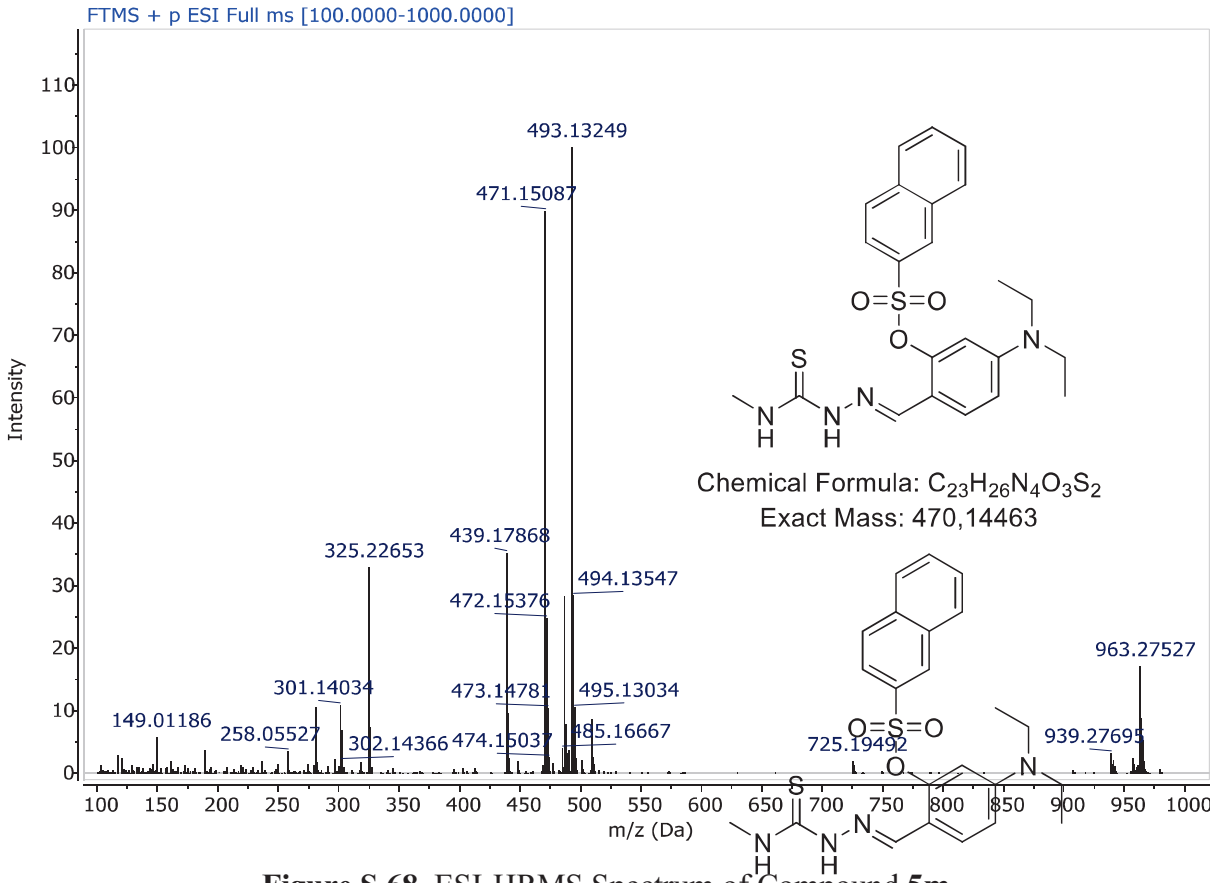

Figure S 68. ESI-HRMS Spectrum of Compound **5m**

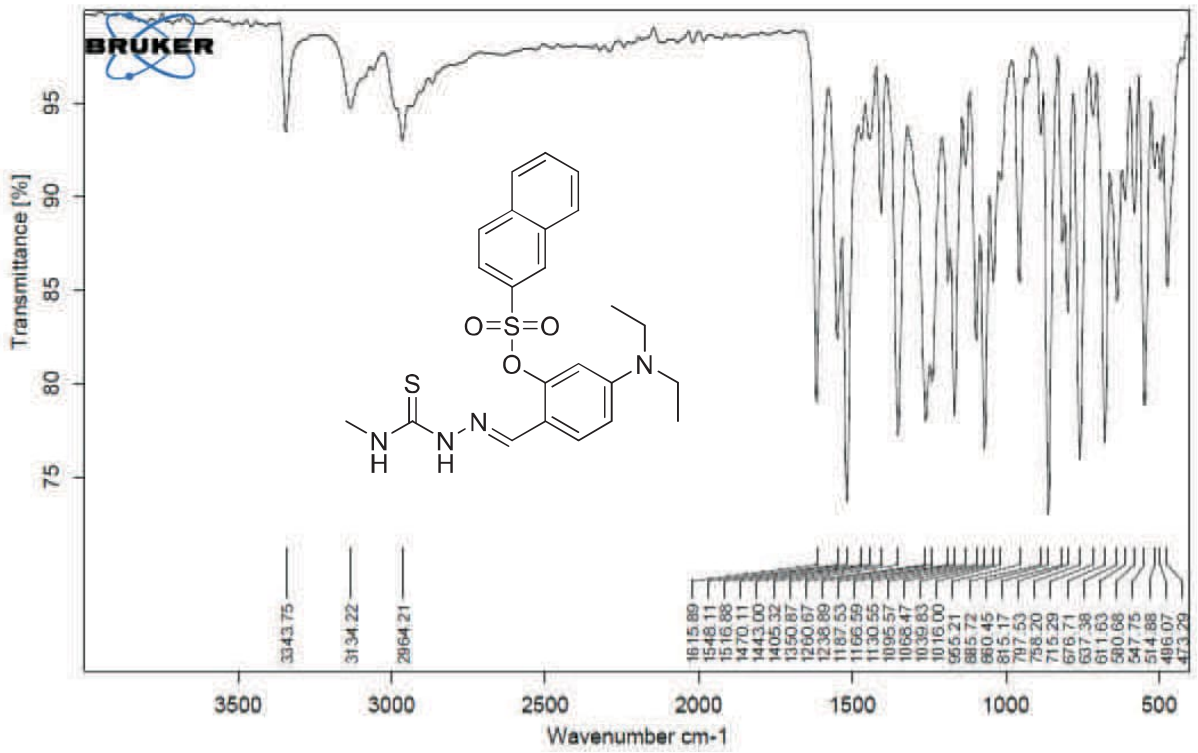

Figure S 69. FT-IR Spectrum of Compound **5m**

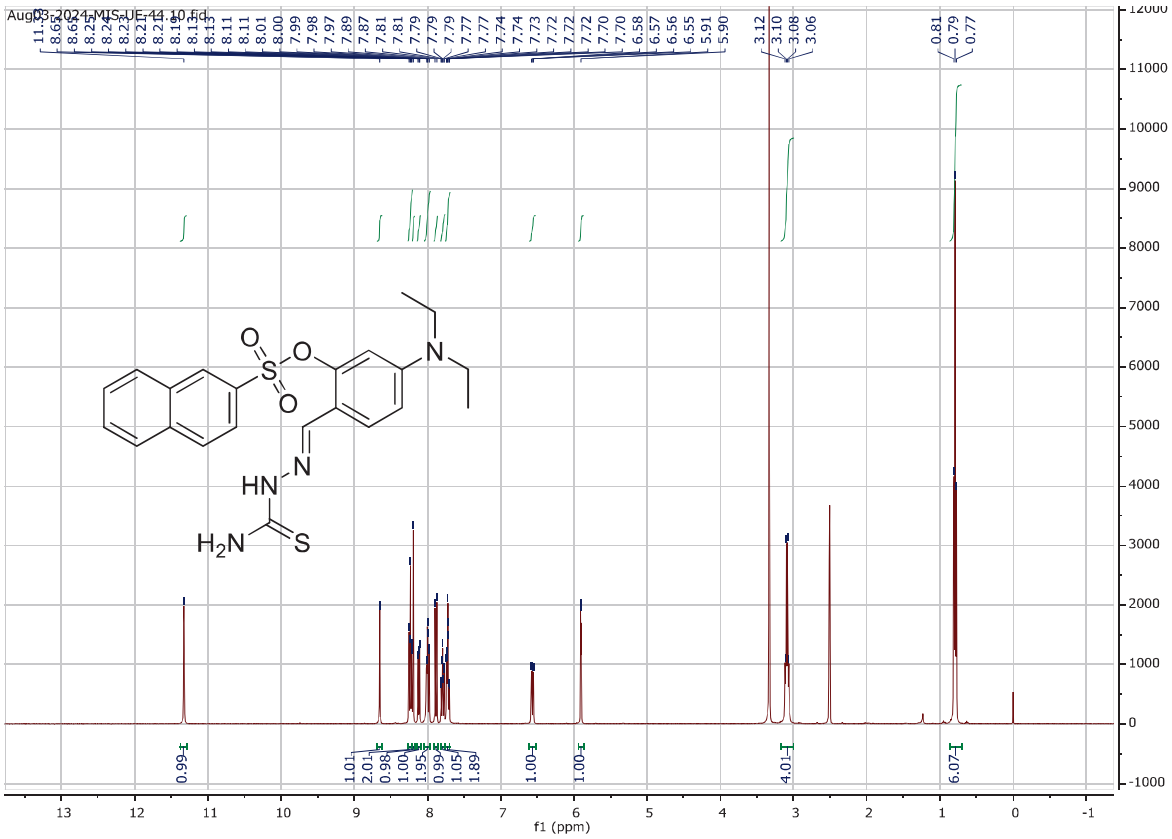

Figure S 70. ^{1}H-NMR Spectrum of Compound **5n** (DMSO-*d6*, 400 MHz)

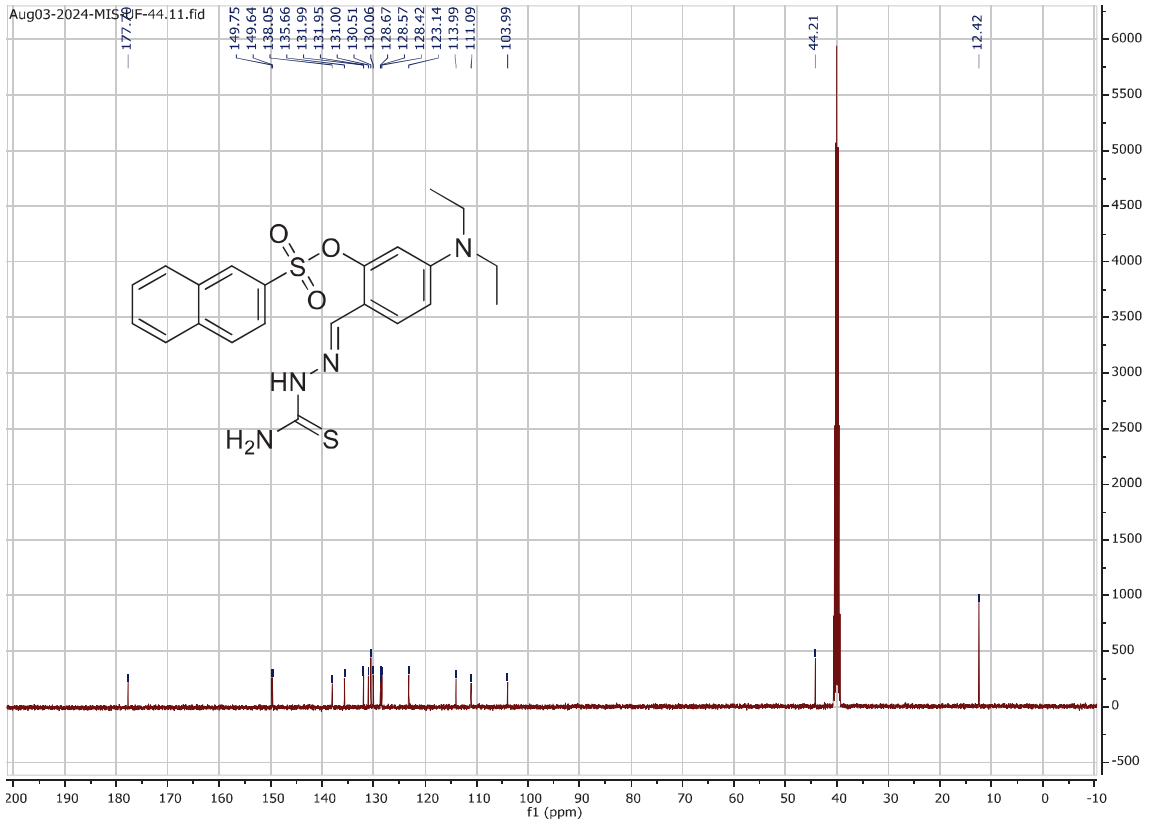

Figure S 71. ^{13}C-NMR Spectrum of Compound **5n** (DMSO-*d6*, 100 MHz)

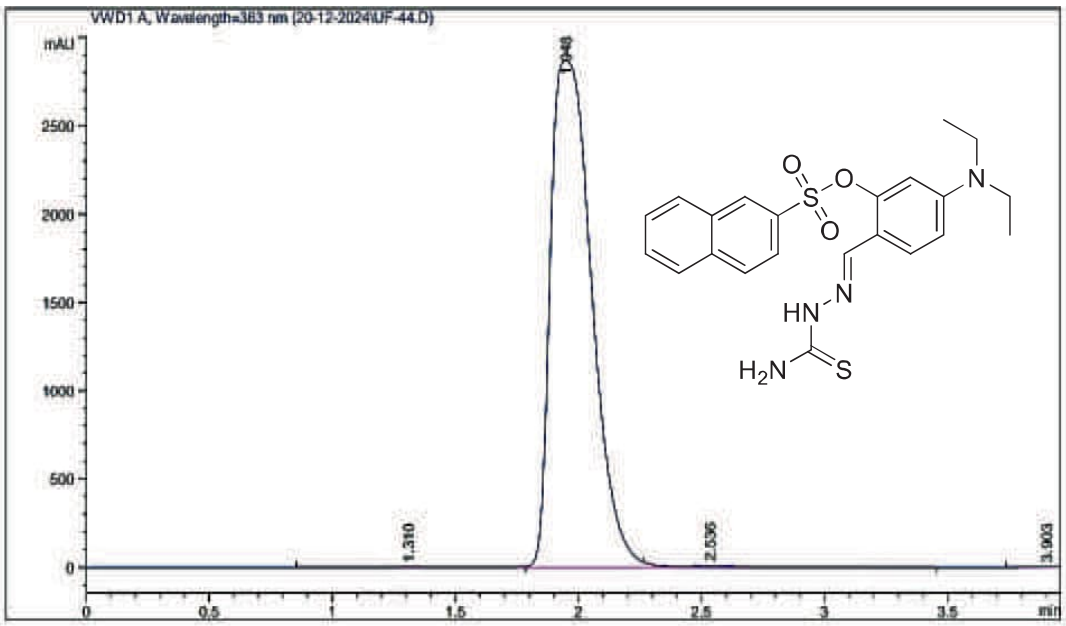

Area Percent Report

Sorted By : Signal
Multiplier : 1.0000
Dilution : 1.0000
Use Multiplier & Dilution Factor with ISTDs

Signal 1: VWD1 A, Wavelength=363 nm

Peak #	RetTime [min]	Type	Width [min]	Area [mAU*s]	Height [mAU]	Area %
1	1.310	BV E	0.1984	61.04853	4.31784	0.1819
2	1.948	VV R	0.1838	3.33529e4	2866.76587	99.3883
3	2.536	VB E	0.2055	142.70123	9.84370	0.4252
4	3.903	BBA	0.1201	1.53341	2.03024e-1	4.569e-3

Totals : 3.35581e4 2881.13044

Figure S 72. HPLC Purity Analysis of Compound **5n**

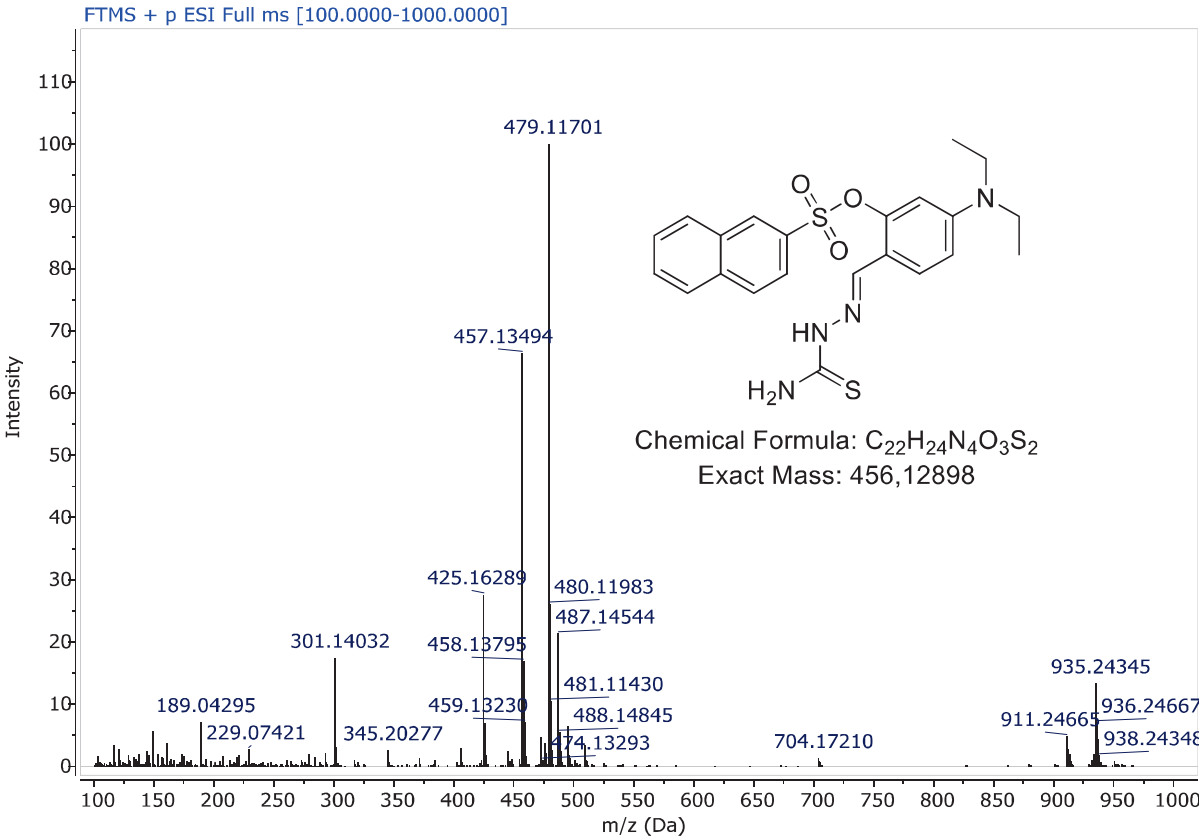

Figure S 73. ESI-HRMS Spectrum of Compound **5n**

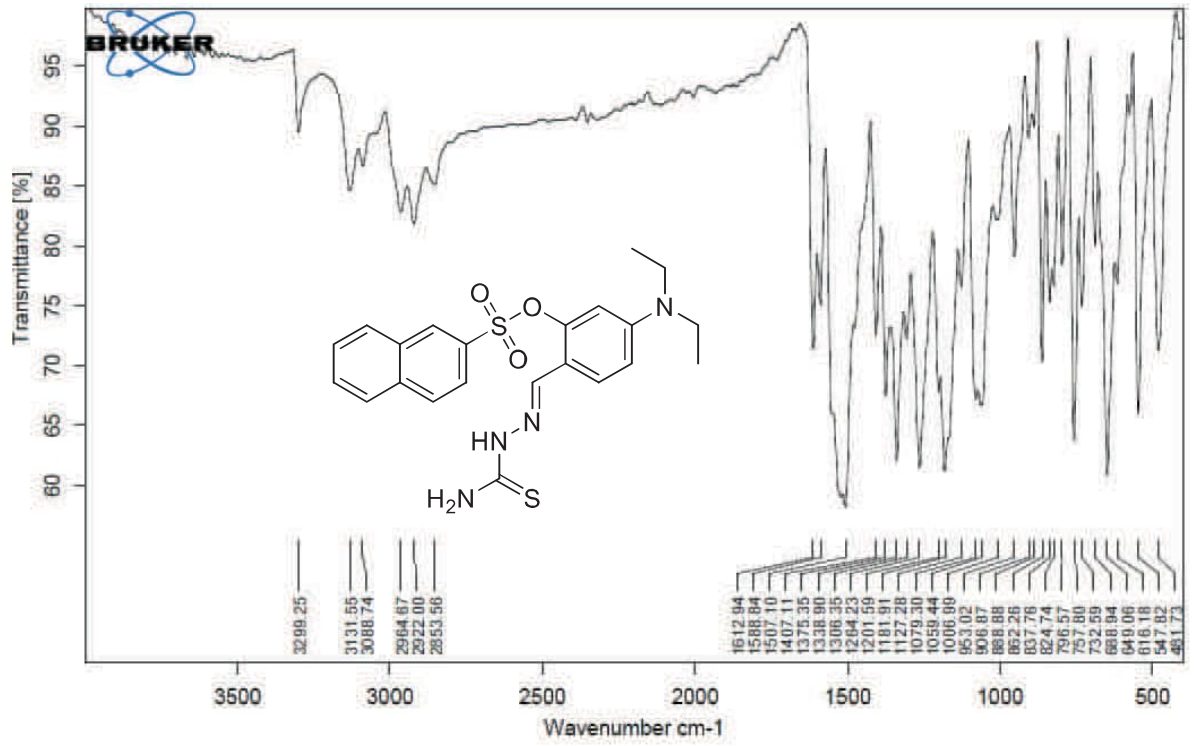

Figure S 74. FT-IR Spectrum of Compound **5n**

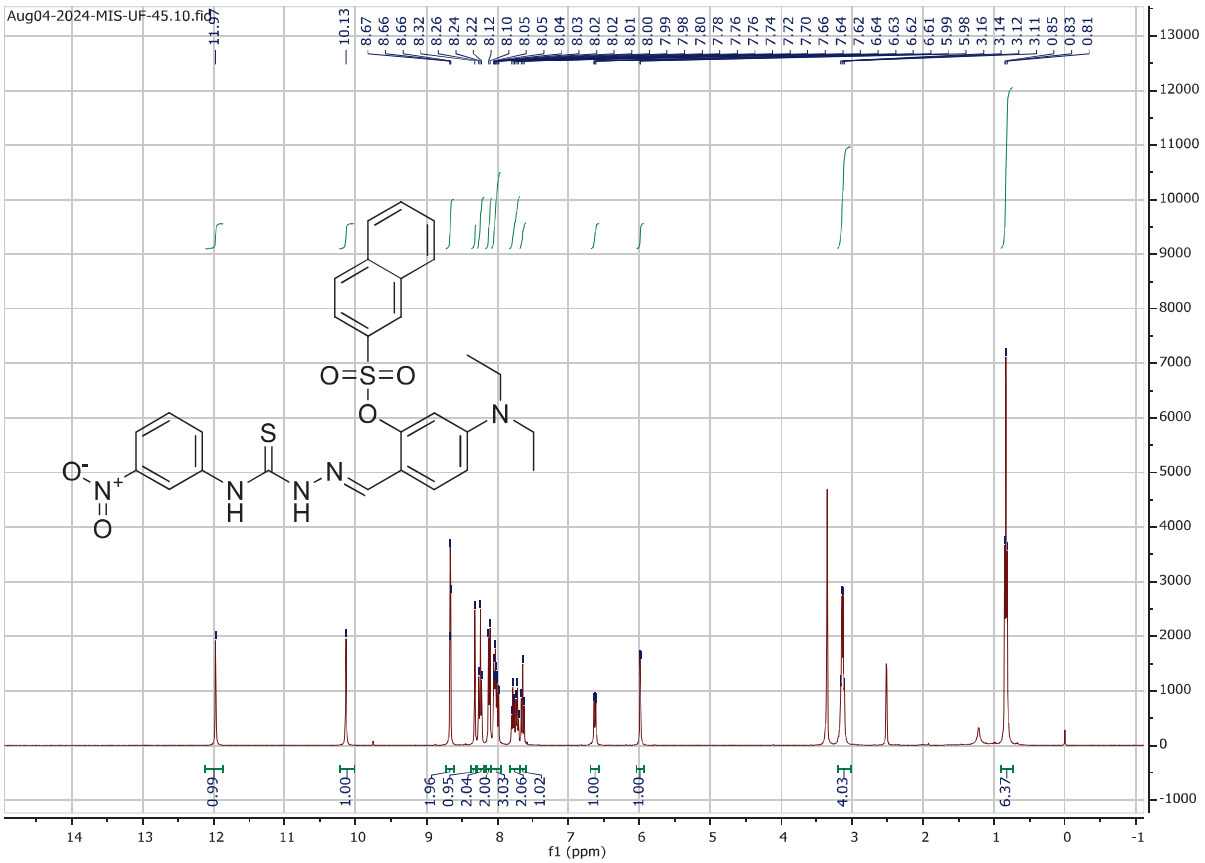

Figure S 75. ^{1}H-NMR Spectrum of Compound **5o** (DMSO-*d6*, 400 MHz)

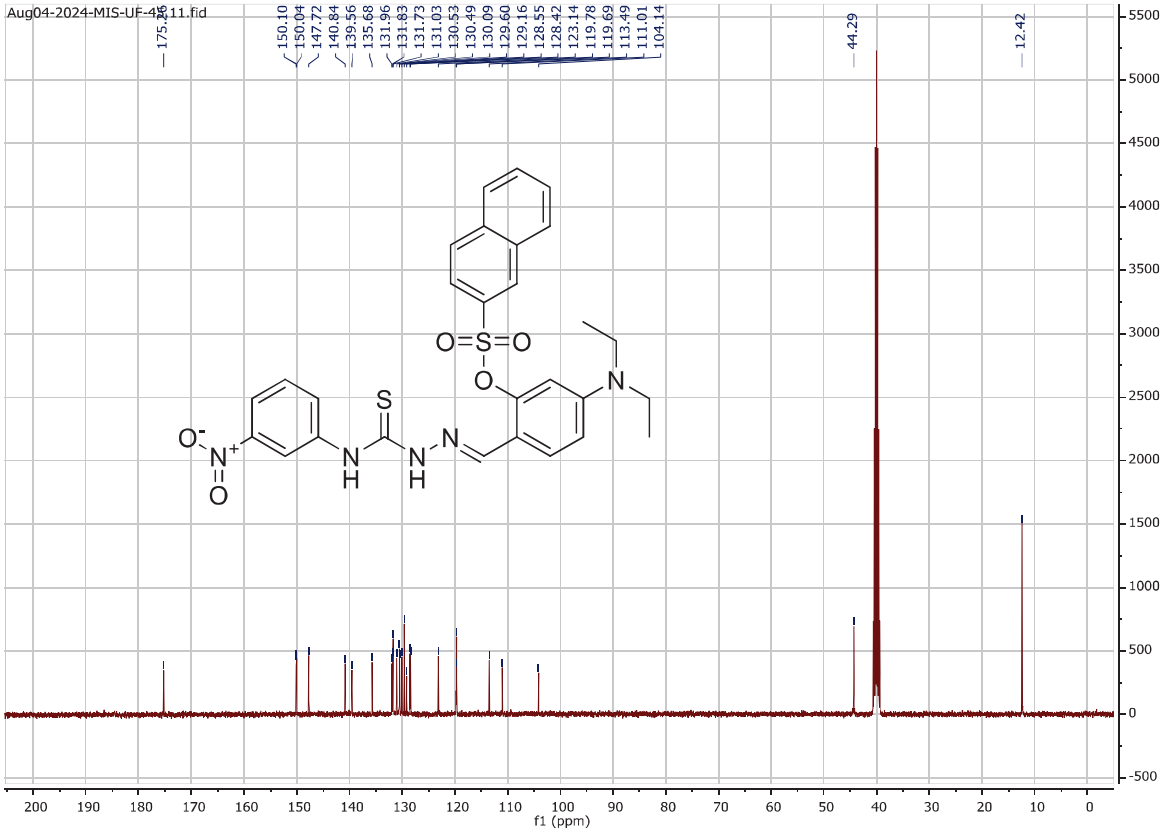

Figure S 76. ^{13}C-NMR Spectrum of Compound **5o** (DMSO-*d6*, 100 MHz)

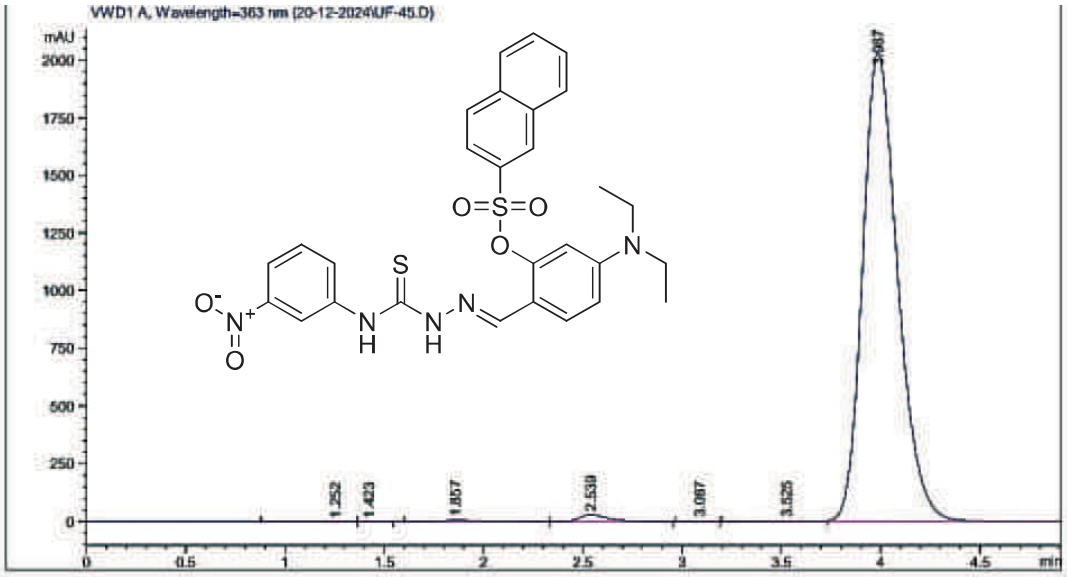

Area Percent Report

Sorted By : Signal
Multiplier : 1.0000
Dilution : 1.0000
Use Multiplier & Dilution Factor with ISTDs

Signal 1: VWD1 A, Wavelength=363 nm

Peak #	RetTime [min]	Type	Width [min]	Area [mAU*s]	Height [mAU]	Area %
1	1.252	BV	0.1621	1.41147	1.10548e-1	5.570e-3
2	1.423	VB	0.0894	6.38199e-1	9.57481e-2	2.519e-3
3	1.857	BV	0.1707	62.80178	5.34108	0.2478
4	2.539	VB	0.1496	280.99582	28.60305	1.1089
5	3.087	BB	0.1297	9.45516e-1	1.20155e-1	3.731e-3
6	3.525	BV E	0.1894	24.16012	1.89643	0.0953
7	3.987	VBAR	0.1869	2.49691e4	2034.59998	98.5361
Totals :				2.53400e4	2070.76698	

Figure S 77. HPLC Purity Analysis of Compound **5o**

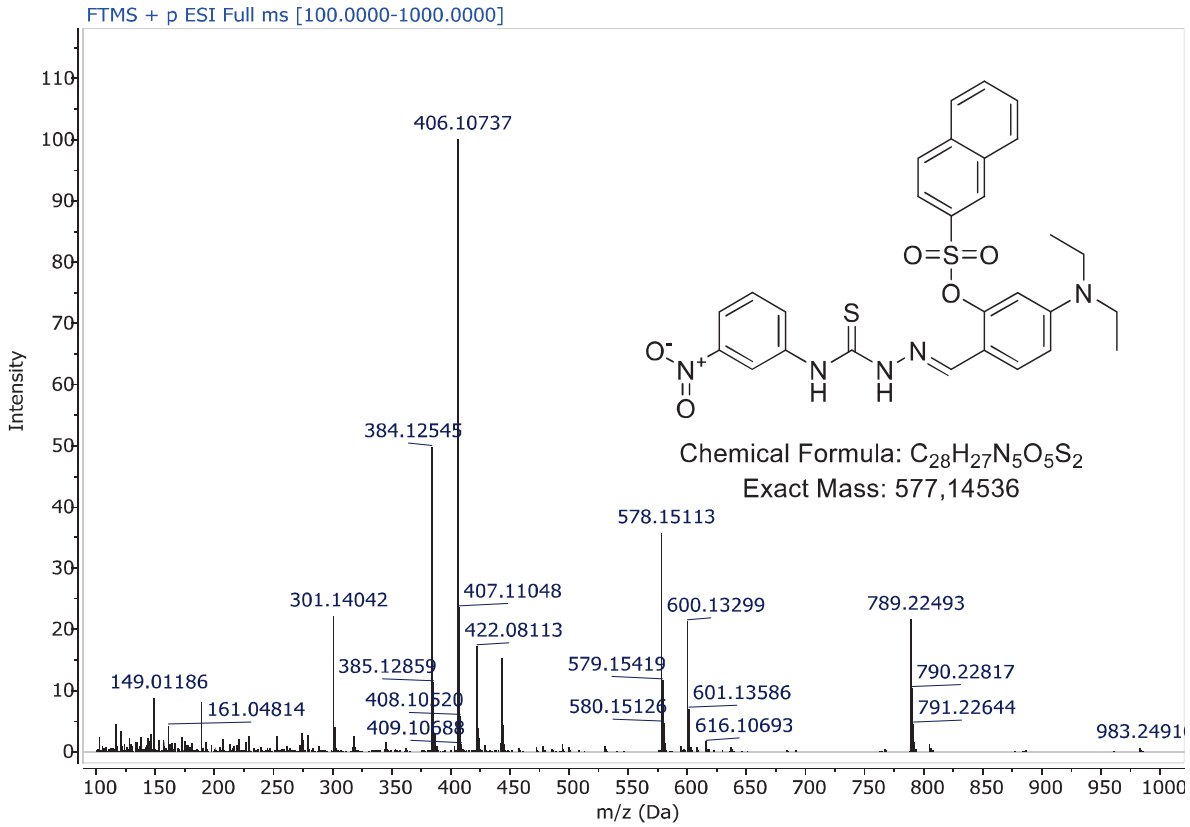

Figure S 78. ESI-HRMS Spectrum of Compound **5o**

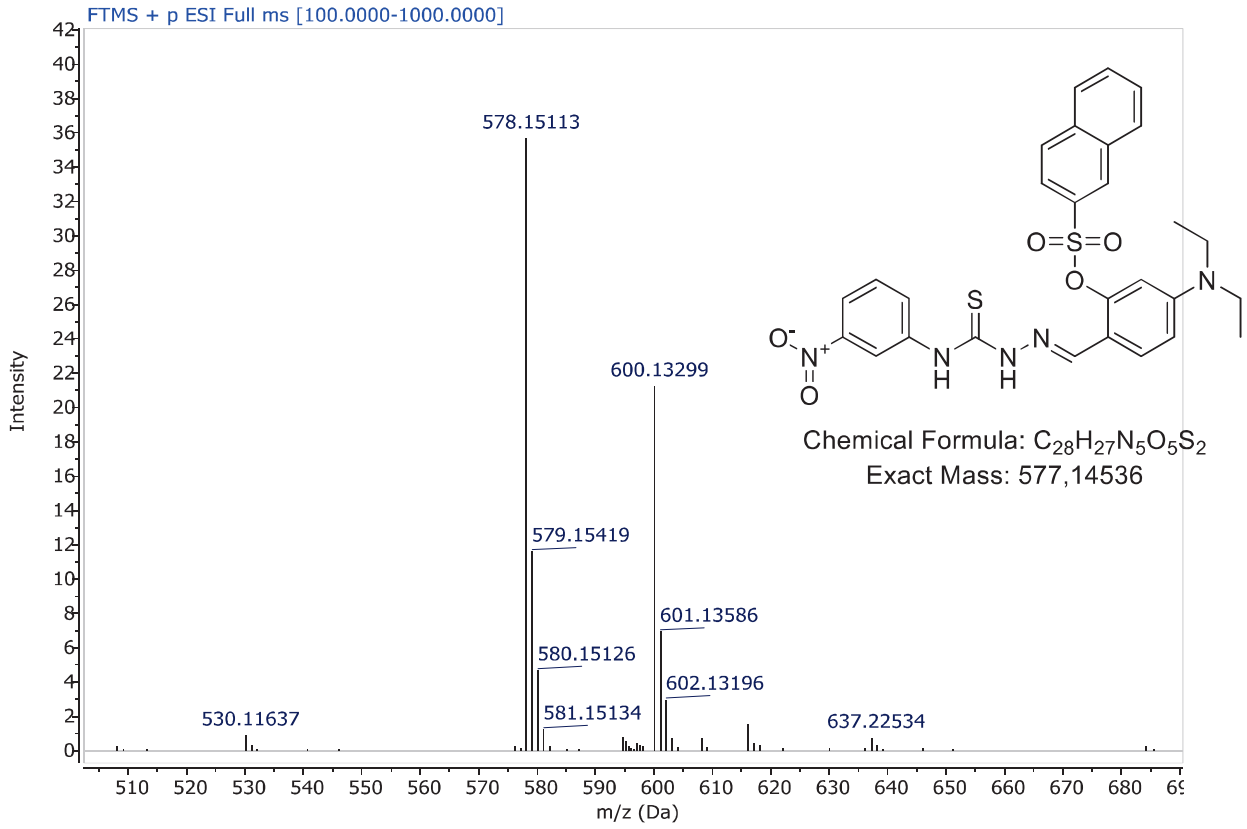

Figure S 79. ESI-HRMS Spectrum of Compound **5o** (extended)

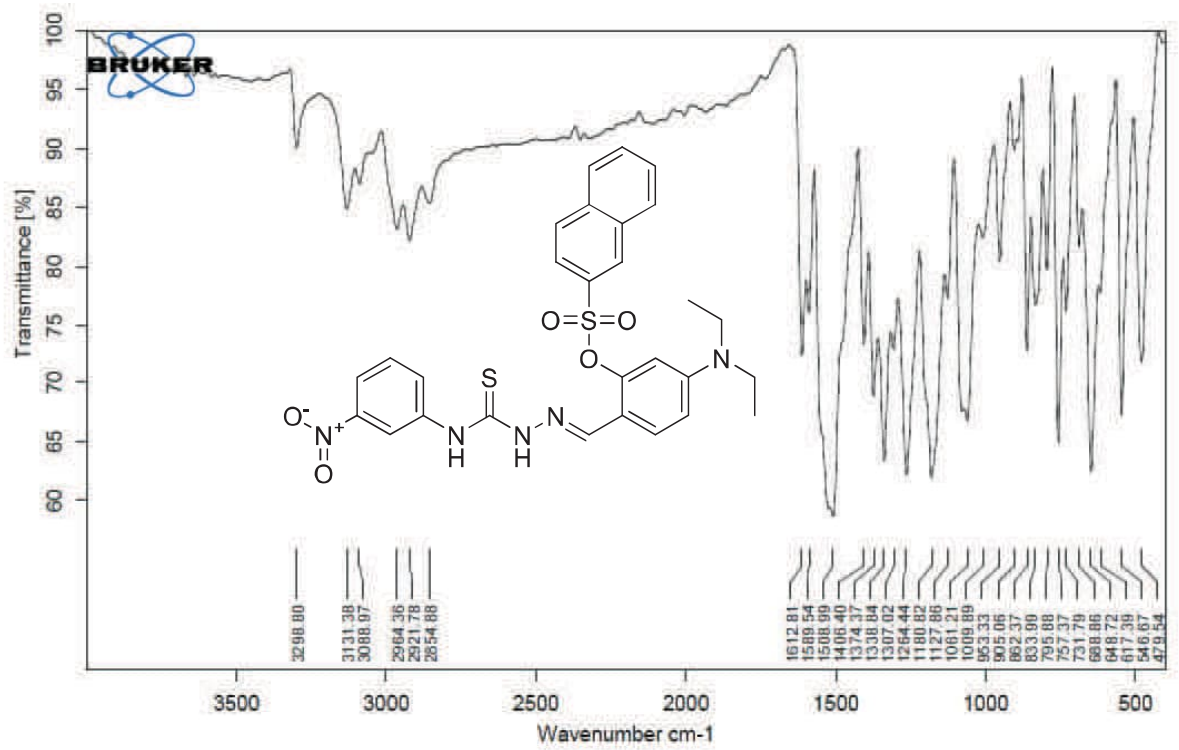

Figure S 80. FT-IR Spectrum of Compound **5o**

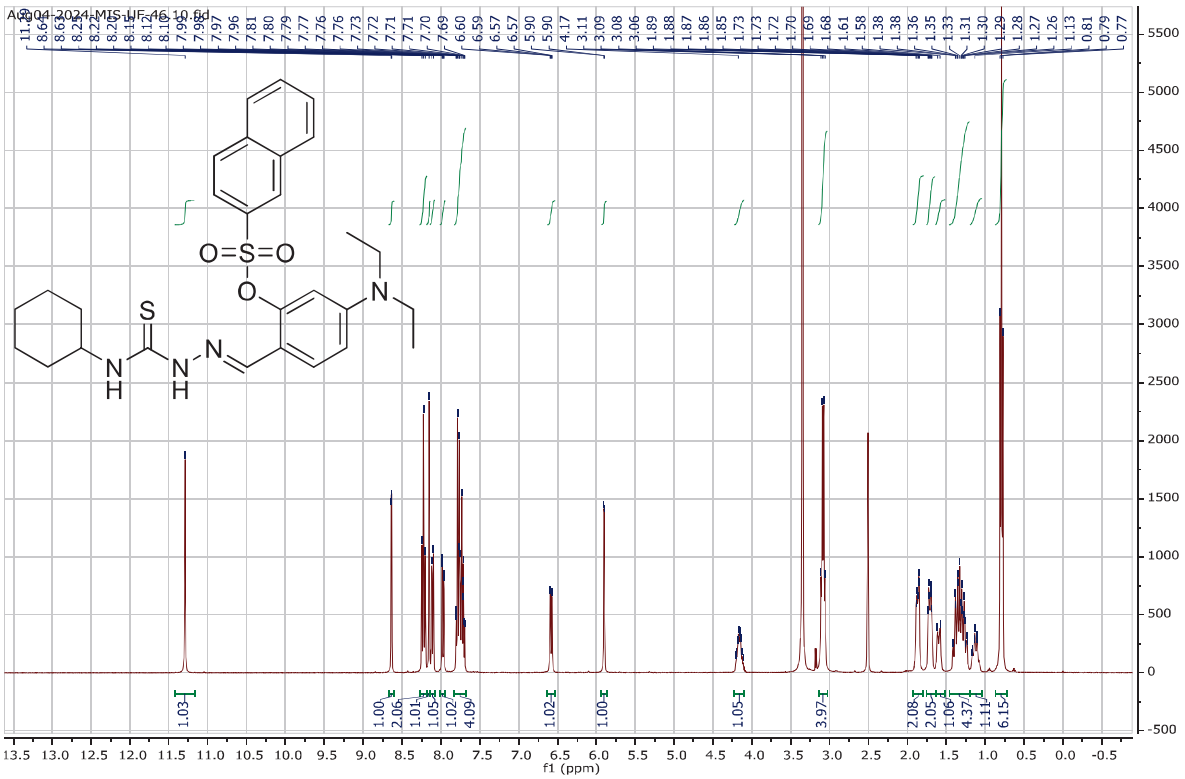

Figure S 81. ^{1}H-NMR Spectrum of Compound **5p** (DMSO-*d6*, 400 MHz)

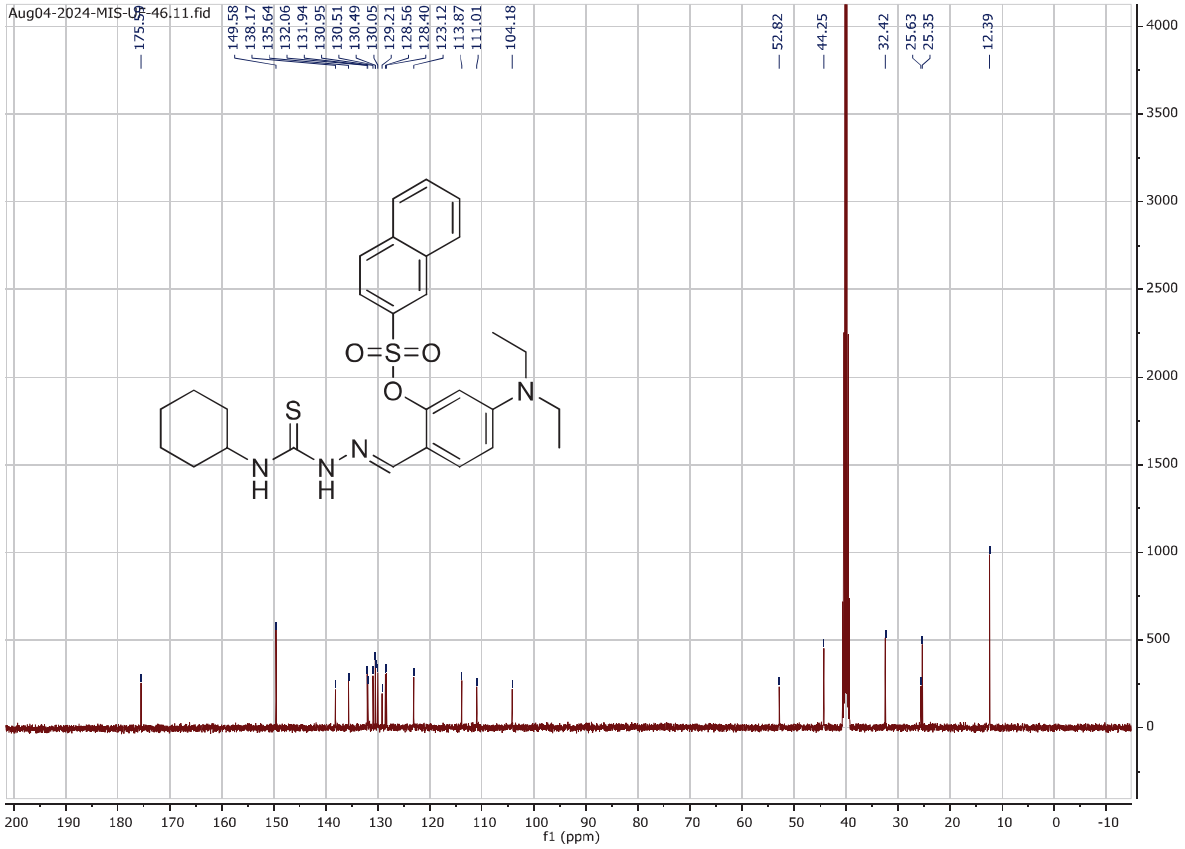

Figure S 82. ^{13}C-NMR Spectrum of Compound **5p** (DMSO-*d6*, 100 MHz)

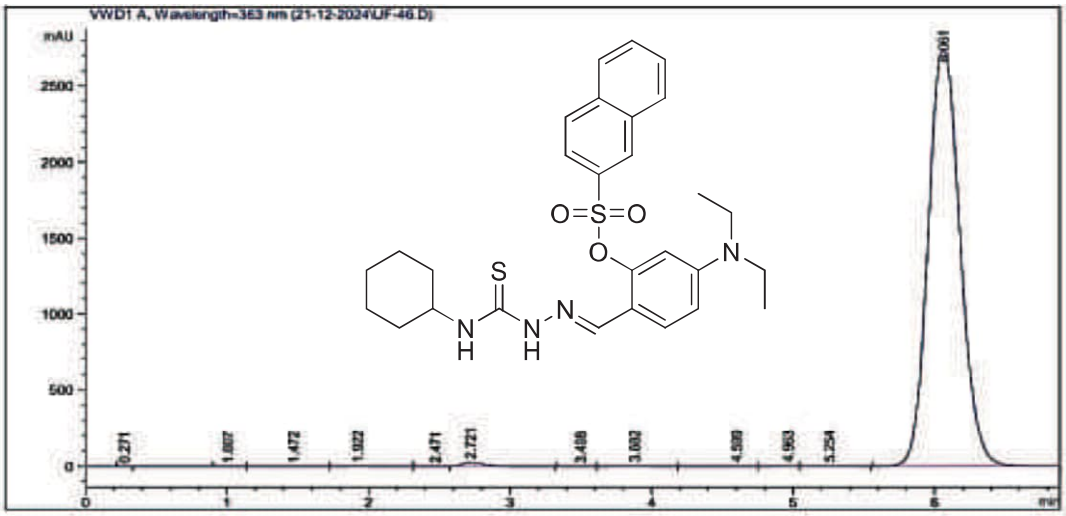

Area Percent Report

Sorted By : Signal
Multiplier : 1.0000
Dilution : 1.0000
Use Multiplier & Dilution Factor with ISTDs

Signal 1: VWD1 A, Wavelength=363 nm

Peak #	RetTime [min]	Type	Width [min]	Area [mAU*s]	Height [mAU]	Area %
1	0.271	BB	0.0469	9.01729e-2	2.86881e-2	2.084e-4
2	1.007	BV	0.1383	7.96371e-1	7.16990e-2	1.840e-3
3	1.472	VB	0.2551	3.51967	1.68655e-1	8.134e-3
4	1.922	BB	0.1479	8.18339	8.03984e-1	0.0189
5	2.471	BV E	0.0942	5.12744e-1	7.12198e-2	1.185e-3
6	2.721	VB R	0.1542	258.94632	25.64293	0.5984
7	3.498	BV	0.1343	2.43296	2.42985e-1	5.623e-3
8	3.882	VB	0.2251	12.49943	7.65070e-1	0.0289
9	4.599	BB	0.1695	2.78652	2.24580e-1	6.440e-3
10	4.963	BV	0.1470	5.37204	5.38273e-1	0.0124

Data File D:\HPLC-DATA\Data\21-12-2024\UF-46.D
Sample Name: UF-46

Peak #	RetTime [min]	Type	Width [min]	Area [mAU*s]	Height [mAU]	Area %
11	5.254	VB	0.2164	33.12867	2.37852	0.0766
12	6.061	BBA	0.2444	4.29414e4	2734.56421	99.2413
Totals :				4.32697e4	2765.52081	

Figure S 83. HPLC Purity Analysis of Compound **5p**

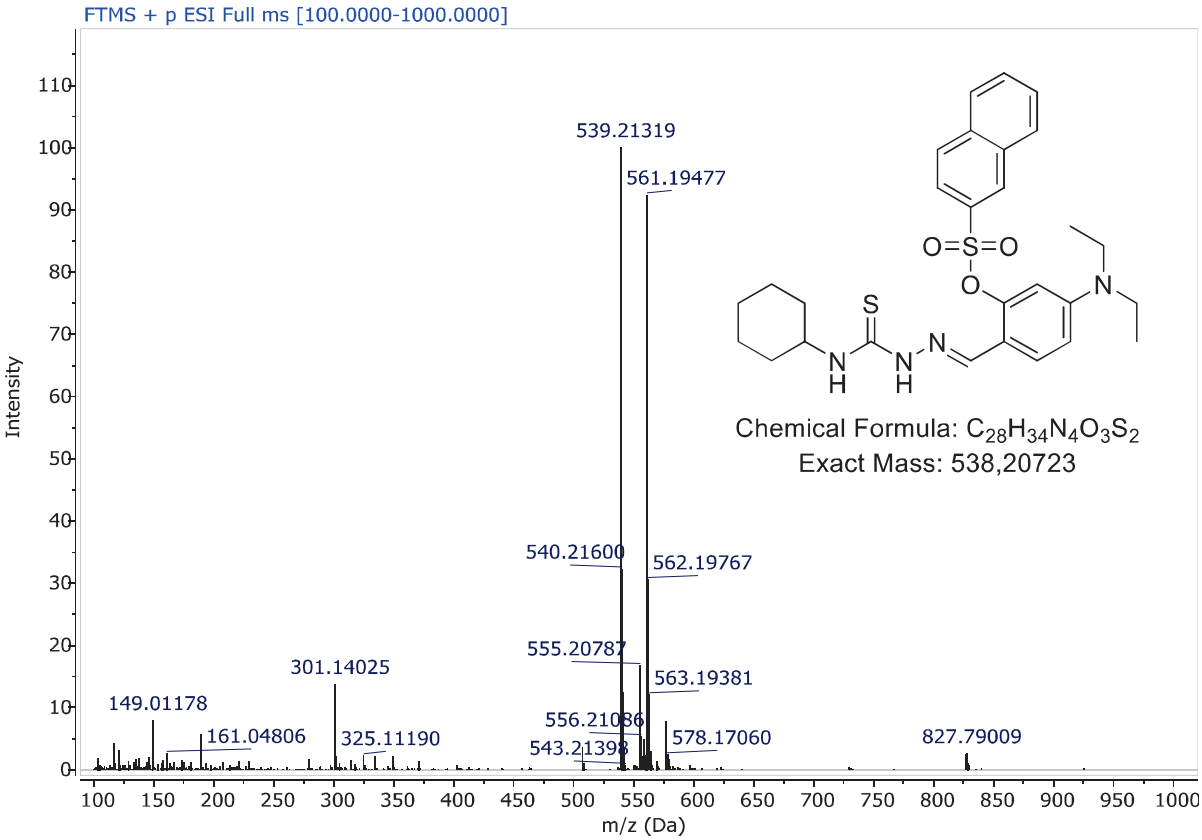

Figure S 84. ESI-HRMS Spectrum of Compound **5p**

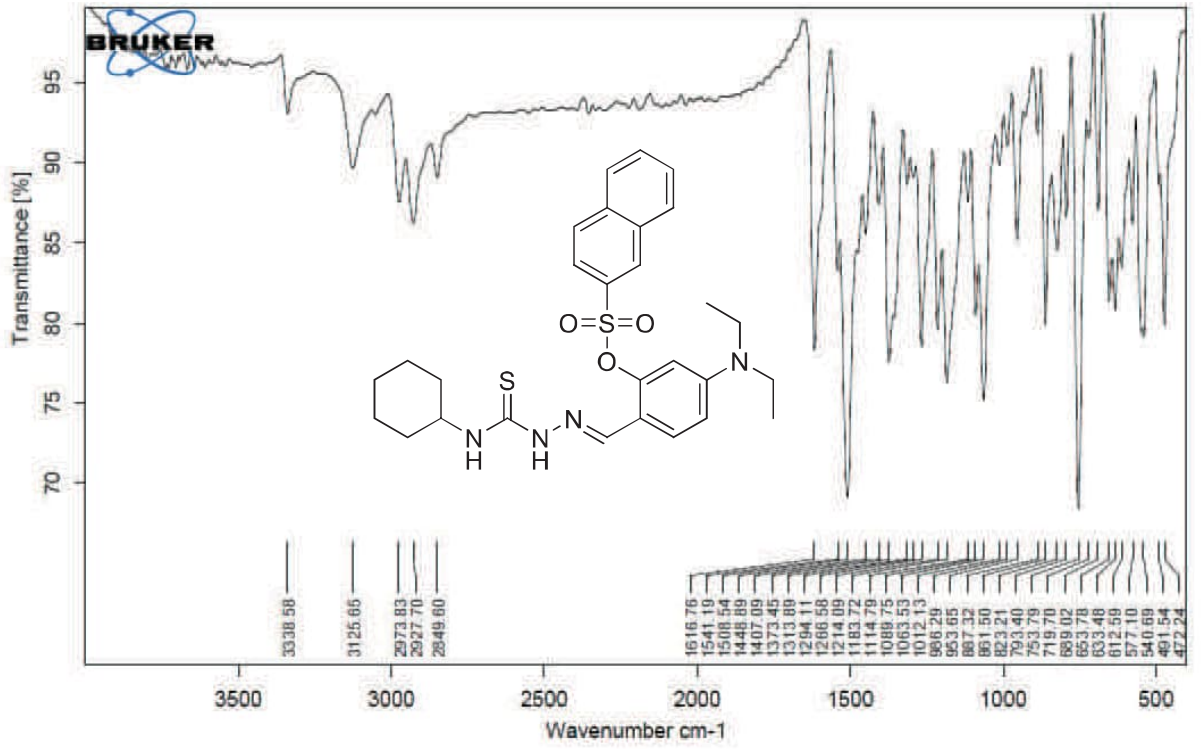

Figure S 85. FT-IR Spectrum of Compound **5p**

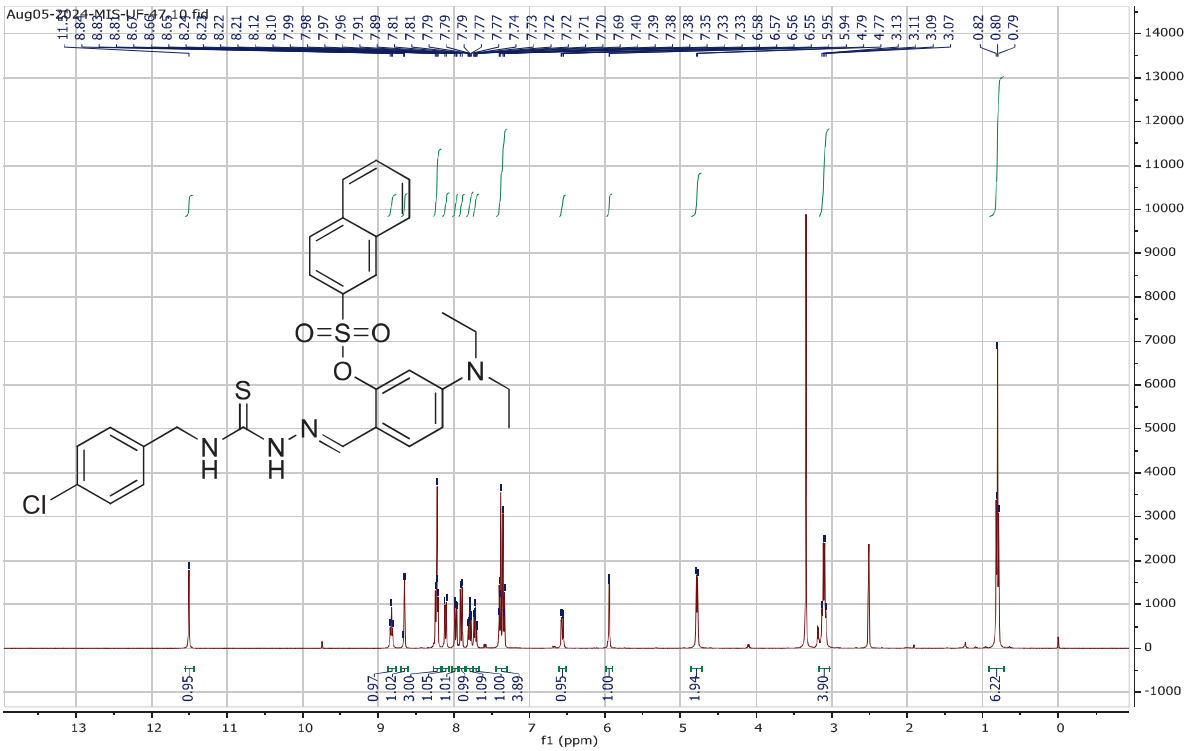

Figure S 86. ^{1}H-NMR Spectrum of Compound **5q** (DMSO-*d6*, 400 MHz)

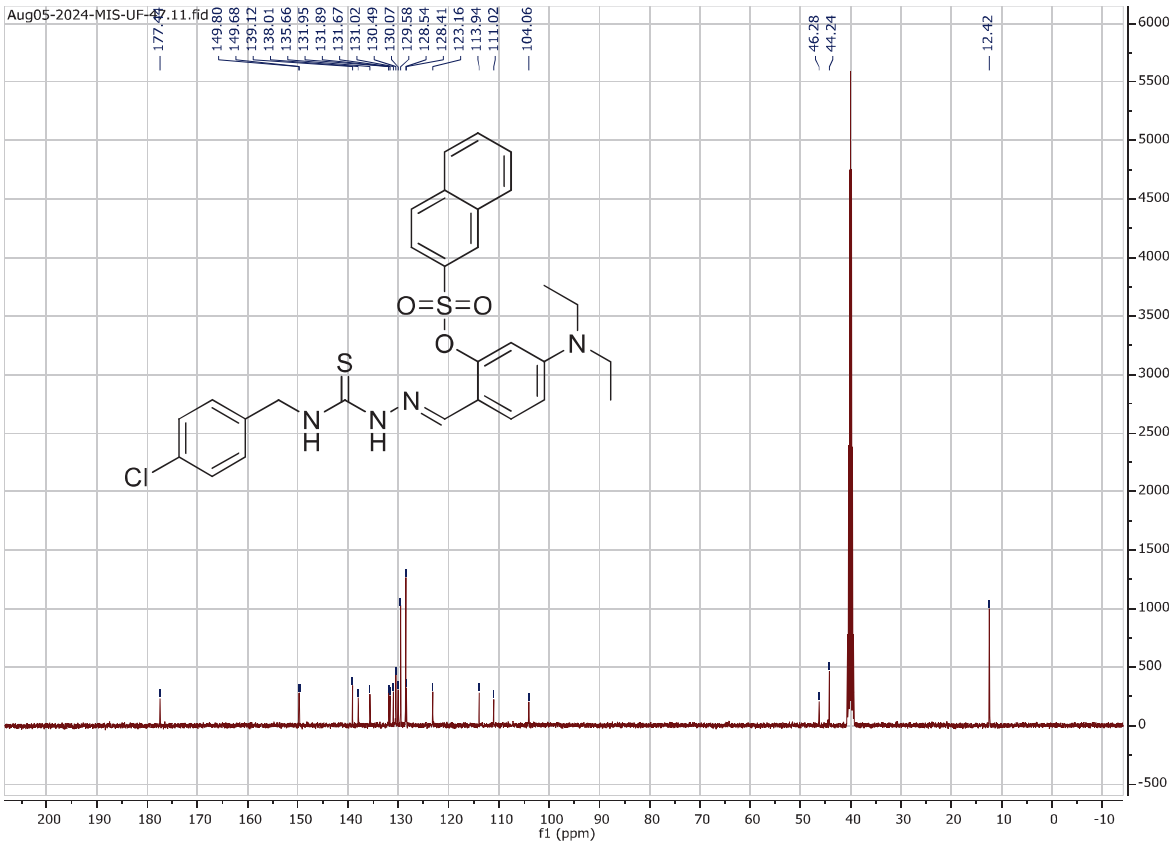

Figure S 87. ^{13}C-NMR Spectrum of Compound **5q** (DMSO-*d6*, 100 MHz)

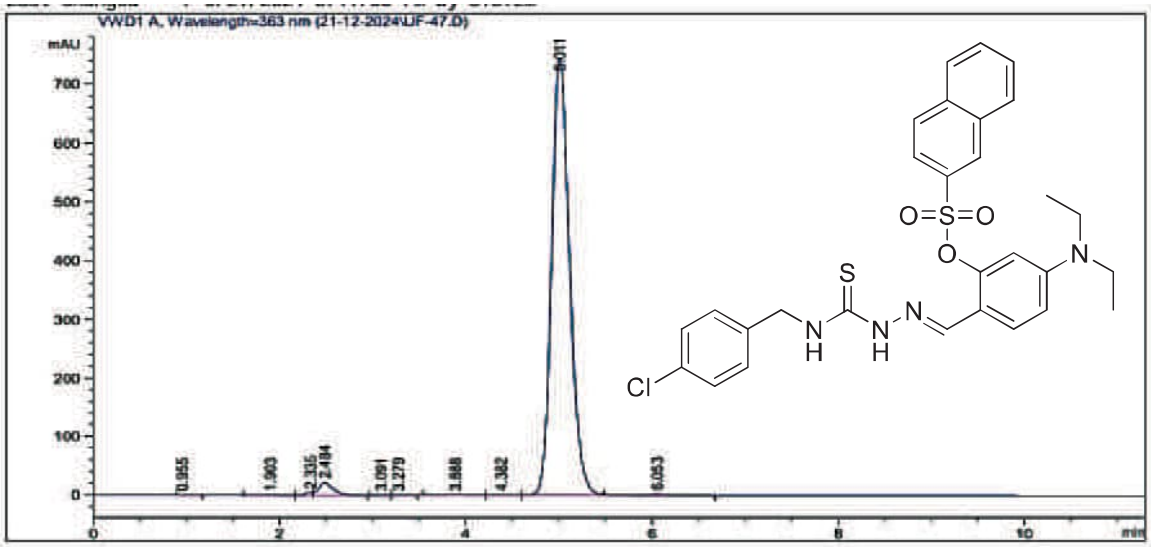

Area Percent Report

Sorted By : Signal
Multiplier : 1.0000
Dilution : 1.0000
Use Multiplier & Dilution Factor with ISTDs

Signal 1: VWD1 A, Wavelength=363 nm

Peak #	RetTime [min]	Type	Width [min]	Area [mAU*s]	Height [mAU]	Area %
1	0.955	BB	0.1288	6.93325e-1	7.46014e-2	6.733e-3
2	1.903	BV	0.1473	6.34860	6.42840e-1	0.0617
3	2.335	VV	0.0823	24.96835	4.70733	0.2425
4	2.484	VB	0.1558	225.25810	21.22508	2.1875
5	3.091	BV	0.1337	1.41315	1.51264e-1	0.0137
6	3.279	VB	0.1409	1.34782	1.30476e-1	0.0131
7	3.888	BV	0.2117	18.34126	1.30772	0.1781
8	4.382	VB	0.1758	6.35814	5.37870e-1	0.0617
9	5.011	BV R	0.2061	9982.56934	743.77142	96.9408
10	6.053	VB E	0.2889	30.29249	1.50387	0.2942

HPLC 12/21/2024 12:26:19 PM SYSTEM Page 1 of 2

Data File D:\HPLC-DATA\Data\21-12-2024\UF-47.D
Sample Name: UF-47

Peak #	RetTime [min]	Type	Width [min]	Area [mAU*s]	Height [mAU]	Area %
Totals :				1.02976e4	774.05248	

Figure S 88. HPLC Purity Analysis of Compound **5q**

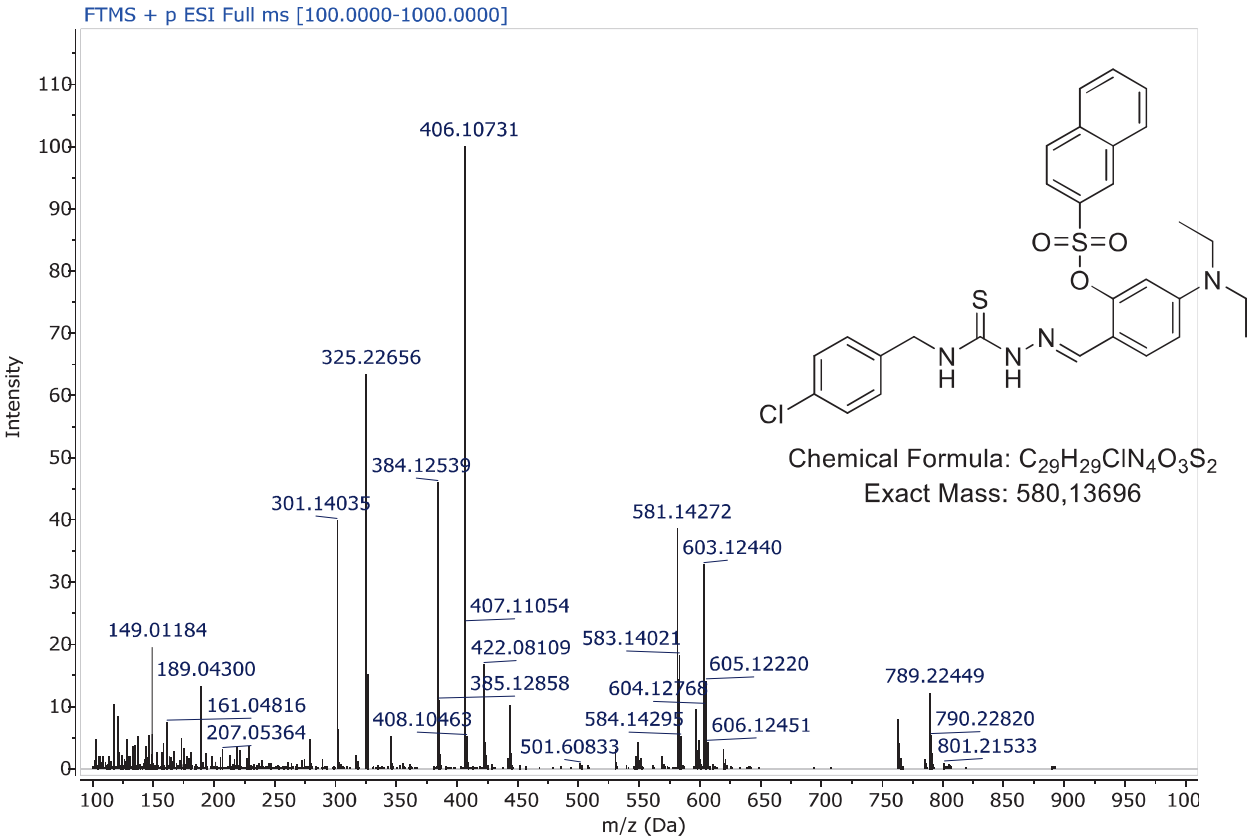

Figure S 89. ESI-HRMS Spectrum of Compound **5q**

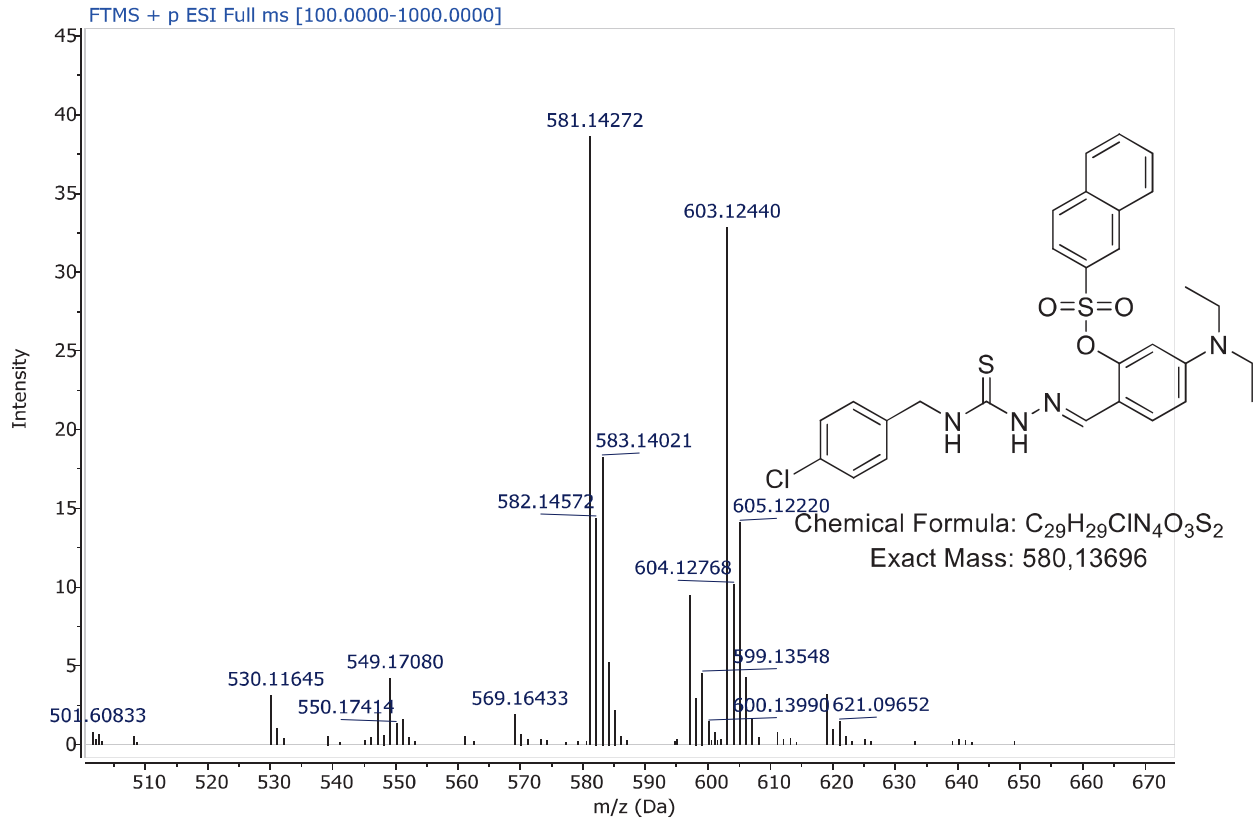

Figure S 90. ESI-HRMS Spectrum of Compound **5q** (extended)

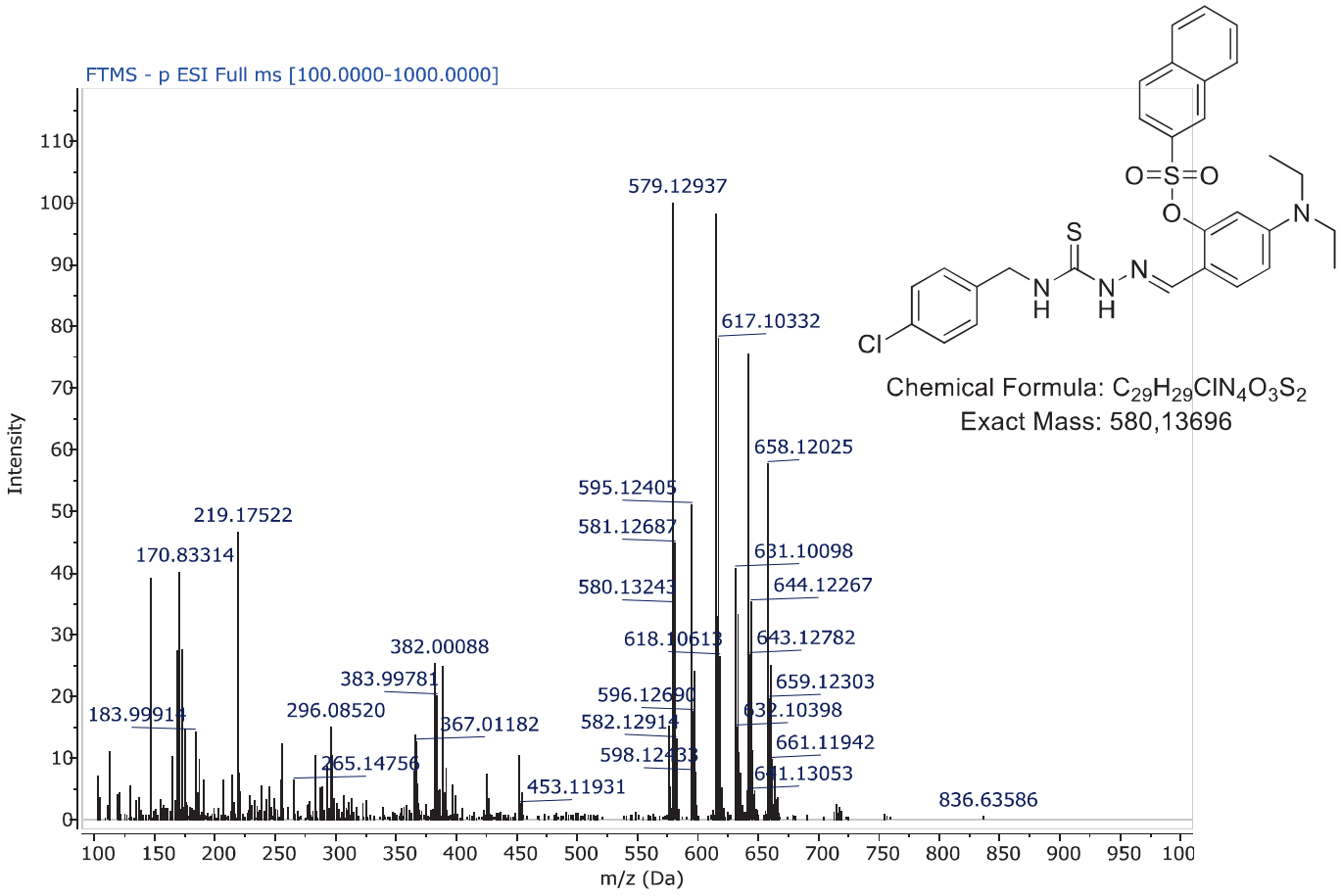

Figure S 91. ESI-HRMS Spectrum of Compound **5q** (negative)

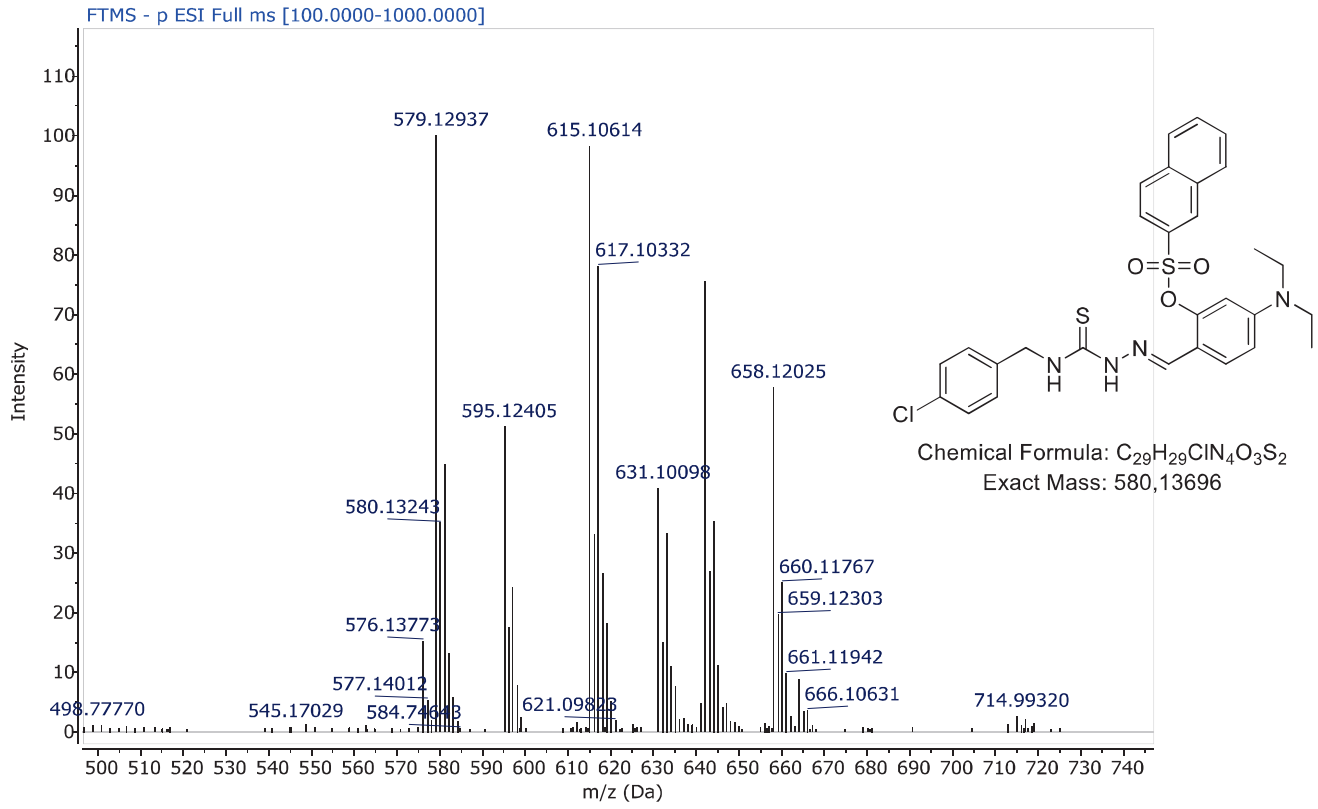

Figure S 92. ESI-HRMS Spectrum of Compound **5q** (negative-extended)

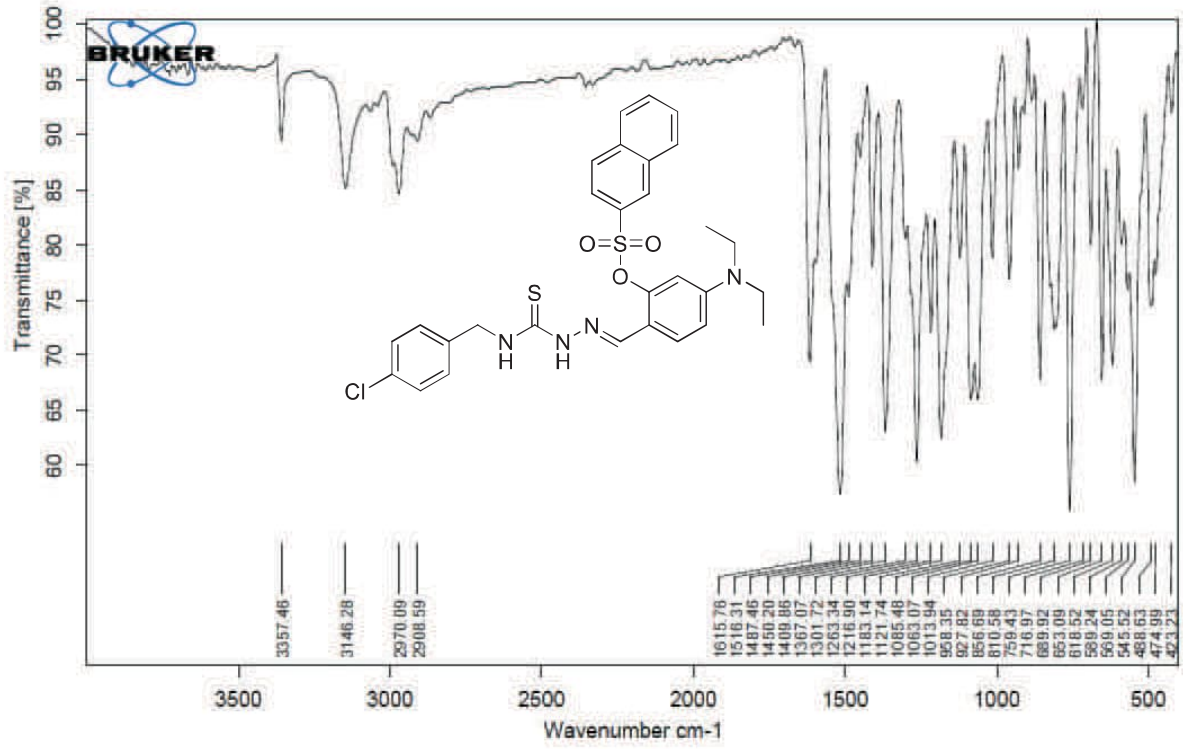

Figure S 93. FT-IR Spectrum of Compound **5q**

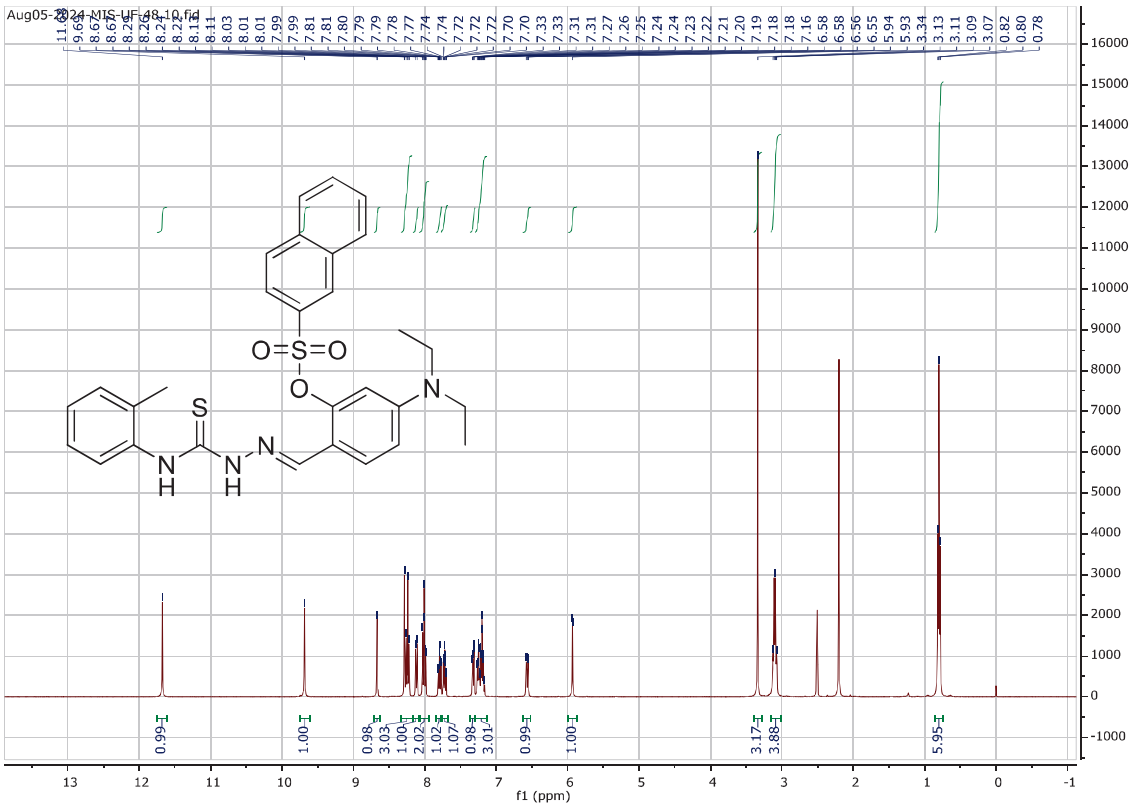

Figure S 94. ^{1}H-NMR Spectrum of Compound **5r** (DMSO-*d6*, 400 MHz)

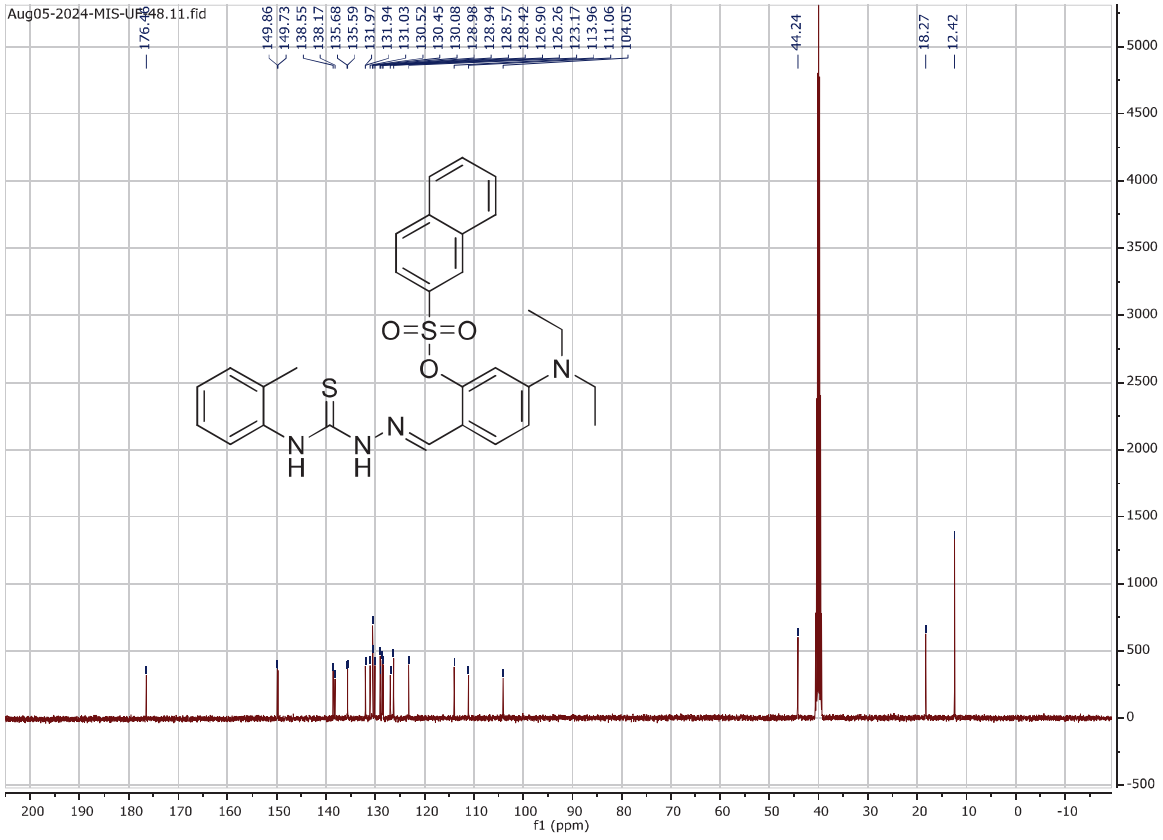

Figure S 95. ^{13}C-NMR Spectrum of Compound **5r** (DMSO-*d6*, 100 MHz)

Acq. Operator : SYSTEM
Sample Operator : SYSTEM
Acq. Instrument : HPLC Location : -
Injection Date : 12/21/2024 12:27:00 PM Inj : 1
Inj Volume : No Inj

Method : D:\HPLC-DATA\Method\BZ-11.M
Last changed : 5/29/2024 5:19:35 PM by SYSTEM

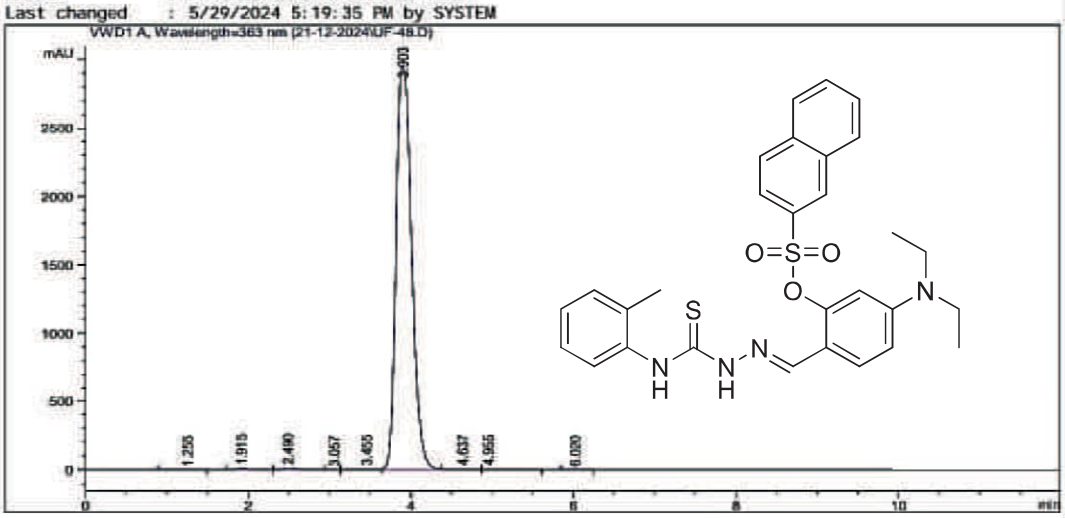

Area Percent Report

Sorted By : Signal
Multiplier : 1.0000
Dilution : 1.0000
Use Multiplier & Dilution Factor with ISTDs

Signal 1: VWD1 A, Wavelength=363 nm

Peak #	RetTime [min]	Type	Width [min]	Area [mAU*s]	Height [mAU]	Area %
1	1.255	BB	0.1811	2.44717	1.65617e-1	6.195e-3
2	1.915	BB	0.1395	78.98338	8.57653	0.1999
3	2.490	BV R	0.1545	120.32886	11.46142	0.3046
4	3.057	VB E	0.0757	3.77875e-1	6.58048e-2	9.565e-4
5	3.455	BV E	0.1823	37.00126	2.98792	0.0937
6	3.903	VV R	0.2077	3.92148e4	2946.11011	99.2663
7	4.637	VV E	0.2554	31.62241	1.74244	0.0800
8	4.955	VB E	0.2429	16.69571	9.91988e-1	0.0423
9	6.020	BB	0.1829	2.37197	1.74945e-1	6.004e-3

Data File D:\HPLC-DATA\Data\21-12-2024\UF-48.D
Sample Name: UF-48

Totals : 3.95046e4 2972.27677

Figure S 96. HPLC Purity Analysis of Compound **5r**

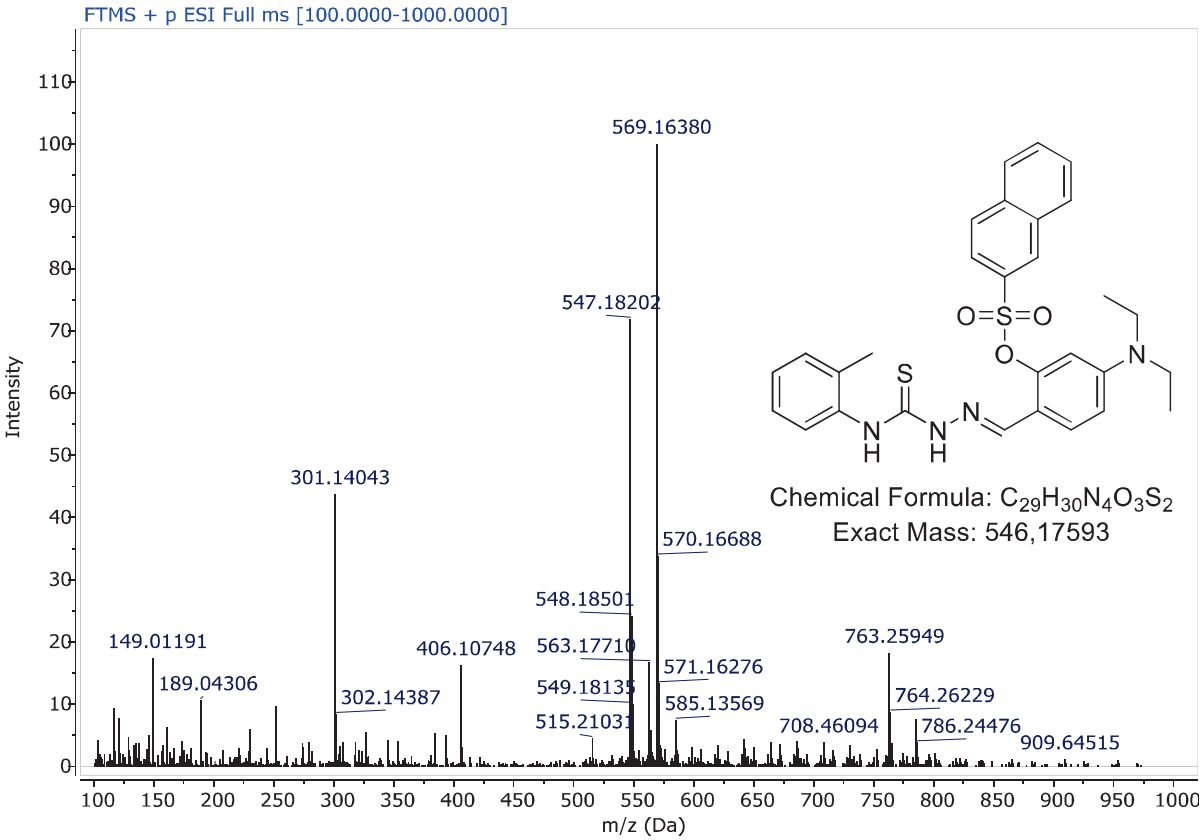

Figure S 97. ESI-HRMS Spectrum of Compound **5r**

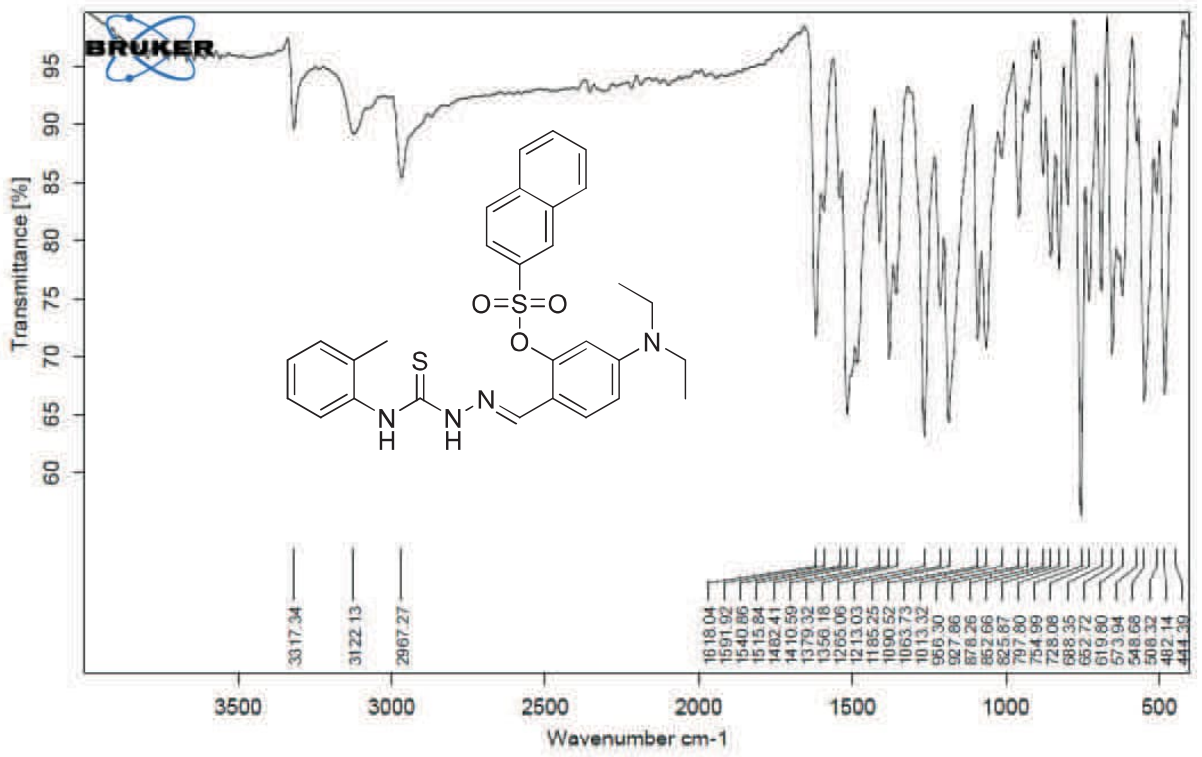

Figure S 98. FT-IR Spectrum of Compound **5r**

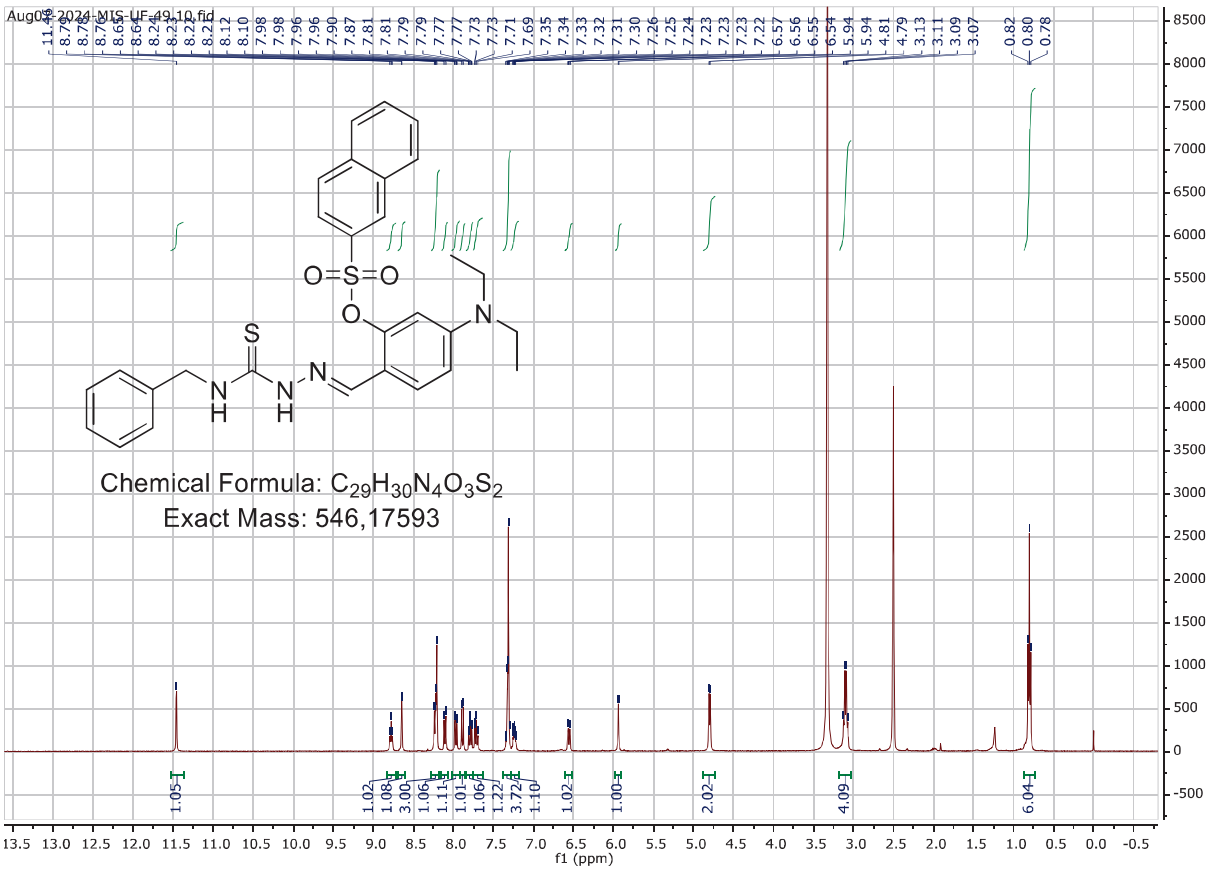

Figure S 99. ^{1}H-NMR Spectrum of Compound **5s** (DMSO-*d6*, 400 MHz)

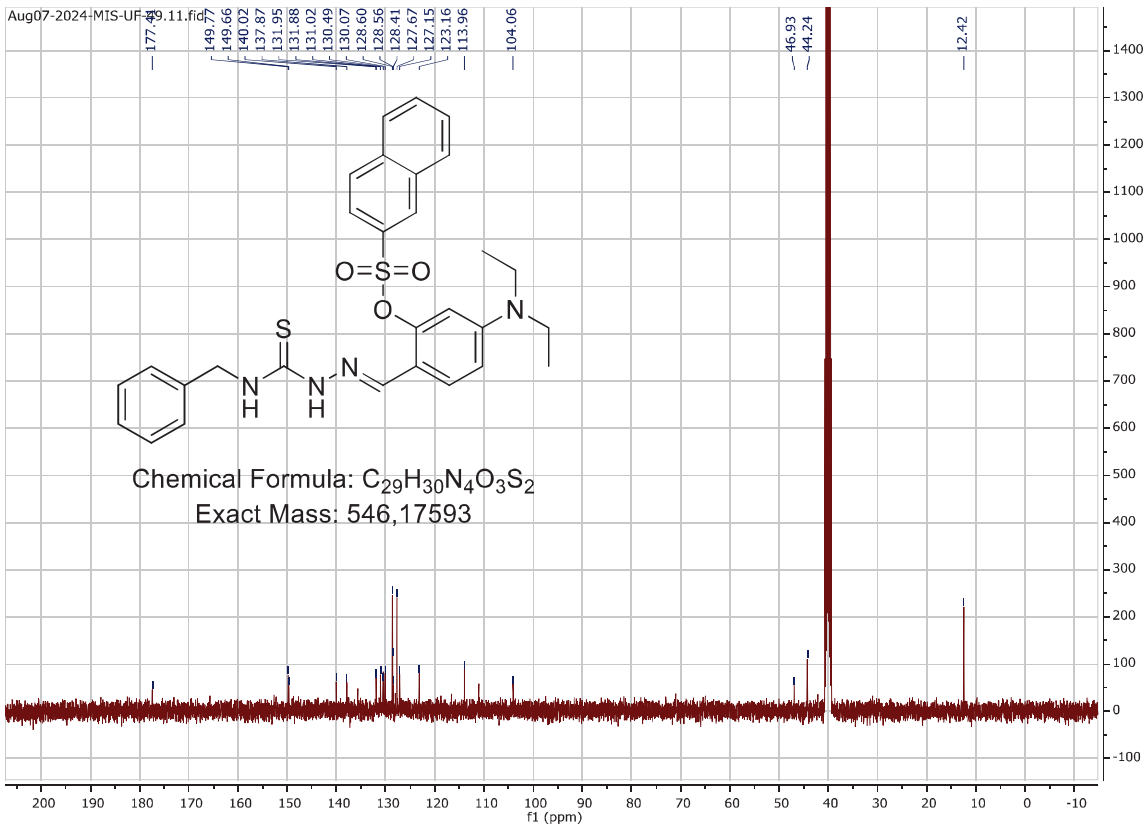

Figure S 100. ^{13}C-NMR Spectrum of Compound **5s** (DMSO-*d6*, 100 MHz)

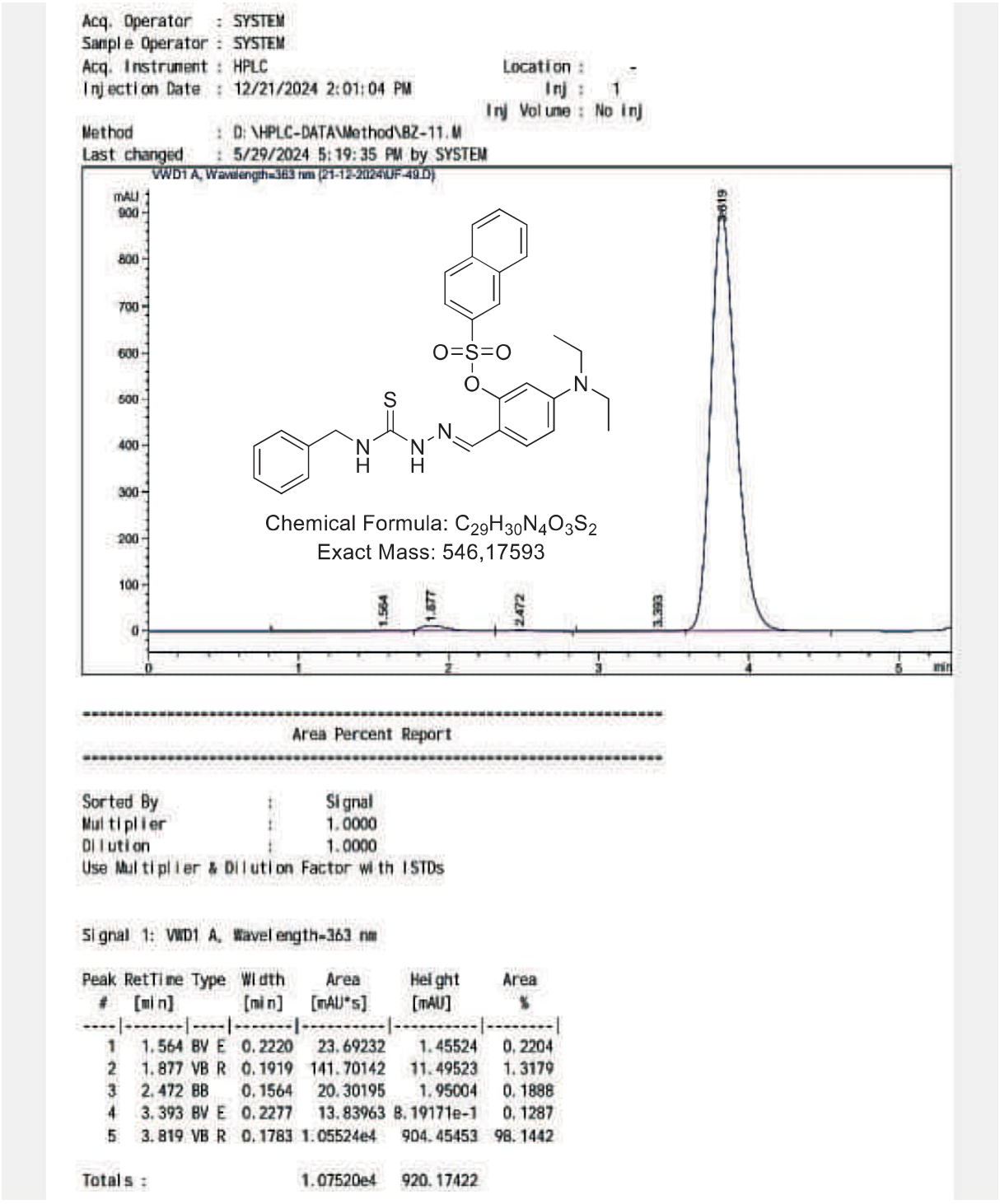

Figure S 101. HPLC Purity Analysis of Compound **5s**

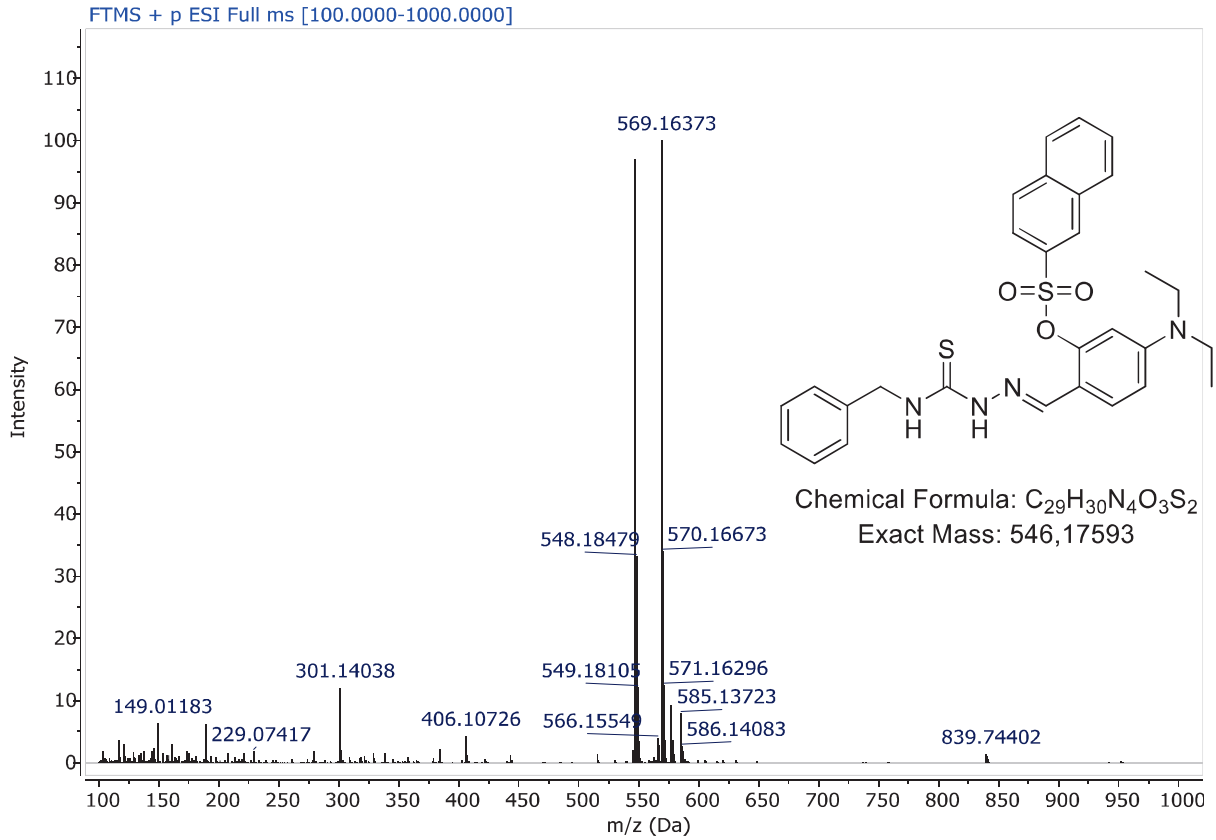

Figure S 102. ESI-HRMS Spectrum of Compound **5s**

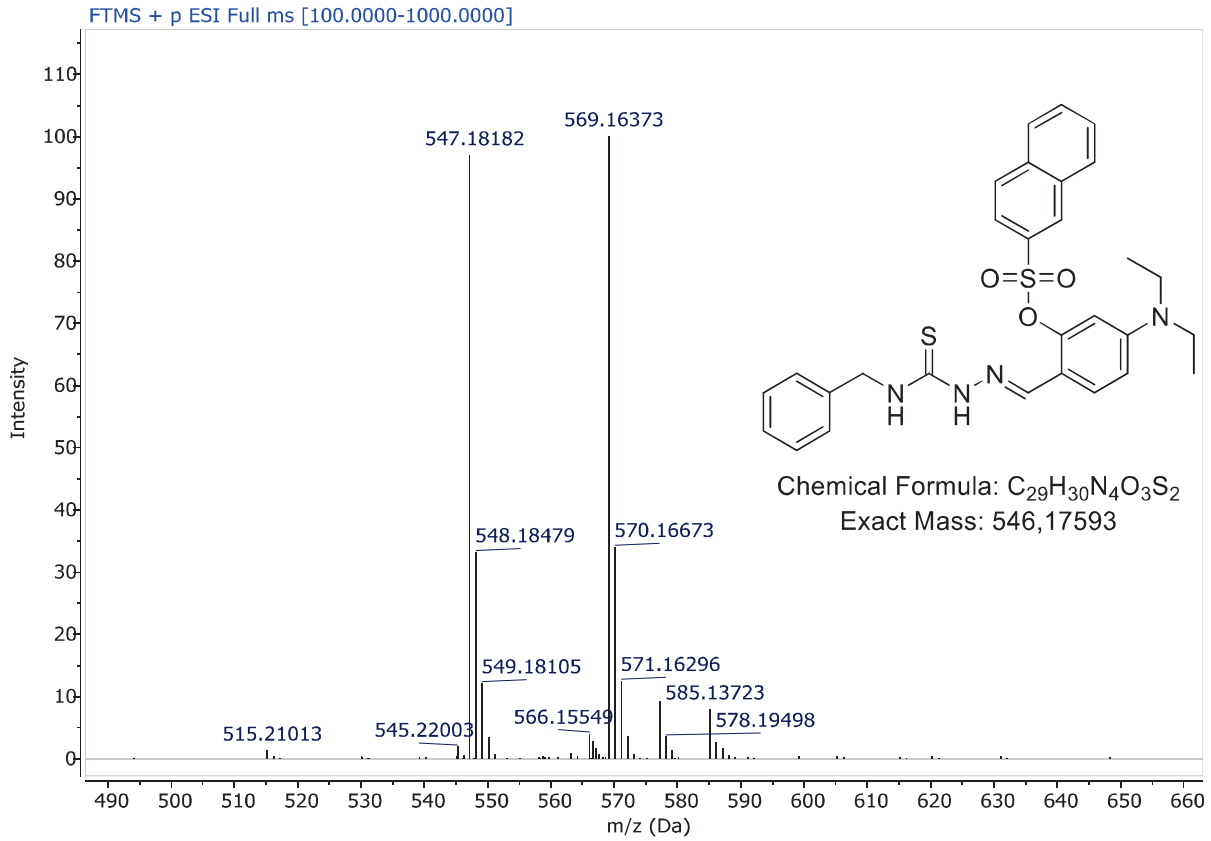

Figure S 103. ESI-HRMS Spectrum of Compound **5s** (extended)

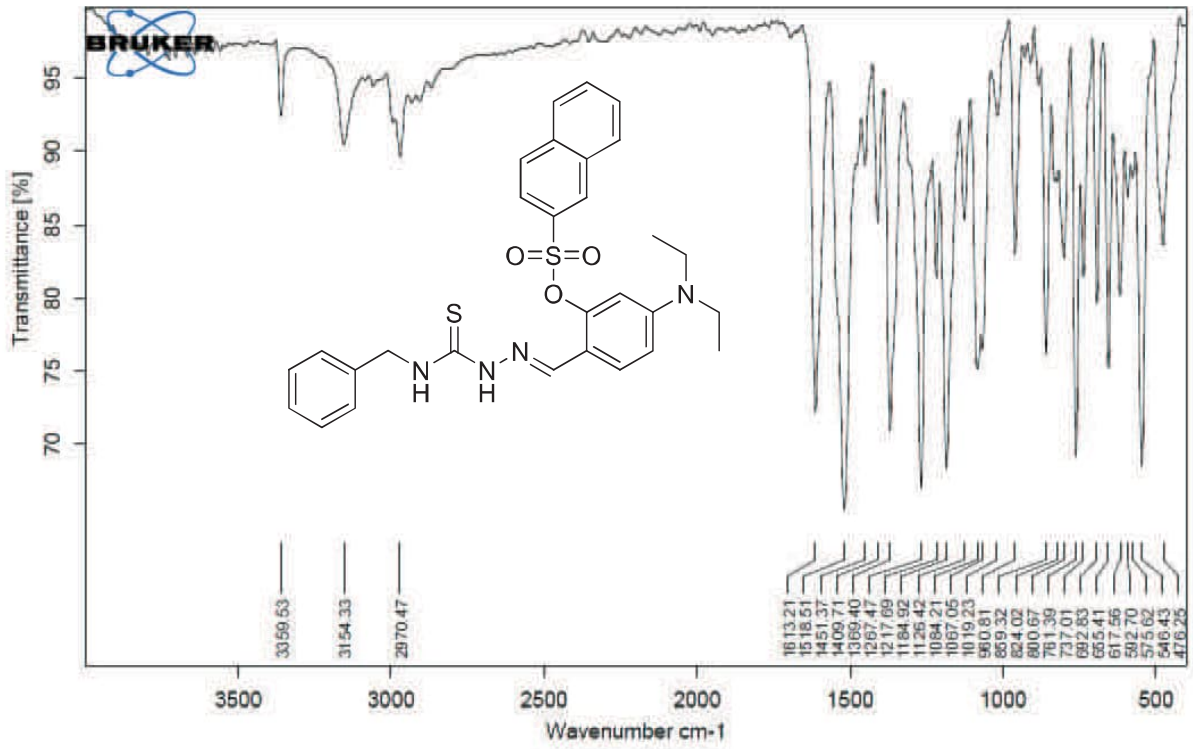

Figure S 104. FT-IR Spectrum of Compound **5s**

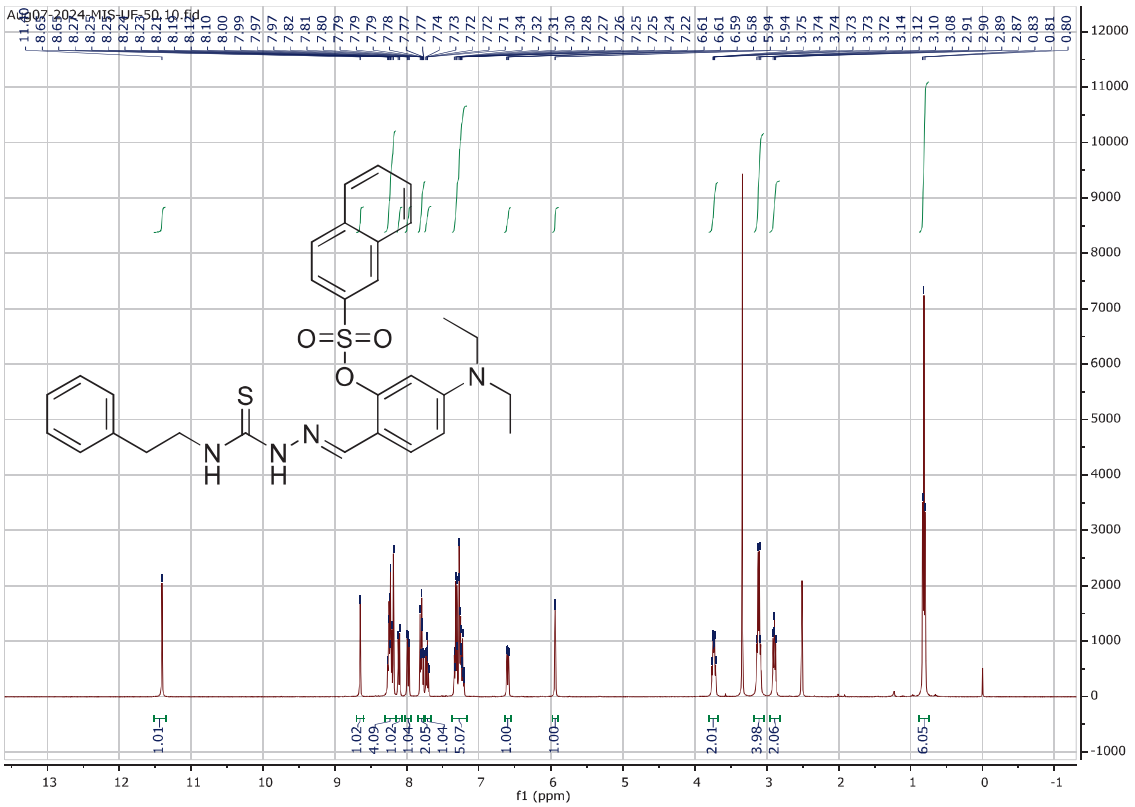

Figure S 105. ^{1}H-NMR Spectrum of Compound **5t** (DMSO-*d6*, 400 MHz)

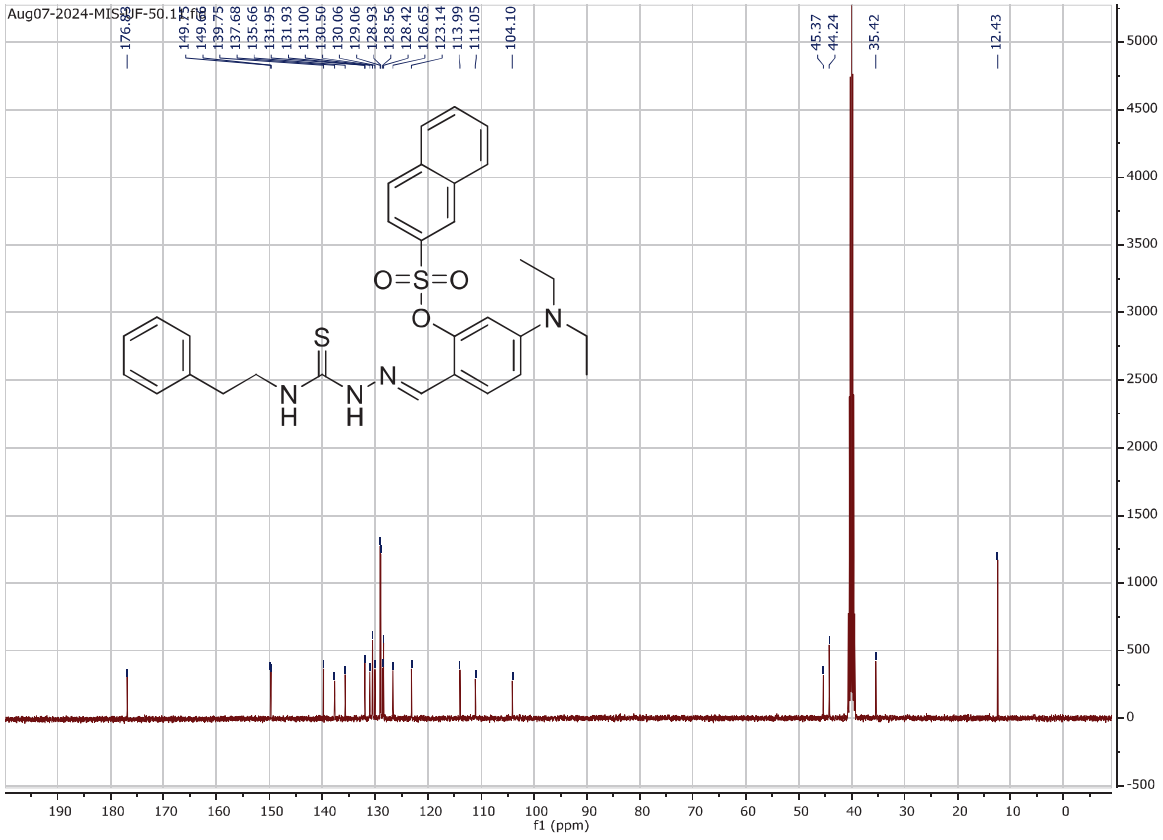

Figure S 106. ^{13}C-NMR Spectrum of Compound **5t** (DMSO-*d6*, 100 MHz)

Acq. Operator : SYSTEM
Sample Operator : SYSTEM
Acq. Instrument : HPLC Location : -
Injection Date : 12/21/2024 1:40:50 PM Inj : 1
Inj Volume : No Inj

Method : D:\HPLC-DATA\Method\BZ-11.M
Last changed : 5/29/2024 5:19:35 PM by SYSTEM

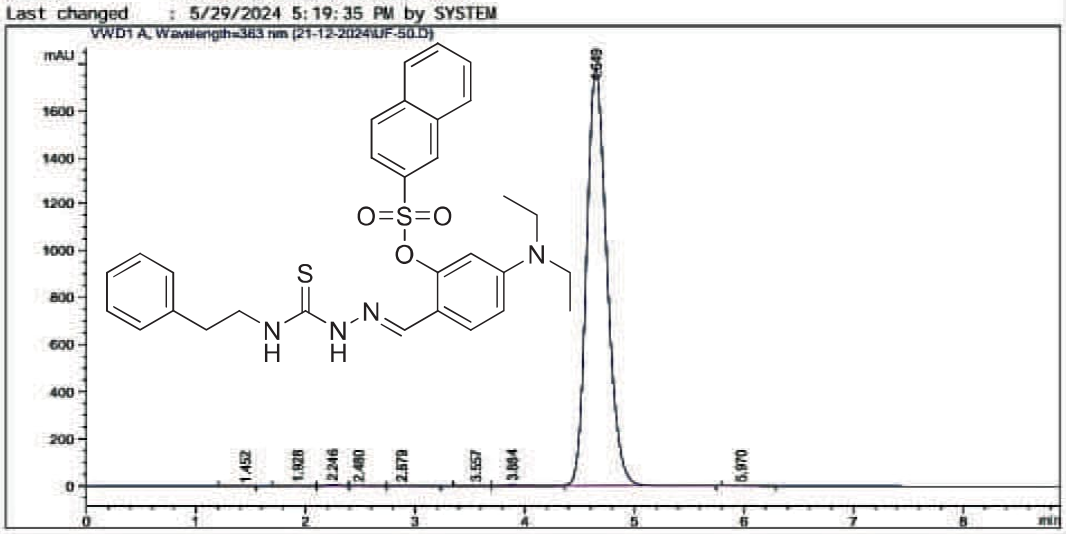

Area Percent Report

Sorted By : Signal
Multiplier : 1.0000
Dilution : 1.0000
Use Multiplier & Dilution Factor with ISTDs

Signal 1: VWD1 A, Wavelength=363 nm

Peak #	RetTime [min]	Type	Width [min]	Area [mAU*s]	Height [mAU]	Area %
1	1.452	BB	0.1612	6.54231e-1	5.05506e-2	2.844e-3
2	1.928	BB	0.1500	3.21834	2.96447e-1	0.0140
3	2.246	BV	0.1373	44.98896	5.05414	0.1955
4	2.480	VB	0.1452	20.86225	2.09753	0.0907
5	2.879	BB	0.1769	10.21445	8.48364e-1	0.0444
6	3.557	BV E	0.1817	8.02471	6.44265e-1	0.0349
7	3.884	VV E	0.2301	63.31086	3.84301	0.2752
8	4.649	VB R	0.1981	2.28522e4	1777.04077	99.3252
9	5.970	BB	0.1938	3.97989	3.09367e-1	0.0173

Data File D:\HPLC-DATA\Data\21-12-2024\UF-50.D
Sample Name: UF-50

Totals : 2.30075e4 1790.18445

Figure S 107. HPLC Purity Analysis of Compound **5t**

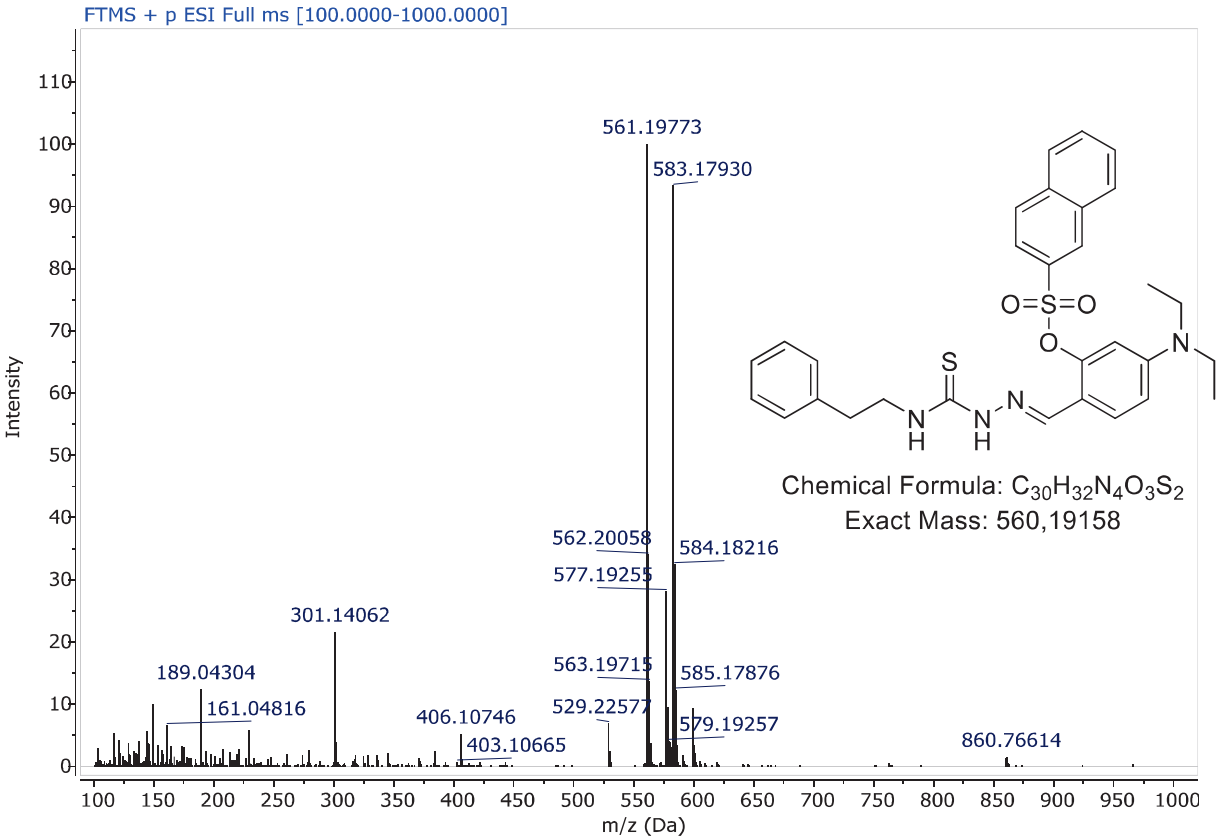

Figure S 108. ESI-HRMS Spectrum of Compound **5t**

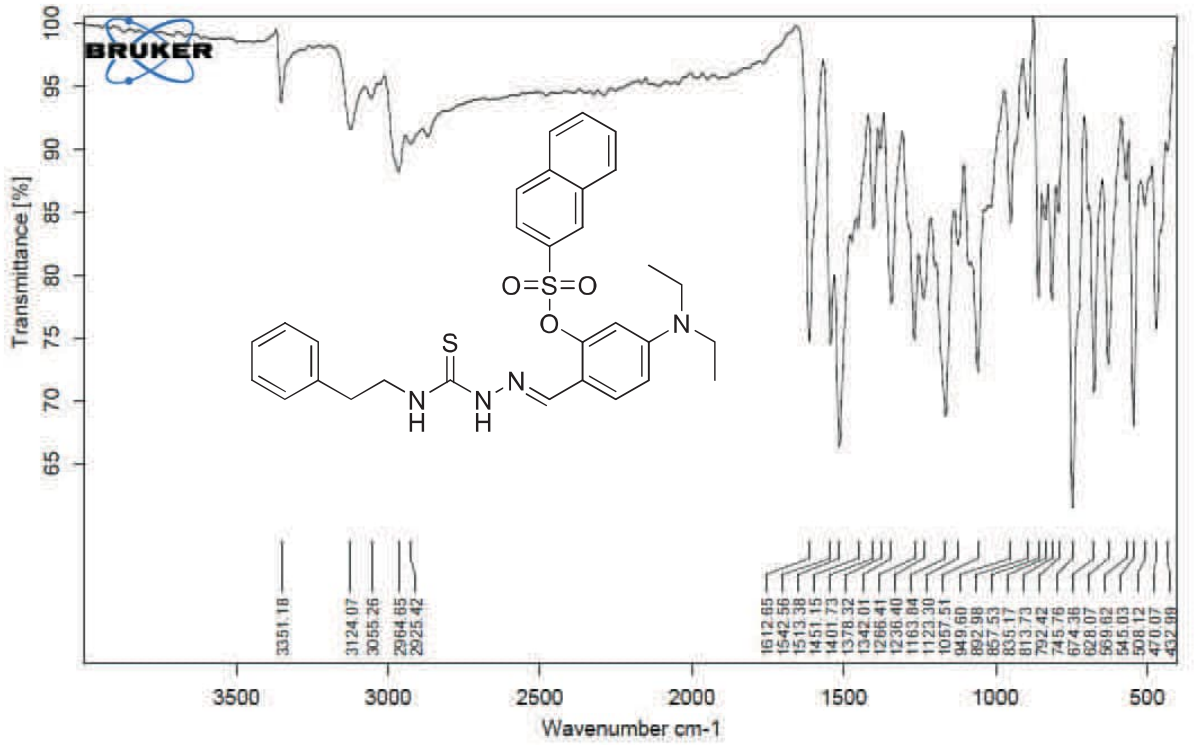

Figure S 109. FT-IR Spectrum of Compound **5t**

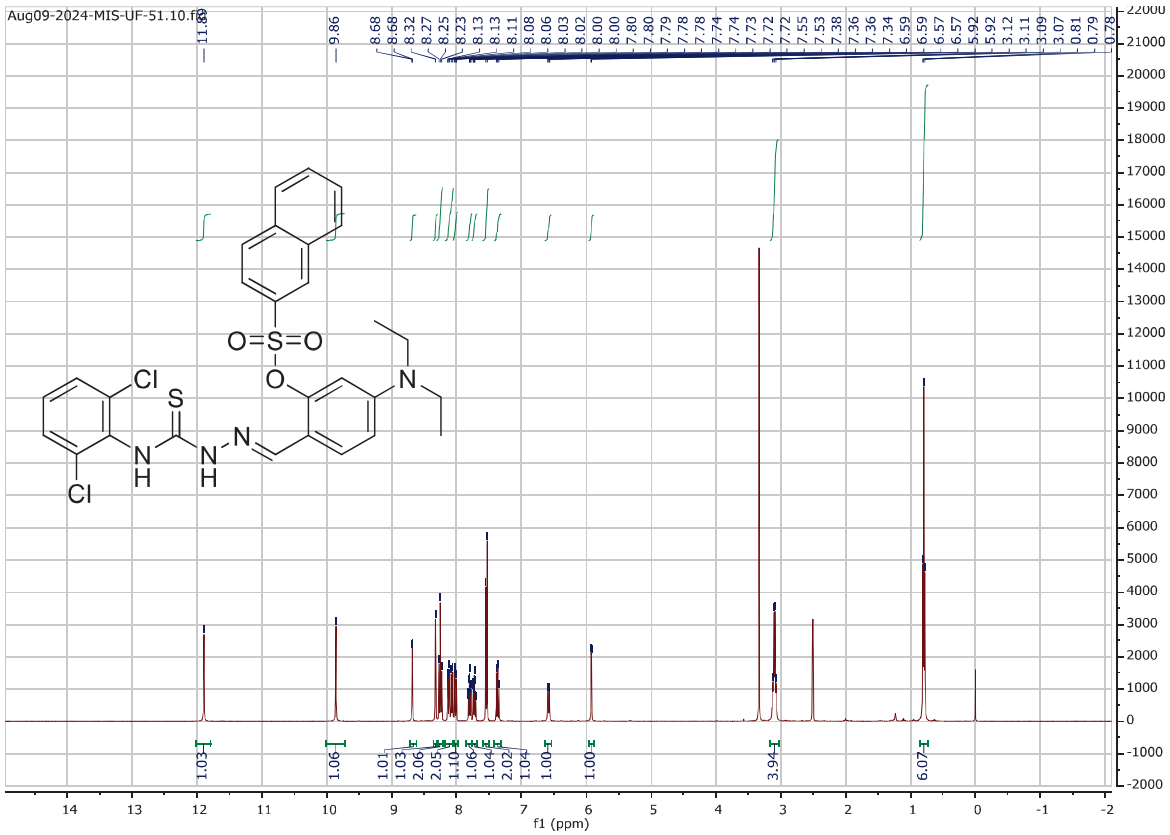

Figure S 110. ^{1}H-NMR Spectrum of Compound **5u** (DMSO-*d6*, 400 MHz)

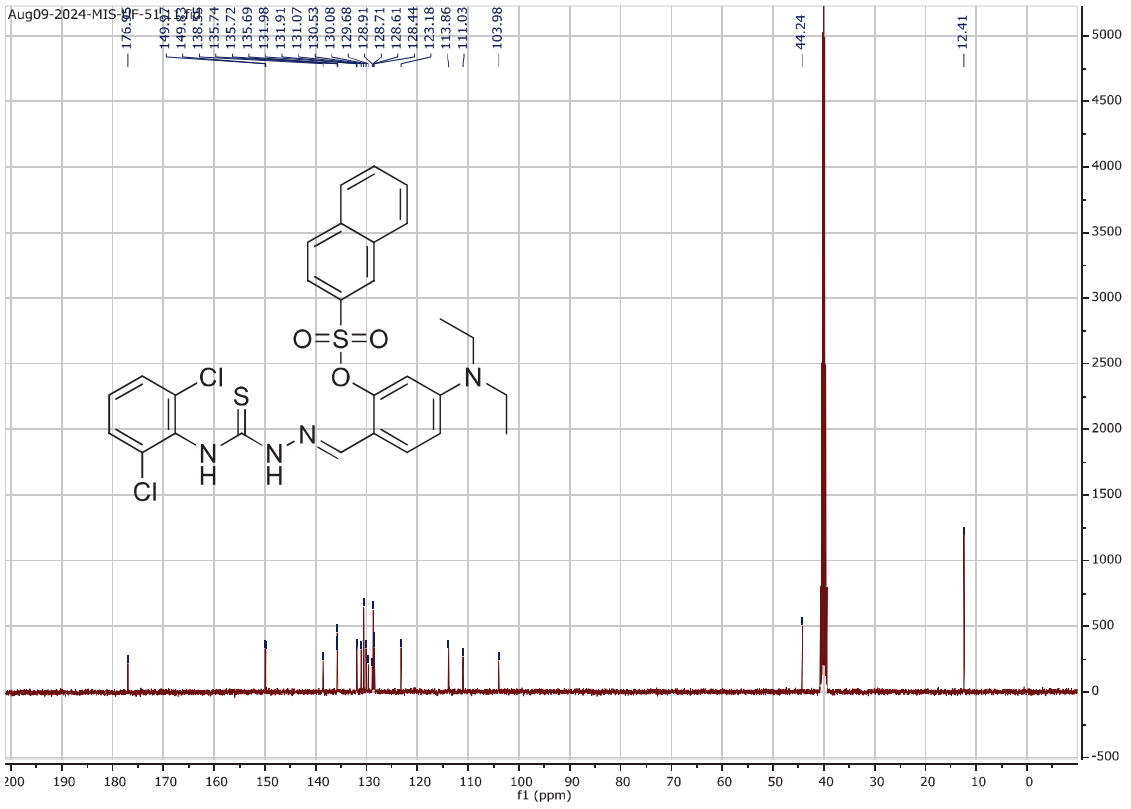

Figure S 111. ^{13}C-NMR Spectrum of Compound **5u** (DMSO-*d6*, 100 MHz)

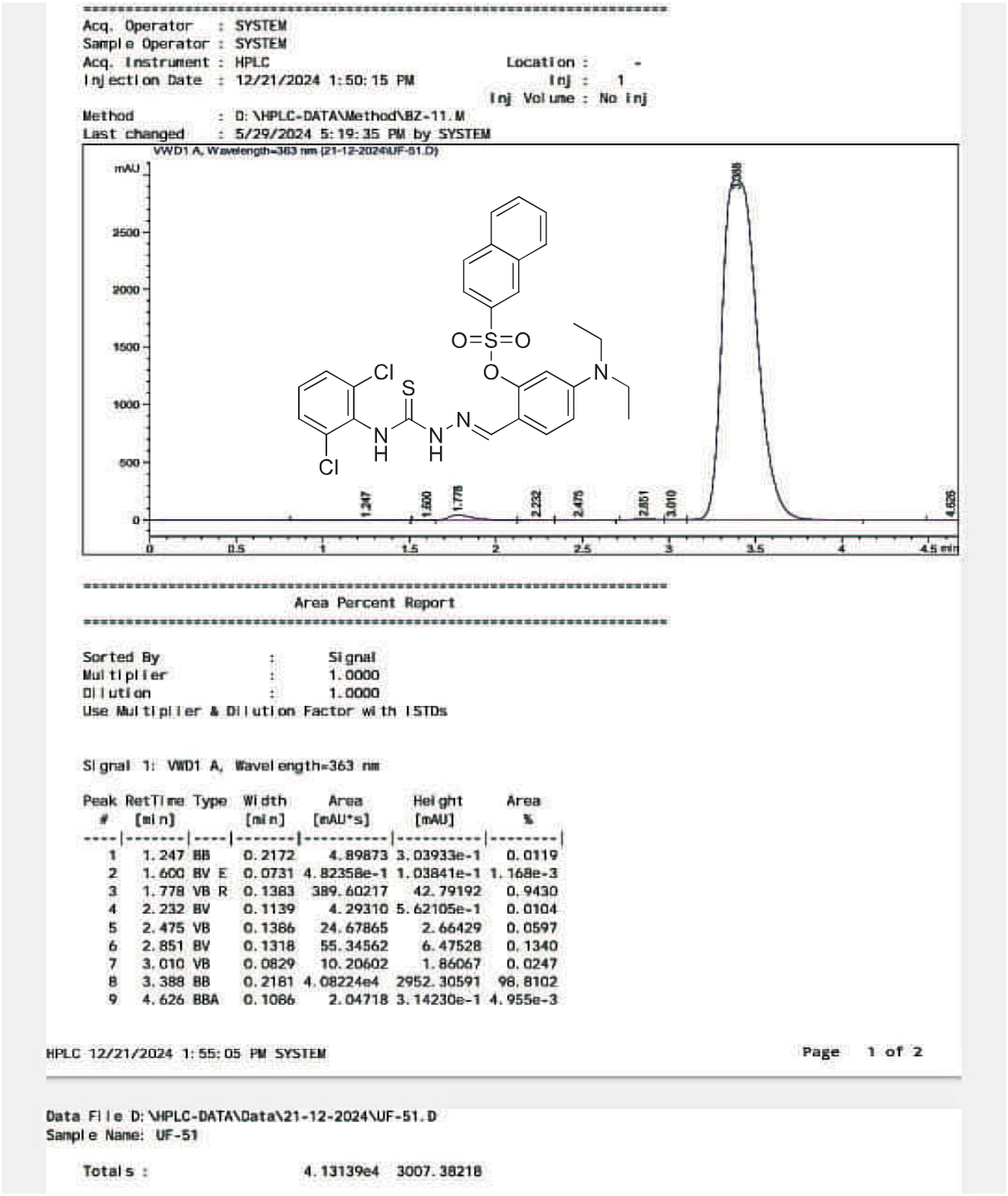

Acq. Operator : SYSTEM
Sample Operator : SYSTEM
Acq. Instrument : HPLC Location : -
Injection Date : 12/21/2024 1:50:15 PM Inj : 1
Inj Volume : No inj

Method : D:\HPLC-DATA\Method\BZ-11.M
Last changed : 5/29/2024 5:19:35 PM by SYSTEM

Area Percent Report

Sorted By : Signal
Multiplier : 1.0000
Dilution : 1.0000
Use Multiplier & Dilution Factor with ISTDs

Signal 1: VWD1 A, Wavelength=363 nm

Peak #	RetTime [min]	Type	Width [min]	Area [mAU*s]	Height [mAU]	Area %
1	1.247	BB	0.2172	4.89873	3.03933e-1	0.0119
2	1.600	BV E	0.0731	4.82358e-1	1.03841e-1	1.168e-3
3	1.778	VB R	0.1383	389.60217	42.79192	0.9430
4	2.232	BV	0.1139	4.29310	5.62105e-1	0.0104
5	2.475	VB	0.1386	24.67865	2.66429	0.0597
6	2.851	BV	0.1318	55.34562	6.47528	0.1340
7	3.010	VB	0.0829	10.20602	1.86067	0.0247
8	3.388	BB	0.2181	4.08224e4	2952.30591	98.8102
9	4.626	BBA	0.1086	2.04718	3.14230e-1	4.955e-3

Data File D:\HPLC-DATA\Data\21-12-2024\UF-51.D
Sample Name: UF-51

Totals : 4.13139e4 3007.38218

Figure S 112. HPLC Purity Analysis of Compound **5u**

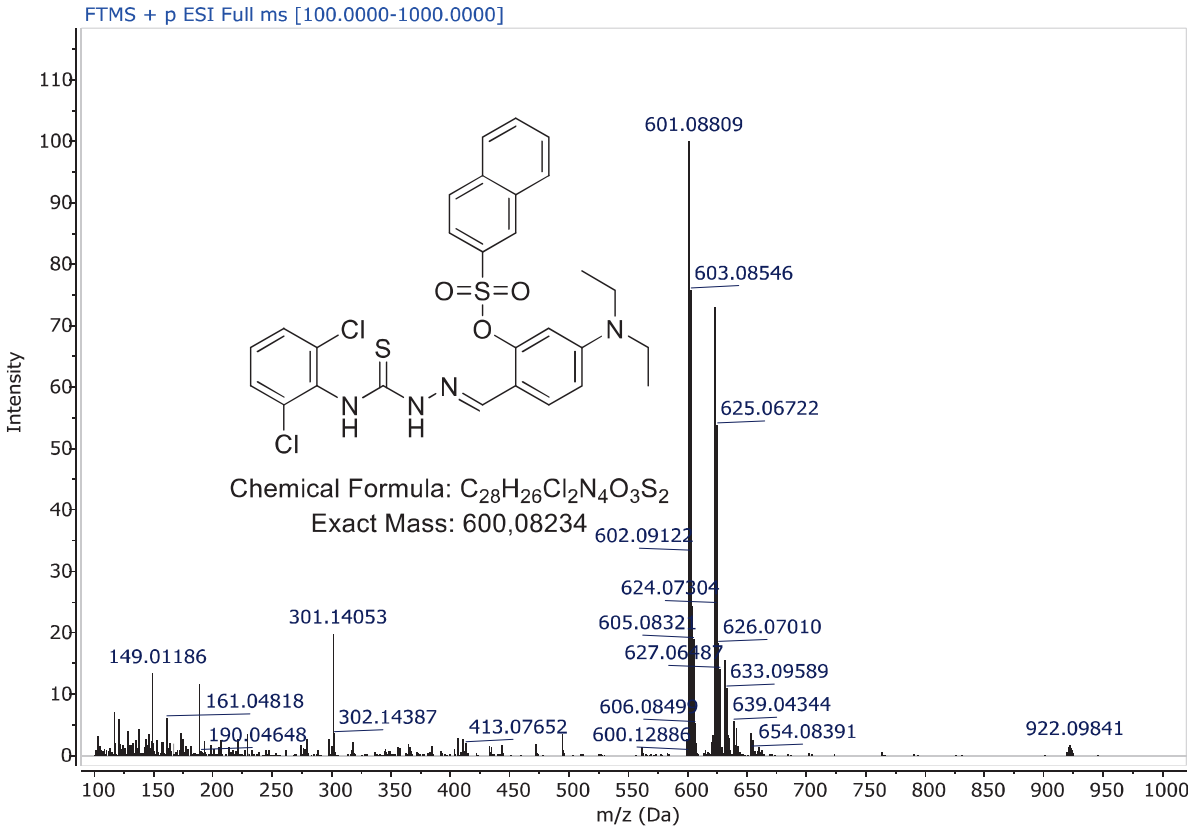

Figure S 113. ESI-HRMS Spectrum of Compound **5u**

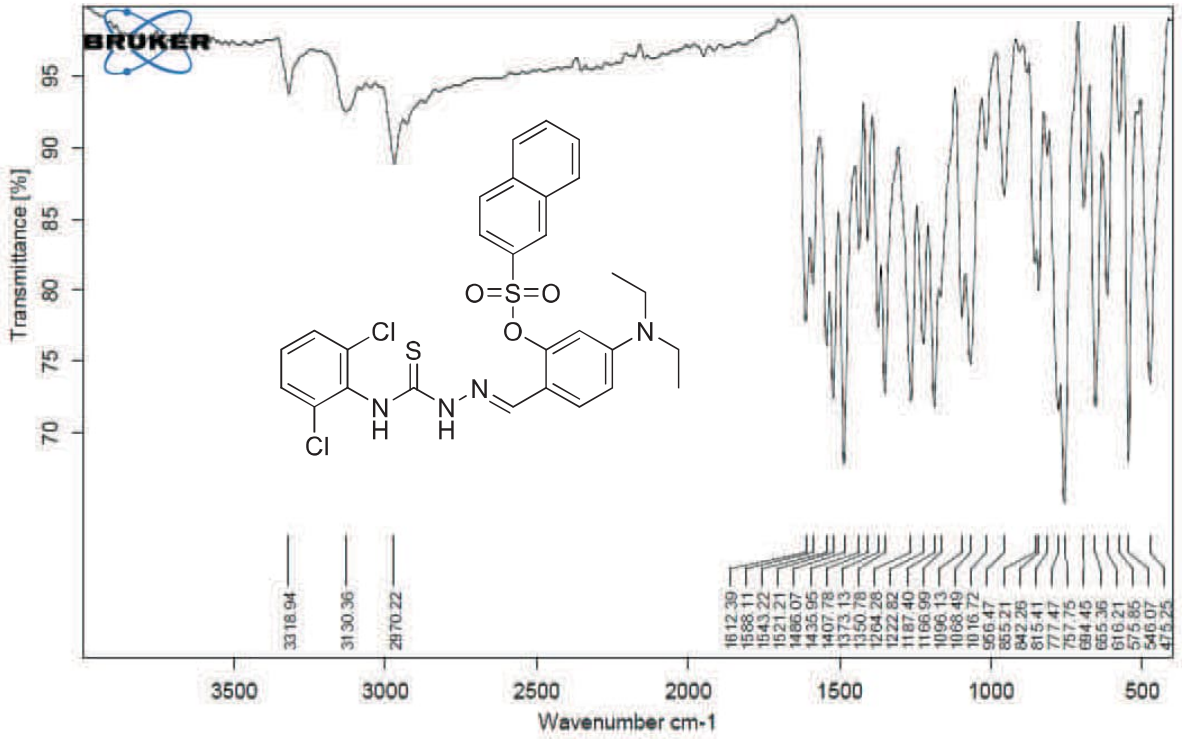

Figure S 114. FT-IR Spectrum of Compound **5u**

0	0.04201	0.07501	0.105603	0.12042	0.140511
100	73.63	65	49.09	41	36.36

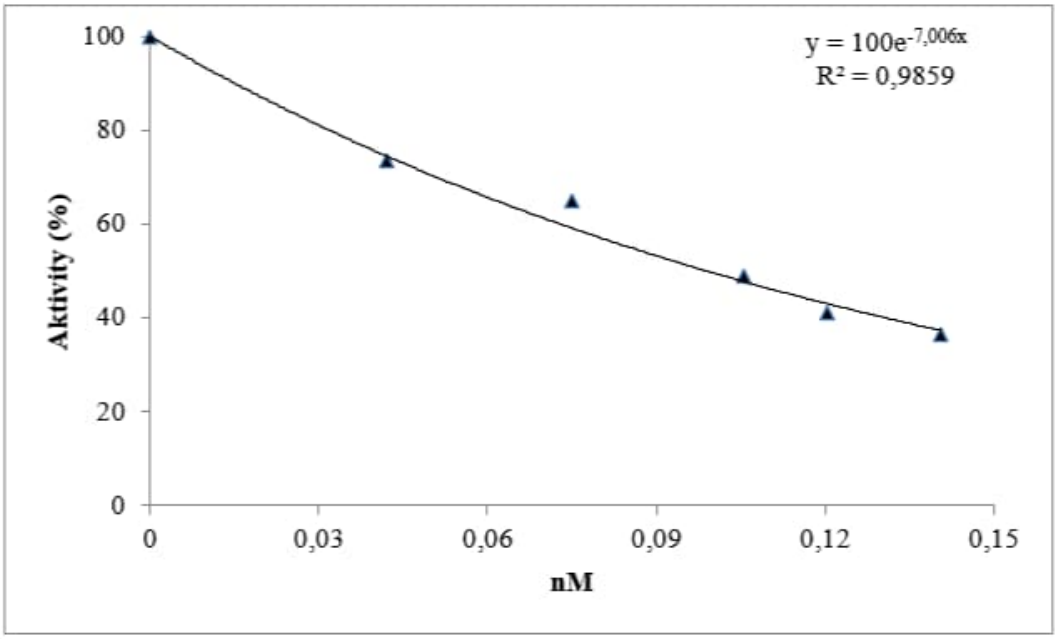

Figure S 115. Inhibition Curve of Compound **5a**

0	0.052469	0.083703	0.135062	0.150802	0.170926
100	73.37	60.68	51.28	42.37	38.46

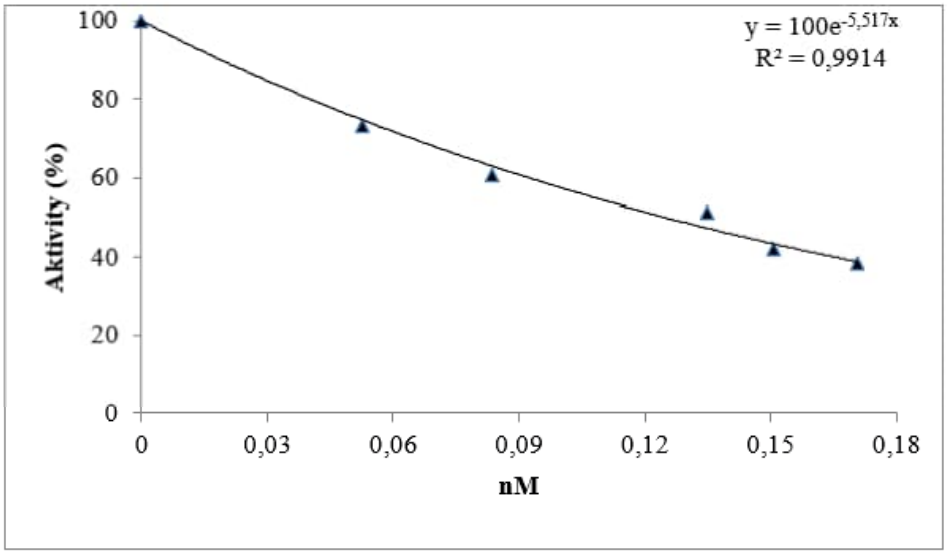

Figure S 116. Inhibition Curve of Compound **5b**

0	0.081315	0.121842	0.19315	0.223947	0.250473
100	68.33	58.33	47.5	37.5	30.83

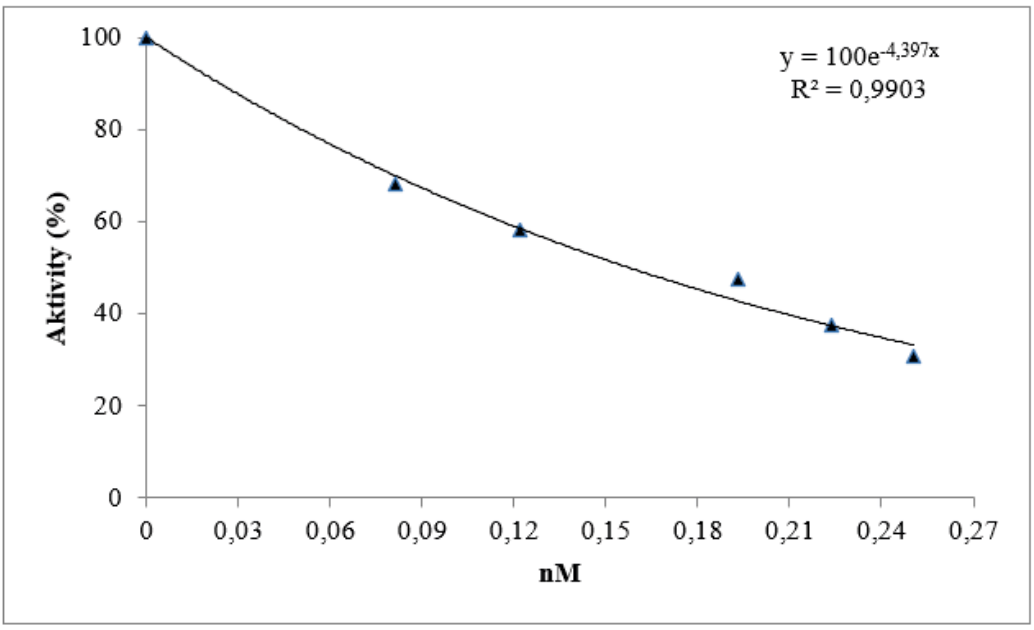

Figure S 117. Inhibition Curve of Compound **5c**

0	0.081015	0.130152	0.180267	0.195036	0.210393
100	80.83	67.5	48.33	40.83	35

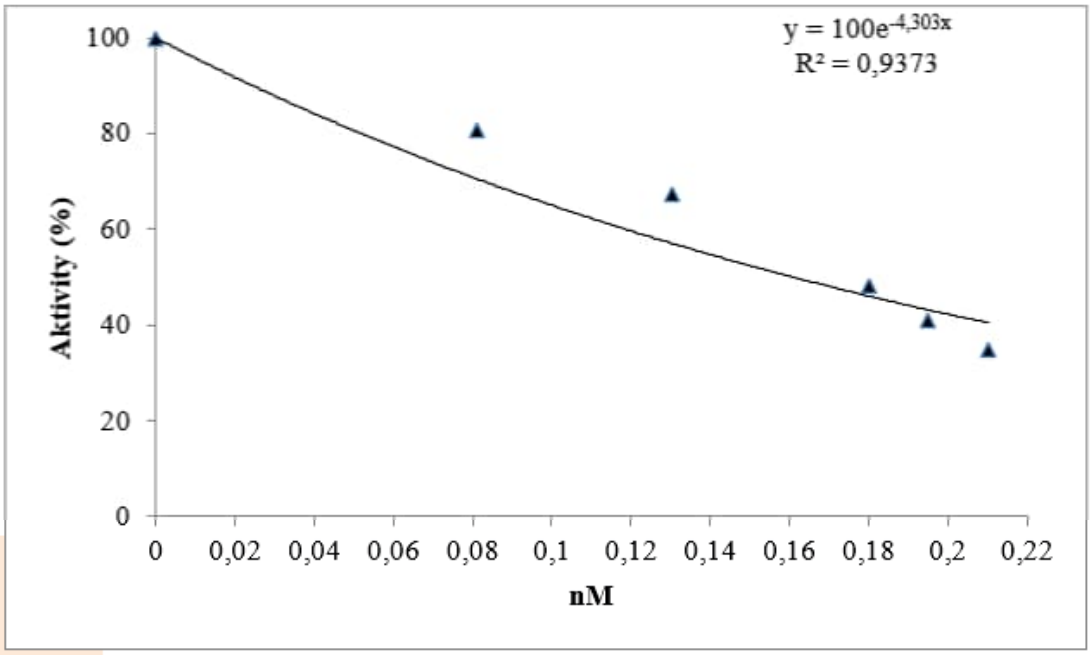

Figure S 118. Inhibition Curve of Compound **5d**

0	0.041522	0.072538	0.120406	0.130507	0.140558
100	76	65	52	40	34

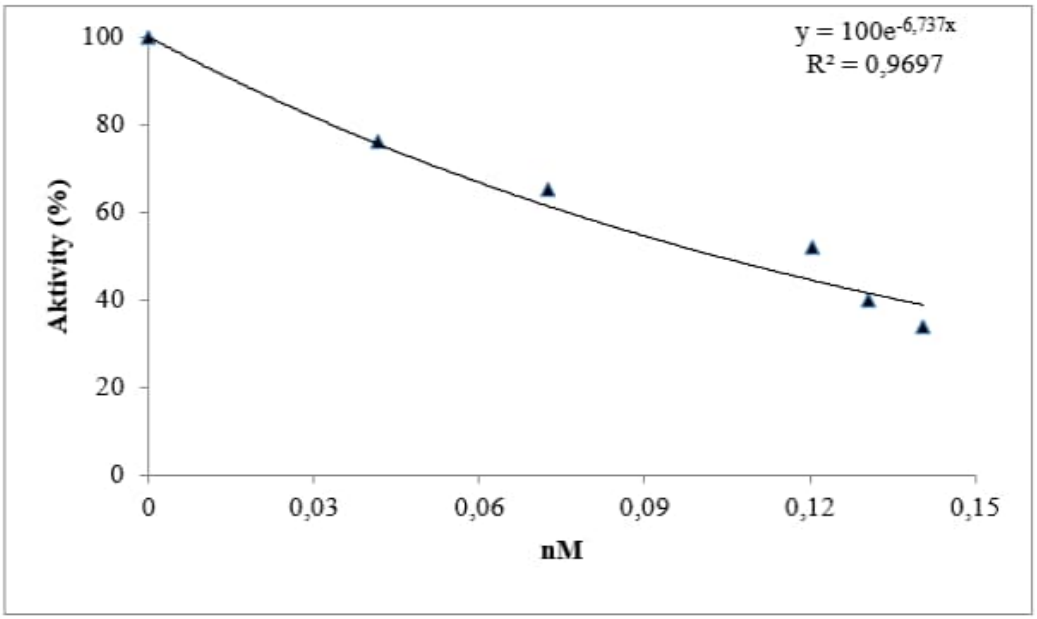

Figure S 119. Inhibition Curve of Compound **5e**

0	0.03127	0.071776	0.140317	0.160406	0.174568
100	78.33	65.83	50	44.16	38.33

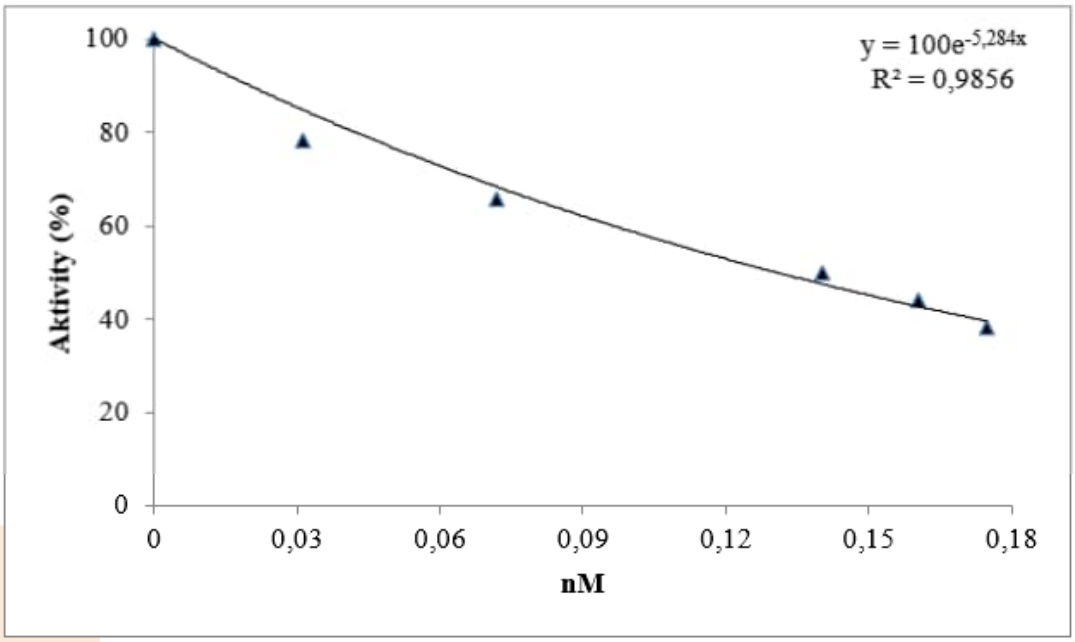

Figure S 120. Inhibition Curve of Compound **5f**

0	0.07906	0.130277	0.190451	0.210519	0.230624
100	72.5	63.33	48.33	41.66	36.66

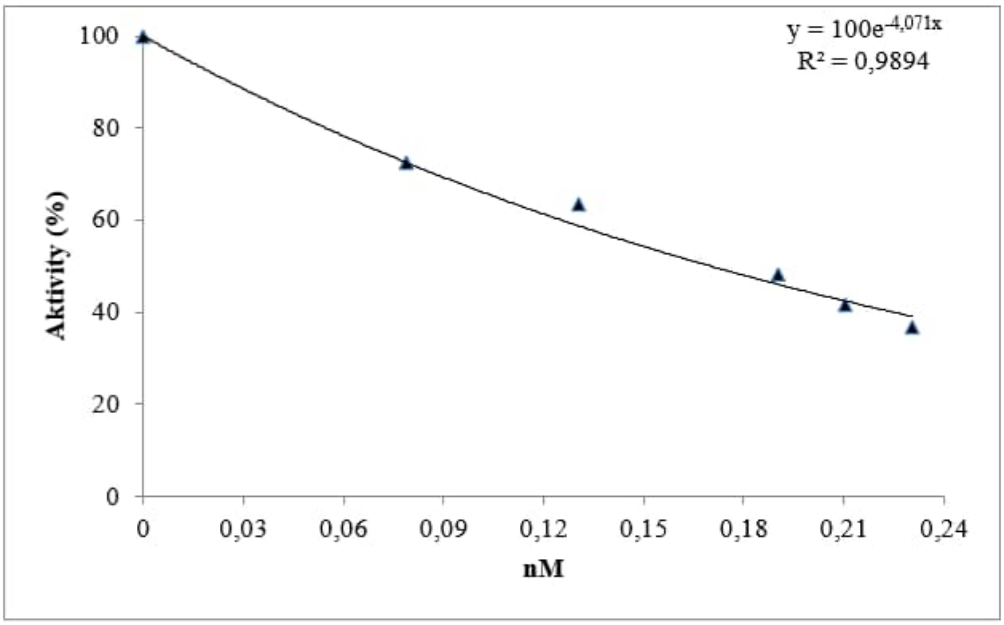

Figure S 121. Inhibition Curve of Compound **5g**

0	0.031317	0.051976	0.103624	0.110461	0.124056
100	75.55	66.66	48.88	44.44	37.77

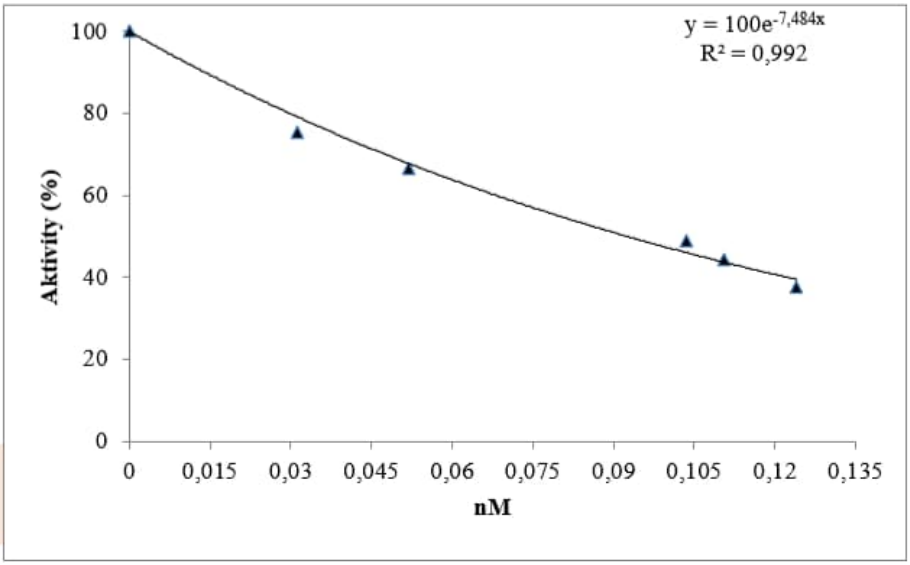

Figure S 122. Inhibition Curve of Compound **5h**

0	0.041317	0.072306	0.124041	0.140461	0.155053
100	72.38	57.14	48.57	38.09	33.33

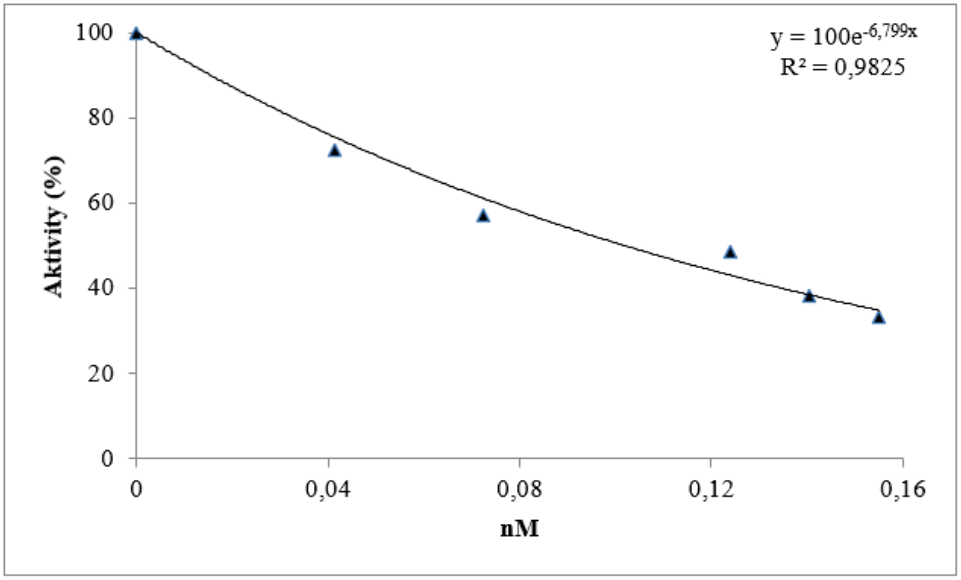

Figure S 123. Inhibition Curve of Compound **5i**

0	0.051812	0.082635	0.139048	0.150527	0.166061
100	76.2	64.76	48.57	40	33.33

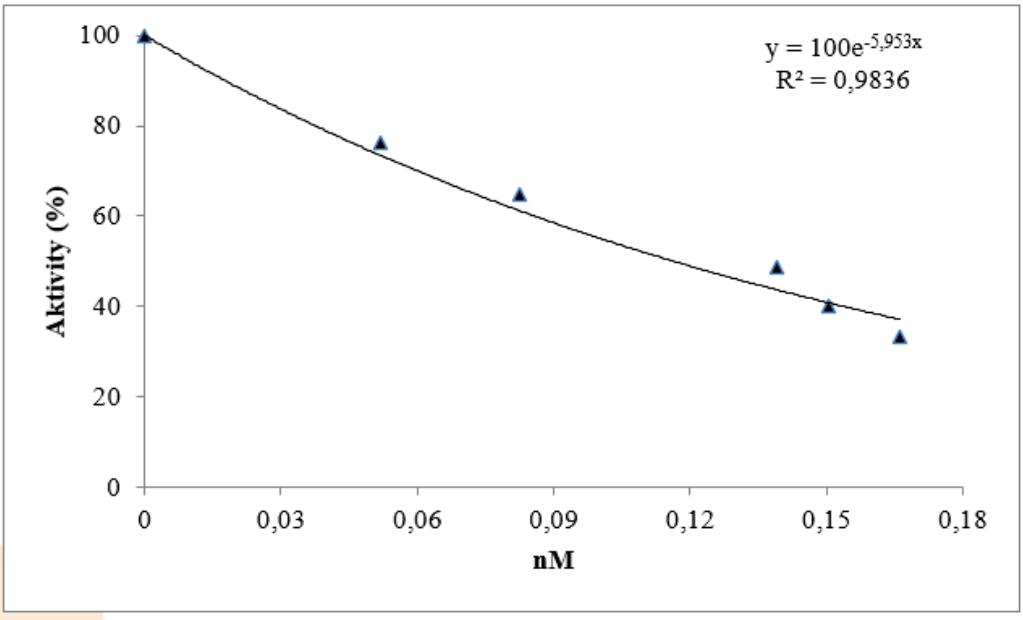

Figure S 124. Inhibition Curve of Compound **5j**

0	0.061497	0.092694	0.149045	0.160538	0.170598
100	77.77	67.77	47.77	41.11	32.22

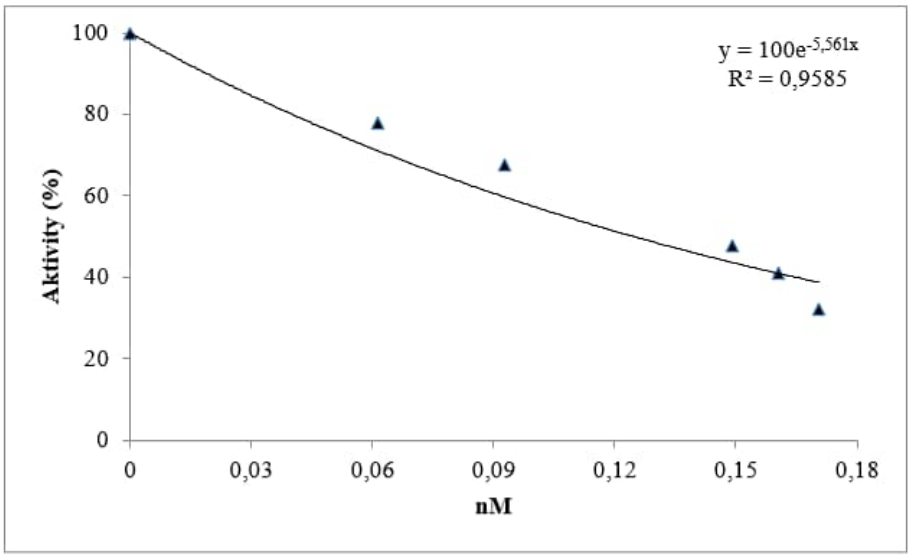

Figure S 125. Inhibition Curve of Compound **5k**

0	0.031644	0.061973	0.115036	0.124049	0.135056
100	71.11	63.33	50	41.11	35.55

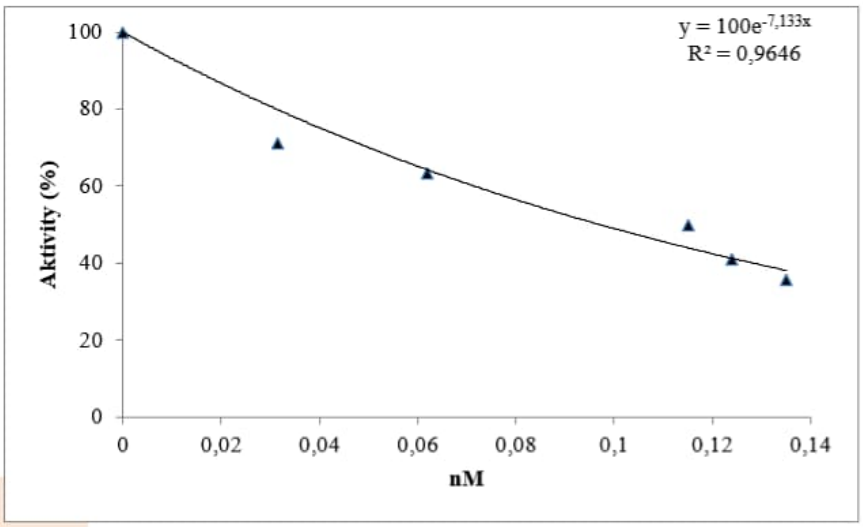

Figure S 126. Inhibition Curve of Compound **5l**

0	0.041506	0.082711	0.140407	0.150422	0.166051
100	76.66	60	48.88	44.44	38.88

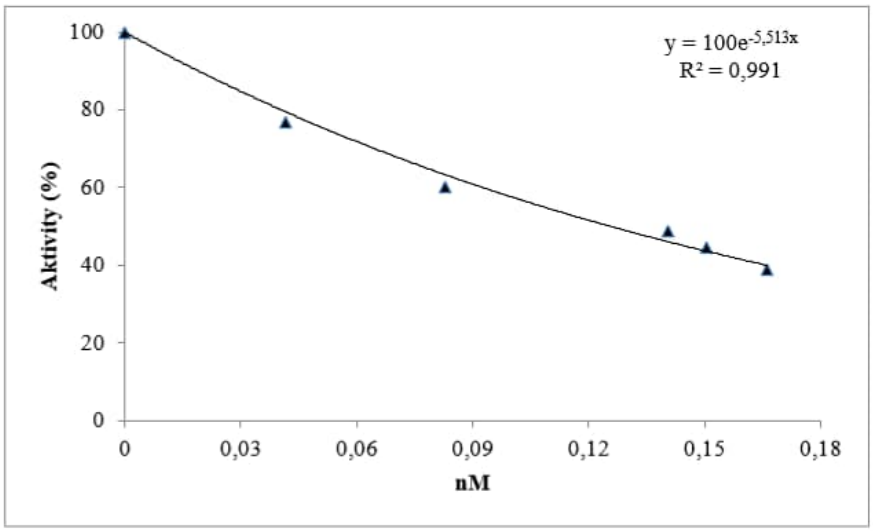

Figure S 127. Inhibition Curve of Compound **5m**

0	0.051257	0.0822	0.140394	0.154044	0.160503
100	74.46	64.89	48.93	42.55	34.04

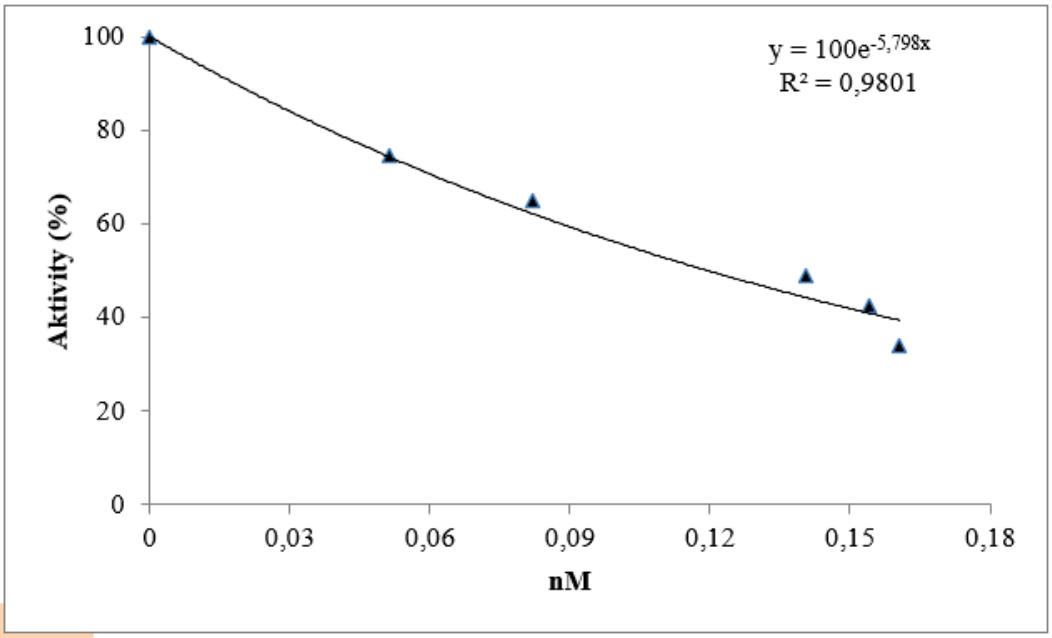

Figure S 128. Inhibition Curve of Compound **5n**

0	0.041256	0.071758	0.125028	0.140302	0.150377
100	72	60	50	45	35

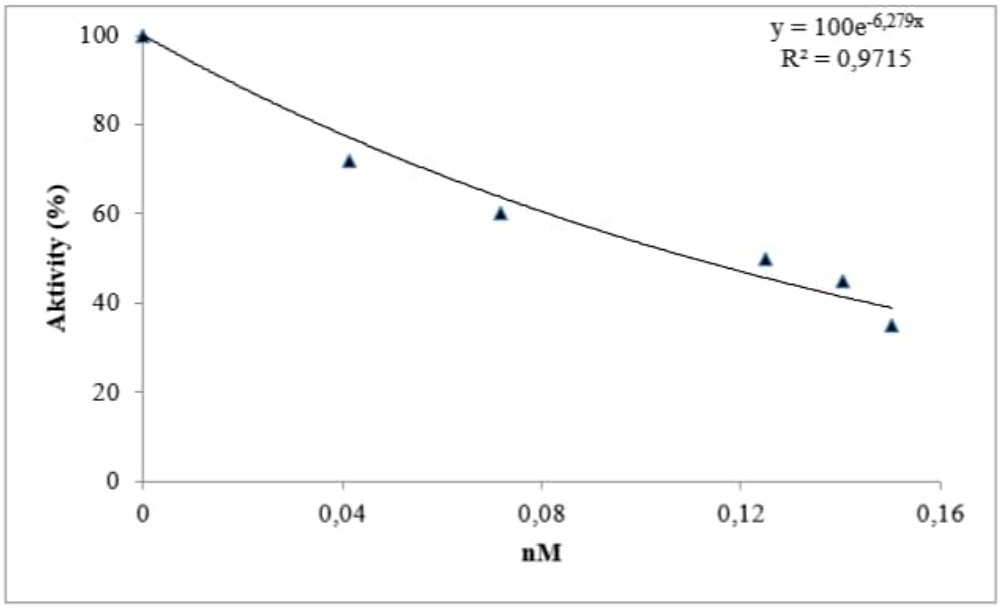

Figure S 129. Inhibition Curve of Compound **5o**

0	0.051716	0.093004	0.146558	0.156866	0.177725
100	80	72	47	40	34

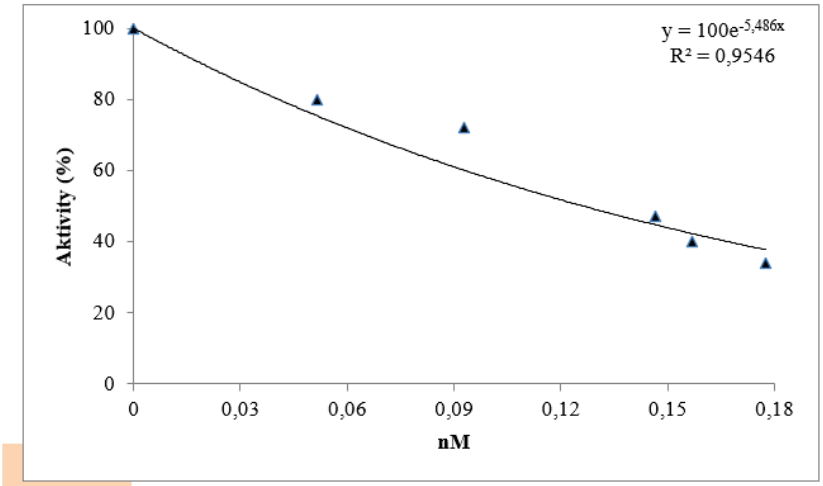

Figure S 130. Inhibition Curve of Compound **5p**

0	0.031087	0.061739	0.123043	0.130391	0.144347
100	75.83	66.66	50	44.16	39.16

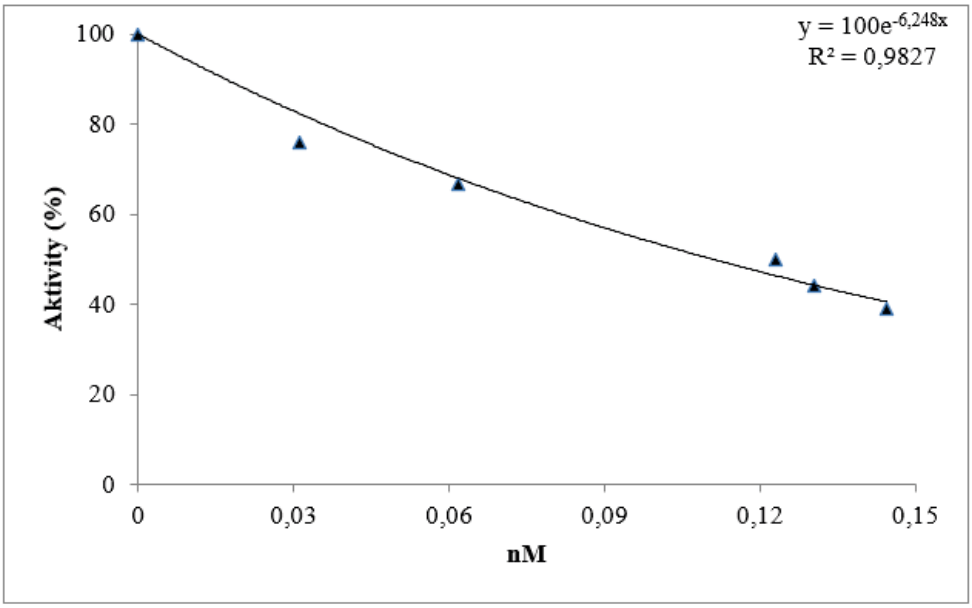

Figure S 131. Inhibition Curve of Compound **5q**

0	0.061121	0.091793	0.145291	0.157314	0.173811
100	73.07	65.38	47.7	45.38	38.46

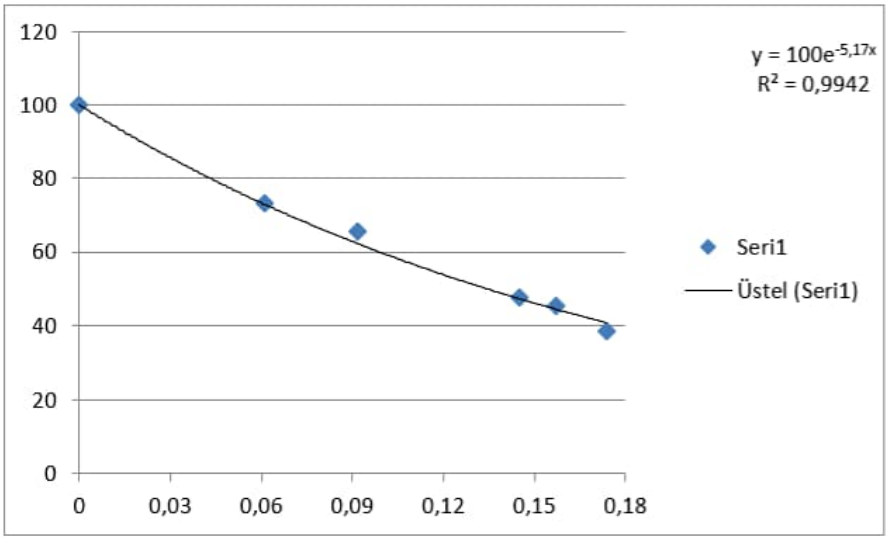

Figure S 132. Inhibition Curve of Compound **5r**

0	0.041674	0.062392	0.133468	0.144067	0.152478
100	70.4	60.8	48.81	42.4	36

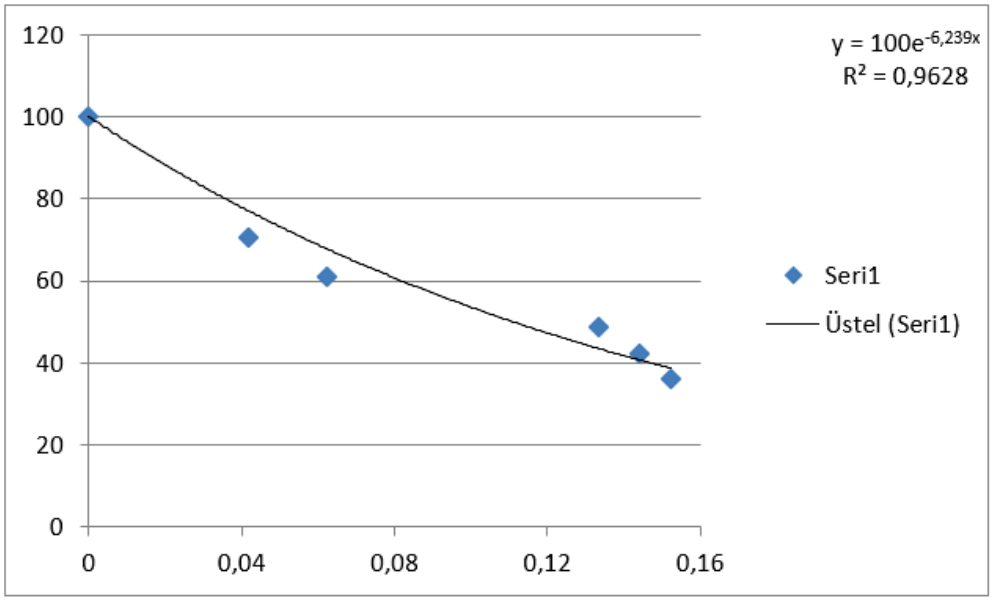

Figure S 133. Inhibition Curve of Compound **5s**

0	0.051674	0.10287	0.143827	0.154545	0.165023
100	70.83	60	47.55	41.66	37.5

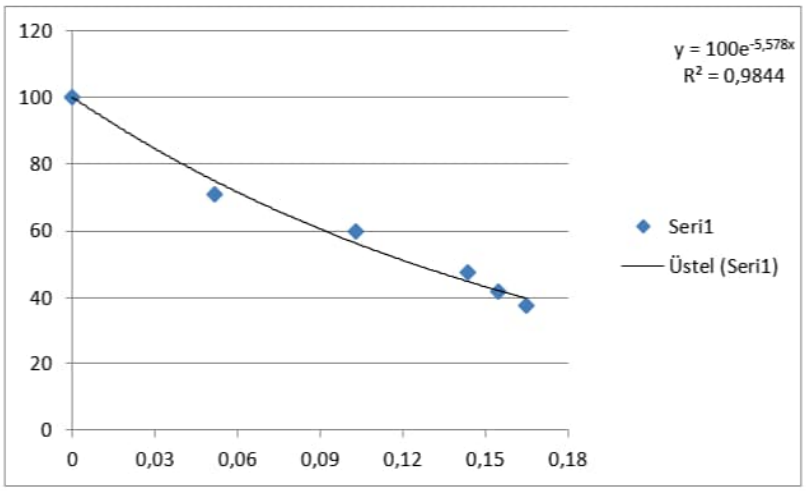

Figure S 134. Inhibition Curve of Compound **5t**

0	0.031054	0.051687	0.098253	0.123375	0.143692
100	76.33	67.93	49.61	43.51	38.16

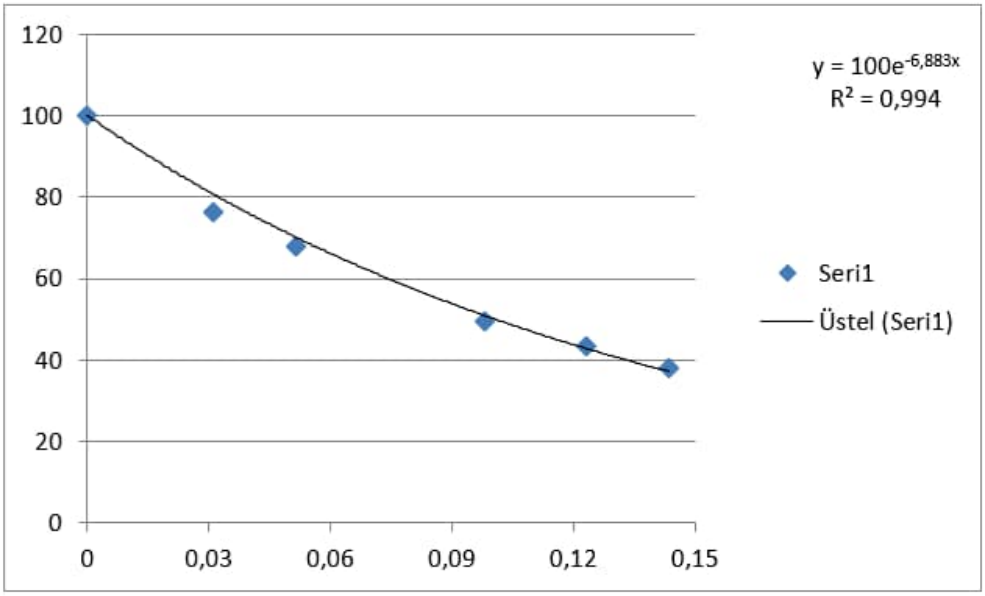

Figure S 135. Inhibition Curve of Compound **5u**

0	0.16237	0.348198	0.473465	0.494207	0.514702
100	72.32	66.07	50	43.75	35.71

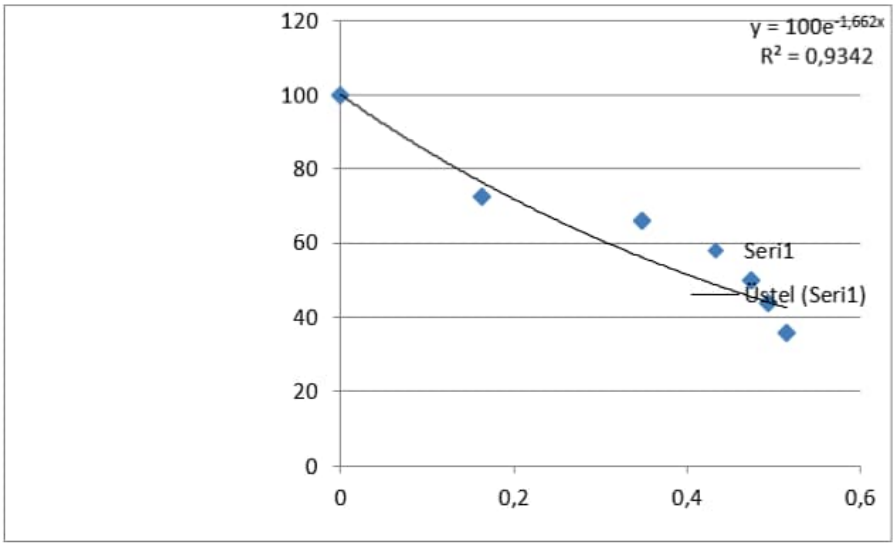

Figure S 136. Inhibition Curve of Compound **Clorgyline**